Philipps Universität Marburg

Neuromediators in the developing olfactory system: 3D-reconstruction towards a functional understanding

Neuromediatoren im sich entwickelnden olfaktorischen System: mittels 3D-Rekonstruktionen zu einem funktionellen Verständnis

Dissertation
zur Erlangung des Doktorgrades
der Naturwissenschaften
(Dr. rer. nat.)

dem
Fachbereich Biologie
der Philipps-Universität Marburg
vorgelegt von

Wolf-Dietmar Hütteroth
aus Erlangen

Marburg/Lahn 2008

Vom Fachbereich Biologie
der Philipps-Universität Marburg als Dissertation am
13. August 2008 angenommen.

Erstgutachter: Prof. Dr. Joachim Schachtner
Zweitgutachter: Prof. Dr. Uwe Homberg

Tag der mündlichen Prüfung am 20.10.2008.

Inhaltsverzeichnis

Eigene Beiträge und veröffentlichte Teile der Arbeit

Laut §8, Absatz 3 der Promotionsordnung der Philipps-Universität Marburg (Fassung vom 28.04.1993) müssen bei den Teilen der Dissertation, die bei gemeinsamer Forschungsarbeit entstanden sind, „die individuellen Leistungen des Doktoranden deutlich abgrenzbar und bewertbar sein." Dies betrifft die Kapitel I-VII. Die Beiträge werden im Folgenden näher erläutert. Die Arbeiten wurden zum Teil über eine Sachbeihilfe der Deutschen Forschungsgemeinschaft für Prof. Dr. J. Schachtner (Scha 678/3-3) gefördert.

Kapitel I: Copper/Zinc superoxide dismutase-like immunoreactivity in the metamorphosing brain of the sphinx moth *Manduca sexta*

- Sämtliche Westernblots und der größte Teil der Immunfärbungen wurden von mir angefertigt. Die TUNEL-Färbungen erfolgten durch J. Schachtner, die Paraffinschnittserien wurden von L. Lennartz angefertigt. Die Analyse der Daten erfolgte durch J. Schachtner und mich.
- Das Manuskript wurde in Zusammenarbeit mit J. Schachtner und H.-W. Honegger verfasst.
- Dieses Kapitel wurde in der vorliegenden Form im „Journal of Comparative Neurology" veröffentlicht (Schachtner J, Huetteroth W, Nighorn A, Honegger HW. 2004. Copper/Zinc Superoxide Dismutase-Like Immunoreactivity in the Metamorphosing Brain of the Sphinx Moth *Manduca sexta*. J Comp Neurol 469:141-152).

Kapitel II: Transient nitric oxide-dependent cyclic GMP formation is involved in metamorphic development of the antennal lobes of *Manduca sexta*

- Weitgehende Durchführung und Auswertung der Experimente durch mich; Fig. 1 beruht auf Daten erhoben durch S. Utz und J. Schachtner.
- Die ODQ-Experimente zu Fig. 2 wurden von S. Utz durchgeführt.
- P. Winterhagen erhob die Daten zu den MsGCα1-, und MsGC-I-Immunfärbungen in Fig. 5.
- Die RIOD-Daten in Fig. 6, deren Auswertung und die zugrunde liegenden Präparate wurden von J. Schachtner und B. Trosowski erstellt.
- U. Müller stellte seine Expertise bei den ELISAs zur Verfügung.
- Das Manuskript wurde in Zusammenarbeit mit J. Schachtner. U. Müller und A. Nighorn verfasst und am 23.07.2008 bei „Developmental Neurobiology" eingereicht (Huetteroth W, Winterhagen P, Utz S, de Vente J, Müller U, Nighorn A, Schachtner J 2008. Transient, nitric oxide-dependent cyclic GMP formation is involved in metamorphic development of the antennal lobes of *Manduca sexta*. Dev Neurobiol).

Kapitel III: Mas-allatotropin in the developing antennal lobe of the sphinx moth *Manduca sexta*: Distribution, time course, developmental regulation and colocalization with other neuropeptides

- Immunzytochemische Mehrfachmarkierungen mit Antiseren gegen Mas-Allatotropin und GABA bzw. TM-MFas II wurden von mir durchgeführt und ausgewertet. Ebenso gehen die im Manuskript gezeigten 3D-Rekonstruktionen des Antennallobus auf mich zurück.
- Die Experimente wurden zu einem großen Teil von S. Utz durchgeführt und ausgewertet. Ein Teil der immunzytochemischen Präparate wurde von der technischen Assistentin Sabine Jesberg bzw. der Auszubildenden Karin Müller angefertigt.
- Die Westernblots wurden großteils von M. Vömel erstellt.
- Das Manuskript wurde in Zusammenarbeit mit S. Utz und J. Schachtner verfasst und wurde in vorliegender Form in der Fachzeitschrift „Developmental Neurobiology“ veröffentlicht (Utz S, Huetteroth W, Schachtner J. 2008. Mas-allatotropin in the developing antennal lobe of the sphinx moth *Manduca sexta*: Distribution, time course, developmental regulation and colocalization with other neuropeptides. Dev Neurobiol 68:123-142).

Kapitel IV: Direct peptide profiling of lateral cell groups of the antennal lobes of *Manduca sexta* reveals specific composition and changes in neuropeptide expression during development

- Immunzytochemische Färbung mit einem Antiserum gegen myoinhibitorische Peptide sowie die 3D-Rekonstruktion des Antennallobus wurden von mir angefertigt.
- Die Experimente wurden größtenteils von S. Utz durchgeführt und ausgewertet. Ausnahme war die im Manuskript aufgeführte Fragmentierung der Peptide Mas-Allatotropin, Cydiastatin 3 und 4, welche von PD Dr. Reinhard Predel (Zoologie, Universität Jena) durchgeführt und ausgewertet wurden.
- Das Manuskript wurde in Zusammenarbeit mit S. Utz und J. Schachtner verfaßt und ist in vorliegender Form in der Fachzeitschrift „Developmental Neurobiology“ veröffentlicht (Utz S, Huetteroth W, Wegener C, Kahnt J, Predel R, Schachtner J. 2007. Direct peptide profiling of lateral cell groups of the antennal lobes of *Manduca sexta* reveals specific composition and changes in neuropeptide expression during development. Dev Neurobiol 67:764-777).

Kapitel V: Standard three-dimensional glomeruli of the *Manduca sexta* antennal lobe: a tool to study both developmental and adult plasticity

- Durchführung und Auswertung sämtlicher Experimente durch mich.
- Verfassen des Manuskriptes in Zusammenarbeit mit J. Schachtner.
- Dieses Kapitel wurde in der vorliegenden Form in „Cell and Tissue Research" veröffentlicht (Huetteroth W, Schachtner J. 2005. Standard three-dimensional glomeruli of the *Manduca sexta* antennal lobe: a tool to study both developmental and adult plasticity. Cell Tissue Res 319:513-524).

Kapitel VI: Anisometric brain dimorphism revisited: implementation of a volumetric 3D standard brain in *Manduca sexta*

- Anleitung und teilweise Durchführung durch den Autor, Anfertigung der Präparate überwiegend durch Basil el Jundi. Die Auswertung erfolgte in Zusammenarbeit mit Basil el Jundi.
- Angela Kurylas erteilte Hilfestellung bei der Standardisierung.
- Das Manuskript wurde in Zusammenarbeit mit Basil el Jundi und J. Schachtner verfasst und am 27.06.2008 bei „Journal of Comparative Neurology" eingereicht (el Jundi B, Huetteroth W, Kurylas AE, Schachtner J 2008. Anisometric brain dimorphism revisited: implementation of a volumetric 3D standard brain in *Manduca sexta*. J Comp Neurol).

Kapitel VII: A 4D representation of antennal lobe output based on an ensemble of identified projection neurons

- Erstellung des Referenz-Antennallobus durch den Autor, ebenso die Identifizierung der innervierten Glomeruli, der Somalage und der Trakte.
- Elektrophysiologie und deren Auswertung, Aufarbeitung der Präparate, Datenaufnahme und Verknüpfung der physiologischen Daten als Farbkodierung mit der 3D Darstellung in Amira durch Dr. Erich M. Staudacher.
- Das Manuskript wurde von E.M. Staudacher und K.C. Daly in Zusammenarbeit mit mir und J. Schachtner verfasst und am 01.07.2008 bei „Journal of Neuroscience Methods" eingereicht (Staudacher EM, Huetteroth W, Schachtner J, Daly KC 2008. A 4D representation of antennal lobe output based on an ensemble of identified projection neurons. J Neurosci Methods).

Die komplette Dissertationsarbeit, die einzelnen Kapitel sowie als "online supplement" zur Verfügung gestellte Teile der vorangehenden Arbeiten (Bilder und Filme) finden sich auf beiliegender CD.

Über den Rahmen dieser Doktorarbeit hinaus stellte ich der Arbeitsgruppe von PD Dr. Reinhard Predel meine Expertise bei der 3D-Darstellung von PBAN-Zellen in *Manduca sexta* zur Verfügung. Im Rahmen der Zusammenarbeit führte ich Immunfärbungen gegen PRXamide und anschliessende dreidimensionale Rekonstruktionen im Gehirn und Bauchmark durch. Die Ergebnisse dieses Projektes stehen kurz vor der Einreichung bei PNAS unter dem Titel: “Peptidomics of pheromone biosynthesis activating neuropeptide (PBAN)-expressing neurons of an insect.”

Weitere kurz vor dem Abschluss stehende Projekte, an denen ich in der AG Schachtner maßgeblich beteiligt bin:

- Vierdimensionale Darstellung der pupalen Metamorphose des Schwärmergehirnes (mit Basil el Jundi). Ein Manuskript hierzu ist in Arbeit.
- Entwicklung eines Stadiumschlüssels zur Altersbestimmung von Tribolium-Puppen (mit Stefan Dippel).
- Auflösung und Neubildung glomerulärer Strukturen im sich entwickelnden Antennallobus des roten Reismehlkäfers (mit Brigitte Götz). Die Ergebnisse werden momentan gemeinsam mit dem vorangehenden Projekt unter dem Titel “The transition from the larval to the adult antennal lobe in the red flour beetle *Tribolium castaneum”* für eine Veröffentlichung zusammengestellt.
- Hirnanatomie und Neuropeptide dreier Collembolenarten (mit Martin Kollmann). Der Inhalt dieser Arbeit soll auf Einladung hin bei “Arthropod Structure and Development” erscheinen.

Die Abfassung der Dissertation in englischer Sprache wurde vom Dekan des Fachbereichs Biologie am 17.07.2008 genehmigt

Zusammenfassung

Während der Ontogenese holometaboler Insekten wie zum Beispiel der Schmetterlinge (Lepidoptera) kommt es zu radikalen Änderungen der Lebensumstände: während das Leben der Larve weitestgehend auf Fressen und Wachsen ausgerichtet ist, verlangt die Möglichkeit des Fluges dem adulten Tier völlig andersgeartete Herausforderungen ab. Auch die Art und Geschwindigkeit der Sinneseindrücke verändert sich rapide. All dies erfordert neben der völligen Neuorganisation des Körpers und der Sinnesorgane auch eine Umorganisation des Gehirnes, das diese um- und neu gebauten Systeme integrieren muß. Seit mehr als drei Dekaden dient der Tabakschwärmer *Manduca sexta* als Modelltier zur Untersuchung dieses Umbaus, welcher unter Laborbedingungen innerhalb von lediglich drei Wochen während der Puppenruhe erfolgt. In dieser Zeit nimmt das Gehirn um etwa das zehnfache an Volumen zu, einige larvenspezifische Zellen sterben, andere adultspezifische Neuroblasten proliferieren und wieder andere Nervenzellen werden umgebaut, um den neuen Anforderungen gewachsen zu sein (Übersichtsartikel: Truman 1996; Weeks 1999).

Viele der hierbei zugrunde liegenden ontogenetischen Prozesse des Auswachsens und der Ausdifferenzierung von Nervenzellen scheinen zwischen Insekten und Vertebraten konserviert zu sein. So finden sich auf molekularer Ebene als auch auf der Ebene der Neuropil-Organisation Parallelen, welche im Insektenmodell meist einfacher und zugänglicher untersucht werden können. Beispiele hierfür wären zum einen die Zielfindung sensorischer Rezeptorneurone, deren Einwachsen in die primären Verarbeitungszentren über gleiche Kontaktrezeptoren gesteuert wird (Luo and Flanagan 2007), und zum anderen die prinzipiell analoge Organisation olfaktorischer Neuropile in duftabhängig aktivierbare Glomeruli (Hildebrand and Shepherd 1997, Eisthen 2002).

Ebenfalls eine stark konservierte Rolle in der Individualentwicklung spielt das gasförmige Signalmolekül Stickstoffmonoxid (NO), dessen Einfluss auf die Neurogenese bereits in mehreren Systemen demonstriert wurde (Übersichtsartikel für Insekten: Bicker 2007, Vertebraten: Cheng et al. 2003, Garthwaite 2008). Auch in *Manduca* wurde eine Einflußnahme auf die Antennallobus-Entwicklung gezeigt (Gibson et al. 2001). Nun sind die Wirkmöglichkeiten von NO mannigfach: es kann sowohl direkt durch ADP-Ribosylierung oder S-Nitrosylierung Proteine beeinflussen, aber auch weitere Signalkaskaden stimulieren. Prominentestes Beispiel hierfür in *Manduca* wäre die transiente cGMP-Synthese durch NO-abhängige lösliche Guanylatzyklasen (Schachtner et al. 1998, 1999). Das gebildete cGMP weist wiederum ein weites Wirkspektrum auf, welches von direkt abhängigen Ionenkanälen (cyclic nucleotide gated channels, CNGs) bis hin zur Aktivierung von Proteinkinasen reicht. Im Rahmen unserer Arbeitshypothese wird durch selektive cGMP-Produktion in einem definierten Zeitfenster der Antennallobus-Entwicklung die Ausschüttung von Neuropeptiden in lokalen Interneuronen bewirkt. Hierdurch bestünde die Möglichkeit, ein weitgehend undifferenziertes Entwicklungssignal zu spezifizieren, um gezielt einzelne synaptische Verbindungen zu stärken.

Sowohl zum NO/cGMP-System als auch zu verschiedenen Neuropeptiden im sich entwickelnden Antennallobus existierten erste Untersuchungen unserer Arbeitsgruppe (Schachtner et al. 1998, 1999, Schachtner et al. 2004, Utz und Schachtner 2005). Die begonnenen Arbeiten zu den Neuropeptiden wurden in Zusammenarbeit mit S. Utz durch anatomische und pharmakologische Arbeiten zu Allatotropin (Kapitel III) sowie der Charakterisierung der lateralen Zellgruppe mittels MALDI-TOF

Massenspektrometrie erweitert (Kapitel IV). Der Schwerpunkt der vorliegenden Arbeit sollte jedoch auf der genaueren Charakterisierung des NO/cGMP-Signalweges im sonst gut etablierten Modellsystem des sich entwickelnden Antennallobus von *Manduca sexta* liegen.

Hierzu wurde zunächst die in Frage kommende Zellgruppe auf deren Fähigkeit zur Verlängerung des NO-Signals untersucht, gefolgt von einem Test auf möglichen Zelltod während der Entwicklung (Kapitel I). Da aufgrund fehlenden Zelltodes von einer stabilen Neuronpopulation in dieser Zellgruppe ausgegangen werden konnte, wurde der Signalweg genauer hinsichtlich seines Zeitfensters, seiner Spezifität sowie der Anzahl beteiligter Neurone untersucht (Kapitel II). Ebenfalls wurde eine Möglichkeit zu seiner Signifikanz für die neuronale Entwicklung aufgezeigt. Hierbei wurden die Arbeiten weiterer Arbeitsgruppenmitglieder integriert. Zudem kam in dieser Arbeit mit der 3D-rekonstruktionsbasierten Volumetrie eine Methode zum Einsatz, die sich im Folgenden auch in anderen Bereichen der Arbeitsgruppe als wichtiges Werkzeug herausstellte. Voraussetzung hierfür war jedoch die Etablierung eines geeigneten Protokolls sowie die Definition leicht identifizierbarer Neuropilbereiche im Antennallobus während der Entwicklung (Kapitel V). Nachdem dieses Protokoll eingeführt war, lag die Ausweitung der Methode auf das gesamte Hirn nahe, was in Zusammenarbeit mit B. el Jundi geschah. Im Anschluss erfolgte die Anwendung des erstellten Volumen-Standardgehirnes in Form einer volumetrischen Erfassung des Geschlechtsdimorphismus (Kapitel VI). Die gewachsene anatomische Expertise wurde im Rahmen einer Kooperation mit K.C. Daly und E.M. Staudacher (West Virginia University, Morgantown, WV, USA) am Antennallobus von *Manduca sexta* angewandt. Hierfür wurden Projektionsneurone intrazellulär abgeleitet und ihre Antwortprofile auf eine Reihe standardisierter Duftreize bestimmt. Nach intrazellulärer Färbung wurden die Glomeruli identifiziert, in denen diese Projektionsneurone dendritische Verzweigungen hatten und in einem 3D-Atlas dargestellt. Eine 4D Darstellung wurde durch Verknüpfen des räumlich-anatomischen 3D-Atlas mit der farbkodierten neuronalen Aktivität der einzelnen Elemente dieses virtuellen Ensembles erreicht (Kapitel VII).

Viele der neu entwickelten Methoden sind parallel im Rahmen von Kooperationen und Laborpraktika, Bachelor- und Diplomarbeiten in *Manduca sexta* vertieft (Staudacher et al. 2007a,b, el Jundi et al. 2007, el Jundi 2008, Rulla 2008, Neupert et al., in prep.) bzw. bei anderen Modellinsekten wie dem rotbraunen Reismehlkäfer *Tribolium castaneum* (Dippel et al. 2006, Dreyer et al. 2006, Schachtner et al. 2006, Dippel et al. 2007, Dreyer et al. 2007, Götz et al. 2007, Schachtner et al. 2007, Götz 2007, Dippel 2008, Dreyer 2008) oder basalen Hexapoden-Vertretern wie Collembolen (Kollmann et al. 2007, Kollmann 2008) durch mich oder unter meiner Anleitung angewendet worden. Hierbei stand die Frage im Vordergrund, inwieweit die in *Manduca* vorgefundenen Mechanismen und deren zu Grunde liegende Neuromediatoren innerhalb der Arthropoden konserviert sind.

Die Arbeit ist in die genannten sieben Kapitel gegliedert, deren Inhalt in den folgenden Absätzen nochmals ausführlicher zusammengefaßt wird.

Kapitel I: Kupfer/Zink Superoxid Dismutase-ähnliche Immunreaktivität im sich entwickelnden Gehirn des Tabakschwärmers *Manduca sexta*

Original-Titel: Copper/Zinc superoxide dismutase-like immunoreactivity in the metamorphosing brain of the sphinx moth *Manduca sexta*

In jedem metabolisch aktiven Gewebe entstehen hochreaktive Moleküle als Nebenprodukte, die die Effizienz der gewünschten Prozesse negativ beeinflussen. Besonders gut charakterisiert sind die reaktiven Sauerstoff-Verbindungen (reactive oxygen species, ROS), welche vor allem in der Atmungskette anfallen und in Zellen zu oxidativem Streß führen. Hierzu gehört auch Superoxid, O_2^-, welches durch rasche Oxidation anderer Proteine deren Funktionalität verändern kann. Die Cu/Zn Superoxid-Dismutase (Cu/Zn-SOD) katalisiert diesen Prozeß und baut vorhandenes Superoxid zusammen mit dem Enzym Katalase zu Sauerstoff und Wasser ab. Auch das Signalmolekül Stickstoffmonoxid (NO) ist in seiner Wirkdauer und –reichweite durch Superoxid als Reaktionspartner stark eingeschränkt, und kann beides in Gegenwart der Cu/Zn-SOD ausweiten.

Mit einem Antikörper gegen Cu/Zn-SOD konnten wir in Western Blots bei etwa 15 KDa das Vorhandensein eines entsprechenden Proteins in Hirngewebe der Insekten *Manduca sexta*, *Drosophila melanogaster*, *Leucophaea maderae*, *Schistocerca gregaria* und *Gryllus bimaculatus* sowie Ratte und Maus nachweisen. Darüberhinaus zeigten wir mit der gleichen Methode die Expression von Cu/Zn-SOD durch die komplette Puppenentwicklung bis in frühe Adultstadien von *Manduca sexta*.

Um eine mögliche protektive Rolle von Cu/Zn-SOD während der Puppenentwicklung genauer zu untersuchen, wurden in diversen Stadien Immunfärbungen an Hirnschnitten vorgenommen. Hierbei zeigte sich eine distinkte Cu/Zn-SOD-Immunreaktivität (SOD-IR) in den Kenyon-Zellen der Pilzkörper, in Zellen der Pars intercerebralis, des lateralen Protocerebrums, des medianen Tritocerebrums, sowie in verschiedenen Zellen der optischen Loben sowie der Antennalloben. Im dorsalen Protocerebrum gab es zudem Hinweise auf SOD-IR in Gliazellen. Während sich die SOD-IR in den meisten protocerebralen Zellen über den kompletten betrachteten Entwicklungszeitraum erstreckte, begann die SOD-IR in Zellen der optischen Loben und Antennalloben erst im Verlauf der Puppenentwicklung bzw. trat lediglich transient auf. So zeigte sich erste SOD-IR in der lateralen Zellgruppe des Antennallobus etwa ab P7/8, parallel zum steigenden 20-Hydroxy-Ecdyson-Titer. In der medianen Zellgruppe des Antennallobus trat nur vereinzelt und unregelmäßig SOD-IR im letzten Drittel der Puppenentwicklung auf. In adulten Tieren ging die SOD-IR innerhalb der ersten vier Tage weitgehend zurück.

Um festzustellen, ob Cu/Zn-SOD tatsächlich in relevanten Zellen eine protektive Rolle übernehmen kann, wurden Doppelfärbungen gegen Cu/Zn-SOD und MsGCα1 (die α1-Untereinheit der löslichen Guanylatzyklase aus *Manduca sexta*) durchgeführt. Die lösliche Guanylatzyklase stellt eines der Hauptziele von NO in Nervengewebe dar und zyklisiert nach Bindung von NO an seine Hämgruppe Guanosintriphosphat zu dem sekundären Botenstoff cGMP. Tatsächlich wiesen sowohl einige Zellen des medianen Tritocerebrums und der lateralen Zellgruppe im Antennallobus Doppelfärbungen auf. Die Befunde für den Antennallobus wurden gestärkt durch Doppelfärbungen gegen Cu/Zn-SOD und cGMP, welches transient ab P7/8 in der lateralen Zellgruppe gebildet wird: faktisch alle Zellen mit

cGMP-Immunreaktivität zeigten ebenso SOD-IR. Desgleichen fanden sich im optischen Lobus Zellen mit sowohl cGMP- als auch Cu/Zn-SOD-Immunreaktivität.
Um die protektive Rolle von Cu/Zn-SOD während der Entwicklung zu untermauern führten wir TUNEL-Färbungen durch, mit deren Hilfe wir sterbende Zellen markierten. Solche Zellen traten vor allem in den optischen Loben und vereinzelt im Protocerebrum auf, jedoch niemals zusammen mit SOD-IR. Dies steht in Übereinstimmung mit einer Schutzfunktion von Cu/Zn-SOD für die Zelle, die in sterbenden Zellen keinen Sinn ergeben würde.
Da wir zu keinem Zeitpunkt der Puppenentwicklung sterbende Zellen im Antennallobus vorfanden, konnten wir in folgenden Untersuchungen immer von einer konstanten Zellpopulation im AL ausgehen.

Kapitel II: Transiente Bildung von Stickstoffmonoxid-abhängigem cGMP im sich entwickelnden Antennallobus des Tabakschwärmers *Manduca sexta*

Original-Titel: Transient, nitric oxide-dependent cyclic GMP formation is involved in metamorphic development of the antennal lobes of *Manduca sexta*

In früheren Arbeiten unserer Arbeitsgruppe wurde bereits ein transienter, induzierbarer Anstieg cGMP-immunreaktiver (cGMP-ir) Zellen in der lateralen Zellgruppe des Antennallobus beschrieben. Hierfür kamen allerdings mehrere Guanylatzyklasen in Frage. Erste Hinweise auf die Abhängigkeit dieses cGMP-Anstieges von Stickstoffmonoxid (NO) bzw. dessen Haupt-Zielprotein, der löslichen Guanylatzyklase (sGC) sollten verdichtet, sowie die Anzahl der beteiligten Zellen und ihr zeitlicher Verlauf mittels pharmakologischer Experimente genauer charakterisiert werden.
Hierzu wurden verschiedene Präparationsprotokolle angewandt, die eine stimulationsabhängige Zuordnung der verschiedenen cGMP-Färbungen ermöglichten. Bei normaler Präparation werden in physiologischer Ringerlösung sämtliche Nerven durchtrennt. In einer früheren Arbeit aus der Arbeitsgruppe konnte gezeigt werden, dass das Durchtrennen der Antennalnerven den gleichen Effekt wie eine elektrische Stimulation bewirkt und in einem definierten Zeitraum der Puppenentwicklung zu cGMP-Immunreaktivität (cGMP-IR) in Neuronen der lateralen Zellgruppe führt.
Diese präparationsbedingte Stimulation in verschiedenen Puppenstadien ergab erste, schwache cGMP-IR in etwa 15 Zellen des Stadiums P5/6, einen sprunghaften Anstieg auf knapp 60 Zellen bei P8/9 gefolgt von einem langsamen Abfallen auf 20 cGMP-ir Zellen bei P12, bis bei P15 keine cGMP-IR mehr durch reine Präparation induziert werden konnte. Im Folgenden sollte die Anzahl derjenigen Zellen bestimmt werden, deren cGMP-Synthese auf sGC-Aktivität zurückzuführen war. Hierfür wurde einmalig systemisch bei P7 der sGC-Inhibitor ODQ in den Thorax der Puppen injiziert, gefolgt von normaler Präparation in den folgenden fünf Tagen. An den ersten zwei Folgetagen nach Injektion ergab sich ein Rückgang um etwa 20 Zellen in den ODQ-behandelten Tieren verglichen zu Puffer-injizierten Tieren, ab dem dritten Tag konnte kein signifikanter Unterschied mehr zwischen den beiden Gruppen festgestellt werden.
Um die Ursache der verbliebenen cGMP-ir Zellen nach ODQ-Injektion zu klären, wurde das Injektionsprotokoll beibehalten, jedoch bei der Präparation an den zwei Folgetagen erst die rechte

Antenne in ihrer Antennentasche durchtrennt, um eine gezielte Stimulation des Antennalnervs herbeizuführen. Nach 10 Minuten wurde das Tier *in situ* fixiert, um andersgeartete präparationsbedingte Stimulation zu unterbinden. Die ODQ-behandelten Tiere wiesen an den Folgetagen keine cGMP-ir Zellen mehr auf, was den Schluß einer exklusiven cGMP-IR über sGC nach Antennalnerv-Stimulation im Antennallobus zuläßt. Dieses Experiment wurde mit gleichem Ergebnis mit Injektionen bei P9 wiederholt, wiederum fanden sich keine cGMP-ir Zellen bei ODQ-Gabe. Somit lassen sich die Ergebnisse der vorangegangenen Experimente durch eine ODQ-Wirkdauer im Gewebe von etwa zwei Tagen erklären.

Da wir trotz unilateraler Deantennierung immer in gleichem Maße cGMP-ir Zellen in beiden Antennalloben fanden, wiederholten wir das ODQ-Experiment in Tieren, die bei P0 einseitig deantenniert wurden. Durch die fehlende sensorische Innervierung während der Antennallobus-Entwicklung entstand nur ein aglomeruläres, verkleinertes Neuropil auf dieser Seite, was die Vollständigkeit der Deantennierung bestätigte. Die großteils über den Antennalnerv kommenden sensorischen Rezeptorneurone des Antennallobus beherbergen die NO-Synthase, deren stimulationsabhängige Aktivierung erst zu NO-Produktion, und im Folgenden zu sGC-Aktivierung in den lokalen Interneuronen des Antennallobus führt.

Nichtsdestotrotz trat auch in diesem Falle bei kontralateraler Antennalnerv-Durchtrennung vor der Präparation komplett ODQ-blockierbare cGMP-IR auf, das heißt auf indirektem Weg wird die kontralaterale Stimulation der sGC erreicht. Einzige verbleibende NO-Quelle auf dieser Seite ist die sensorische Innervierung des ansonsten deafferentierten Antennallobus aus dem Labialpalpus. Dass diese sensorische Innervierung tatsächlich unbelangt blieb, wurde durch Immunfärbung gegen Fasciclin II nachgewiesen. Die in diesen Zellen vorhandene NO-Synthase scheint ausreichend, um cGMP im kompletten Set von Zellen hochzuregulieren

Das Vorhandensein der NO-sensitiven löslichen Guanylatzyklase während der Puppenentwicklung wurde mittels eines Antikörpers gegen die α-Untereinheit des Heterodimers (MsGCα1) gezeigt. Das Auswerten der MsGCα1-immunreaktiven (MsGCα1-ir) Zellen der lateralen Zellgruppe im Antennallobus während der Entwicklung ergab keine MsGCα1-ir Zellen bis etwa P5, gefolgt von einem Anstieg auf knapp 30 Zellen bei P8. Ein weiterer Anstieg an MsGCα1-ir Zellen auf etwa 60 Zellen erfolgte zum Adultschlupf. Die Zahlen und das zeitliche Erscheinen der gefundenen Zellen fügen sich gut ein in das Bild der gefundenen cGMP-ir Zellen der vorangegangenen pharmakologischen Experimente mit ODQ.

Einen Hinweis auf eine mögliche Quelle für die verbleibenden, nicht Antennalnerv-stimulierten NO-abhängigen cGMP-ir Zellen wird mit dem immunzytochemischen Nachweis der membranständigen Guanylatzyklase MsGC-I geboten. Bereits vor den ersten MsGCα1-ir Zellen zeigt sich MsGC-I-Immunreaktivität im zentralen unstrukturierten Neuropil des Antennallobus, später weisen mehrere Zellen der lateralen Zellgruppe bis in das adulte Stadium hinein MsGC-I-Immunreaktivität auf.

Nachdem der zeitliche Verlauf des Antennalnerv-stimulierten NO/sGC/cGMP-Signalwegs weitgehend geklärt war, wurde mit Antikörpern gegen Synaptotagmin und Synapsin - beides Proteine beteiligt bei der synaptischen Vesikelausschüttung - eine mögliche Rolle dieses Signalweges auf die Neuropilbildung im Antennallobus untersucht. Vergleichende Messungen der optischen Dichte von Synaptotagmin-Immunfärbungen in Antennalloben pharmakologisch behandelter Tiere ergaben einen

deutlichen Rückgang an Synaptotagmin-Immunreaktivität (Syt-IR) in den Glomeruli von ODQ-injizierten Tieren.
Ähnliche Ergebnisse ergaben sich mittels eines Enzyme-linked immunosorbent assay (ELISA), wobei das Hirngewebe aufgeteilt wurde in Antennalloben, optische Loben und restliches Gehirn. Während die Antennalloben nach ODQ-Injektion einen Rückgang der Immunantwort auf etwa 70% aufwiesen, war die Immunantwort in den anderen beiden Geweben um nur etwa 10% reduziert. Diese Ergebnisse sprechen für einen Einfluß des transienten, NO-abhängigen cGMP-Signals auf die Ausbildung aktiver Synapsen während der Entwicklung des Antennallobus.
Um festzustellen, inwieweit dieser Effekt das Volumen identifizierbarer Neuropile beeinflußt, wurden bei P12 die Volumen von zehn zuvor definierten Glomeruli nach ODQ-Injektion bei P7 mit den Glomerulus-Volumen kontroll-injizierter Tiere verglichen. Offensichtlich ist die Wirkung des NO-abhängigen cGMP auf die Ausbildung aktiver Synapsen beschränkt, zumindest konnte ein Effekt auf das Volumen weitgehend ausgeschlossen werden.

Kapitel III: Mas-Allatotropin im sich entwickelnden Antennallobus des Tabakschwärmers *Manduca sexta*: Verteilung, zeitlicher Verlauf, entwicklungsabhängige Regulierung und Kolokalisation mit anderen Neuropeptiden

Original-Titel: Mas-allatotropin in the developing antennal lobe of the sphinx moth *Manduca sexta*: Distribution, time course, developmental regulation and colocalization with other neuropeptides

Ursprünglich beschrieben wurde das Neuropeptid Allatotropin (AT) als Neurohormon, welches an den corpora allata die Juvenilhormon-Synthese und -Sekretion stimuliert. Darüberhinaus finden sich jedoch eine Vielzahl an Mas-AT-immunreaktiven (AT-ir) Interneuronen im Gehirn des Tabakschwärmers, unter anderem im sich bildenden Antennallobus. Basierend auf unserem Vorwissen zu anderen Neuropeptiden wurden AT-ir Zellen hinsichtlich ihres Typs, ihres zeitlichen Auftretens sowie ihrer 20-Hydroxyecdyson (20E)-abhängigen Regulation hin im sich entwickelnden Antennallobus untersucht. Darüberhinaus wurden Kolokalisationen mit GABA, Allatostatin-A (AST-A) und RFamid durchgeführt und quantitativ ausgewertet.
Im Rahmen der Spezifitätstests der verwendeten Antikörper wurden Western Blots mit allen drei verwendeten Neuropeptid-Antikörpern an verschiedenen Puppenstadien von *Manduca sexta* durchgeführt, im Falle des Antiserums gegen RFamid sogar vergleichend an adulten *Schistocerca gregaria* und *Leucophaea maderae*. Zusätzlich wurde erstmals ein vergleichender Western Blot mit dem Antikörper gegen das synaptische Vesikelprotein Synapsin an *Manduca sexta*, *Tribolium castaneum* und als Referenz *Drosophila melanogaster* durchgeführt, was in allen drei Spezies zu der für *Drosophila* beschriebenen typischen Doppelbande bei etwa 63 KDa führte.
Die im Antennallobus von *Manduca sexta* auftretenden AT-ir Zellen wurden im Rahmen der Arbeit sieben verschiedenen Zelltypen zugeordnet, wobei lokale Interneurone der lateralen Zellgruppe den größten Anteil einnehmen. Es konnten aber auch AT-ir Projektions- und Zentrifugalneurone nachgewiesen werden. Bereits in der lateralen Zellgruppe des larvalen antennalen Zentrums finden sich etwa 10 AT-ir Zellen, so genannte larvale lokale AT-ir Neurone (lLATn), die jedoch ihre

Immunreaktivität mit Beginn der Verpuppung wieder verlieren. Erst gegen P6/7, ausgelöst durch den steigenden 20E-Titer, treten erneut AT-ir lokale Interneurone in der lateralen Zellgruppe auf. Inwieweit dies wieder die alten larvalen AT-ir Zellen bzw. neu geborene lokale Interneurone (LATn) sind, konnte nicht unterschieden werden. Bis etwa P13 werden so in einem einzigen Anstieg circa 100 Zellen der lateralen Zellgruppe AT-ir, die bis in die adulten Stadien bestehen bleiben. Die Abhängigkeit dieses Anstieges von 20E wurde durch Hormoninjektion demonstriert; durch 20E-Injektionen bei P1 konnte der Anstieg der AT-ir Zellen in der lateralen Zellgruppe signifikant vorverlegt werden.

Eine mögliche Rolle von AT bei der Glomerulusbildung wird basierend auf Dreifachfärbungen gegen das Zelladhäsionsmolekül Fasciclin II als Marker der einwachsenden olfaktorischen Rezeptorneurone und dem synaptischen Vesikelprotein Synapsin diskutiert; hierbei zeigt sich bereits früh ein Einwachsen der lokalen AT-ir Neurite in die sich bildenden Glomeruli.

Ein median gelegenes, sehr großes Projektionsneuron, das sogenannte „large median AT-ir neuron“ (lmATn), weist ebenfalls ab P7/8 AT-Immunreaktivität auf. Der Primärneurit dieser Zelle zieht entlang des antenno-subösophageal-Traktes in Richtung Unterschlundganglion, konnte aber aufgrund schwächer werdender Färbung nicht weiter verfolgt werden. Hier verliert sich auch der Neurit des einzeln auftretenden zentrifugalen AT-ir Neurons – ab etwa P7/8 verläuft so ein AT-ir Neurit in einem charakteristischen Bogen durch den Antennallobus, das andere Ende verliert sich im Verlauf des inneren antennocerebralen Traktes. Auch die sehr unregelmäßig auftretenden ein bis drei bzw. ein bis zwei AT-ir Zellen der anterioren (aATn) und dorsolateralen Zellgruppe (dlATn) lassen sich frühestens ab P7/8 nachweisen.

Die einzigen AT-ir Zellen des Antennallobus, die ihre AT-Peptididentität durch die gesamte Entwicklung beibehalten sind die beiden „early AT-ir neurons“ (eATn), die ebenfalls wie die lmATn als Projektionsneurone in Richtung Unterschlundganglion oder Tritocerebrum ziehen.

Die LATn weisen auch Immunreaktivität gegen den inhibitorischen Transmitter GABA auf, was deren Identität als lokale Interneurone untermauert. Hinsichtlich der Neuropeptid-Doppelfärbungen wurden unter den LATn sowohl AT/AST-A-ir Zellen als auch AT/RFamid-ir Zellen gefunden. Auch die drei Projektionsneurone (2 eATn und 1 lmATn) lassen sich mit dem Antiserum gegen RFamid markieren. Aufgrund der vorgefundenen Doppelfärbungsmuster lassen sich erstmalig mindestend drei biochemisch unterschiedliche Populationen innerhalb der morphologisch recht homogenen Gruppe der lokalen Interneurone im Antennallobus unterscheiden.

Zur besseren Visualisierung der Somalage bzw. der AT-ir Traktverläufe wurden dreidimensionale Modelle der AT-ir Zellen für drei repräsentativen Stadien (P3, P7 und adult) erstellt und im Falle des adulten Antennallobus als animierte Version als „Supplement“ beigefügt.

Kapitel IV: Direktes „Peptid-Profiling“ lateraler Zellgruppen des Antennallobus von *Manduca sexta* zur Ermittlung spezifischer Zusammensetzung und Veränderungen der Neuropeptid-Expression während der Entwicklung

Original-Titel: Direct peptide profiling of lateral cell groups of the antennal lobes of *Manduca sexta* reveals specific composition and changes in neuropeptide expression during development

Nachdem mit Hilfe immunzytochemischer Techniken das zelluläre und zeitliche Auftreten verschiedener Neuropeptidfamilien während der AL-Metamorphose gezeigt wurde (siehe vorangehendes Kapitel), sollten in dieser Arbeit die Neuropeptid-Isoformen innerhalb der Peptidfamilien aufgelöst werden. Hierzu wurde mittels massenspektrometrischer Analyse der Antennallobus-Zellgruppen erstmals das komplette Peptidom eines definierten Neuropils bzw. seiner Zellgruppen durch die Puppenentwicklung analysiert.

Zwölf Peptidmassen konnten vier Peptidfamilien zugewiesen werden: der AST-A-Familie (Helicostatin 1, Cydiastatin 2, 3 und 4), der Mas-FLRFamid-Familie (Mas-FLRFamid I-III, Mas-QFLRFamid I), der Mas-Myoinhibitory Peptide-Familie (Mas-MIP III, V, und VI) sowie Mas-Allatotropin aus der Allatotropin-Familie. Durch Peptidfragmentierung mittels MALDI-TOF/TOF konnte die Identität von Mas-AT, Cydiastatin 3 und 4 eindeutig bestätigt werden. Zu den Allatostatinen und RFamiden wurden durch unsere Arbeitsgruppe bereits immunzytochemische Arbeiten vorgelegt, ebenso zu Allatotropin (siehe vorangegangenes Kapitel). In dieser Arbeit wurde mit einem Antiserum gegen Myoinhibitory Peptide immunzytochemisch das Vorhandensein dieser Peptidfamilie in einem Teil der lateralen Zellgruppe bestätigt.

Die Analyse der relativen Häufigkeit der verschiedenen Massenpeaks zu den unterschiedlichen Entwicklungszeiten bestätigte weitgehend die immunzytochemischen Arbeiten; so zeigte sich eine generelle Zunahme an Massenpeaks im Verlauf der Puppenentwicklung. Insbesondere gegen P7/8 konnte eine starke Zunahme verzeichnet werden, was nicht nur mit dem steigenden 20E-Titer korreliert, sondern auch mit dem Beginn der Glomerulibildung im Antennallobus. Einige Massepeaks traten lediglich in adulten Tieren auf, so z.B. Mas-MIP V. Durch das Auflösen der einzelnen Isoformen der Peptidfamilien konnte mit dieser Arbeit unter anderem gezeigt werden, dass sich im Antennallobus lediglich Mas-AT und nicht zusätzlich „Mas-AT like peptides“ befinden. Zudem läßt das heterogene Auftreten der verschiedenen Allatostatin-A-Isoformen während der Entwicklung eine zeitlich differentielle Expression z.B. des Allatostatin-A-Precursors vermuten. Ebenso denkbar wäre eine posttranslationelle Regulierung der verschiedenen Isoformen; in beiden Fällen jedoch spricht dies für eine aktive, differenzierte Rolle der beteiligten Neuropeptide in der Antennallobus-Entwicklung.

Kapitel V: Standardisierte dreidimensionale Glomeruli im Antennallobus von *Manduca sexta*: ein Werkzeug zur Untersuchung von Plastizität während der Puppen- und Adult-Entwicklung.
Original-Titel: Standard three-dimensional glomeruli of the *Manduca sexta* antennal lobe: a tool to study both developmental and adult plasticity

Trotz mehreren morphologischen Untersuchungen am Antennallobus des Tabakschwärmers *Manduca sexta* und einer Festlegung der Glomeruluszahl auf 63 ±1 durch Rospars und Hildebrand (1992, 2000) waren die bestehenden Arbeiten nicht auf wiederholte Identifizierung normaler Glomeruli ausgelegt und zudem auf adulte Tiere beschränkt. Klar identifizierbare Glomeruli blieben bis dato die drei geschlechtspezifischen Glomeruli unmittelbar am Übergang des Antennalnerv in den Antennallobus - der distale „Cumulus“, der ringförmige „Toroid“ und der hufeisenförmige „Toroid 2“ oder auch „Horseshoe“.
Zusammenhängende Bildstapel dank konfokaler Laserscan-Mikroskopie in Kombination mit leistungsfähiger 3D-Rekonstruktions-Software boten erstmals die Möglichkeit, mit überschaubarem Aufwand eine wirklichkeitsgetreue Darstellung des räumlichen Aufbaus der Antennalloben zu generieren, die zudem eine quantitative Auswertung der markierten Strukturen gestattet. Um eine anatomische Vergleichsbasis für pharmakologische Experimente zu schaffen, wurden aus drei verschiedenen Entwicklungsstadien zehn leicht zu identifizierende Glomeruli von insgesamt 30 männlichen Antennalloben rekonstruiert. Diese Rekonstruktionen basieren auf Immunfärbungen mit einem Antikörper gegen das ubiquitär vorhandene präsynaptische Vesikelprotein Synaptotagmin, dessen generelle Verwendbarkeit in *Manduca sexta* bereits zuvor an Schnittpräparaten gezeigt wurde (Dubuque et al. 2001). Für die Arbeit dieses Kapitels wurde das Färbeprotokoll für ganze Gehirne von *Manduca sexta* optimiert.
Neben den bereits erwähnten geschlechtsspezifischen Glomeruli „Cumulus“, „Toroid“ und „Horseshoe“ sind die gewählten Glomeruli der basal sitzende „labial pit organ glomerulus“ („LPOG“), der seinen sensorischen Eingang aus Sensillen der Labialpalpen bezieht, „G20“, der größte normale Glomerulus posterior im Antennallobus, die anterior lokalisierten benachbarten Glomeruli „Disc“ und „Discbase“, der ventromedian liegende kleine Glomerulus „Cap“ und der darunter liegende Glomerulus „Base“, sowie der ebenso ventral positionierte elongierte Glomerulus „Club“.
Als erstes Stadium wurde P13 gewählt; zu diesem Zeitpunkt ist die Haupt-Synaptogenesewelle im Antennallobus abgeschlossen, alle Glomeruli sind ausgebildet und die zehn ausgewählten Glomeruli eindeutig identifizierbar. Deweiteren wurden diese zehn Glomeruli in frisch geschlüpften Adulttieren (A0) sowie vier Tage alten Adulttieren (A4) untersucht. Frisch geschlüpfte Adulttiere stehen für naive Tiere, die erstmals mit ihrer olfaktorischen Umwelt in Kontakt treten, vier Tage alte Tiere repräsentieren adulte Falter mit erster Dufterfahrung. Der Vergleich der glomerulären Volumina ergab massives Größenwachstum zwischen P13 und A0 um 40-130%, sowie - nach Normalisierung der Werte auf das Antennallobus-Volumen - signifikantes Größenwachstum in den geschlechtsspezifischen Glomeruli „Cumulus“ und „Toroid“ innerhalb der ersten vier Tage der Adulttiere.
Trotz genereller Form- und Lagekonstanz wiesen die zehn untersuchten Glomeruli auch diesbezüglich eine gewisse Plastizität auf – die namengebende Ringform des „Toroid“ beispielsweise konnte nur in

etwa der Hälfte der untersuchten Tiere vorgefunden werden, die restlichen Tiere besaßen einen anteroventral geöffneten „Toroid“. Der „Horsehoe“ hingegen schien in mehreren Antennalloben in zwei oder mehr separierte Teile zerfallen zu sein.
Repräsentative Antennalloben der drei Stadien wurden in ein internetfähiges, interaktives Protokoll exportiert (virtual reality modeling language, vrml) und gemeinsam mit Filmen von sich drehenden 3D-rekonstruierten Antennalloben auf einer Homepage zugänglich gemacht (www.3D-insectbrain.de).

Kapitel VI: Ein Standardgehirn des Tabakschwärmers *Manduca sexta* und seine funktionelle Anwendung

Original-Titel: Anisometric brain dimorphism revisited: implementation of a volumetric 3D standard brain in *Manduca sexta*

Da in den letzten Jahren zu anderen Insektengehirnen 3D-Standards entstanden sind, lag es nahe, die zuvor etablierten Methoden der 3D-Rekonstruktion in *Manduca sexta* auch erstmals auf ein komplettes Lepidopteren-Gehirn anzuwenden. Hierdurch ergab sich die Möglichkeit, die für den Antennallobus angewandte Volumen-Standardisierung auch auf andere Neuropile auszuweiten.
Basierend auf zwölf frisch geschlüpften weiblichen Individuen (A0) wurde aus 30 klar abgrenzbaren Neuropilen ein Standardgehirn als volumetrische und anatomische Referenz zukünftiger pharmakologischer und ethologischer Studien erstellt. Hierbei konnte erstmals bei einem Insekten-Standardgehirn die Lamina als das äußerste Neuropil des optischen Lobus mit einbezogen werden. Da die ausgewählten zwölf Tiere die bei *Manduca sexta* vorkommenden Gewichtsvarianzen recht gut repräsentierten, konnte zudem gezeigt werden dass bei den untersuchten Neuropil-Volumina kein allometrisches Verhalten auftritt.
Der Tabakschwärmer ist bekannt für seinen ausgeprägten Geschlechtsdimorphismus im Antennallobus. Ein Haupt-Augenmerk dieser Arbeit lag auf der Untersuchung weiterer möglicher volumetrischer Repräsentationen des Geschlechtsdimorphismus in höheren Hirnzentren wie zum Beispiel den Calyces, die die nächste Station zur Verarbeitung olfaktorischer Information bilden. Hierzu wurden vergleichend sechs männliche Gehirne (A0) rekonstruiert und hinsichtlich des Großteils der 30 Neuropile mit dem weiblichen Standardgehirn verglichen. In nahezu allen Neuropilen wies das weibliche Gehirn signifikant größere Volumina als in den Männchen auf. Dieser isometrische Dimorphismus war in Übereinstimmung mit den signifikant höheren Gewichten der Weibchen, auch wenn zuvor keine intrasexuelle Allometrie gezeigt werden konnte. Prominente Ausnahme blieb der Antennallobus, in dem die zuvor etablierten zehn Glomeruli vergleichend zwischen den Geschlechtern betrachtet wurden. Somit konnte erstmals der bekannte Dimorphismus im Neuropil des Antennallobus zwischen den Geschlechtern quantifiziert und - nach Abzug des isometrischen Dimorphismus - auf die geschlechtsspezifischen Glomeruli reduziert werden.
Das Vorhandensein ähnlich erstellter volumetrischer Daten aus Gehirnen der Hymenopteren (Biene) und Orthopteren (Heuschrecke) ermöglichte einen Vergleich der Neuropil-Volumenverhältnisse zwischen verschiedenen Insektenordnungen. Hierdurch ergaben sich erste Rückschlüsse auf evolutive, soziale oder Lebensraum-angepasste Adaptationen der Hirnneuropile dieser Tierklasse.

Insbesondere die unterschiedliche Repräsentation der primären sensorischen Neuropile sowie die ausgeprägteren Pilzkörper des sozialen Insekts Biene konnten hierbei volumetrisch eindruckvoll herausgearbeitet werden. Die dreidimensionalen Ergebnisse wurden wiederum auf der entsprechend erweiterten Internetseite verfügbar gemacht (www.3D-insectbrain.de).

Kapitel VII: Eine 4D-Repräsentation von Antennallobus-Aktivität basierend auf einem Ensemble identifizierter Projektionsneurone

Original-Titel: A 4D representation of antennal lobe output based on an ensemble of identified projection neurons

Wie bereits erwähnt, stellt der Antennallobus von *Manduca sexta* seit Dekaden ein etabliertes Modellsystem der olfaktorischen Forschung dar. Die gängigen Methoden zur Untersuchung der Duftcodierung im kompletten System des Antennallobus haben zwei sich gegenseitig ausschliessende Eigenschaften. Während die intrazelluläre Ableitung aus Einzelzellen hohe zeitliche Auflösung einer Duftantwort liefert, bleibt doch die systemische Antwort des kompletten Systems der interagierenden Glomeruli verborgen. Diese Information wiederum wird in Ca^{2+}-Imaging-Studien aufgedeckt, auf Kosten der zeitlichen Auflösung, sowie beschränkt auf den sichtbaren Teil des Antennallobus.
In dieser Arbeit wird das Dilemma umgangen durch Intrazellulär-Ableitungen an Projektionsneuronen mit einem standardisierten Stimulierungsprotokoll, der nachträglichen Identifizierung der innervierten Glomeruli und der gemeinsamen 3D-Visualisierung der Duftantworten aus dem stetig wachsenden Ensemble aus einzeln abgeleiteten Zellen in einem Referenz-Antennallobus. Hierbei wird die bereits mehrfach erwähnte hohe Invarianz und übersichtliche Struktur des Insekten-Antennallobus ausgenutzt. Die Methode ist zudem erweiterbar auf andere Zelltypen und bietet die Möglichkeit anderweitig erhobene Daten aus Imaging-Studien oder Tetrodenableitungen zu integrieren. Angestrebt ist die Repräsentation eines jeden Glomerulus durch mindestens ein abgeleitetes Projektionsneuron kurz vor, während und kurz nach der standardisierten Duftstimulierung, um ein Gesamtbild der Duftantwort auf Einzelzell-Ebene mit hoher zeitlicher Auflösung zu erhalten.
Um die Machbarkeit zu demonstrieren, wurden aus Einzelzellableitungen an 25 Projektionsneuronen die Zellgruppe der Somata, die antennocerebralen Trakte sowie die innervierten Glomeruli identifiziert. In sechs Fällen wurden zwei Projektionsneurone dem gleichen Glomerulus zugeordnet. Das Stimulationsregime bestand aus fünf Duftpulsen á 100 ms pro Duft und Konzentration, unterbrochen durch 10 s reine Luftgabe. Die verwendeten Düfte beinhalteten unverdünntes 2-Hexanon, 1-Hexanol, 2-Octanon, 1-Octanol, 2-Decanon sowie 1-Decanol; alles Düfte, für die bereits gezeigt wurde dass *Manduca sexta* sie unterscheiden kann.
Etwa 50% der 25 Zellen reagierten exzitatorisch, 25% inhibitorisch und 25% zeigten keine Reaktion auf die präsentierten Duftstimuli. Nach Alignierung der Datenspuren auf den Stimulusbeginn wurden die Aktionspotentiale aller Zellen durch entsprechende Schwellenlegung in 500 zeitlichen Bins von je 20 ms ausgezählt. Diese Daten wurden für jeden Duft als Peri-Stimulus-Zeithistogramm dargestellt sowie zur Anpassung individueller Unterschiede der Ableitungen in Z-Wert basierte Daten transformiert. Der Z-Wert liefert ein Maß dafür, um wie viele Standardabweichungen ein Wert von

einem auf Null gesetzten Mittelwert abweicht. Die Z-Werte jeder Zelle wurden in Falschfarben umcodiert und auf die rekonstruierten Oberflächen der zugehörigen identifizierten Glomeruli eines Referenz-Antennallobus projiziert, um eine 4D-Repräsentation der Duftantwort des Zell-Ensembles zu erhalten.

Referenzen

Bicker G. 2007. Pharmacological approaches to nitric oxide signalling during neural development of locusts and other model insects. Arch Insect Biochem Physiol 64:43-58.

Cheng A, Wang S, Cai J, Rao MS, and Mattson MP. 2003. Nitric oxide acts in a positive feedback loop with BDNF to regulate neural progenitor cell proliferation and differentiation in the mammalian brain. Dev Biol 258:319-333.

Dippel S, Dreyer D, Huetteroth W, and Schachtner J. 2006. Staging of pupal development and brain metamorphosis of the red flour beetle *Tribolium castaneum*. 99th DZG meeting Münster PM_NB_1.20, p44.

Dippel S, Goetz B, Dreyer D, Huetteroth W, and Schachtner J. 2007. Pupal staging and metamorphic development of the antennal lobes of the red flour beetle *Tribolium castaneum*. 7th NWG meeting, Göttingen TS8-5B.

Dippel S. 2008. Der Einfluss von Tachykinin-verwandten Peptiden auf die Gehirnentwicklung von *Tribolium castaneum* während der Metamorphose. Diplomarbeit Philipps-Universität Marburg.

Dreyer D, Dippel S, el Jundi B, Huetteroth W, and Schachtner J. 2006. 3D reconstruction of the *Tribolium* brain: a tool to study developmental and adult plasticity. 99th DZG meeting Münster PM_NB_1.19, p44.

Dreyer D, Dippel S, Huetteroth W, and Schachtner J. 2007. The *Tribolium* brain: 3D reconstruction and immunocytochemical mapping during metamorphosis and in the adult. 7th NWG meeting, Göttingen TS8-6B.

Dreyer D. 2008. Erstellung eines standardisierten 3D Neuropilatlas und die Plastizität des Gehirns von Tribolium castaneum. Diplomarbeit Philipps-Universität Marburg.

Eisthen HL. 2002. Why are olfactory systems of different animals so similar? Brain Behav Evol 59:273-293.

el Jundi B, Huetteroth W, and Schachtner J. 2007. 3D reconstruction of *Manduca sexta* adult brain and of brains during metamorphic development. 7th NWG meeting, Göttingen TS8-7B.

el Jundi B. 2008. Erstellung eines 3D Standardgehirnes des Tabakschwärmers *Manduca sexta:* Ontogenie und Geschlechtsdimorphismus. Diplomarbeit Philipps-Universität Marburg.

Garthwaite J. 2008. Concepts of neural nitric oxide-mediated transmission. European Journal of Neuroscience 27:2783-2802.

Gibson NJ, Rössler W, Nighorn AJ, Oland LA, Hildebrand JG, and Tolbert LP. 2001. Neuron-glia communication via nitric oxide is essential in establishing antennal-lobe structure in *Manduca sexta*. Dev Biol 240:326-339.

Götz B. 2007. Entwicklung der Antennalloben während der Metamorphose des roten Reismehlkäfers *Tribolium castaneum*. Bachelorarbeit Philipps-Universität Marburg.

Götz B, Dippel S, Dreyer D, Huetteroth W, and Schachtner J. 2007. Ontogeny of the antennal lobes of the red flour beetle *Tribolium castaneum.* 100. DZG meeting Köln N14, p107.

Hildebrand JG and Shepherd GM. 1997. Mechanisms of olfactory discrimination: converging evidence for common principles across phyla. Annu Rev Neurosci 20:595-631.

Kollmann M, Huetteroth W, and Schachtner J. 2007. Studies on a collembolan brain: 3D reconstruction and neurochemistry. 100th DZG meeting Köln N47, p124.

Kollmann M. 2008. Anatomische und immunzytochemische Untersuchungen am Gehirn der Collembolen. Diplomarbeit Philipps-Universität Marburg.

Luo L and Flanagan JG. 2007. Development of continuous and discrete neural maps. Neuron 56:284-300.

Neupert S, Huetteroth W, Schachtner J, and Predel R. 2008. Peptidomics of pheromone biosynthesis activating neuropeptide (PBAN)-expressing neurons of an insect. in preparation.

Rulla S. 2008. Immunhistochemisch-anatomische Analyse des Antennallobus von *Manduca sexta* nach Injektion von Na^{+}- und Ca^{2+}-Kanalblockern. Bachelorarbeit Philipps-Universität Marburg.

Schachtner J, Klaassen L, and Truman JW. 1998. Metamorphic control of cyclic guanosine monophosphate expression in the nervous system of the tobacco hornworm, *Manduca sexta*. J Comp Neurol 396:238-252.

Schachtner J, Homberg U, and Truman JW. 1999. Regulation of cyclic GMP elevation in the developing antennal lobe of the Sphinx moth, *Manduca sexta*. J Neurobiol 41:359-375.

Schachtner J, Trosowski B, D'Hanis W, Stubner S, and Homberg U. 2004. Development and steroid regulation of RFamide immunoreactivity in antennal-lobe neurons of the sphinx moth *Manduca sexta*. J Exp Biol 207:2389-2400.

Schachtner J, Huetteroth W, Dreyer D, Dippel S, and el Jundi B. 2006. 3D-reconstructions of the *Tribolium* brain: a tool to study developmental and adult plasticity. 36th meeting of the Society for Neuroscience, Atlanta.

Schachtner J, Goetz B, Dippel S, Dreyer D, and Huetteroth W. 2007. Metamorphic development of the antennal lobes of the red flour beetle *Tribolium castaneum*: 3D-reconstruction and neurochemistry. 37th SfN meeting, San Diego, California, USA, 135.2/F14.

Staudacher EM, Huetteroth W, Schachtner J, and Daly KC. 2007a. Ensemble analysis of projection neurons from identified glomeruli in the moth *Manduca sexta*: Towards a 4D representation of odor processing in a virtual antennal lobe. 37th SfN meeting, San Diego, California, USA 612.15(LL16).

Staudacher EM, Huetteroth W, Schachtner J, and Daly KC. 2007b. Glomerular response mapping using virtual projection neuron populations: A step towards representing whole antennal lobe activity in realtime. 29th AChemS meeting, Sarasota, Florida, USA.

Truman JW. 1996. Steroid receptors and nervous system metamorphosis in insects. Dev Neurosci 18:87-101.

Utz S and Schachtner J. 2005. Development of A-type allatostatin immunoreactivity in antennal lobe neurons of the sphinx moth *Manduca sexta*. Cell Tissue Res 320:149-162.

Weeks JC. 1999. Steroid hormones, dendritic remodeling and neuronal death: insights from insect metamorphosis. Brain Behav Evol 54:51-60.

INTRODUCTION

With approximately 1 million known species (estimations go as far as 20-30 millions), insects provide the most successful animal group on earth (Fig. 1). Being pollinators like honeybees or just diet for other animals, most ecosystems rely on the involvement of insects. On the other hand, insects also pose a major challenge to humans, either as pests on major crops or as vectors of diseases like malaria, chagas' disease, yellow fever or sleeping sickness.

Fig. 1 By far the most species in all metazoan groups are found in insects (Grimaldi and Engel 2005).

Those economic and medicinal challenges call for applied research as well as basic research on this extraordinary animal group, along with another good reason: especially in neurosciences the relative simple neural systems of insects are regarded as important models to better understand basic questions with respect to brain functions (e.g. learning, orientation, olfaction, motoric control) or the ontogenic development of the nervous system.

Olfaction plays a major role in the whole animal kingdom regarding orientation and communication (e.g. finding food or mating partners, intraspecies communication). The primary olfactory center of insects, the antennal lobes, share a common layout with those of most animals with a sense of smell, e.g. the olfactory lobe in crustaceans or the olfactory bulb in vertebrates (Schachtner et al. 2005). The universal feature in these cases is provided by so-called olfactory glomeruli, sphere-like neuropilar substructures, in which olfactory sensory neurons interlink with second-order olfactory neurons (Hildebrand and Shepherd 1997, Eisthen 2002). Regarding development, the underlying principles in nervous systems are also astoundingly conserved in nature. Solutions to recurring problems in neural development like aquisition of neural cell identity, pathfinding, or connecting to proper target cells were shown to be regulated by same or similar mechanisms across animal groups (Luo and Flanagan 2007).

Already several decades ago the antennal lobe of the sphinx moth *Manduca sexta* emerged as one of those model systems covering both olfactory system development and olfaction research; easy rearing, staging, and its large accessible antennal lobes with few individually attributable glomeruli are still advantageous features today.

The main aim of this study was to use *Manduca sexta* to clarify if certain neuromodulators might be involved in developmental decisions for building a proper olfactory neural network. Therefore the quality, the quantity, the timing and the regulation of certain neuromodulators in the antennal lobe was examined, focussing on neuropeptides and the gaseous signal molecule nitric oxide (NO). Within the framework of this question, brain 3D reconstruction techniques were employed and refined, and became an essential part in the second half of this thesis.

For a better understanding of the subsequent chapters the model system, its development and neuromodulators as well as the used techniques are shortly introduced.

The moth brain

Like in most insects, the brain of *Manduca sexta* consists of three condensed neuromeres, the proto-, deuto-, and tritocerebrum. Additionally, the subesophageal ganglion fuses with those supraesophageal neuromeres during pupal metamorphosis, leading to its characteristic shape with esophageal foramen in the adult (Fig. 2, chapter II, VI). The large lateral optic lobes of the brain build up the most prominent part of the protocerebrum, whereas the deutocerebrum forms its most conspicuous brain part on the anterior side - the antennal lobes. They obtain their main sensory input via the antennal nerve from the antennae, where olfactory information is perceived. The remains of the small tritocerebrum lie on the inner side of the esophageal foramen and exhibit no clearly separated structures.

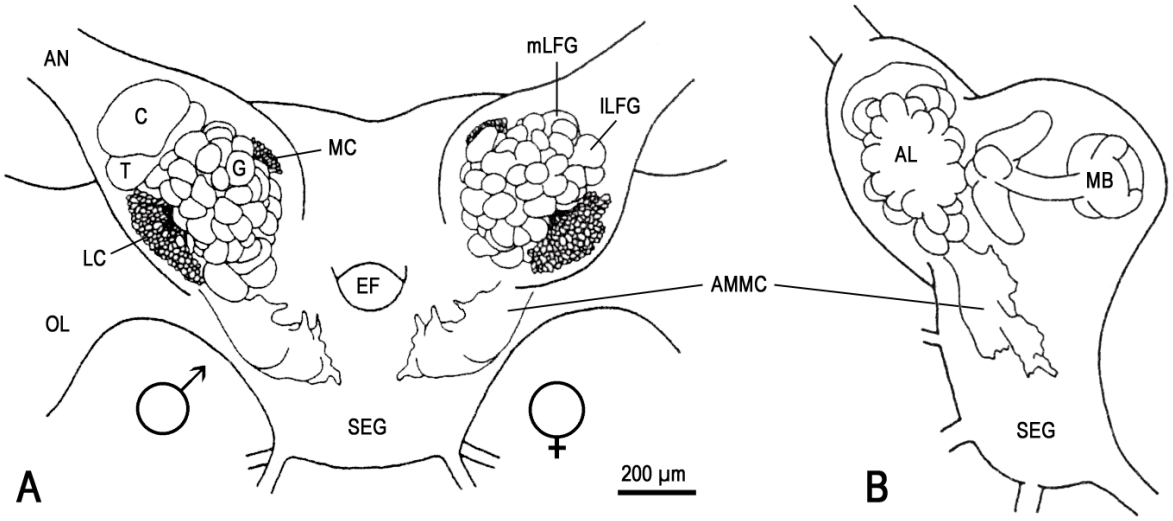

Fig. 2 Anterior (A) and sagittal (B) view on a schematic adult brain of *Manduca sexta*. The subesophageal ganglion (SEG) is fused to the protocerebrum, thus forming the esophageal foramen (EF). On the lateral sides of the central brain are the optic lobes (OL, cut off), while the sex-dimorphic deutocerebral antennal lobes (AL) sit dorso-anteriorly (right side – male, left side - female). Beside isomorphic glomeruli (G), distally situated glomeruli are enlarged in males (C, cumulus; T, toroid) and integrate female pheromone signals, while their female counterparts (lateral large female glomerulus, lLFG; medial large female glomerulus, mLFG) process host-plant odors. The third sex-dimorphic glomerulus, the horseshoe in males i.e. the small female glomerulus (SFG) in females, is occluded by normal glomeruli. Most somata of second order AL neurons reside either in the lateral (LC), median (MC), or anterior (AC) cell group (see Fig. 3). Posterior to the AL lie the mushroom bodies (MB), multisensory integration centers of the brain. The remaining deutocerebrum is organized in the antennal mechanosensory and motoric center (AMMC; after Anton and Homberg 1999).

The antennal lobe – functional anatomy

The antennal lobe (AL) is organized into glomeruli, spheroidal neuropils which are, to different extents, separated by glial processes (*Manduca sexta*: Tolbert and Hildebrand 1981, *Drosophila melanogaster*: Stocker et al. 1990; cockroach: Boeckh and Tolbert 1993; *Apis mellifera*: Hähnlein and Bicker 1996; orthoptera: Ignell et al. 2001; mosquito: Ignell et al. 2005; for a recent review see Schachtner et al. 2005).

All glomeruli are innervated by four major cell types (Fig. 3): 1. olfactory receptor neurons (ORN) which project into distal parts of single glomeruli, 2. multiglomerular local interneurons (LN) and 3. centrifugal neurons (CN), which both modulate the olfactory information, and finally 4. projection neurons (PN). PN transfer the odor

information from glomeruli into higher brain centers including the calyces of the mushroom bodies and the lateral protocerebrum, which are innervated via several antennocerebral tracts (Homberg et al. 1988; Homberg 1990; Anton and Homberg 1999). While the cell bodies of ORN and CN usually lie outside the innervated AL, all somata of PN reside in one of three cell groups around the AL neuropil. The largest is the lateral cell group, which also houses exclusively the LN. The other cell groups are the smaller median and the even smaller anterior cell group (Fig. 2, 3, chapter IV).

The glomerulus number is species-specific and can reach up to about 460 in insects (ants; Zube et al. 2008). Few insect groups show no glomerular organization of the AL neuropil (Palaeoptera) or exhibit thousands of isomorphic microglomeruli (Ensifera, reviewed in Schachtner et al. 2005). 3D reconstructions of several insect ALs allowed individual identification of distinct glomeruli within insect species (*Apis mellifera*: Galizia et al. 1999; *Drosophila melanogaster*: Laissue et al. 1999; *Cotesia glomerata* and *rubecula*: SMID et al. 2003; *Spodoptera littoralis*: Sadek et al. 2002; *Helicoverpa assulta* and *virescens*: Berg et al. 2002; *Agrotis ipsilon*: Greiner et al. 2004; *Manduca sexta*: chapter V; *Helicoverpa armigera*: Skiri et al. 2005; *Anopheles gambiae* and *Aedes aegyptii*: Ignell et al. 2005). This was simplified in animals with pronounced sex-specific glomerulus dimorphism like Dictyoptera, Hymenoptera and Lepidoptera (Rospars 1988; Anton and Homberg 1999; Hansson and Anton 2000). In Lepidoptera however, this dimorphism seems to be restricted to moths, since sex-specific differences were never observed in the ALs of butterflies (*Pieris brassicae*: Rospars 1983; *Papilio xuthus*: Michiyo Kinoshita, *Caligo eurilochus*: pers. observation).

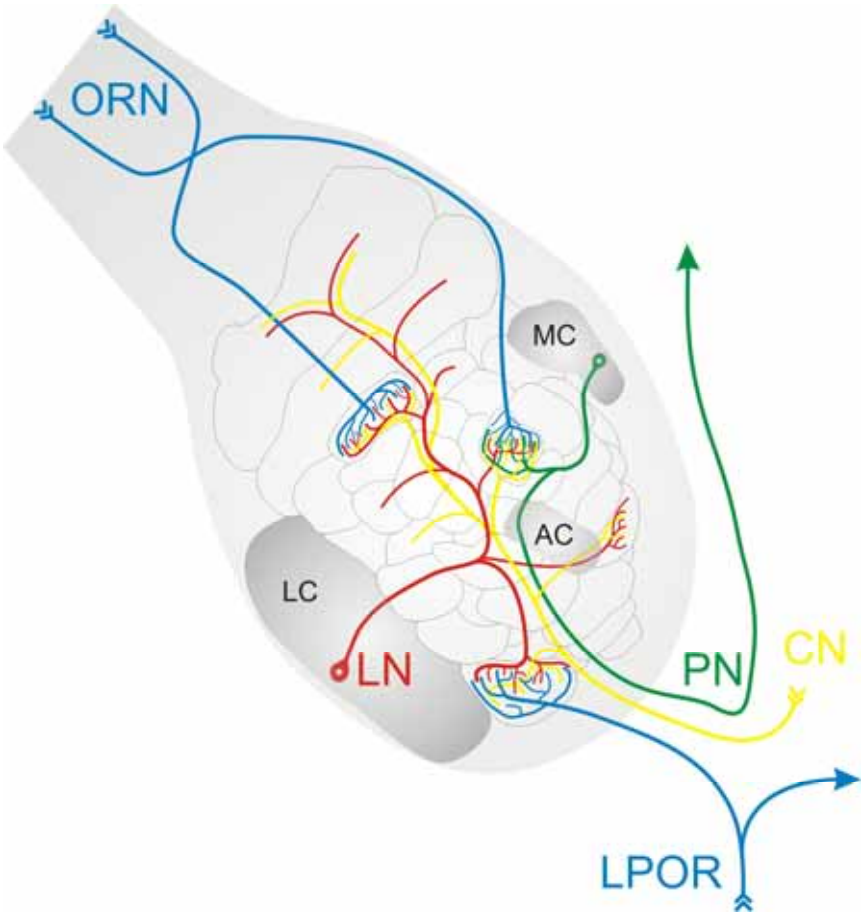

Fig. 3 Scheme of *Manduca sexta* antennal lobe (AL) organization. Olfactory receptor neurons (ORN) coming from the antennae via the antennal nerve innervate single glomeruli. Sensory axons of the CO_2-sensitive labial palp organ (LPOR) bilaterally innervate a defined large ventral glomerulus (see chapter II, V). Almost all somata of AL neurons are located in three cell groups: the anterior (AC), median (MC) and lateral cell group (LC). Local interneurons (LN) have their somata exclusively in the LC, and exhibit multi- or omniglomerular dendritic ramifications. Projection neurons (PN) mainly innervate single glomeruli, and, to a lesser extent, few glomeruli, before they leave the AL towards the protocerebrum via different antennocerebral tracts. In the protocerebrum, main target areas include the calyces of the pedunculi, the lateral horn, or the inferior lateral protocerebrum. Additional modulatory input in the AL comes from multiglomerular centrifugal neurons (CN); their somata reside outside the innervated AL.

The AL of *Manduca sexta* contains beside its three sex-specific glomeruli 60 ±1 "normal" glomeruli (Rospars and Hildebrand 2000; chapter V - VII). The male-specific glomeruli are the cumulus, toroid, and horseshoe, which together form the macroglomerular complex at the entrance of the antennal nerve. Homologous to these male glomeruli are in the female AL the lateral and medial large female glomerulus and the small female glomerulus (Fig. 2). Extracellular recordings of the MGC showed specific pheromone responses (Heinbockel et al. 1998a), and intracellular recordings of MGC-specific PN revealed distinct responses in cumulus and toroid according to pheromone compound (Christensen and Hildebrand 1987; Heinbockel et al. 1998b, 1999). In intracellular recordings from the corresponding glomeruli in females specific responses to Linalool can be found. This volatile compound is emitted by Solanaceae like tobacco, the main food plant of *Manduca sexta* (King et al. 2000; Reisenman et al. 2004). Another special glomerulus is the labial pit organ glomerulus (LPOG), a large ventrally located glomerulus which receives its sensory input from the labial palp organ and was shown to react specifically to CO_2 (Kent et al. 1986; Guerenstein et al. 2004; Guerenstein and Hildebrand 2008). All other glomeruli are regarded as "normal" glomeruli which process odors other than pheromones (Hansson et al. 2003; Schachtner et al. 2005).

In vivo-imaging studies in ALs of several animal species revealed unique sets of active glomeruli, depending on stimulus quality (*Apis mellifera*: Galizia and Menzel 2001; *Spodoptera littoralis*; Carlsson et al. 2002; *Manduca sexta*: Hansson et al. 2003; *Drosophila melanogaster*: Wang et al. 2003; *Heliothis virescens*: Skiri et al. 2004; *Camponotus floridanus*: Zube et al. 2008). Target patterning studies of ORN expressing the same odorant binding protein in *Drosophila*, mouse and zebrafish exhibited discrete innervation of the same glomeruli (Vosshall et al. 2000; Korsching 2002; Leon and Johnson 2003). This led to the hypothesis of odor coding in the AL and olfactory bulb respectively via activation of certain species-specific glomeruli organized in a conserved spatial pattern - an odor map. Apparently this glomerular activation pattern is concentration- and context-dependent, while the olfactory coding itself exhibits - apart from a spatial component - also a time-dependent component (Axel 1995; Hildebrand and Shepherd 1997; Buck 2000; Laurent et al. 2001; Korsching 2002; Leon and Johnson 2003, Knüsel et al. 2007).

Development of the antennal lobe

Under laboratory conditions, the adult antennal lobe develops within three weeks of pupation (P0 – P19 or pharate stage), which ends with the adult ecdysis (A0). Those three weeks can be subdivided into three distinct phases: preparation (I), formation (II), and maturation (III; Fig. 4; Dubuque et al. 2001). Usually, the adults live for about three weeks and extend their whole adult behavioural program not before 3-4 days after eclosion (A2-3).

During phase I, which lasts about 7 to 8 days (P0 to P7/8), all neurons involved in building the AL are born (until P2; Hildebrand et al. 1997). The ORN start to grow into the AL (from P3 to P10), and the protoglomeruli - matrices of the later glomeruli - are laid out (around P6; Oland and Tolbert 1996).

Phase II (P7/8 to P12) is dominated by massive synaptogenesis in the forming glomeruli. A general framework of synapses is built, paralleled by first neuronal activity in ORN (Oland et al. 1996). The other players in the AL network, namely local interneurons and centrifugal neurons join the projection neurons by ingrowing into glomeruli. The formation of glomeruli is stabilized by glial cells, which migrate along glomerular borders (Tolbert et al. 2004). From P13 onwards most synapses appear to be functional (Tolbert et al. 1983). Two main mechanisms seem to regulate developmental processes during phase II: hormonal control by 20-hydroxy-

ecdysone (20E, Schachtner et al. 1999, 2004; Utz and Schachtner 2005; chapter III) and spontaneous neuronal activity (Oland et al. 1996; Schachtner et al. 1999; Lohr et al. 2005). Early injections of 20E lead to precocious glomerulus formation, including precocious rises of GABA- and neuropeptide-immunoreactive cells in the AL (Homberg and Hildebrand 1994; Schachtner et al. 1999; 2004; Utz and Schachtner 2005; chapter III). ORN exhibit spontaneous activity in vivo starting around phase II (Oland et al. 1996), and at least in cell culture also local interneurons and projection neurons show calcium-driven plateau potentials during this time window (Mercer and Hildebrand 2002; Mercer et al. 2005). Glial cells as well depend on voltage-dependent calcium channels for glomerular border migration (Lohr et al. 2005).

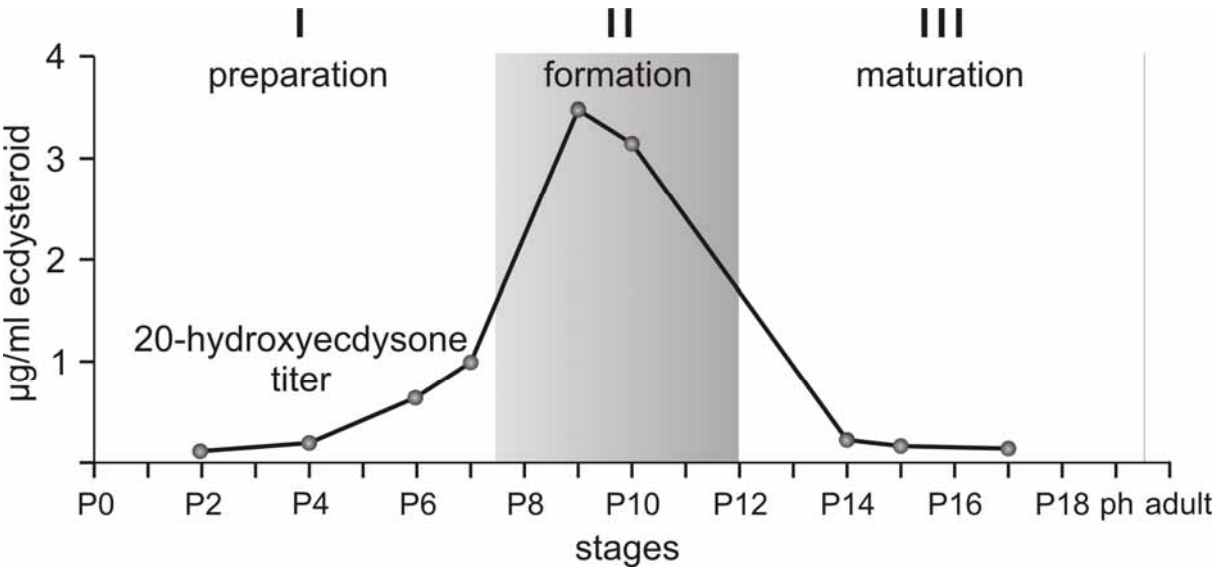

Fig. 4 The antennal lobe development during the pupation period (three weeks, P0 – ph, pharate animal) can be subdivided into three phases I-III which correspond to the titer of 20-hydroxyecdysone (titer after Warren and Gilbert 1986; phases according to Dubuque et al. 2001 and chapter III).

The last phase of pupal AL development, phase III, is marked by only sparse synaptogenesis (Tolbert et al. 1983; Tolbert 1989; Oland et al. 1990; Dubuque et al. 2001). Glomeruli increase in size (chapter V) and refine their synapses (Dubuque et al. 2001). From P15/16 onwards ORN prove to react on odor stimuli (Schweitzer et al. 1976). An additional phase of AL development is probably formed by the first days of adult life, when the animal encounters odors for the first time and possibly undergoes a sensible phase (Anton et al. 2007). This is substanciated by additional adult glomerular size increases between freshly eclosed and four day old adults (chapter V) and unclear results after odor stimulation within first days of adult life in intracellular recordings and behavioral studies (Daly et al. 2004).

Transmitters and neuromodulators in the antennal lobe

In several insect species the antennal lobe was examined regarding its neurochemical organization. These studies revealed a widespread repertoire of neuromediators in the AL; apart from the classical transmitters acetylcholine (ACh), or γ-amino butyric acid (GABA) also biogenic amines, neuropeptides or the gaseous signaling molecule nitric oxide (NO) were found (reviewed in Schachtner et al. 2005).

Classical neurotransmitters

ACh is most likely the principal transmitter of ORN in insects; besides that, ACh is found in subsets of PN (reviewed in Schachtner et al. 2005). At least in *Drosophila*, also some LN exhibit choline acetyltransferase immunoreactivity, an enzyme crucial for ACh synthesis (Shang et al. 2007). Binding studies with the snake poison α-bungarotoxin in *Manduca sexta* and *Apis mellifera* together with physiological studies in *Manduca sexta* point to nicotinic acetylcholine receptors in the AL (Hildebrand et al. 1979; Scheidler et al. 1990; Lohr 2003).

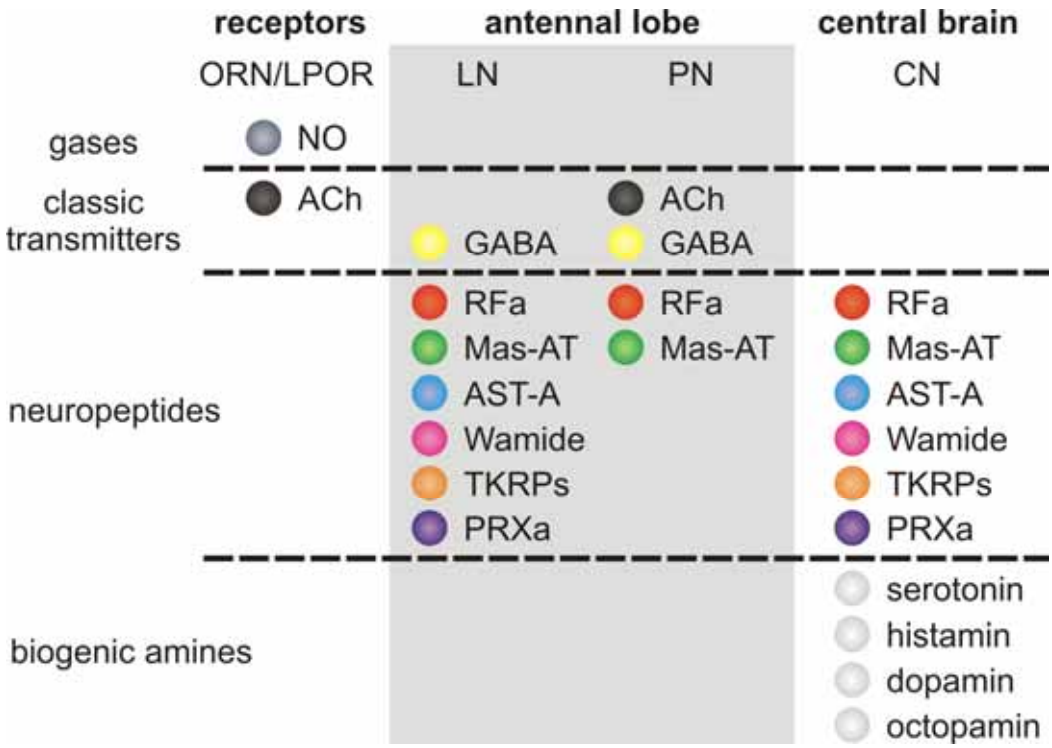

Fig. 5 Neurochemistry in the adult olfactory system of *M. sexta.* The primary olfactory system consists of the following main neuron classes: the olfactory (ORN) and labial palp organ receptor neurons (LPOR), local neurons (LN), projection neurons (PN), and centrifugal neurons (CN). Across those neuron classes, four types of neuromediators are unevenly distributed, 1. signaling gases like nitric oxide (NO), 2. classical transmitters like acetylcholine (ACh) or γ-aminobutyric acid (GABA), 3. neuropeptides like RFamides (RFa), *M. sexta* – allatotropin (Mas-AT), allatostatin-A (AST-A), Wamide, tachykinin-related peptides (TKRPs), PRXamide (PRXa), and 4. biogenic amines.

As an inhibitory signal, GABA seems to be the principal transmitter of LN in insects (reviewed in Schachtner et al. 2005). Physiological studies in several insects reveal the involvement of GABA in inhibitory interactions which lead to odor-dependent snychronization of PN activity (*Schistocerca gregaria*: Laurent 2002; *Manduca sexta*: Lei et al. 2002; *Apis mellifera*: Sachse and Galizia 2002; *Drosophila melanogaster*: Wilson and Laurent 2005). Additionally, Lei et al. (2002) demonstrated a role for GABA in interglomerular inhibition.

Biogenic amines

In the insect nervous system, biogenic amines serve as neurotransmitters, neuromodulators and neurohormones (reviewed in Bicker 1999; Homberg and Müller 1999; Monastirioti 1999; Nässel 1999; Roeder 2005; Hansson and Anton 2000; Homberg 2002). Histochemical and immunocytochemical studies mainly focus on the four biogenic amines serotonin, histamin, dopamin, and octopamin in the ALs of various insect species. In most

cases, biogenic amines innervate the AL via a small number of centrifugal neurons; in some cases, however, local aminergic neurons are described (reviewed in Schachtner et al. 2005).

Neuropeptides

Neuropeptides provide the largest group of signal molecules in the nervous system. Frequently described as cotransmitters of classical transmitters (Vilim et al. 2000; Nässel 2002), it is believed that neuropeptides mainly regulate the state of activity in neuronal networks of the CNS, and therefore specify the input and output properties of these networks (Hökfelt 1991; Hökfeldt et al. 2000; Marder and Bucher 2001; Nusbaum et al. 2001; Nässel 2002; Nässel and Homberg 2006).

A common feature of AL and olfactory bulb (OB) is the expression of various neuropeptides (Smith et al. 1993; Caillol et al. 2003; Moody and Meraly 2004; Schachtner et al. 2005; Gutierrez-Mecinas et al. 2005). Until now, neither in the AL nor in the OB the exact amount of neuropeptides and their cellular localization is known. Few studies in mammals point to important functions of peptides in the olfactory system (e.g. neurogenesis induction by neuropeptide Y and PACAP in the olfactory epithelium of the rat, Hansel et al. 2001a, b; Prokineticin 2 as a trophic signal in mouse olfactory bulb neurogenesis induction, Ng et al. 2005).

So far there exist no studies about a possible role of (neuro)peptides in the insect olfactory system. Most of peptidergic neurons in the AL belong to the lateral cell group (reviewed in Schachtner et al. 2005, chapter III, IV). With GABA being the principal transmitter of local interneurons colocalization of neuropeptides implies their involvement as modulating cotransmitters in the inhibitory GABA signal transduction pathway. Besides, neuropeptides were also found in projection and centrifugal neurons of the AL (Fig. 5). Analogous to the local interneurons, neuropeptides most likely act as cotransmitters to the dominant transmitters ACh or GABA in projection neurons. Centrifugal neurons usually innervate all glomeruli, or exhibit a varicose mesh covering all glomeruli (e.g. allatostatin, Utz and Schachtner 2005). This innervation pattern points to a possible paracrine function, with a more general influence on the AL neuronal network.

In general, only sparse information is available on neuropeptide function in neuronal networks. This is mainly due to missing information about the complete peptidome of the neurons involved. Until now, triple labelling studies using antisera against three different neuropeptide families (AST-A, AT, RFamide, see chapter III) show colocalization of at least two neuropeptide families in subpopulations of local interneurons. Since the number of neuropeptides in the lateral cell group detected with MALDI-TOF exceeds this (chapter IV), we expect further subpopulations of local interneurons with individual peptide identities.

Nitric oxide (NO)

Since its discovery in the nervous system manyfold functions were found for NO (Dawson and Snyder 1994; Garthwaite and Boulton 1995; Müller 1997; Bicker 2001, 2005, 2007; Boehning and Snyder 2003; Garthwaite 2008). Calcium-triggered conversion of L-arginine to L-citrulline by the enzyme NO-synthase leads to nitric oxide production (Fig. 6). NO as a highly diffusible gaseous messenger molecule is able to signal in a certain volume around its production site without being limited by cellular boundaries or transmission directions (Philippides et al. 2005). Main physiological target of NO is the heme group of soluble guanylyl cyclases (sGC, Elphick et al. 1993; Garthwaite 2008), which in turn produce the second messenger cyclic 3',5'-guanylyl monophosphate (cGMP). Main targets of cGMP include ion channels, protein kinases, and phosphodiesterases (Schmidt et al. 1993; Friebe and Koesling 2003; Matulef and Zagotta 2003; Krumenacker et al. 2004). The

lifetime of NO is significantly reduced by reactive oxygen species (ROS) like superoxide, which are - among other sources – a byproduct of the respiratory chain in mitochondria. Superoxide in turn becomes systematically catabolized by the enzyme Cu/Zn-superoxide dismutase, thus indirectly prolonging the range of NO.

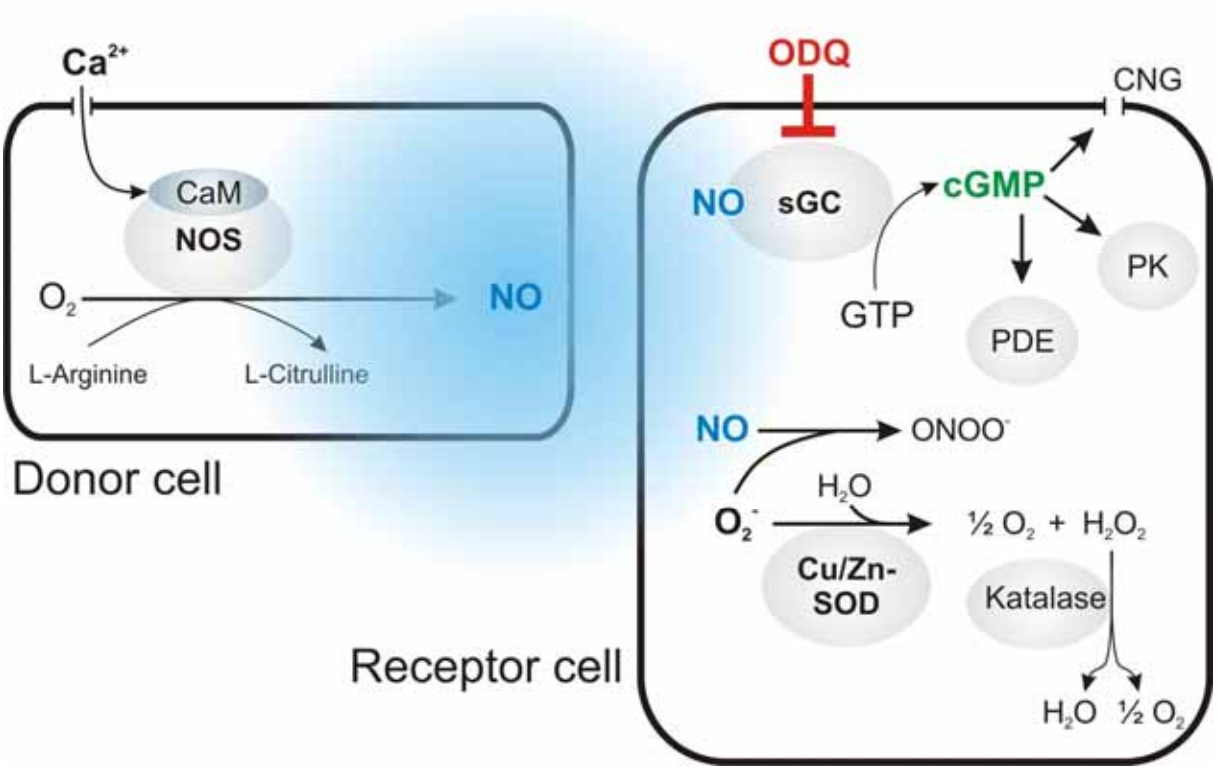

Fig. 6 The nitric oxide (NO) / soluble guanylyl cyclase (sGC) / cGMP signaling pathway. In a donor cell, calcium ion influx (Ca^{2+}) leads to activation of nitric oxide synthase (NOS). The NOS enzyme in turn generates nitric oxide (NO) by oxydation of the amino acid L-arginine to L-citrulline. The highly mobile signaling molecule NO is able to diffuse through cell membranes, until it eventually will activate the soluble guanylyl cyclase (sGC). This leads to the conversion of guanylyl triphosphate (GTP) to cyclic guanylyl monophosphate (cGMP), an important second messenger within cells. cGMP can directly activate cyclic nucleotide gated channels (CNG), protein kinases (PK), and phosphodiesterases (PDE). Pharmacological application of ODQ leads to irreversible inhibition of sGC. Degradation of NO often takes place by reactive oxygen species like superoxide (O_2^-), which oxidize NO to peroxynitrite ($ONOO^-$). The copper/zinc-superoxide dismutase (Cu/Zn-SOD) however scavenges excessive superoxide and catalizes its reaction to dioxygen (O_2) and hydrogen peroxide (H_2O_2). The latter is further broken down by a catalase to O_2 and water (H_2O).

Both in the vertebrate olfactoy bulb and in the insect AL NO-triggered cGMP seems to play a role in signal processing (Breer and Shepherd 1993; Hopkins et al. 1996; Kendrick et al. 1997; Müller 1997; Bicker 1998; Collmann et al. 2004, Wilson et al. 2007). In adult *Manduca sexta*, Collmann et al. (2004) demonstrated in an imaging study odor-specific NO production in different subsets of glomeruli. Intracellular recordings combined with pharmacological interference revealed a functional link between NO production and proper odor processing within the AL (Wilson et al. 2007). The special propensities of NO suggest a role in synchronization of the olfactory signal between several neurons within single activated glomeruli as a functional unit (Breer and Shepherd 1993; Müller 1997).

Apparently, during neural development NO and NO-stimulated cGMP seem to play additional instructive roles apart from those known in adult neural systems, including cell proliferation, axogenesis, growth cone differentiation and instruction, and synaptogenesis (Davies 2000, Gibson et al. 2001, Bicker 2005, 2007; Garthwaite 2008). More information on the developmental role of NO and cGMP can be found in chapter II.

3D reconstruction

By now, virtual 3D brain reconstruction based on immunohistological data became an almost common tool in insect neuroscience. It helps in such diverse questions as fitting single neurons – either intracellularly or genetically labeled - of several preparations into one reference (Brandt et al. 2005; Jefferis et al. 2007; Kurylas et al. 2008), or comparing brain volumes between different species, genders, ages, or pharmacologically treated animals (Kühn-Bühlmann and Wehner 2006; chapter V, VI; Rulla 2008).

In chapter V, a protocol for optimized labeling in antennal lobes is presented, and with this publication a web presence was established: http://www.3d-insectbrain.com. This website shall serve as a platform for ongoing research on 3D insect brains and brain parts. With a standard brain of the desert locust *Schistocerca gregaria* (Kurylas et al. 2008), and the *Manduca sexta* standard brain (chapter VI) already two other projects came online. Further planned additions include standard brains of the cockroaches *Leucophaea maderae* (Wei 2007) and *Periplaneta americana* (in cooperation with P. Kloppenburg, University of Cologne, Germany), the red flour beetle *Tribolium castaneum* (Dreyer 2008), a 3D-4D representation of the developing *Manduca* brain (el Jundi 2008), and a standardized central complex of the desert locust *Schistocerca gregaria* (Lenschow 2008).

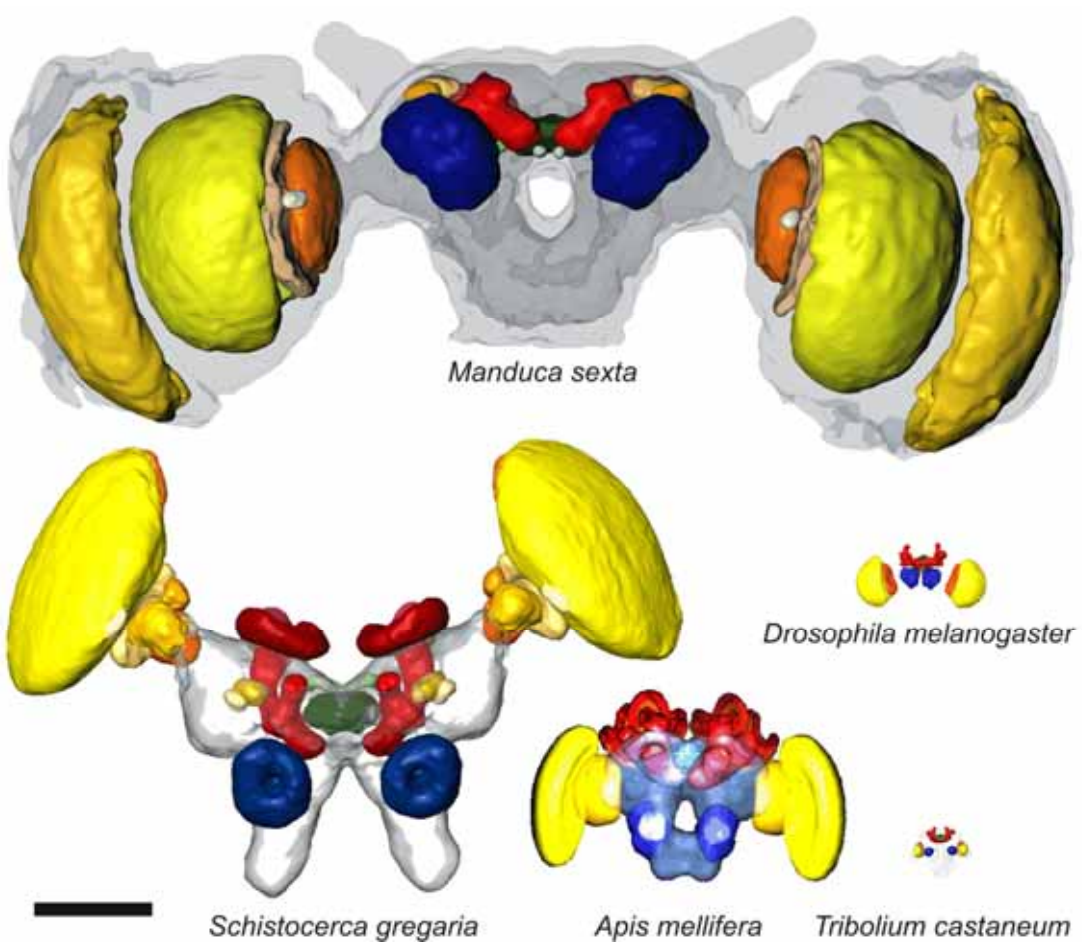

Fig. 7 All five standard insect 3D brains existing so far. For the color code and further explanations, see chapter VI. Scale bar = 500 µm (after Brandt et al. 2005, Jenett et al. 2006, Kurylas et al. 2008, chapter VI, and Dreyer 2008).

All chapters and additional supplementary material (pictures, movies) can be found on the attached CD (last page).

LITERATURE

Anton S and Homberg U. 1999. Antennal lobe structure. In Hansson BS, editor. Insect Olfaction. Berlin: Springer. p 97-124.

Anton S, Dufour MC, and Gadenne C. 2007. Plasticity of olfactory-guided behaviour and its neurobiological basis: lessons from moths and locusts. Entomologia Experimentalis et Applicata 123:1-11.

Axel R. 1995. The molecular logic of smell. Sci Am 273:154-159.

Berg BG, Galizia CG, Brandt R, and Mustaparta H. 2002. Digital atlases of the antennal lobe in two species of tobacco budworm moths, the Oriental *Helicoverpa assulta* (male) and the American *Heliothis virescens* (male and female). J Comp Neurol 446:123-134.

Bicker G. 1998. NO news from insect brains. Trends Neurosci 21:349-355.

Bicker G. 1999. Histochemistry of classical neurotransmitters in antennal lobes and mushroom bodies of the honeybee. Microsc Res Tech 45:174-183.

Bicker G. 2001. Sources and targets of nitric oxide signalling in insect nervous systems. Cell Tissue Res 303:137-146.

Bicker G. 2005. STOP and GO with NO: nitric oxide as a regulator of cell motility in simple brains. Bioessays 27:495-505.

Bicker G. 2007. Pharmacological approaches to nitric oxide signalling during neural development of locusts and other model insects. Arch Insect Biochem Physiol 64:43-58.

Boeckh J and Tolbert LP. 1993. Synaptic organization and development of the antennal lobe in insects. Microsc Res Tech 24:260-280.

Boehning D and Snyder SH. 2003. Novel neural modulators. Annu Rev Neurosci 26:105-131.

Brandt R, Rohlfing T, Rybak J, Krofczik S, Maye A, Westerhoff M, Hege HC, and Menzel R. 2005. Three-dimensional average-shape atlas of the honeybee brain and its applications. J Comp Neurol 492:1-19.

Breer H and Shepherd GM. 1993. Implications of the NO/cGMP system for olfaction. Trends Neurosci 16:5-9.

Buck LB. 2000. The molecular architecture of odor and pheromone sensing in mammals. Cell 100:611-618.

Caillol M, Aioun J, Baly C, Persuy MA, and Salesse R. 2003. Localization of orexins and their receptors in the rat olfactory system: possible modulation of olfactory perception by a neuropeptide synthetized centrally or locally. Brain Res 960:48-61.

Carlsson MA, Galizia CG, and Hansson BS. 2002. Spatial representation of odours in the antennal lobe of the moth *Spodoptera littoralis* (Lepidoptera: Noctuidae). Chem Senses 27:231-244.

Christensen TA and Hildebrand JG. 1987. Male-specific, sex pheromone-selective projection neurons in the antennal lobes of the moth *Manduca sexta*. J Comp Physiol [A] 160:553-569.

Collmann C, Carlsson MA, Hansson BS, and Nighorn A. 2004. Odorant-evoked nitric oxide signals in the antennal lobe of *Manduca sexta*. J Neurosci 24:6070-6077.

Daly KC, Christensen TA, Lei H, Smith BH, and Hildebrand JG. 2004. Learning modulates the ensemble representations for odors in primary olfactory networks. Proc Natl Acad Sci U S A.

Davies S. 2000. Nitric oxide signalling in insects. Insect Biochem Mol Biol 30:1123-1138.

Dawson TM and Snyder SH. 1994. Gases as biological messengers: nitric oxide and carbon monoxide in the brain. J Neurosci 14:5147-5159.

Dreyer D. 2008. Erstellung eines standardisierten 3D Neuropilatlas und die Plastizität des Gehirns von *Tribolium castaneum*. Diploma thesis, Philipps-University Marburg.

Dubuque SH, Schachtner J, Nighorn AJ, Menon KP, Zinn K, and Tolbert LP. 2001. Immunolocalization of synaptotagmin for the study of synapses in the developing antennal lobe of *Manduca sexta*. J Comp Neurol 441:277-287.

Eisthen HL. 2002. Why are olfactory systems of different animals so similar? Brain Behav Evol 59:273-293.

el Jundi B. 2008. Erstellung eines 3D Standardgehirnes des Tabakschwärmers *Manduca sexta:* Ontogenie und Geschlechtsdimorphismus. Diploma thesis, Philipps-University Marburg.

Elphick MR, Green IC, and O'Shea M. 1993. Nitric oxide synthesis and action in an invertebrate brain. Brain Res 619:344-346.

Friebe A and Koesling D. 2003. Regulation of nitric oxide-sensitive guanylyl cyclase. Circ Res 93:96-105.

Galizia CG, McIlwrath SL, and Menzel R. 1999. A digital three-dimensional atlas of the honeybee antennal lobe based on optical sections acquired by confocal microscopy. Cell Tissue Res 295:383-394.

Galizia CG and Menzel R. 2001. The role of glomeruli in the neural representation of odours: results from optical recording studies. J Insect Physiol 47:115-130.

Garthwaite J and Boulton CL. 1995. Nitric oxide signaling in the central nervous system. Annu Rev Physiol 57:683-706.

Garthwaite J. 2008. Concepts of neural nitric oxide-mediated transmission. European Journal of Neuroscience 27:2783-2802.

Gibson NJ, Rössler W, Nighorn AJ, Oland LA, Hildebrand JG, and Tolbert LP. 2001. Neuron-glia communication via nitric oxide is essential in establishing antennal-lobe structure in *Manduca sexta*. Dev Biol 240:326-339.

Greiner B, Gadenne C, and Anton S. 2004. Three-dimensional antennal lobe atlas of the male moth, *Agrotis ipsilon*: A tool to study structure-function correlation. J Comp Neurol 475:202-210.

Grimaldi DA and Engel MS. 2005. Evolution of the insects. Cambridge, UK: Cambridge University Press.

Guerenstein PG, Christensen TA, and Hildebrand JG. 2004. Sensory processing of ambient CO_2 information in the brain of *Manduca sexta*. J Comp Physiol A Neuroethol Sens Neural Behav Physiol 190:707-725.

Guerenstein PG and Hildebrand JG. 2008. Roles and effects of environmental carbon dioxide in insect life. Annu Rev Entomol 53:161-178.

Gutierrez-Mecinas M, Crespo C, Blasco-Ibanez JM, Gracia-Llanes FJ, Marques-Mari AI, and Martinez-Guijarro FJ. 2005. Characterization of somatostatin- and cholecystokinin-immunoreactive periglomerular cells in the rat olfactory bulb. J Comp Neurol 489:467-479.

Hansel DE, Eipper BA, and Ronnett GV. 2001a. Neuropeptide Y functions as a neuroproliferative factor. Nature 410:940-944.

Hansel DE, Eipper BA, and Ronnett GV. 2001b. Regulation of olfactory neurogenesis by amidated neuropeptides. J Neurosci Res 66:1-7.

Hansson BS and Anton S. 2000. Function and morphology of the antennal lobe: new developments. Annu Rev Entomol 45:203-231.

Hansson BS, Carlsson MA, and Kalinova B. 2003. Olfactory activation patterns in the antennal lobe of the sphinx moth, *Manduca sexta*. J Comp Physiol A Neuroethol Sens Neural Behav Physiol 189:301-308.

Hähnlein I and Bicker G. 1996. Morphology of neuroglia in the antennal lobes and mushroom bodies of the brain of the honeybee. J Comp Neurol 367:235-245.

Heinbockel T and Hildebrand JG. 1998a. Antennal receptive fields of pheromone-responsive projection neurons in the antennal lobes of the male sphinx moth *Manduca sexta*. J Comp Physiol [A] 183:121-133.

Heinbockel T, Kloppenburg P, and Hildebrand JG. 1998b. Pheromone-evoked potentials and oscillations in the antennal lobes of the sphinx moth *Manduca sexta*. J Comp Physiol [A] 182:703-714.

Heinbockel T, Christensen TA, and Hildebrand JG. 1999. Temporal tuning of odor responses in pheromone-responsive projection neurons in the brain of the sphinx moth *Manduca sexta*. J Comp Neurol 409:1-12.

Hildebrand JG, Hall LM, and Osmond BC. 1979. Distribution of binding sites for 125I-labeled alpha-bungarotoxin in normal and deafferented antennal lobes of *Manduca sexta*. Proc Natl Acad Sci U S A 76:499-503.

Hildebrand JG and Shepherd GM. 1997. Mechanisms of olfactory discrimination: converging evidence for common principles across phyla. Annu Rev Neurosci 20:595-631.

Hildebrand JG, Rössler W, and Tolbert LP. 1997. Postembryonic development of the olfactory system in the moth *Manduca sexta*: primary-afferent control of glomerular development. Semin Cell Dev Biol 8:163-170.

Homberg U, Montague RA, and Hildebrand JG. 1988. Anatomy of antenno-cerebral pathways in the brain of the sphinx moth *Manduca sexta*. Cell Tissue Res 254:255-281.

Homberg U. 1990. Immunocytochemical demonstration of transmitter candidates in the central olfactory pathways in the sphinx moth *Manduca sexta*. In Døving KB, editor. Olfaction and Taste. Oslo: GSC A/S. p 151-158.

Homberg U and Hildebrand JG. 1994. Postembryonic development of gamma-aminobutyric acid-like immunoreactivity in the brain of the sphinx moth *Manduca sexta*. J Comp Neurol 339:132-149.

Homberg U and Müller U. 1999. Neuroactive Substances in the Antennal Lobe. In Hansson BS, editor. Insect Olfaction. p 181-206.

Homberg U. 2002. Neurotransmitters and neuropeptides in the brain of the locust. Microsc Res Tech 56:189-209.

Hopkins DA, Steinbusch HW, Markerink-van Ittersum M, and De Vente J. 1996. Nitric oxide synthase, cGMP, and NO-mediated cGMP production in the olfactory bulb of the rat. J Comp Neurol 375:641-658.

Hökfelt T. 1991. Neuropeptides in perspective: the last ten years. Neuron 7:867-879.

Hökfelt T, Broberger C, Xu ZQ, Sergeyev V, Ubink R, and Diez M. 2000. Neuropeptides--an overview. Neuropharmacology 39:1337-1356.

Ignell R, Anton S, and Hansson BS. 2001. The antennal lobe of orthoptera - anatomy and evolution. Brain Behav Evol 57:1-17.

Ignell R, Dekker T, Ghaninia M, and Hansson BS. 2005. Neuronal architecture of the mosquito deutocerebrum. J Comp Neurol 493:207-240.

Jefferis GS, Potter CJ, Chan AM, Marin EC, Rohlfing T, Maurer CR, Jr., and Luo L. 2007. Comprehensive maps of *Drosophila* higher olfactory centers: spatially segregated fruit and pheromone representation. Cell 128:1187-1203.

Jenett A, Schindelin JE, and Heisenberg M. 2006. The Virtual Insect Brain protocol: creating and comparing standardized neuroanatomy. BMC Bioinformatics 7:544.

Kendrick KM, Guevara-Guzman R, Zorrilla J, Hinton MR, Broad KD, Mimmack M, and Ohkura S. 1997. Formation of olfactory memories mediated by nitric oxide. Nature 388:670-674.

Kent KS, Harrow ID, Quartararo P, and Hildebrand JG. 1986. An accessory olfactory pathway in Lepidoptera: the labial pit organ and its central projections in *Manduca sexta* and certain other sphinx moths and silk moths. Cell Tissue Res 245:237-245.

King JR, Christensen TA, and Hildebrand JG. 2000. Response characteristics of an identified, sexually dimorphic olfactory glomerulus. J Neurosci 20:2391-2399.

Knüsel P, Carlsson MA, Hansson BS, Pearce TC, and Verschure PF. 2007. Time and space are complementary encoding dimensions in the moth antennal lobe. Network 18:35-62.

Korsching S. 2002. Olfactory maps and odor images. Curr Opin Neurobiol 12:387-392.

Krumenacker JS, Hanafy KA, and Murad F. 2004. Regulation of nitric oxide and soluble guanylyl cyclase. Brain Res Bull 62:505-515.

Kühn-Bühlmann S and Wehner R. 2006. Age-dependent and task-related volume changes in the mushroom bodies of visually guided desert ants, *Cataglyphis bicolor*. J Neurobiol 66:511-521.

Kurylas AE, Rohlfing T, Krofczik S, Jenett A, and Homberg U. 2008. Standardized atlas of the brain of the desert locust, *Schistocerca gregaria*. Cell Tissue Res 333:125-145.

Laissue PP, Reiter C, Hiesinger PR, Halter S, Fischbach KF, and Stocker RF. 1999. Three-dimensional reconstruction of the antennal lobe in *Drosophila melanogaster*. J Comp Neurol 405:543-552.

Laurent G, Stopfer M, Friedrich RW, Rabinovich MI, Volkovskii A, and Abarbanel HD. 2001. Odor encoding as an active, dynamical process: experiments, computation, and theory. Annu Rev Neurosci 24:263-297.

Laurent G. 2002. Olfactory network dynamics and the coding of multidimensional signals. Nat Rev Neurosci 3:884-895.

Lei H, Christensen TA, and Hildebrand JG. 2002. Local inhibition modulates odor-evoked synchronization of glomerulus-specific output neurons. Nat Neurosci 5:557-565.

Lenschow C. 2008. 3D-Rekonstruktion und Standardisierung des Zentralkomplexes bei *Schistocerca gregaria*. Bachelor thesis, Philipps-University Marburg.

Leon M and Johnson BA. 2003. Olfactory coding in the mammalian olfactory bulb. Brain Res Brain Res Rev 42:23-32.

Lohr C. 2003. Monitoring neuronal calcium signalling using a new method for ratiometric confocal calcium imaging. Cell Calcium 34:295-303.

Lohr C, Heil JE, and Deitmer JW. 2005. Blockage of voltage-gated calcium signaling impairs migration of glial cells in vivo. Glia 50:198-211.

Luo L and Flanagan JG. 2007. Development of continuous and discrete neural maps. Neuron 56:284-300.

Marder E and Bucher D. 2001. Central pattern generators and the control of rhythmic movements. Curr Biol 11:R986-R996.

Matulef K and Zagotta WN. 2003. Cyclic nucleotide-gated ion channels. Annu Rev Cell Dev Biol 19:23-44.

Mercer AR and Hildebrand JG. 2002. Developmental changes in the electrophysiological properties and response characteristics of *Manduca* antennal-lobe neurons. J Neurophysiol 87:2650-2663.

Mercer AR, Kloppenburg P, and Hildebrand JG. 2005. Plateau potentials in developing antennal-lobe neurons of the moth, *Manduca sexta*. J Neurophysiol 93:1949-1958.

Monastirioti M. 1999. Biogenic amine systems in the fruit fly *Drosophila melanogaster*. Microsc Res Tech 45:106-121.

Moody TW and Merali Z. 2004. Bombesin-like peptides and associated receptors within the brain: distribution and behavioral implications. Peptides 25:511-520.

Müller U. 1997. The nitric oxide system in insects. Prog Neurobiol 51:363-381.

Nässel DR. 1999. Histamine in the brain of insects: a review. Microsc Res Tech 44:121-136.

Nässel DR. 2002. Neuropeptides in the nervous system of *Drosophila* and other insects: multiple roles as neuromodulators and neurohormones. Prog Neurobiol 68:1-84.

Nässel DR and Homberg U. 2006. Neuropeptides in interneurons of the insect brain. Cell Tissue Res 326:1-24.

Ng KL, Li JD, Cheng MY, Leslie FM, Lee AG, and Zhou QY. 2005. Dependence of olfactory bulb neurogenesis on prokineticin 2 signaling. Science 308:1923-1927.

Nusbaum MP, Blitz DM, Swensen AM, Wood D, and Marder E. 2001. The roles of co-transmission in neural network modulation. Trends Neurosci 24:146-154.

Oland LA, Orr G, and Tolbert LP. 1990. Construction of a protoglomerular template by olfactory axons initiates the formation of olfactory glomeruli in the insect brain. J Neurosci 10:2096-2112.

Oland LA and Tolbert LP. 1996. Multiple factors shape development of olfactory glomeruli: insights from an insect model system. J Neurobiol 30:92-109.

Oland LA, Pott WM, Bukhman G, Sun XJ, and Tolbert LP. 1996. Activity blockade does not prevent the construction of olfactory glomeruli in the moth *Manduca sexta*. Int J Dev Neurosci 14:983-996.

Philippides A, Ott SR, Husbands P, Lovick TA, and O'Shea M. 2005. Modeling cooperative volume signaling in a plexus of nitric oxide synthase-expressing neurons. J Neurosci 25:6520-6532.

Reisenman CE, Christensen TA, Francke W, and Hildebrand JG. 2004. Enantioselectivity of projection neurons innervating identified olfactory glomeruli. J Neurosci 24:2602-2611.

Roeder T. 2005. Tyramine and Octopamine: Ruling Behavior and Metabolism. Annu Rev Entomol 50:447-477.

Rospars JP. 1983. Invariance and sex-specific variations of the glomerular organization in the antennal lobes of a moth, *Mamestra brassicae*, and a butterfly, *Pieris brassicae*. J Comp Neurol 220:80-96.

Rospars JP. 1988. Structure and Development of the Insect Antennodeutocerebral System. International Journal of Insect Morphology & Embryology 17:243-294.

Rospars JP and Hildebrand JG. 2000. Sexually dimorphic and isomorphic glomeruli in the antennal lobes of the sphinx moth *Manduca sexta*. Chem Senses 25:119-129.

Rulla S. 2008. Immunhistochemisch-anatomische Analyse des Antennallobus von *Manduca sexta* nach Injektion von Na^{+}- und Ca^{2+}-Kanalblockern. Bachelor thesis, Philipps-University Marburg.

Sachse S and Galizia CG. 2002. Role of inhibition for temporal and spatial odor representation in olfactory output neurons: a calcium imaging study. J Neurophysiol 87:1106-1117.

Sadek MM, Hansson BS, Rospars JP, and Anton S. 2002. Glomerular representation of plant volatiles and sex pheromone components in the antennal lobe of the female *Spodoptera littoralis*. J Exp Biol 205:1363-1376.

Schachtner J, Homberg U, and Truman JW. 1999. Regulation of cyclic GMP elevation in the developing antennal lobe of the Sphinx moth, *Manduca sexta*. J Neurobiol 41:359-375.

Schachtner J, Trosowski B, D'Hanis W, Stubner S, and Homberg U. 2004. Development and steroid regulation of RFamide immunoreactivity in antennal-lobe neurons of the sphinx moth *Manduca sexta*. J Exp Biol 207:2389-2400.

Schachtner J, Schmidt M, and Homberg U. 2005. Organization and evolutionary trends of primary olfactory brain centers in Tetraconata (Crustacea + Hexapoda). Arthropod Structure and Development 34:257-299.

Scheidler A, Kaulen P, Bruning G, and Erber J. 1990. Quantitative autoradiographic localization of [125I]alpha-bungarotoxin binding sites in the honeybee brain. Brain Res 534:332-335.

Schmidt HH, Lohmann SM, and Walter U. 1993. The nitric oxide and cGMP signal transduction system: regulation and mechanism of action. Biochim Biophys Acta 1178:153-175.

Schweitzer ES, Sanes JR, and Hildebrand JG. 1976. Ontogeny of electroantennogram responses in the moth, *Manduca sexta*. J Insect Physiol 2:955-960.

Shang Y, Claridge-Chang A, Sjulson L, Pypaert M, and Miesenböck G. 2007. Excitatory local circuits and their implications for olfactory processing in the fly antennal lobe. Cell 128:601-612.

Skiri HT, Galizia CG, and Mustaparta H. 2004. Representation of Primary Plant Odorants in the Antennal Lobe of the Moth *Heliothis virescens* Using Calcium Imaging. Chem Senses 29:253-267.

Skiri HT, Rø H, Berg BG, and Mustaparta H. 2005. Consistent organization of glomeruli in the antennal lobes of related species of heliothine moths. J Comp Neurol 491:367-380.

SMID HM, Bleeker MA, van Loon JJ, and Vet LE. 2003. Three-dimensional organization of the glomeruli in the antennal lobe of the parasitoid wasps *Cotesia glomerata* and *C. rubecula*. Cell Tissue Res 312:237-248.

Smith RL, Baker H, and Greer CA. 1993. Immunohistochemical analyses of the human olfactory bulb. J Comp Neurol 333:519-530.

Stocker RF, Lienhard MC, Borst A, and Fischbach KF. 1990. Neuronal architecture of the antennal lobe in *Drosophila melanogaster*. Cell Tissue Res 262:9-34.

Tolbert LP and Hildebrand JG. 1981. Organization and synaptic ultrastructure of glomeruli in the antennal lobes of the moth *Manduca sexta*: a study using thin sections and freeze fracture. Proc R Soc Lond B 213:279-301.

Tolbert LP, Matsumoto SG, and Hildebrand JG. 1983. Development of synapses in the antennal lobes of the moth *Manduca sexta* during metamorphosis. J Neurosci 3:1158-1175.

Tolbert LP. 1989. Afferent axons from the antenna influence the number and placement of intrinsic synapses in the antennal lobes of *Manduca sexta*. Synapse 3:83-95.

Tolbert LP, Oland LA, Tucker ES, Gibson NJ, Higgins MR, and Lipscomb BW. 2004. Bidirectional influences between neurons and glial cells in the developing olfactory system. Prog Neurobiol 73:73-105.

Utz S and Schachtner J. 2005. Development of A-type allatostatin immunoreactivity in antennal lobe neurons of the sphinx moth *Manduca sexta*. Cell Tissue Res 320:149-162.

Vilim FS, Cropper EC, Price DA, Kupfermann I, and Weiss KR. 2000. Peptide cotransmitter release from motorneuron B16 in *Aplysia californica*: costorage, corelease, and functional implications. J Neurosci 20:2036-2042.

Vosshall LB, Wong AM, and Axel R. 2000. An olfactory sensory map in the fly brain. Cell 102:147-159.

Wang JW, Wong AM, Flores J, Vosshall LB, and Axel R. 2003. Two-photon calcium imaging reveals an odor-evoked map of activity in the fly brain. Cell 112:271-282.

Warren JT and Gilbert LI. 1986. Ecdysone metabolism and distribution during the pupal-adult development of *Manduca sexta*. Insect Biochemistry 16:65-82.

Wei, H. 2007. A three-dimensional standardized atlas of the brain of the cockroach *Leucophaea maderae*. Bachelor thesis, Philipps-University Marburg.

Wilson CH, Christensen TA, and Nighorn AJ. 2007. Inhibition of nitric oxide and soluble guanylyl cyclase signaling affects olfactory neuron activity in the moth, *Manduca sexta*. J Comp Physiol A Neuroethol Sens Neural Behav Physiol 193:715-728.

Wilson RI and Laurent G. 2005. Role of GABAergic inhibition in shaping odor-evoked spatiotemporal patterns in the *Drosophila* antennal lobe. J Neurosci 25:9069-9079.

Zube C, Kleineidam CJ, Kirschner S, Neef J, and Rössler W. 2008. Organization of the olfactory pathway and odor processing in the antennal lobe of the ant *Camponotus floridanus*. J Comp Neurol 506:425-441.

CHAPTER I:

Copper/Zinc Superoxide Dismutase-Like Immunoreactivity in the Metamorphosing Brain of the Sphinx Moth *Manduca sexta*

THE JOURNAL OF COMPARATIVE NEUROLOGY 469:141–152 (2004)

Copper/Zinc Superoxide Dismutase-Like Immunoreactivity in the Metamorphosing Brain of the Sphinx Moth *Manduca sexta*

JOACHIM SCHACHTNER,[1]* WOLF HUETTEROTH,[1] ALAN NIGHORN,[2] AND HANS-WILLI HONEGGER[3]

[1]Fachbereich Biologie, Tierphysiologie, Philipps-Universität, 35032 Marburg, Germany
[2]Arizona Research Laboratories Division of Neurobiology, University of Arizona, Tucson, Arizona 85721
[3]Department of Biological Sciences, Vanderbilt University, Nashville, Tennessee 37325

ABSTRACT

Cu/Zn superoxide dismutase (SOD) is part of the defense mechanism that protects cells from being damaged by reactive oxygen species. During metamorphosis of the nervous system, neurons undergo various fates, which are all coupled to high metabolic activities, such as proliferation, differentiation, pathfinding, and synaptogenesis. We describe the pattern of SOD immunoreactivity of identified neurons and neuron groups in the brain of *Manduca sexta* from the late larva through metamorphosis into adult. We focused on neurons of the developing antennal lobes, the optic lobes, and the central brain. Our results indicate the transient expression of SOD during phases in which the neurons develop their final adult identities. Our data also suggest that the SOD immunoreactivity may be used as an indicator for the period in which developing neurons form their synapses. We also observed SOD immunoreactivity within nitric oxide-sensitive cells as characterized by immunolabeling against 3′5′-cyclic guanosine monophosphate and soluble guanylyl cyclase, a novel finding in insects. J. Comp. Neurol. 469:141–152, 2004.

Indexing terms: development; oxidative stress; cell fate; nitric oxide

In all aerobic organisms, a byproduct of oxygen metabolism is the generation of reactive oxygen species (ROS), which can cause serious damage to any molecule of a cell (Fridovich, 1999). To protect cells against this oxidative threat, cellular defense mechanisms exist. One major player is Cu/Zn superoxide dismutase (SOD) which, together with catalase, eliminates superoxides and eventually converts them to O_2 and H_2O (Fridovich, 1986, 1999). According to the oxidative stress hypothesis of aging, ROS are involved in the physiological deterioration of cells that accompanies aging (Ames et al., 1993; Sohal, 1993; Stadtman, 2001; Nagy, 2001; Linton et al., 2001). Nerve cells, with their high metabolic rates (Frayn, 1996), are particularly endangered. Thus, ROS may play a major role in neurodegenerative disorders such as Alzheimer's disease, Parkinson's disease, and amyotropic lateral sclerosis (Markesbery, 1997; Floyd, 1999; Tabner et al., 2001; Beckman et al., 2001; Maier and Chan, 2002; Okado-Matsumoto and Fridovich, 2002).

In developing nervous systems, neuron proliferation, differentiation, pathfinding to final target areas, and synaptogenesis involve high metabolic rates and, thus, more production of ROS. To prevent oxidative damage, maturing neurons that are in the process of axon and dendrite extension and/or synapse formation may be especially safeguarded by transient defense mechanisms, e.g., by the up-regulation of key antioxidant enzymes.

Grant sponsor: Deutsche Forschungsgemeinschaft; Grant number: Scha 678/3-3 (J.S.).

*Correspondence to: Joachim Schachtner, Fachbereich Biologie, Tierphysiologie, Philipps-Universität, 35032 Marburg, Germany.
E-mail: schachtj@staff.uni-marburg.de

Received 4 June 2003; Revised 14 August 2003; Accepted 19 September 2003

DOI 10.1002/cne.10992

Published online the week of December 8, 2003 in Wiley InterScience (www.interscience.wiley.com).

For *Manduca sexta* a large body of knowledge exists regarding the various developmental fates of identified neurons in the metamorphosing nervous system (for review see Truman, 1996). Most nerve cells of the adult brain that differentiate during metamorphosis arise from neuroblasts that have been arrested during early larval stages and that start a second phase of proliferation in late larval stages. Among these cells are the neurons of the developing optic and antennal lobes, which have been well examined in terms of the developmental time course of their proliferation and differentiation phases (Monsma and Booker, 1996a, b; Oland and Tolbert, 1996; Hildebrand et al., 1997; Champlin and Truman, 1998, 2000). Other neurons of the CNS, which were functional in the larva, are remodeled during metamorphosis to fit the requirements of the adult animal (Truman, 1996; Weeks, 1999). Another fate of neurons during metamorphosis is programmed cell death, which has been described for many regions of the insect CNS (Ewer et al., 1998; Draizen et al. 1999; Weeks, 1999). We hypothesize that SOD might be up-regulated during phases of neuronal maturation but not in neurons that undergo programmed cell death.

Superoxide also acts as a major limiting factor for the survival of the free radical gas nitric oxide (NO; Ku, 1996). It rapidly reacts with NO to build peroxynitrite and, thus, drastically limits the signaling abilities of NO. Thus, SOD may enhance NO stability and, additionally, prevents the production of cytotoxic peroxynitrite (Beckman and Koppenol, 1996; Friebe et al., 1998).

To test the hypothesis that developing neurons in the metamorphosing nervous system of *M. sexta* up-regulate SOD as a possible protection mechanism against oxidative damage, we investigated the pattern of antibody staining obtained with a specific antiserum against SOD (Kostron et al., 1999). Here we describe SOD labeling for selected neurons throughout metamorphosis of the *M. sexta* brain. For many of the neurons examined, we show a colocalization of SOD immunoreactivity with either NO-induced 3′5′-cyclic guanosine monophosphate (cGMP) elevation or an antiserum against the α_1 subunit of soluble guanylyl cyclase, which NO-dependently produces cGMP (Gibson and Nighorn, 2000).

MATERIALS AND METHODS

Animals

M. sexta (Lepidoptera: Sphingidae) were reared on an artificial diet under a long-day photoperiod (L:D = 17:7) at 26°C in walk-in environmental chambers. Under these conditions, the time required from hatching to pupal ecdysis is about 18 days and the time from pupal to adult ecdysis about 20 days. The start of the wandering stage (W0) occurs 3–4 days into the fifth larval instar and is characterized by the appearance of a red pigment along the heart. The following days are referred to as W1 up to W4. At about noon of W2, the animals go into a quiescent prepupal stage. Pupal ecdysis occurs on day W4, and the newly formed pupa is designated as day P0. Subsequent days of pupal development are counted as P1–P20. Adult eclosion occurs around stage P20, and subsequent days of adult life are counted as A0 (freshly eclosed) to A3 (3 days after adult eclosion). Larvae and pupae were staged according to the criteria described by Jindra et al. (1997) and Schwartz and Truman (1983). The criteria involve changes in structures that are either superficial or readily visible through the pupal cuticle under a dissecting microscope.

Western blot analysis

SDS-PAGE. Brains of various insect species [*M. sexta* (various developmental stages), *Drosophila melanogaster* (white puparia), *Gryllus bimaculatus* (adult), *Leucophaea maderae* (adult), *Schistocerca gregaria* (adult)] and pieces of cortices of rat (*Rattus norvegicus*) and mouse (*Mus musculus*) were homogenized in phosphate-buffered saline containing protease and phosphatase inhibitors [0.5 mM Na_3VO_4, 0.5 mM phenylmethylsulfonyl fluoride (PMSF); both Sigma-Aldrich Chemie GmbH, Munich, Germany]. After determination of protein concentration of the samples after Bradford (1976), homogenates were diluted to an equal total protein concentration of 7.5 μg or 6 μg/9 μl. To 9 μl of homogenate 9 μl reducing sample buffer, pH 6.8, was added. After 3 minutes of boiling, samples were loaded onto a discontinuous sodium dodecyl sulfate (SDS)-polyacrylamide gel (3% stacking gel, 12.5% running gel) in a Bio-Rad Mini-Protean 3 chamber and blotted to a nitrocellulose membrane (Hybond C; Amersham Biosciences Europe, Freiburg, Germany), with a semidry transfer apparatus (Bio-Rad, Hercules, CA). To control the efficiency of protein transfer, nitrocellulose membranes were stained after transfer with Ponceau red.

Immunoblot. Blots were blocked in phosphate-buffered saline (PBS; 0.1 M, pH 7.4) containing 0.05% Tween 20, 1% casein, and 20% fetal bovine serum for 1 hour and then incubated with the SOD antiserum (S2; 1:1,000) at 4°C overnight in PBS (0.1 M) containing 0.05% Tween 20 (PBST). For preabsorption, the SOD antibody (Kostron et al., 1999; 1:1,000) was incubated for 30 minutes at room temperature with 100 μmol of synthetic peptide. Blots were washed three times for 10 minutes each in PBST, 1% Triton X-100, and 1% SDS. A horseradish peroxidase (HRP)-coupled goat anti-rabbit secondary antiserum (1:5,000; Jackson Immunoresearch, West Grove, PA) was applied for 1 hour at room temperature in PBST. After being washed, blots were developed by chemiluminescence using Supersignal from Pierce (Rockford, IL) according to the instructions of the manufacturer. The signal was visualized with X-ray films (Fuji), digitized, and further processed in Adobe Photoshop 6.0 and Microsoft's PowerPoint.

Immunocytochemistry

We used as primary antibodies a polyclonal anti-SOD antiserum from rabbit (S2; 1:10,000; Kostron et al., 1999), a polyclonal anti-cGMP antiserum from sheep (1:4,000; kindly provided by Jan DeVente, Limburg University, Maastricht, The Netherlands), a polyclonal anti-sGCα1 against *M. sexta* soluble guanylyl cyclase α1 subunit from goat at 1:5,000, and a monoclonal anti-synaptotagmin antibody from mouse (1:2,500; kindly provided by Kaushiki Menon, Caltech). Specificity controls for the anti-SOD, anti-cGMP, anti-sGCα1, and anti-synaptotagmin antibodies were described by Kostron et al. (1999), De Vente et al. (1987), Ewer et al. (1994), Gibson and Nighorn (2000), and Dubuque et al. (2001). The following secondary antibodies (from Jackson Immunoresearch) were used at a dilution of 1:300: HRP-coupled goat anti-rabbit, Cy2-coupled donkey anti-sheep, Cy3-coupled donkey/goat anti-rabbit/goat, and Cy5-coupled donkey/goat anti-mouse antibodies.

After dissection in cold saline (Weevers, 1966) or PBS, brains of various developmental stages of *M. sexta* were fixed in 4% PBS-buffered formaldehyde, pH 7.4, for 2 hours at room temperature or overnight at 4°C. After fixation, brains were embedded in gelatin/albumin, post-fixed overnight in 8% buffered formaldehyde, and cut at 40 μm with a Vibratome (Leica VT 1000S) in the frontal plane. Vibratome sections were rinsed in 0.1 M Tris HCl (Sigma-Aldrich Chemie GmbH)/0.3 M NaCl (SST; pH 7.4) with 0.1% Triton X-100 (SST-TX 0.1) for 1 hour at room temperature, then preincubated for another hour with 5% normal goat or donkey serum (Jackson Immunoresearch) in SST-TX 0.5. Primary antibodies were then diluted in SST-TX 0.5 with 1% normal goat or donkey serum. After incubation with the primary and secondary antisera, sections were rinsed three times over 30 minutes in SST-TX 0.1 at room temperature.

For multiple labeling, the cGMP antibody and the corresponding secondary antibody were used first, and afterward anti-SOD and anti-synaptotagmin antisera were applied simultaneously and also after washing of the corresponding secondary antisera. HRP was visualized on free-floating sections with 3.3′-diaminobenzidine (DAB; Sigma-Aldrich Chemie GmbH) by using the glucose oxidase (Sigma-Aldrich Chemie GmbH) technique according to Watson and Burrows (1981). Sections were mounted on chromalaun/gelatin-coated coverslips and then dehydrated in ethanol, cleared in xylene, and mounted in Entellan (Merck, Darmstadt, Germany). Alternatively, brains after the fixation process (see above) were dehydrated through a graded ethanol series and xylene and then embedded in Paraplast Plus (Monoject Scientific, St. Louis, MO). Sections were cut at 8 μm on a rotatory microtome, dried on gelatin-coated slides, deparaffinized, and rehydrated. The anti-SOD antiserum (S2) was used at a dilution of 1:1,000, the secondary goat anti-rabbit HRP-coupled antiserum at 1:300. Incubation times and solutions were used as described above. Visualization of HRP was carried out with DAB as a chromophore as described in detail by Homberg et al. (1987). Afterward, sections were rehydrated in ethanol and mounted in Entellan. Sections were photographed with a Polaroid DMCe digital camera mounted on a Zeiss Axioscope, imported into Adobe Photoshop 6.0, and annotated in Microsoft PowerPoint. Doubly or triply fluorescence-labeled sections were analyzed with a confocal laser scanning microscope (Leica TCS-SP2).

Detection of programmed neuronal death

To detect cells undergoing programmed cell death, a detection kit from Roche Diagnostics (Mannheim, Germany) was used. The kit is based on the terminal deoxynucleotidyl tranferase (TdT)-mediated dUTP nick-end labeling (TUNEL) method and was used according to the manufacturer's manual. Vibratome sections of *Manduca* brains were produced as described above. Sections were rinsed three times over 30 minutes in SST-TX 0.1 at room temperature and then incubated in wellplates (Falcon) for 15 minutes in 500 μl reaction buffer (pH 6.6) containing 200 mM Na-cacodylate, 25 mM Tris HCl, 1 mM cobaltic chloride, 0.25 mg/ml bovine serum albumin, and 0.1% Triton X. The reaction buffer was then exchanged with 225 μl of the reaction solution (120 μl distilled water, 30 μl reaction buffer; ×5), 67.5 μl of the kit's nucleotide solution (TMR red dUTP), and 7.5 μl of the kit's enzyme solution (TdT). Controls were processed without the enzyme solution. Sections were incubated in the dark in the reaction buffer for 4 hours at 37°C on a shaker. Then, sections were rinsed four times for 15 minutes each in PBS TX 0.1 and then for a further 10 minutes in PBS alone. Sections were then arranged on coverslips, dehydrated, cleared, and mounted in Entellan as described above. TMR red was visualized by using a confocal laser scanning microscope (Leica TCS-SP2). TUNEL labeling was combined with antibody staining by performing the protocol described above after finishing the TUNEL reaction. Secondary antibodies coupled to Cy2 or Cy5 were used because they can be distinguished from the red fluorescence of TMR red.

RESULTS

Western blot analysis

The antibody used in this study was produced against residues 40–55 of SOD of *Drosophila virilis* (Kostron et al., 1999). Residues 40–55 represent a highly conserved sequence of SODs of all animal species so far examined (Kostron et al., 1999). In this region, SOD binds a copper molecule that is involved in electron transport (Fridovich, 1986).

To demonstrate the specificity of this antiserum and to show its ability to detect SOD from different species, we performed Western blots from SDS gels run under reducing conditions and loaded with brain tissue homogenates of various insects [*M. sexta*, *D. melanogaster* (white puparia), *Leucophaea maderae*, *Schistocerca gregaria*, *Gryllus bimaculatus*] and two mammalian species (mouse, rat). In all lanes, one prominent protein band at about 15 kDa was labeled (Fig. 1A,B). Preadsorption of the SOD antiserum with the synthetic 15-residue peptide abolished all labeling in the Western blots (Fig. 1A) and in the sectioned material (not shown), demonstrating that the antiserum used specifically recognizes the monomeric form of SOD throughout all species tested. The SOD antiserum detects the 15-kDa band in all developmental stages, from fifth-instar larva during metamorphosis to the adult (Fig. 1C).

Developmental pattern of SOD-like immunoreactivity

During metamorphosis the SOD antiserum transiently labeled many cells virtually in every part of the brain of *M. sexta*, including neurons in the optic lobes, antennal lobes, central brain, and subesophageal ganglion (Figs. 2–4). During all phases of development, the antiserum labeled neurons and, rarely, glial material (Fig. 5). The antiserum labeled only the neuronal cell bodies and, in a few cases, small parts of the neurite leaving the cell body (Figs. 2–5).

With only the somata labeled, it was difficult to identify neurons unequivocally by comparison with published data and also to recognize the same neurons in different stages, in that neighboring cell bodies might gain SOD immunoreactivity (-ir). In spite of these ambiguities, some cells and especially cell groups could reliably be identified. For example, in the antennal and optic lobes, the time course of the SOD-ir could be followed throughout late larval and pupal development (Fig. 6). The results show that, in the brain areas investigated, most neurons expressed SOD-ir through distinct developmental stages, whereas some neurons showed expression at all times examined. We focused on those cell types that showed changes in expression.

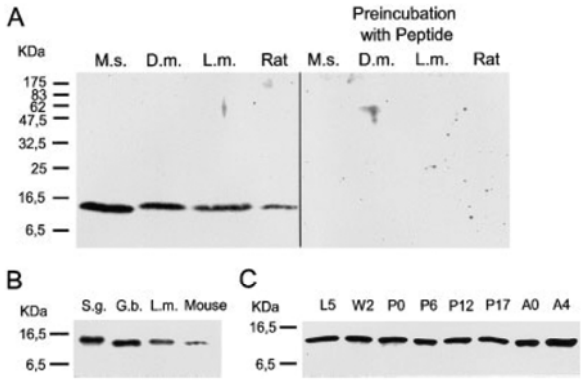

Fig. 1. Immunodetection of SOD in nervous system homogenates of various animals with the anti-SOD antiserum. **A:** The SOD antiserum labels a unique protein band at about 15 kDa in blots of polyacrylamide gels loaded with brain homogenates of *Manduca sexta* adult (M.s.), *Drosophila melanogaster* white puparia (D.m.), *Leucophaea maderae* adult (L.m.), and rat cortex (rat) and run under reducing conditions. After preincubation with synthetic peptide, no signal was detectable in either of the homogenates. **B:** Brain homogenates of further species tested show a labeled protein band at about 15 kDa. *Schistocerca gregaria* adult (S.g.), *Gryllus bimaculatus* adult (G.b.), cortex of mouse brain (mouse). **C:** SOD immunodetection during *M. sexta* brain metamorphosis. The approximately 15-kDa band was detected in all developmental stages. L5, fifth-instar larva; W2, 2-day-old wandering larva (fifth instar); P0–P17, pupal stages of *M. sexta*; A0, freshly eclosed adult; A4, 4-day-old adult. In A and B, single brains were homogenized and a total of 7.5 μg protein/lane was loaded; in C, four brains for each stage were homogenized and a total of 6 μg protein/lane was loaded.

Neurons in the antennal lobe

We followed SOD-ir in the lateral (LC) and the medial cell group (MC; defined by Homberg et al., 1988) in the antennal lobe. The neurons with somata in these two groups together with the olfactory receptor neurons are the principal neurons organizing the glomeruli. These neurons are present from early pupal stage P3, and the cell groups can be unequivocally identified during metamorphosis (Hildebrand et al., 1997). In any given stage from P7 to adulthood, the SOD antiserum labels cell bodies in LC (n = 35; Figs. 2, 6). However, in the different developmental stages, the number of cells stained, and the staining intensity within those cells, varied appreciably (Fig. 2). We distinguished, according to the pattern of SOD-ir in LC, five metamorphic phases. In the first phase from P0 up to P6, no SOD-ir was detected in the LC (n = 16). In a second phase from P7 to P11/12, most cells of LC were labeled with the SOD antiserum (n = 14). The labeled cells in this second phase can be distinguished into two groups: a smaller group consisting of very robustly stained cells and a much larger group of very faintly stained cells (Fig. 2A). Double labeling with the cGMP antiserum showed that all cGMP-immunoreactive cells were also intensely labeled with the anti-SOD antiserum (Fig. 2A–C). As previously described (Schachtner et al., 1999), the cGMP-immunoreactive cells in the LC belong to the group of local neurons, and they account during this time of development for about one-tenth of the approximately 1,000 cells in the LC. In a third metamorphic phase spanning stages P12/13 up to adult eclosion, faint SOD-ir appeared in small populations of cells in LC (n = 15). In a fourth phase starting at adult eclosion (A0) and ending on adult day one to two (A1/2), scattered cells with robust and weakly labeled SOD-ir were found among nonlabeled cells (n = 8; Fig. 2C,D). A subpopulation of the weak SOD-immunoreactive neurons showed additional staining with an antiserum against the α1 subunit of NO-sensitive guanylyl cyclase (sGCα1; Fig. 2D; Gibson and Nighorn, 2000). Somata with strong SOD-ir never colocalized sGCα1-ir (double arrowheads in Fig. 2D). Most of the approximately 60 sGCα1-positive cells (n = 6 antennal lobes) in A0 and A1 showed weak SOD-ir, and there are only a few sGCα1-immunoreactive cells that do not stain with the SOD antiserum (arrowhead in Fig. 2D). Phase five, lasting from A3 until the death of the animal, showed no SOD-ir in the LC (n = 5).

In neurons of the MC, SOD-ir can be detected in a window ranging from stage P13/14 up to P17 (n = 12; Figs. 2, 6). SOD-ir in MC resembles that seen in LC in the same developmental window (phase three): very faint SOD-ir occurring in varying numbers of cells (Fig. 2B).

Neurons in the optic lobes

SOD-ir was detectable in cell cortices of the developing optic neuropils from the onset of the wandering stage (W0; n = 5). At, or shortly before, pupal ecdysis (P0), SOD-ir disappeared and was again detectable at P1 (n = 3). SOD-ir was never observed in the optic anlagen themselves (Fig. 3A). The optic anlagen house the neuroblasts of the optic lobes (for details, see Discussion). From P3/4 on, cell bodies of the appearing three optic neuropils are labeled with the SOD antiserum (layers 1–3 in Fig. 3C). Most cells distal to the lobula and the medulla neuropil showed strong SOD-ir from P3/4 to P11 (n = 23). After P11 and up to adult eclosion, a few weakly labeled somata could occasionally be seen in these areas (n = 19). Somata of the medulla cortex belonging to the medulla stripe (MS; Schachtner et al., 1998) showed intense SOD labeling from P5 to P15 (n = 30). In the outer optic neuropil, the lamina, presumptive second-order visual neurons (lamina monopolar cells) robustly labeled with the SOD antiserum from P3/4 up to P8 (n = 18). From P9–P11, a few weakly labeled somata could be found in this area (n = 7).

Another group of neurons that showed SOD-ir from P1/2 into adulthood was located at the base of the lobula and medulla (bLM neurons; Fig. 3B,D–F,J; n = 57). These neurons with cell bodies of varying sizes probably belong to neurons innervating the lobula and medulla (Homberg and Hildebrand, 1989; Homberg et al., 1990). Among these neurons were a ventrally and a dorsally located cell cluster consisting of somata (VCl and DCl, respectively, both consisting of a few hundred cells) that transiently elevated cGMP levels during optic lobe development (VCl from P4 to P15; DCl from P7 to P15; Schachtner et al., 1998). Double-labeling experiments in a P8 optic lobe showed that most if not all of the DCL neurons colocalize SOD-ir and cGMP-ir (Fig. 3F). In the VCl, a group of the cGMP-positive cells did not stain with the SOD antiserum (Fig. 3E). Additionally, cell bodies of similar size in close proximity to VCl and DCl showed equally strong SOD-ir but no cGMP-ir (Fig. 3E,F).

From P2/3 up to P15, two to four large cell bodies located dorsoposteriorly in the vicinity between the optic lobe and central brain showed robust SOD-ir (Fig. 3C; n = 35). From P15 to adult eclosion, these putative lobula giant neurons (Homberg and Hildebrand, 1994) showed only

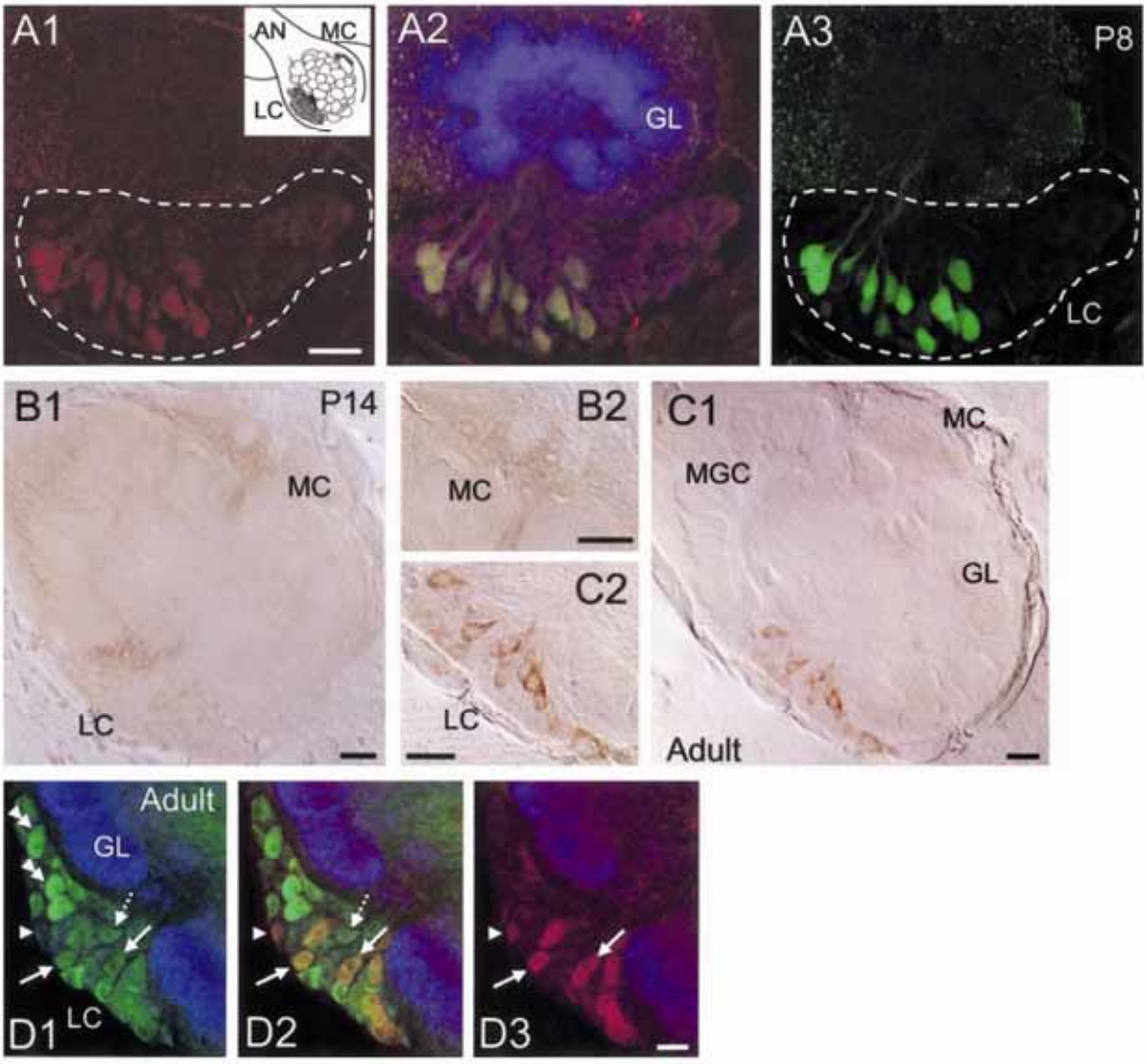

Fig. 2. SOD-ir during antennal lobe (AL) development and colocalization with cGMP-ir and sGCα1-ir. **A1–A3:** Triple labeling in a P8 AL: SOD-ir (red), synaptotagmin-ir (blue), cGMP-ir (green). SOD-ir in the lateral cell group (LC; encircled) is colocalized with cGMP-ir. Other cells of LC are not labeled or are weakly labeled with the SOD antiserum. A2 is a merged image of A1 and A3. Synaptotagmin-ir in A2 labels the developing glomeruli. Inset in A1 shows the orientation of the AL. **B:** SOD-ir in P14 AL is weak in LC and in the medial cell group (MC). B2 shows a magnification of the MC in B1. **C:** SOD-ir in adult ALs is restricted to LC. C2 shows a magnification of LC in C1. Note the differences in the intensities of the labeled cell bodies. **D1–D3:** Triple labeling in an adult AL: SOD-ir (green), synaptotagmin-ir (blue), sGCα1-ir (red). SOD-ir and sGCα1-ir colocalize in LC cell bodies weakly labeled with the SOD antiserum (solid arrows). The strongest SOD-ir labeled cells never show sGCα1-ir (double arrowheads). The arrowhead marks a cell body labeled with sGCα1-ir but not SOD-ir. The dotted arrow points to a weakly SOD-positive cell that is not labeled with sGCα1. Vibratome 40 μm sections, frontal views. Scale bars = 40 μm in A,D, 50 μm in B,C.

weak SOD-ir (Fig. 3H, n = 10). This changed again to very robust SOD labeling at adult eclosion (Figs. 3I, 6; n = 3). In the adult, SOD-ir colocalized in these cells and in most of the bLM neurons with sGCα1 labeling (Fig. 3I,J). SOD-ir in the putative lobula giant neurons and in the bLM neurons faded from adult day 1 (A1) and was then absent in A3 (Fig. 6) and older animals (n = 7).

Neurons in the central brain

In the central brain, many neurons label with the SOD antiserum (Figs. 4, 6). We choose four different groups to follow through pupal development, according to their location. 1) Large cell bodies in the pars intercerebralis (PI) showed robust SOD-ir already in the late fifth larval in-

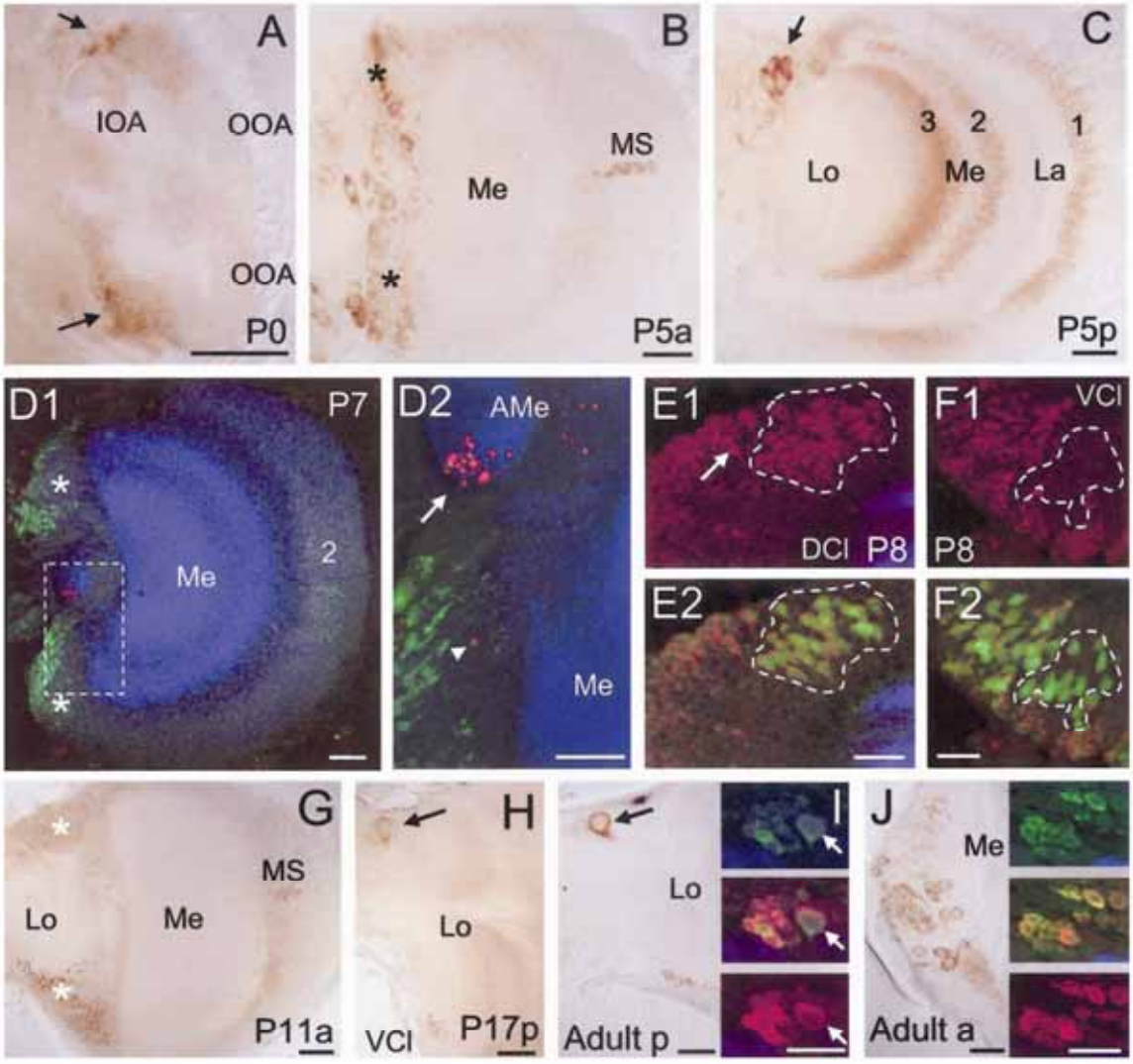

Fig. 3. SOD-ir during optic lobe development. **A:** At P0, cells in the optic lobe cortex stain with the SOD antiserum (arrows). Neuroblasts in the inner (IOA) and outer optic anlagen (OOA) are not labeled. **B,C:** Anterior (P5a) and posterior (P5p) sections of a P5 OL. **B:** Cell bodies of variable size at the basis of lobula and medulla (bLM neurons) showed robust SOD-ir (asterisks). **C:** Most of the neurons surrounding the three optic neuropils (layers 1–3) show strong SOD-ir; neurons in layer 1 are mainly putative lamina monopolar cells. The arrow marks putative lobula giant (LoG) neurons. **D:** Triple labeling with the SOD antiserum (green), synaptotagmin antibody (blue), and TUNEL labeling (red) in a P7 optic lobe. D2 is a magnification of the boxed area in D1 showing dying neuroblasts of the IOA (arrow) and one TUNEL-labeled nucleus in the area of the medulla (arrowhead) of an SOD-negative cell. **E,F:** Triple immunolabeling in the dorsal (DCl; E) and the ventral (VCl; F) cell cluster of a P8 optic lobe; SOD-ir (red), Syt-ir (blue), cGMP-ir (green). **E1,2:** In DCl all cGMP-ir cells show SOD-ir (stippled area). There are additional SOD-immunoreactive neurons that do not label with the cGMP antiserum (left of the encircled area). **F1,2:** In VCl, many SOD-positive neurons colabel with cGMP-ir. The encircled area shows VCl neurons that label only with the cGMP antiserum. **G:** Anterior section of a P11 OL showing SOD-ir in the ventral and dorsal cell cortices of lobula and medulla. **H:** P17. Faint SOD-ir in LoG neurons (arrow) and some cells in the area of VCl. **I,J:** Robust SOD-ir in adult OL can be found in putative LoG neurons (arrows) and in many bLM neurons. **Upper insets** in I and J show SOD-ir (green), **lower insets** sGCα1-ir, and **middle insets** an overlay of both. a, Anterior; b, posterior; La, lamina. Vibratome 40 μm sections, frontal views. Scale bars = 80 μm in A–C,D1,G–J, 40 μm in D2,E,F.

star (the earliest time we looked at SOD-ir) up to adulthood (Fig. 4E; n = 66). It is uncertain whether the same cells were labeled in the different developmental stages. 2) In the Kenyon cells of the mushroom bodies (MB) in *M. sexta*, transient SOD-ir can be divided into five phases. In a first phase from P0 to P3/4, a few Kenyon cells weakly labeled with the SOD antiserum (n = 6). A second phase lasting for about 12–13 days (from P3/4 to P15/16) is

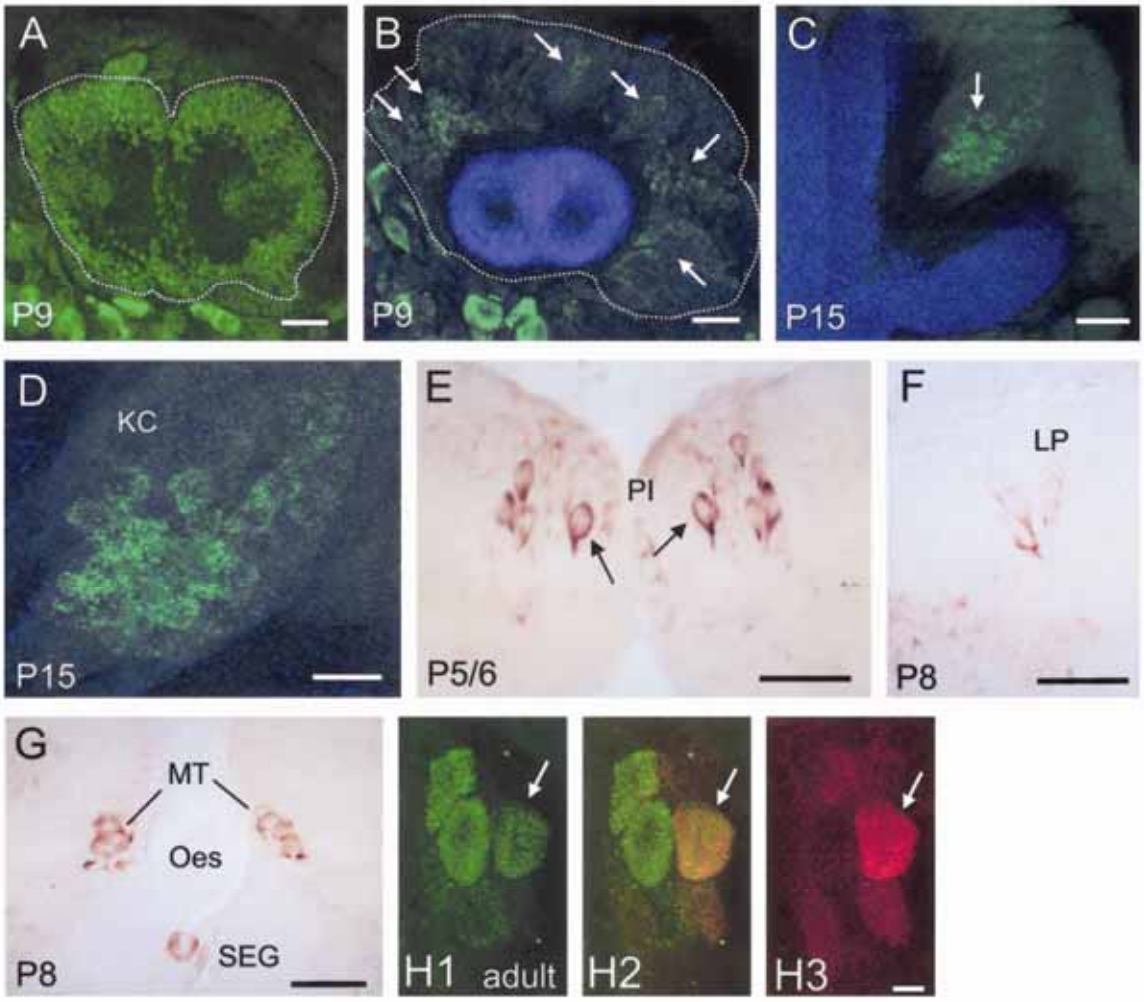

Fig. 4. SOD-ir during central brain development. **A–D:** SOD-ir (green) in the Kenyon cells (KC) of the mushroom bodies. Blue, synatotagmin-ir. A and B are sections of the same mushroom body of a P9 pupal brain, A being posterior to B. Typically for a more posterior view (A), most if not all of the Kenyon cells of the MB (encircled) are labeled with the antiserum. Typically for a more anterior position (B), single clusters of KC show SOD-ir (MB area encircled). **C:** A typical cluster of SOD-immunoreactive KC (arrow) in a P15 pupa. **D:** shows a magnification of the KC cluster in C. **E:** Strong transient SOD-ir in large cell bodies (arrows) of the pars intercerebralis (PI) in a P5/6 pupa. **F:** SOD-ir in large neurons in the lateral dorsal protocerebrum (LP) at stage P8. **G:** Labeling of large neurons in the medial tritocerebrum (MT neurons) and in large cells at the anterior dorsal end of the subesophageal ganglion (SEG). **H:** Double labeling of cells in the medial tritocerebrum of an adult animal with SOD-ir in green (H1) and sGCα1-ir in red (H3). H2 shows an overlay of both. Vibratome sections, 40 μm frontal views. Scale bars = 40 μm in A–C, 100 μm in E–G, 20 μm in D,H.

characterized by robust SOD-ir in many Kenyon cells (Fig. 4A–D). Most if not all Kenyon cells in the posterior part of the MB showed staining in many of these preparations (23 of 26; Fig. 4A). In the middle and anterior portions of the MB, SOD-ir occurred only in clustered groups of Kenyon cells (Fig. 4B). In a third phase spanning the rest of pupal development, no or very weak overall SOD-ir could be detected (n = 7). The fourth phase spans the time right after adult eclosion (A0) when most if not all Kenyon cells showed SOD-ir (not shown; n = 3). In a fifth phase starting from 1-day-old adults (A1) and lasting probably for the rest of the animals' lives, no SOD-ir occurs in Kenyon cells (n = 10). 3) In the lateral protocerebrum, a prominent group of two to four large cell bodies stains positively with the SOD antiserum from L5 up to adulthood (Fig. 4F; n = 64). As for the PI neurons, we are uncertain whether the same cells were labeled in the different developmental stages. 4) In the median tritocerebrum, on each side of the gut opening, a group of two to six large SOD-immunoreactive cell bodies could be followed from P0 up to adulthood (Fig. 4G; n = 58). In the adult, at least one of these cells could be double labeled with the anti-sGCα1 antiserum (Fig. 4H). It connects both tritocerebral areas via a neurite crossing the midline above the gut opening

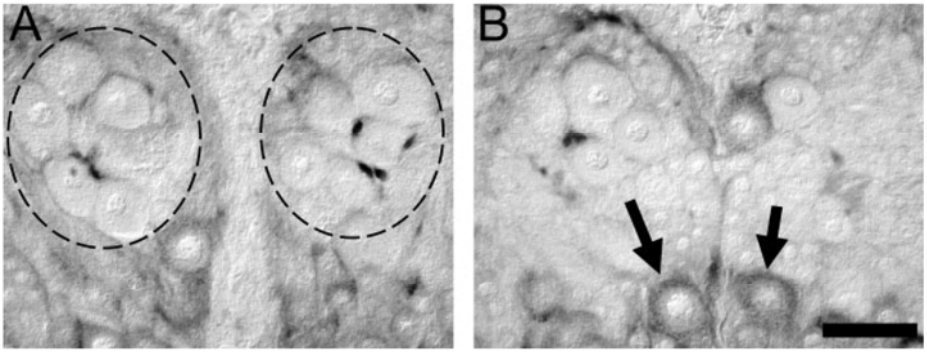

Fig. 5. SOD staining in the dorsal protocerebrum of a P10 pupa. **A:** SOD-ir in prospective glial material between neuronal cells (encircled regions). **B:** Typical staining of neuronal cell bodies (arrows). Paraffin sections (10 μm), frontal views. Scale bar = 50 μm.

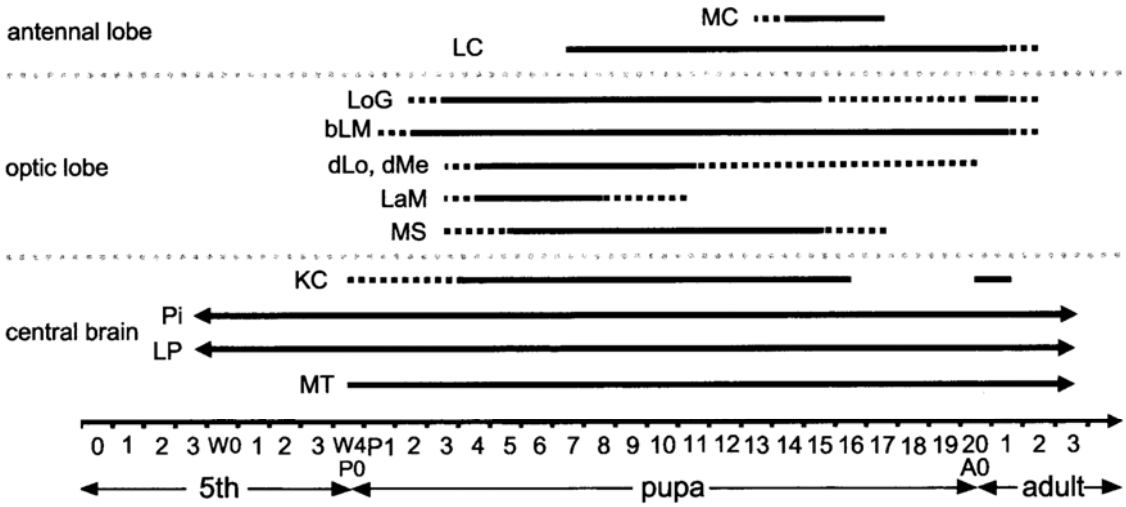

Fig. 6. Diagram showing transient SOD-ir in identified neurons or neuron populations during *M. sexta* development. For further explanation, see text. bLM, Neurons at the basis of lamina and medulla; dLo and dMe, neurons distal to the lobula and medulla, respectively; KC, Kenyon cells; LaM, lamina monopolar cells; LC, lateral cell group of the antennal lobe; LoG, lobula giant neuron; LP, lateral protocerebrum cells; MC, medial cell group of the antennal lobe; MS, medulla stripe; MT, median tritocerebrum cells; Pi, pars intercerebralis cells; W0, start of wandering behavior; W4, 4 days after start of wandering. Scale is days of larval and pupal development.

(Schachtner et al., 1998). Inducible cGMP-ir in this MT cell started with the prepupal stage (W2) and lasted up to pupal stage P14.

TUNEL labeling

TUNEL labeling (Gavrielli et al., 1992) is an indicator for programmed cell death. Cells that undergo programmed cell death may not show any SOD-ir. We found many cells with TUNEL-labeled nuclei throughout development in the optic lobes but only a few cells in the central brain. We never detected TUNEL-labeled nuclei in the antennal lobe neurons. In the optic lobes, TUNEL-labeled nuclei could be detected from W0 all over the optic lobe cortices and from P7 in neuroblasts of the inner and outer optic anlagen. Figure 3D shows an example of putative dying neuroblasts of the inner optic anlagen. Colocalization of SOD-ir in cells with TUNEL-labeled nuclei was never observed.

DISCUSSION

SOD

Cu/Zn SOD, the cytoplasmic form of SOD, together with catalase converts superoxide to molecular oxygen and water (Fridovich, 1986; Oury et al., 1999). *Drosophila* mutants lacking SOD and/or catalase showed greatly reduced life spans (Mackay and Bewley, 1989; Phillips et al., 1989; Kwiatowski et al., 1991; Orr et al., 1992; Griswold et al., 1993). *Drosophila* that overexpressed either Cu/Zn or Mn SOD (another form of SOD in mitochondria) showed longer life spans than were observed in wild-type animals

(Sun and Tower, 1999; Sun et al., 2002; Mockett et al., 2002). Both types of mutants strongly support the idea that both SODs are crucial for protection against ROS.

In this work, we used a previously produced specific antiserum against Cu/Zn SOD from *D. virilis* (Kostron et al., 1999). The antiserum was made against a sequence of 15 amino acids located in the highly conserved copper-binding domain of the enzyme. As expected, we could label SOD in various species, including mammals and insects (Fig. 1). In adult Wistar rats as well as in adult *Periplaneta americana*, SOD seems to be restricted mainly to glial cells (Kostron et al., 1999; Lindenau et al., 2000). We observed Cu/Zn SOD-ir mainly in neurons during metamorphosis and in the early adult and found some SOD-ir in glial-like material (Fig. 5). SOD labeling in rats and *P. americana* was never examined during development, so transient neuronal expression of SOD during development cannot be excluded. We observed SOD-ir in *M. sexta* only in very few brain neurons of adult animals older than 3 days. Similar to the case in *Manduca*, in *Drosophila* little or no SOD seems to be expressed in the adult, as shown by reporter gene expression, suggesting that other antioxidants might compensate for this deficit (Klichko et al., 1999).

SOD expression during metamorphosis

During all stages of pupal development, and in the early adult, many cells in the brain were labeled with the SOD antiserum. Three days after adult eclosion, the SOD signal ceased totally in most of the neurons but was detectable in some of the cell types in the central brain (Fig. 6). We followed SOD-ir in only a small number of neurons or neuron groups that we could reliably identify and investigated the immunoreactivity only during defined developmental stages. The majority of other neurons that did or did not show SOD-ir during these stages was not examined further. The unlabeled cells may express SOD at some point of their development that we did not investigate. Alternatively, other protection mechanisms against ROS might play a role in those cells.

Antennal lobe development

The antennal lobe is the first integration center for odor information in the insect brain. Building blocks of the antennal lobe are the glomeruli, which in *M. sexta* are formed during metamorphosis (Oland and Tolbert, 1996). Each glomerulus consists of thousands of synapses between olfactory receptor neurons, local and projection neurons. A wave of synaptogenesis starts at stage P7/8 at the sexual-specific glomeruli near the entrance of the antennal nerve and ends within the most basally located glomeruli of the antennal lobe. This synaptogenic wave over the antennal lobe ends at P12/13, with glomeruli showing a dense synaptic pattern (Dubuque et al., 2001). From P13, the glomeruli increase in size, but the number of synapses seems not to increase until adult eclosion (Tolbert et al., 1983; Tolbert, 1989).

Most neurons of the antennal lobe belong to the group of adult-specific neurons, which are all born by P3 (Hildebrand et al., 1997). At stage P7/8, when the antennal lobe neurons start to form synapses and the glomeruli mature, neurons in the lateral cell group became SOD immunoreactive (Fig. 2). As shown by double-labeling experiments with an antiserum against cGMP, the most robust SOD-ir was expressed by neurons showing cGMP-ir (Fig. 2). Previously we showed that, between P7/8 and P12/13, 50–100 local interneurons in the lateral cell group are rendered cGMP positive (Schachtner et al., 1998). cGMP elevation in these neurons seems to be due mainly to NO-sensitive soluble guanylyl cyclases (Schachtner et al., 1999; Schachtner, unpublished data) with NO likely released from the olfactory receptor neurons (Gibson and Nighorn, 2000). SOD-ir especially in these local interneurons suggests that SOD may play a role in prolonging NO signaling. Preliminary results obtained from pharmacological experiments during this time of development suggest a role of the NO/cGMP signaling pathway in enhancing synaptogenesis in the developing glomeruli (Schachtner, 2001; Schachtner, unpublished results).

Malun et al. (1994) showed that uniglomerular projection neurons (uPNs) of the medial cell group are the first antennal lobe neurons contacting olfactory receptor neurons before glomeruli formation. These uPNs, as with the olfactory receptor neurons, are able to form tufted dendritic trees and are thought to play a role in building the glomerular template (Malun et al., 1994). During this period of extensive dendritic and axonal growth, no SOD-ir was detected in the medial cell group. We hypothesize that SOD-ir may be a correlate of metabolic activity. The correlation of SOD-ir with synaptogenesis in the lateral cell group may indicate that the metabolism is particularly high during massive synapse formation, i.e., higher than during axonal and dendritic growth. Thus, SOD-ir might be primarily a marker for neuronal maturation, but not for neuronal growth. Then, the cells of the lateral cell group might be more involved in building up the primary glomerular network than the medial cell group between P7/8 and P11/12.

The pattern of SOD-ir in the lateral cell group changed dramatically after adult eclosion, with some somata showing robust SOD-ir, comparable to the signal intensity observed earlier in development, whereas others showing weak staining. Double-labeling experiments with the sGCα1 antiserum revealed colocalization of sGCα1-ir in a subpopulation of the weakly SOD-immunoreactive cells (Fig. 2D). As discussed earlier, SOD in the sGCα1-positive cells might help to increase the longevity of NO. The function of the strongly SOD-positive neurons is unknown, but it is possible that they undergo a last refinement of synaptic connectivity in the glomeruli to cope with odor information provided from the olfactory receptor neurons.

Optic lobe development

The optic lobe is a highly retinotopically ordered neuropil that consists of three distinguishable neuropils, most distally the lamina, followed by the medulla and the lobula complex, the anterior lobula, and the posterior lobula plate (Bullock and Horridge, 1965; Strausfeld, 1976; Homberg, 1994). In *M. sexta*, the optic anlagen, from which the optic lobes develop, are readily apparent in the third larval instar (Monsma and Booker 1996a). We never observed SOD-ir in the optic anlagen, which contrasts with findings of Klichko et al. (1999), who found reporter gene expression of the promoter domain of Cu/Zn SOD in proliferating neuroblasts of *D. melanogaster*. Because we began to test for SOD labeling only after the beginning of wandering behavior (W0), we may have missed a large part of the neuroblasts' proliferation period, during which they could have transiently expressed SOD. On the other

hand, the neuroblasts of the optic anlagen produce ganglion mother cells far into pupal development, and programmed cell death of these neuroblasts does not occur before P7 (Monsma and Booker, 1996a; Champlin and Truman, 1998). Also, we never found SOD-ir in neuroblasts undergoing programmed cell death (shown by using the TUNEL technique; Fig. 3D), supporting the hypothesis that such cells do not up-regulate SOD for protection against ROS.

In addition, it has been reported that neuroblasts of the optic anlagen in *M. sexta* contain NO synthase (NOS) from the beginning of the fifth larval instar, which is the time when the neuroblasts shift to produce optic lobe neurons (Champlin and Truman 2000). Because no SOD-ir could be found, we suggest that the neuroblasts in the optic anlagen in *M. sexta* are protected against ROS by mechanisms other than SOD.

From stage P3/4 onward, most somata located distally and adjacent to the three developing optic neuropils showed strong SOD-ir. This pattern of SOD-ir terminated first (at P8) in the cells distal to the lamina, then in the cells distal to the medulla, followed by cells in the lobula complex (at P11). Most, if not all, of the cells distal to the lamina are probably lamina monopolar cells that form the lamina neuropil together with the axons of the photoreceptor cells. The cells distal to medulla and lobula complex, together with the neurons at the basis of the lamina and medulla (bLM neurons) form the other two optic lobe neuropils. Because of their location, the bLM neurons may develop into tangential neurons of the medulla and lobula complex and into the putative lobula giant neurons LoGs (Homberg and Hildebrand, 1994). They are SOD positive from P1/2 to A1/2.

If our hypothesis is correct that SOD expression is an indicator for synaptogenesis, the network assemblage of the three optic lobes would start at P1/2 in the medulla and lobula complex (at P1/2) with the bLM neurons and the LoGs. One to two days later (at P3/4), cells distal to all three optic lobe neuropils are recruited. Because of their position, these cells are very likely to be involved in building the columnar organization of the optic neuropils, which is finished at P11. According to the time course of the SOD-ir of the cells distal to the lamina (lamina monopolar cells), the assemblage of lamina neuropil would start at P3/4 and would then mostly be finished at P8, whereas some areas might be under construction up to P11, insofar as some scattered cells showed SOD-ir up to this time.

The involvement of NO in optic lobe development has been shown for *Drosophila* and *Manduca* (Gibbs and Truman, 1998; Champlin and Truman, 2000). In *Manduca*, NO in concert with the developmental hormone 20-hydroxyecdysone, but without the involvement of cGMP, stops neuroblast proliferation (Champlin and Truman 2000). Previously, we described neurons of the group of bLM neurons that transiently enhanced their cGMP levels during optic lobe metamorphosis (Schachtner et al. 1998). These ventral (VCl) and dorsal (DCl) cluster neurons show additional immunolabeling with the antiserum against the α1 subunit of soluble guanylyl cyclase (Schachtner et al., 1998; Schachtner, unpublished results). Transient cGMP increases in both cell clusters occur in the developmental window of robust SOD-ir within the bLM neurons. Double labeling with the SOD and cGMP antisera revealed that in the VCl all neurons showing cGMP-ir colocalized SOD-ir, whereas in the DCl not all neurons positive for cGMP contained SOD-ir. Thus, in most neurons of the two cell clusters, SOD might support NO signaling during development by protecting NO from being degraded by ROS.

Other brain areas

In the central brain, many neurons showed SOD-ir. We followed four groups of cells during metamorphosis, which occupied similar positions in the brain throughout development. As for the Kenyon cells and the large medial tritocerebral neurons (MT neurons; Schachtner et al., 1998), we are confident that we described SOD-ir pattern in the same neurons throughout metamorphosis. As far the neurons in the pars intercerebralis (PI neurons) and the neurons in the lateral protocerebrum (LP neurons) are concerned, we might have described different neurons with changing SOD-ir in a similar location.

The Kenyon cells are the principal neurons of the mushroom bodies (MBs; Heisenberg, 1998; Menzel, 2001). The cell bodies of the Kenyon cells reside in the calyx area, with their neurites projecting into the calyx and their axons projecting into the pedunculus and the various lobes (Schürmann, 1987; Homberg, 1994). In contrast to the antennal and optic lobes, the MBs exist already in the larva. In *Drosophila*, the MBs are built from four neuroblasts per hemisphere, which continue to proliferate from the embryo up to late metamorphosis (Ito and Hotta, 1992). In other insects, the proliferation phase continues into adulthood, underscoring the plasticity of this brain structure (Cayre et al., 1996). Elegant experiments in *Drosophila* showed that Kenyon cell axons degenerate during the first 24 hours of pupal development and that pruning of new imaginal fibers occurs later, while new cell bodies are added steadily (Technau and Heisenberg, 1982).

In *M. sexta* development of the MB has so far not been studied. Transient SOD-ir in their Kenyon cells can be divided into five phases. If SOD expression is an indicator for synapse formation, the changes in SOD-ir during phases 1–5 may reflect the dynamics of the MB network assemblage as described above for *Drosophila*.

In conclusion, our data indicate changes of SOD-ir during larval, pupal, and adult development in *M. sexta*, suggesting that SOD may be an important defense mechanism against ROS in developing brain structures. This conclusion is supported by the fact that SOD-ir appears transiently during phases of neuronal maturation. SOD may protect cells from oxidative stress, so the presence of SOD-ir during synapse formation might indicate that, during this event, the buildup of ROSs is greater than during other developmental events, i.e., axon growth and dendrite formation. However, we also found neurons in the pars intercerebralis, in the lateral protocerebrum, and in the median tritocerebrum, which showed SOD-ir during long periods. These cells have large diameters and are in areas in which many neurosecretory cells are located. SOD-ir within these cells might thus reflect high metabolic rates in terms of producing and releasing peptides or biogenic amines. Additionally, many NO-sensitive neurons showed SOD-ir, suggesting a role of SOD in securing NO action.

ACKNOWLEDGMENTS

We thank Dr. Jan DeVente for kindly providing the cGMP antiserum and Dr. Kaushiki P. Menon for providing the synaptotagmin antibody. We also thank Drs. Uwe Homberg, Achim Paululat, and Martin Klingenspor for providing the various brain tissues and Lucia Lennarts and Sabine Jesberg for their expert technical assistance.

LITERATURE CITED

Ames BN, Shigenaga MK, Hagen TM. 1993. Oxidants, antioxidants, and the degenerative diseases of aging. Proc Natl Acad Sci USA 90:7915–7922.

Beckman JS, Koppenol WH. 1996. Nitric oxide, superoxide, and peroxynitrite: the good, the bad, and ugly. Am J Physiol 271:1424–1437.

Beckman JS, Estevez AG, Crow JP, Barbeito L. 2001. Superoxide dismutase and the death of motoneurons in ALS. Trends Neurosci 24:15–20.

Bradford MM. 1976. A rapid and sensitive method for the quantitation of microgram quantities of protein utilizing the principle of protein-dye binding. Anal Biochem 72:248–254.

Bullock TH, Horridge GA. 1965. Structure and function in the nervous system of invertebrates, vol II. San Francisco: W.H. Freeman.

Cayre M, Strambi C, Charpin P, Augier R, Meyer MR, Edwards JS, Strambi A. 1996. Neurogenesis in adult insect mushroom bodies. J Comp Neurol 371:300–310.

Champlin DT, Truman JW. 1998. Ecdysteroid control of cell proliferation during optic lobe neurogenesis in the moth *Manduca sexta*. Development 125:269–277.

Champlin DT, Truman JW. 2000. Ecdysteroid coordinates optic lobe neurogenesis via a nitric oxide signaling pathway. Development 127:3543–3551.

DeVente J, Steinbusch HWM, Schipper J. 1987. A new approach to immunocytochemistry of 3′5′-cyclic guanosine monophosphate: preparation, specificity, and initial application of a new antiserum against formaldehyde fixed 3′5′-cyclic guanosine monophosphate. Neuroscience 22:361–373.

Draizen TA, Ewer J, Robinow S. 1999. Genetic and hormonal regulation of the death of peptidergic neurons in the *Drosophila* central nervous system. J Neurobiol 38:455–465.

Dubuque SH, Schachtner J, Nighorn AJ, Menon KP, Zinn K, Tolbert LP. 2001. Immunolocalization of synaptotagmin for the study of synapses in the developing antennal lobe of *Manduca sexta*. J Comp Neurol 441:277–287.

Ewer J, De VJ, Truman JW. 1994. Neuropeptide induction of cyclic GMP increases in the insect CNS: resolution at the level of single identifiable neurons. J Neurosci 14:7704–7712.

Ewer J, Wang CM, Klukas KA, Mesce KA, Truman JW, Fahrbach SE. 1998. Programmed cell death of identified peptidergic neurons involved in ecdysis behavior in the moth, *Manduca sexta*. J Neurobiol 37:265–280.

Floyd RA. 1999. Antioxidants, oxidative stress, and degenerative neurological disorders. Proc Soc Exp Biol Med 222:236–245.

Frayn KN. 1996. Metabolic regulation. In: Snell K, editor. Frontiers in metabolism, 1 series. Portland: Portland Press.

Fridovich I. 1986. Superoxide dismutases. Adv Enzymol Relat Areas Mol Biol 58:61–97.

Fridovich I. 1999. Fundamental aspects of reactive oxygen species, or what's the matter with oxygen? Ann N Y Acad Sci 893:13–18.

Friebe A, Schultz G, Koesling D. 1998. Stimulation of soluble guanylate cyclase by superoxide dismutase is mediated by NO. Biochem J 335: 527–531.

Gavrielli Y, Sherman Y, Ben-Sasson SA. 1992. Identification of programmed cell death in situ via specific labeling of nuclear DNA fragmentation. J Cell Biol 119:493–501.

Gibbs SM, Truman JW. 1998. Nitric oxide and cyclic GMP regulate retinal patterning in the optic lobe of *Drosophila*. Neuron 20:83–93.

Gibson NJ, Nighorn A. 2000. Expression of nitric oxide synthase and soluble guanylyl cyclase in the developing olfactory system of *Manduca sexta*. J Comp Neurol 422:191–205.

Griswold CM, Matthews AL, Bewley KE, Mahaffey JW. 1993. Molecular characterization and rescue of acatalasemic mutants of *Drosophila melanogaster*. Genetics 134:781–788.

Heisenberg M. 1998. What do the mushroom bodies do for the insect brain? An introduction. Learn Mem 5:1–10.

Hildebrand JG, Rössler W, Tolbert LP. 1997. Postembryonic development of the olfactory system in the moth *Manduca sexta*: primary-afferent control of glomerular development. Cell Dev Biol 8:163–170.

Homberg U. 1994. Distribution of neurotransmitters in the insect brain. Stuttgart: Gustav Fischer Verlag.

Homberg U, Hildebrand JG. 1989. Serotonin immunoreactivity in the optic lobes of the sphinx moth *Manduca sexta* and colocalisation with FMRF-amide and SCPB immunoreactivity. J Comp Neurol 288:243–253.

Homberg U, Hildebrand JG. 1994. Postembryonic development of gamma-aminobutyric acid-like immunoreactivity in the brain of the sphinx moth *Manduca sexta*. J Comp Neurol 339:132–149.

Homberg U, Kingan TG, Hildebrand JG. 1987. Immunocytochemistry of GABA in the brain and suboesophageal ganglion of *Manduca sexta*. Cell Tissue Res 248:1–24.

Homberg U, Montague RA, Hildebrand JG. 1988. Anatomy of antennocerebral pathways in the brain of the sphinx moth *Manduca sexta*. Cell Tissue Res 254:255–281.

Homberg U, Kingan TG, Hildebrand JG. 1990. Distribution of FMRF amide-like immunoreactivity in the brain and suboesophageal ganglion of the sphinx moth *Manduca sexta* and colocalization with SCPB-, BPP-, and GABA-like immunoreactivity. Cell Tissue Res 259:401–419.

Ito K, Hotta Y. 1992. Proliferation pattern of postembryonic neuroblasts in the brain of *Drosophila melanogaster*. Dev Biol 149:134–148.

Jindra M, Huang JY, Malone F, Asahina M, Riddiford LM. 1997. Identification of mRNA developmental profiles of two ultraspiracle isoforms in the epidermis and wings of *Manduca sexta*. Insect Mol Biol 6:41–53.

Klichko VI, Radyuk SN, Orr WC. 1999. CuZn-SOD promoter-driven expression in the *Drosophila* central nervous system. Neurobiol Aging 20:537–543.

Kostron B, Market D, Kellermann J, Carter CE, Honegger HW. 1999. Antisera against *Periplaneta americana* Cu,Zn-superoxide dismutase (SOD): separation of the neurohormone bursicon from SOD, and immunodetection of SOD in the central nervous system. Insect Biochem Mol Biol 29:861–871.

Ku DK. 1996. Nitric oxide and nitric oxide donor-induced relaxation. In: Packer L, editor. Methods in enzymology, vol 269, part B. New York: Academic Press. p 107–119.

Kwiatowski J, Skarecky D, Tyler R, Pascual M, Ayala FJ. 1991. A truncated P element is inserted in the transcribed region of the Cu,Zn SOD gene of an SOD "null" strain of *Drosophila melanogaster*. Free Radic Res Commun 12/13:429–435.

Lindenau J, Noack H, Possel H, Asayama K, Wolf G. 2000. Cellular distribution of superoxide dismutases in the rat CNS. Glia 29:25–34.

Linton S, Davies MJ, Dean RT. 2001. Protein oxidation and ageing. Exp Gerontol 36:1503–1518.

Mackay WJ, Bewley GC. 1989. The genetics of catalase in *Drosophila melanogaster*: isolation and characterization of acatalasemic mutants. Genetics 122:643–652.

Maier CM, Chan PH. 2002. Role of superoxide dismutases in oxidative damage and neurodegenerative disorders. Neuroscientist 8:323–334.

Malun D, Oland LA, Tolbert LP. 1994. Uniglomerular projection neurons participate in early development of olfactory glomeruli in the moth *Manduca sexta*. J Comp Neurol 350:1–22.

Markesbery WR. 1997. Oxidative stress hypothesis in Alzheimer's disease. Free Radic Biol Med 23:134–147.

Menzel R. 2001. Searching for the memory trace in a mini-brain, the honeybee. Learn Mem 8:53–62.

Mockett RJ, Orr WC, Sohal RS. 2002. Overexpression of Cu,ZnSOD and MnSOD in transgenic *Drosophila*. Methods Enzymol 349:213–220.

Monsma SA, Booker R. 1996a. Genesis of the adult retina and outer optic lobes of the moth, *Manduca sexta*. I. Patterns of proliferation and cell death. J Comp Neurol 367:10–20.

Monsma SA, Booker R. 1996b. Genesis of the adult retina and outer optic lobes of the moth *Manduca sexta*. II. Effects of deafferentiation and developmental hormone manipulation. J Comp Neurol 367:21–35.

Nagy IZ. 2001. On the true role of oxygen free radicals in the living state, aging, and degenerative disorders. Ann N Y Acad Sci 928:187–199.

Okado-Matsumoto A, Fridovich I. 2002. Amyotrophic lateral sclerosis: a proposed mechanism. Proc Natl Acad Sci USA 99:9010–9014.

Oland LA, Tolbert LP. 1996. Multiple factors shape development of olfactory glomeruli: insights from an insect model system. J Neurobiol 30:92–109.

Oland LA, Tolbert LP. 1998. Glomerulus development in the absence of a set of mitral-like neurons in the insect olfactory lobe. J Neurobiol 36:41–52.

Orr WC, Arnold LA, Sohal RS. 1992. Relationship between catalase activity, life span and some parameters associated with antioxidant defenses in *Drosophila melanogaster*. Mech Ageing Dev 63:287–296.

Oury TD, Card JP, Klann E. 1999. Localization of extracellular superoxide dismutase in adult mouse brain. Brain Res 850:96–103.

Phillips JP, Campbell SD, Michaud D, Charbonneau M, Hilliker AJ. 1989. Null mutation of copper/zinc superoxide dismutase in *Drosophila* confers hypersensitivity to paraquat and reduced longevity. Proc Natl Acad Sci USA 86:2761–2765.

Schachtner J. 2001. Involvement of NO and cGMP in antennal lobe development of the sphinx moth *Manduca sexta*. Soc Neurosci Abstr 27: 140.6.

Schachtner J, Klaassen L, Truman JW. 1998. Metamorphic control of cyclic guanosine monophosphate expression in the nervous system of the tobacco hornworm, *Manduca sexta*. J Comp Neurol 396:238–252.

Schachtner J, Homberg U, Truman JW. 1999. Regulation of cyclic GMP elevation in the developing antennal lobe of the sphinx moth, *Manduca sexta*. J Neurobiol 41:359–375.

Schürmann F-W. 1987. The architecture of the mushroom bodies and related neuropiles in the insect brain. In: Gupta AP, editor. Arthropod brain: its evolution, development, structure and functions. New York: John Wiley & Sons. p 231–264.

Schwartz LM, Truman JW. 1983. Hormonal control of rates of metamorphic development in the tobacco hornworm *Manduca sexta*. Dev Biol 99:103–114.

Sohal RS. 1993. The free radical hypothesis of aging: an appraisal of the current status. Aging 5:3–17.

Stadtman ER. 2001. Protein oxidation in aging and age-related diseases. Ann N Y Acad Sci 928:22–38.

Strausfeld NJ. 1976. Atlas of an insect brain. Berlin: Springer.

Sun J, Tower J. 1999. FLP recombinase-mediated induction of Cu/Zn-superoxide dismutase transgene expression can extend the life span of adult *Drosophila melanogaster* flies. Mol Cell Biol 19:216–228.

Sun J, Folk D, Bradley TJ, Tower J. 2002. Induced overexpression of mitochondrial Mn-superoxide dismutase extends the life span of adult *Drosophila melanogaster*. Genetics 161:661–672.

Tabner BJ, Turnbull S, El Agnaf O, Allsop D. 2001. Production of reactive oxygen species from aggregating proteins implicated in Alzheimer's disease, Parkinson's disease and other neurodegenerative diseases. Curr Top Med Chem 1:507–517.

Technau G, Heisenberg M. 1982. Neural reorganization during metamorphosis of the corpora pedunculata in *Drosophila melanogaster*. Nature 295:405–407.

Tolbert LP. 1989. Afferent axons from the antenna influence number and placement of intrinsic synapses in the antennal lobe of *Manduca sexta*. Synapse 3:83–95.

Tolbert LP, Matsumoto SG, Hildebrand JG. 1983. Development of synapses in the antennal lobes of the moth *Manduca sexta* during metamorphosis. J Neurosci 3:1158–1175.

Truman JW. 1996. Metamorphosis of the insect nervous system. In: Gilbert LI, editor. Metamorphosis: postembryonic reprogramming of gene expression in amphibian and insect cells. Orlando, FL: Academic Press. p 283–320.

Watson AHD, Burrows M. 1981. Input and output synapses on identified motor neurones of a locust revealed by intracellular injection of horseradish peroxidase. Cell Tissue Res 215:325–332.

Weeks JC. 1999. Steroid hormones, dendritic remodeling and neuronal death: insights from insect metamorphosis. Brain Behav Evol 54:51–60.

Weevers RD. 1966. A lepidopteran saline: the effects of inorganic cation concentrations on sensory reflex and motor responses in a herbivorous insect. J Exp Biol 44:163–176.

CHAPTER II:

Transient nitric oxide-dependent cyclic GMP formation is involved in metamorphic development of the antennal lobes of *Manduca sexta*

Transient nitric oxide-dependent cGMP formation is involved in metamorphic development of the antennal lobes of *Manduca sexta*

Wolf Huetteroth[1], Sandra Utz[1], Patrick Winterhagen[1,2], Jan de Vente[3], Uli Müller[4], Alan Nighorn[5], Joachim Schachtner[1]*

[1]Fachbereich Biologie, Tierphysiologie, Philipps-Universität Marburg, Karl-von-Frisch-Str. 8, 35032 Marburg, Germany

[2]Department of Agriculture, Missouri State University, Mountain Grove, MO 65711, USA

[3]European Graduate School of Neuroscience (EURON), Psychiatry and Neuropsychology, University of Maastricht, Maastricht, The Netherlands

[4]Department 8.3-Biosciences-Zoology and Physiology, Saarland University, Postfach 151150, 66041 Saarbruecken, Germany

[5]Arizona Research Laboratories, Division of Neurobiology, University of Arizona, Tucson, AZ 85721, USA

ABSTRACT: The paired antennal lobes (ALs) of the sphinx moth *Manduca sexta* serve as a well-established model for studying development of the primary integration centers for odor information in the brain. In this study, we report evidence for an involvement of the nitric oxide / soluble guanylyl cyclase (sGC) / cGMP-pathway in the formation of the olfactory glomeruli in the developing ALs of *M. sexta*. Antennal nerve stimulation and pharmacological manipulation revealed approximately 20 local neurons of the developing AL exhibiting a transient NO and sGC-dependent rise in cGMP-immunoreactivity. The activity dependent and transient cGMP-increases in this defined set of local neurons are restricted to the phase of glomerulus formation which is characterized by massive synaptogenesis. Injection of ODQ, a specific inhibitor of sGC at the beginning of the phase of glomeruli formation resulted in the decrease of synaptic vesicle protein synaptotagmin as revealed by immunocytochemistry and ELISA. Although 3D-reconstructions did not show obvious differences in the morphology of glomeruli, we postulate an involvement of the NO/cGMP signaling pathway in the generation or strengthening of synapses during formation of the olfactory glomeruli.
Keywords: insect, olfactory system, metamorphosis, soluble guanylyl cyclase, nitric oxide

INTRODUCTION

The antennal lobes (ALs) of the sphinx moth *Manduca sexta* serve as a well-established model for studying the neuronal development of the primary integration centers for odor information in the brain (Tolbert et al. 2004). ALs of insects compare to olfactory bulbs of vertebrates by sharing their principal morphological organization into so-called olfactory glomeruli, but also by a number of basic physiological properties with respect to information processing (Hildebrand and Shepherd 1997, Strausfeld and Hildebrand 1999, Eisthen 2002).

In *M. sexta* the ALs arise during metamorphosis, a hormonally-controlled postembryonic period lasting about three weeks. During this time, the whole brain undergoes reorganization and small larval antennal centers develop into the adult ALs. AL development in *M. sexta* can be roughly divided into three phases (Oland and Tolbert 1996, Dubuque et al. 2001). The preparation phase (phase I) lasts about seven to eight days beginning at pupal formation. It includes the birth of all AL neurons, the arrival of the axons of the olfactory receptor neurons (ORNs) in the ALs, and the formation of the protoglomeruli, the sites where the glomeruli

Correspondence to:
J. Schachtner (schachtner@staff.uni-marburg.de)
Contract grant sponsor:
DFG; contract grant number: Scha 678/3-3.

form during phase II. The glomerulus formation phase (phase II) lasts about five days and is characterized by massive synaptogenesis between the involved neurons. It is assumed, that during phase II a basic network of synaptic contacts within and between the glomeruli is established, which ensures the principal correlation of in- and output components of the AL (Dubuque et al. 2001). In contrast to phase II, in phase III, which lasts about eight days up to adult eclosion, little synaptogenesis occurs. During this last phase, the glomeruli grow in size between 40 and 130% (Huetteroth and Schachtner 2005), probably because of the increasing neurite diameters, and the synaptic wiring in the glomeruli is thought to undergo further refinement and maturation (Tolbert et al. 1983, Tolbert 1989, Dubuque et al. 2001). None of the neurons of the ALs undergo programmed cell death during phases I to III (Schachtner et al. 2004a), and, as all neurons of the ALs are born early in AL development (Hildebrand et al. 1997), the neuronal composition of the ALs does not change throughout the formation of the ALs.

Studies in vertebrates and invertebrates on the role of nitric oxide (NO) during nervous system development find this gaseous signaling molecule mainly associated with three phases: Proliferation and differentiation, axonal growth, and synaptogenesis (Truman et al. 1996, Davies 2000, Gibbs 2003, Krumenacker and Murad 2006, Bicker 2001, 2007, Garthwaite 2008). On one hand, these findings suggest a variety of mechanisms for NO action, but also a high evolutionary conservation of NO function during nervous system development. The most prominent target for NO is the soluble guanylyl cyclase which typically consists of an α- and β-subunit. This enzyme forms the second messenger cGMP which in turn has several targets in the cell, including e.g. cGMP dependent ion channels, kinases, and phosphodiesterases (Boehning and Snyder 2003, Friebe and Koesling 2003, Koesling et al. 2004, Bicker 2007, Garthwaite 2008).

Previous studies showed that during metamorphic development of the *M. sexta* AL NO-synthase (NOS) and soluble guanylyl cyclase (sGC) are expressed in different cell populations: while NOS is constitutively produced in ORNs as soon as they grow into the developing AL, sGC is expressed in AL neurons (Gibson and Nighorn 2000). Studies on cGMP regulation in the developing *M. sexta* AL revealed a transient cGMP upregulation mainly in a subset of local interneurons (LNs) during the phase of glomerulus formation, which at least partly seemed to be induced via activity dependent release of NO from the ORNs (Schachtner et al. 1998, 1999). Spontaneous activity from the antennal nerve can be recorded extracellularly from stage P7 onwards (Oland et al. 1996). Together this led to the hypothesis that NO release triggered by spontaneous activity of the ORNs induces cGMP upregulation in LNs during the phase of glomerulus formation (phase II, Schachtner et al. 1999).

In the present study we characterize the cells that respond to NO during development and show that this transient NO-derived cGMP is likely to play a role in the synapse formation necessary for the appropriate development of the antennal lobe.

MATERIALS AND METHODS

Animals

Animals (*Manduca sexta*; Lepidoptera: Sphingidae) were kept in walk-in environmental chambers at 26°C under a long-day photoperiod (L:D = 17:7) and were fed with artificial diet as described before (Bell and Joachim 1978). Under this regime pupal development from the day of pupal ecdysis (P0) until adult eclosion (A0) takes approximately 21 days, each day corresponding to a pupal stage (P0-P20). Pupae were staged according to criteria described in Jindra et al. (1997) and Schwartz and Truman (1983). The criteria involve changes in structures that are either superficial or readily visible through the pupal cuticle under a dissecting microscope.

Dissection and Preparation

Depending on the dissection protocol, different results regarding cGMP-immunoreactivity were achieved. Therefore we distinguish between the following two methods: 1. Standard: Animals were chilled on ice for 2-15 minutes followed by dissection of the brain under cold saline (Weevers 1966). The whole dissection lasted 10 minutes; subsequently brains were transferred to cold phosphate-buffered 4 % formaldehyde solution (4% FA; PBS 0.01 M, pH 7). 2. Antennal stimulation: Animals were chilled on ice for 2 minutes. The right antennal pocket was opened and the developing antenna was cut (according to Schachtner et al. 1999). After leaving the pupa 10 min at room temperature it was transferred into cold phosphate-buffered 4 % formaldehyde solution (4% FA; PBS 0,01 M, pH 7) for 30 min to stop further stimulation; to ensure better perfusion of fixative, immediately before prefixation, thorax and head were opened dorsally and the proboscis pocket was cut off. In the deantennation experiment (Fig. 4) the complete left antennal pocket with antennal anlage was twisted off immediately after pupa formation (P0) before the dissection was performed as described. Since the cuticle at early P0 still was green and soft, the wound closed by itself and did not have to be sealed artificially.

Immunocytochemistry

After dissection, all brains were fixed for 2-4 h at room temperature or overnight at 4° C. Brains were then processed following immunocytochemistry

standard protocols for vibrating microtome sections (see Utz and Schachtner 2005) or for wholemounts (see Huetteroth and Schachtner 2005). The following primary antisera were used: Polyclonal anti-cGMP antibody raised in sheep (1:4000 on vibratome sections, 1:100.000 in wholemounts; kindly provided by Dr. Jan de Vente, University of Utrecht, The Netherlands). The antibody was produced by immunization of sheep with cGMP-coupled Glutathione-S-Transferase fusion protein and subsequent purification. Specificity controls for the anti-cGMP antiserum is described in de Vente et al. (1987, 1996) and for *M. sexta* tissue in Ewer et al. (1994) and in Schachtner et al. (1999). Polyclonal goat antiserum against the α1 subunit of *M. sexta* soluble guanylyl cyclase (anti-MsGCα1; 1:5000; Bethyl Laboratories Inc., Montgomery, TX, USA). For immunization, the amino acid sequence c-IREALKDYGIGQANSTDVDT was used (amino acids 676-695 of the MsGCα1 protein, which are specific for this guanylyl cyclase). In western blots of adult *M. sexta* brain homogenate the antiserum detects a single band of approximately 78 KDa which matches approximately the predicted size of 78,4 KDa (Collmann et al. 2004). In adult *M. sexta* this antiserum labels cells in the lateral, medial, and anterior cell groups of the AL (Wilson et al. 2007). Preadsorption tests were performed in western blots and in tissue sections and exhibited no nonspecific interactions (Collmann et al., 2004). Polyclonal rabbit antiserum against the atypical receptor guanylyl cyclase I from *M. sexta* (anti-MsGC-I; 1:2000; kindly provided by Dr. David Morton, Simpson et al. 1999). In western blots of adult *M. sexta* the antiserum detects a single band of approximately 55 KDa; preadsorption of the antiserum with MsGC-I GST fusion protein abolished all staining in tissue sections (Nighorn et al. 2001). Monoclonal anti-synaptotagmin antibody from mouse (anti-syt; 1:4000; kindly provided by Dr. K. Menon, Division of Biology, Caltech, CA, USA), which was either used to label neuropilar structures for better orientation, or to detect optical density differences in sections of ODQ-treated animals; its specificity in *M. sexta* tissue was described in Dubuque et al. (2001). Monoclonal anti-synapsin antibody from mouse (anti-syn; 1:100; kindly provided by Dr. E Buchner, University of Würzburg, Germany). Since the anti-synaptotagmin antiserum could not be obtained in the same quality as before, we switched to the anti-synapsin antiserum to label neuropilar structures. Specificity of this antibody for *M. sexta* nervous tissue was published previously (Utz et al. 2008). Polyclonal antiserum against the transmembrane form of *M. sexta* fasciclin II, raised in guinea pig (anti-TM-MFasII; 1:2000; kindly provided by Dr. P.F. Copenhaver, OHSU, OR, USA). The staining was used to identify remaining sensory AL inputs in early deantennated animals (Fig. 4). The specificity of the anti-TM-MFasII antiserum for *M. sexta* tissue was shown in western blots (Wright and Copenhaver 2000). As secondary antibodies we used affinity-purified Cy2-, Cy3-, and Cy5-coupled anti-sheep, anti-mouse, anti-rabbit, anti-guinea pig, or anti-goat antisera, either raised in goat or donkey (all Jackson ImmunoResearch, Westgrove, PA, USA).

Pharmacology

Based on external markers pupae at stage P7 or P9 were chilled on ice for 2 min, followed by an injection of 15 µl ODQ (1H-[1,2,4]Oxadiazolo[4,3-a]quinoxalin-1-one; 1 mM; Alexis) per g body weight, dissolved in saline (Ephrussi and Beadle 1936) with 1 % DMSO into the dorsolateral thorax. ODQ has been shown to be a potent blocker of soluble guanylyl cyclase in a variety of animals (Garthwaite et al. 1995, Friebe and Koesling 2003, for a review in insects see e.g. Bicker 2007) including *M. sexta* nervous tissue (e.g. Zayas and Trimmer 2007). Control animals were injected with saline + 1 % DMSO only. All injections were performed as described in Schachtner et al. (1999).

Cell counting

Immunostained sections or wholemounts were scanned with a confocal laserscan microscope (Leica TCS SP2). In sections, counting of cells was performed as described before (Schachtner et al. 2004b); in short, up to 35 cells were counted by individual identification, higher numbers were corrected for double counts across sections using a correction factor (Abercrombie 1946). In wholemounts we used the 3D visualization software Amira 4.1 (Mercury Computer Systems, San Diego, CA, USA) to count cell numbers and to reconstruct identified single glomeruli (see below). Further processing of pictures was done with Adobe Photoshop 6.0 - CS2 and Corel Draw 12, diagrams were created with Microsoft Excel 2003. Statistical calculations were performed in Microsoft Excel 2003 or Statistica ’99.

Measurement and comparison of optical densities

Brains were dissected and fixed according to the standard protocol described above. Frontal 40 µm thick brains sections of gelatine embedded brains were obtained with a vibrating microtome (Leica, Bensheim, Germany). Sections were then labeled with the anti synaptotagmin antiserum (1:4000) and subsequently with a secondary HRP coupled goat anti-mouse antibody (1:300, Jackson ImmunoResearch). HRP was visualized on free-floating sections with 3,3′-diaminobenzidine tetrahydrochloride (DAB; Sigma-Aldrich) by using the glucose oxidase (Sigma-Aldrich) technique according to Watson and Burrows (1981). Sections were mounted on chromalum/gelatin-coated microscope slides, dehydrated in ethanol, cleared in xylene, and mounted in entellan (Merck, Darmstadt, Germany).

For a detailed description of the staining procedure refer to Utz et al. (2005). Each experimental series which was equally treated in terms of the staining procedure and incubation times consisted of two vehicle (saline according to Ephrussi and Beadle, 1936) injected animals (controls) and three to five ODQ injected animals. Animals were injected at stage P7 and dissected at stage P12/13. At stage P12/13 each AL consisted of a series of 10 frontal 40 µm sections. These sections were digitized with a Polaroid DMCe camera (8bit grayscale, 800x600 dpi resolution) mounted on a Zeiss Axioscope (objective x20 oil). Settings of the microscope (light intensity) and of the Polaroid camera software were standardized for all sections. Analysis of sections was then performed offline with Scion Image (Scion Corporation). Analysis was performed by first defining a threshold gray level which best described the stained glomeruli in sections of control animals. Gray value threshold was usually either 75 or 85. This procedure assured that only labeled pixel within glomeruli were used for optical density analysis. The same threshold was used for analyzing sections of all ALs of an experimental series including controls and ODQ treated animals. Next the mean gray value over all ten sections of an AL was calculated and then multiplied with all pixels with gray values above threshold. This integrated optical density (IOD) gives a measure of mean optical density combined with an area covered by pixels over the gray value threshold. To estimate the difference between IODs of ALs of control and treated animals the ratios between IODs of ODQ injected and the control animals were formed. This ratio of integrated density (RIOD) is 1 if the IODs of treated and control animals are equal, is >1 if the IOD of the treated animals is larger than the IOD of the control, and is <1 if the IOD of the treated is smaller than of the control animal.

Determination of protein amounts by ELISA

To compare relative amounts of synaptotagmin protein in defined brain areas (AL, optic lobes, central brain) between ODQ and vehicle injected animals we used the ELISA (Enzyme-linked immunosorbent assay) technique. The protocol used was modified from Fiala et al. (1999). ODQ and vehicle injections were performed as described above at P7, brains were dissected out at P12/13, and subsequently each brain was separated in two AL, two optic lobes and the rest of the brain (central brain). Three series of experiments were performed. One consisted of five ODQ injected and five controls, the other two experimental series consisted each of three ODQ and three vehicle injected animals. For each series, the different brain parts were separately collected on ice in 100 µl buffer containing 0.1 M PBS / 1 mM EGTA (ethylene glycol-bis(2- aminoethyl ether)

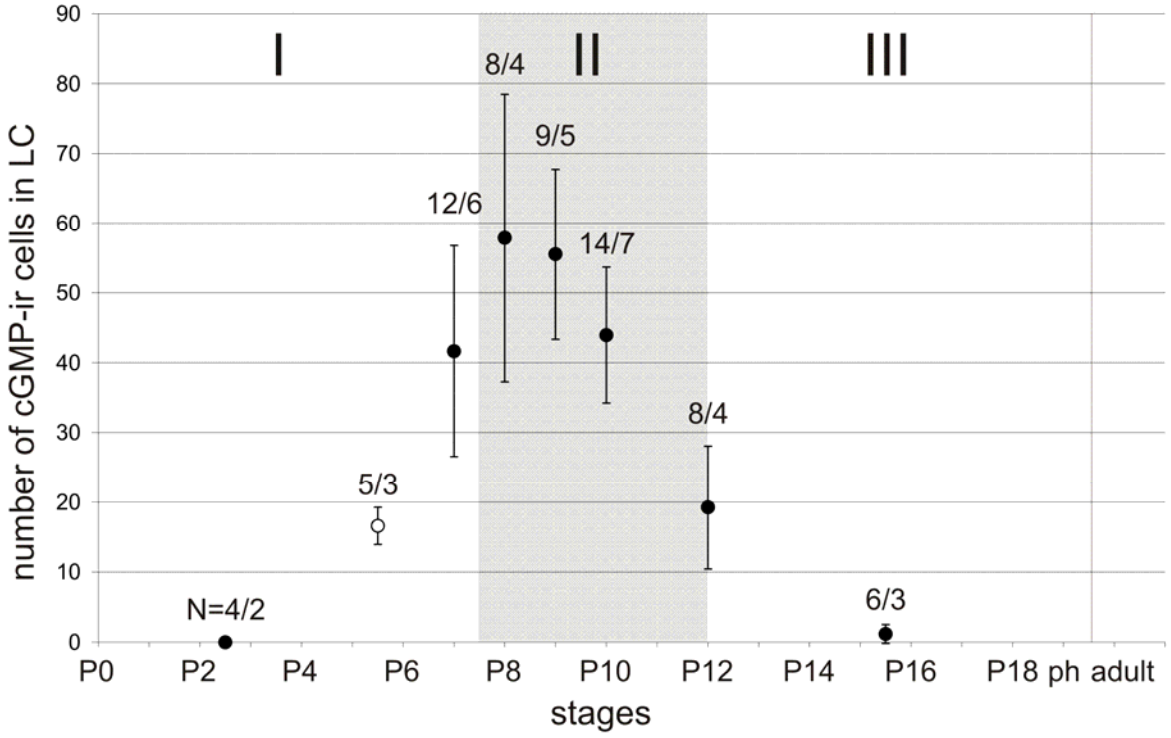

Figure 1 Numbers of cGMP-immunoreactive cells in the lateral cell group at different times of pupal development. After standard dissection, the ALs exhibited a characteristic, stage-dependent number of cGMP-ir cells in LC. At the earliest stage examined (P2/3), no cGMP-immunoreactivity was found. At P5/6, some weakly stained cells appeared (open circle). Shortly before phase II of AL development, robust staining occurred in about 40 cells (P7). cGMP-ir cell number peaks at P8 (about 60 cells) and subsequently declines during the following stages (P9: 55; P10: 45; P12: 20). In the middle of phase III at stage P15/16, almost no cGMP-ir cells are left in the lateral cell group. N = ALs/animals, bars = standard deviation.

N,N,N´,N´-tetraacetic acid; Sigma-Aldrich). Samples were homogenized for a couple of seconds in an ultrasonic bath (Elma Transsonic 310, Hans Schmidbauer GmbH & Co. KG, Singen, Germany) and frozen in liquid oxygen over night. After thawing, polystyrene micro titre plates (Falcon) were coated with the samples for 1 hour at 4°C. Coating was performed by diluting samples (1:1) within a row of 4 wells, starting with 100 µl of the different homogenates using identical protein concentrations. Buffer only served as negative control. Protein concentration of each homogenate was calculated by comparison with a linear calibration curve, performed with a commercially available kit (BCA Protein Assay Kit, Pierce). After short wash with PBS, the remaining binding sites in each well were blocked for 1 hr with 300 µl PBS containing 1 % BSA at 4°C. After washing with PBS, the primary antibody (anti-syt 1:4000) was applied (50 µl/well) over night at 4°C. After washing (3 x 5 min PBS) the secondary antibody (biotin-conjugated goat anti-mouse IgG (H+L); Jackson ImmunoResearch) was added (100 µl/well; 1:4000 in 0.1 M / 1 % BSA) for 1.5 hours at room temperature, followed by another washing step (3 x 5 min PBS). Then the enzyme solution (alkaline phophatase-conjugated streptavidin; Jackson ImmunoResearch) was added (100 µl / well; 1:10.000 in 1% BSA in PBS) for 40 min at room temperature. After washing (3 x 5 min PBS), the substrate (4-nitrophenylphosphate disodium salt hexahydrate; AppliChem) was added (200 µl / well; 1 mM in RXN-buffer: 0.1 M TrisHCl / 1 mM MgCl; pH 8.8). For color development plates were incubated at 36 °C for at least 1.5 hours. The absorbance was measured spectrophotometrically at 420 nm using a microplate reader (Dynatech MR4000). For analysis, the absorbance of control measurements has been set to 100 %. Percentage deviation of the absorbance of corresponding dilutions of the treated samples was then quantified. The average of two dilutions / sample has been taken into account for analysis. Only measurements from the same micro titre plate were compared.

3D reconstruction

Before injection appropriate pairs of animals with similar weight and developmental stage were chosen and injected with ODQ or buffer respectively. After fixation the brains of related controls and ODQ-injected animals underwent exactly the same immunohistochemical procedure by processing them together in one well and finally mounting them in one spacer hole according to Huetteroth and Schachtner (2005). Confocal image acquisition took place with identical settings, optimized for best dynamic intensity range (256 gray values) of the anti-mouse-Cy5 synapsin signal of the control AL. Following glomerulus identification, reconstruction and measurement was

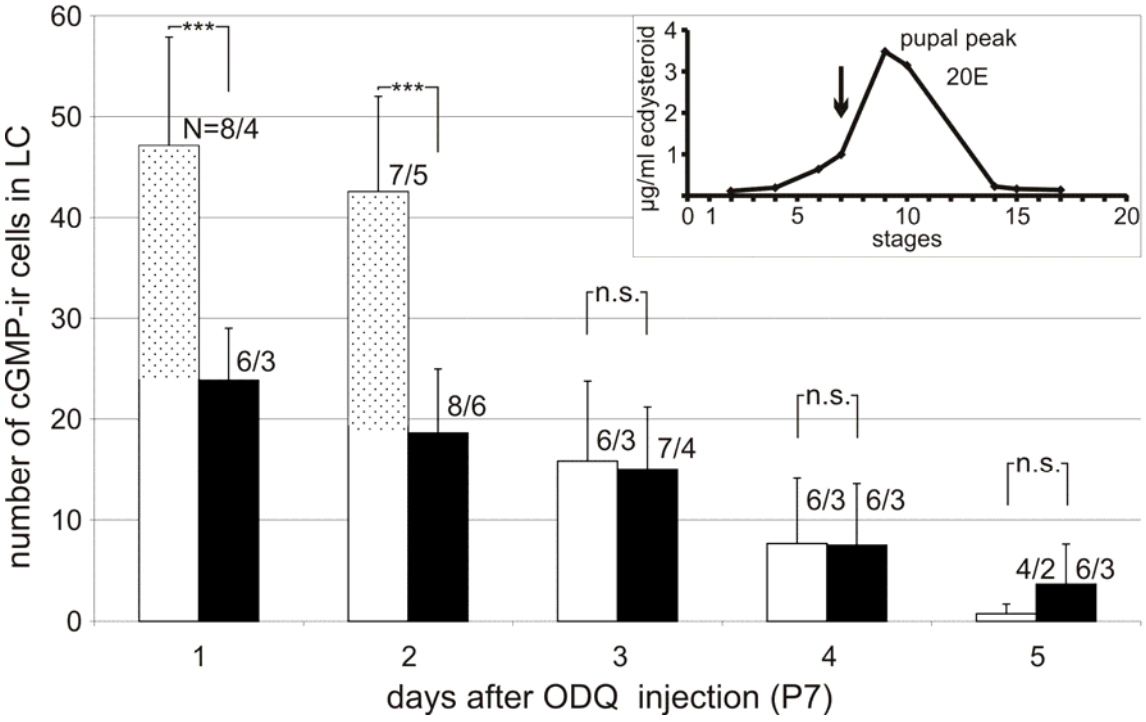

Figure 2 Effect of the soluble guanylyl cyclase inhibitor ODQ on cGMP-immunoreactivity in the lateral cell group. After injection of ODQ (black columns) or the solvent DMSO (1% in saline) as control (white columns) shortly before the beginning of phase II (P7, arrow in inset), animals were standard dissected and monitored for cGMP-immunoreactivity on five subsequent days. While control animals exhibit cGMP-ir cell numbers comparable to cell numbers in Fig. 1, ODQ-injected animals have significantly less cGMP-ir cells (~ 20 somata, dotted areas) during the first two days. In animals dissected later than two days after injection, no significant differences in numbers of cGMP-ir cells between ODQ-injected and control animals were found. N = ALs/animals, Bars = standard deviation, *** = P<0.001; n.s. = not significant.

performed with the 3D reconstruction software AMIRA 4.1 (Huetteroth and Schachtner 2005), followed by additional data evaluation using Microsoft Excel 2003.

RESULTS

Time course of dissection-induced cGMP-immunoreactivity

During the phase of glomerulus formation (phase II) a set of local interneurons in the lateral cell group of the AL shows robust cGMP-elevations after dissection (Schachtner et al. 1998). Analyzing this phenomenon revealed that the transient cGMP-elevations depend on a hormonal (20-hydroxyecdysone, 20E) and an activity dependent component (Schachtner et al. 1999). Artificially shifting the pupal 20E peak to an earlier developmental stage resulted in premature formation of glomeruli and early ability of AL neurons to elevate cGMP-concentrations, demonstrating a developmental regulation of the cGMP-signaling. An approach using pharmacology and electrophysiology revealed that part of the cGMP-signal depended selectively on electrical activity of the ORNs which via release of NO lead to the increases of cGMP-concentrations in a set of local neurons.

The identity of dissection-inducible cGMP-immunoreactive (cGMP-ir) somata in the lateral cell group (LC) of the developing antennal lobe (AL) was described previously (Schachtner et al. 1999). Here we focus on the quantity and exact time course of dissection-induced cGMP-ir somata in LC (Fig. 1). Depending on pupal stage, normal dissection of brains under physiological saline for ten minutes led to different numbers of cGMP-ir cells in the LC. While no cGMP-immunoreactivity was seen at P2/3 (N=4 ALs/2 animals), some weak staining was found around P5/6 in about 18 cells (N=5/3). At P7 a steep increase in cGMP-immunoreactivity to about 40 cells occurred (N=12/6), which peaks with about 60 cells around P8 (N=8/4). cGMP-immunoreactivity remained high with about 55 cells at P9 (N=9/5) and about 45 cells at P10 (N=14/7), before it decreased to about 20 cells at P12 (N=8/4) and to nearly zero cells after P15/16 (N=6/3; Fig. 1). In summary, our data show that the ability to generate activity-induced cGMP in the LC is found in a variable number of cells depending on pupal stage. Those cell numbers exhibit a characteristic transient pattern, peaking around the beginning of phase II (Fig. 1).

Several GC sources contribute to dissection-induced cGMP-immunoreactivity

To begin to determine which GC was responsible for this phenomenon, we performed single systemic injections of the soluble guanylyl cyclase blocker 1H-[1,2,4]oxadiazolo[4,3-a]quinoxalin-1-one (ODQ) at the beginning of phase II (around P7/8). This led to a reduction of cGMP-ir cells in the LC of more than 20 cells, lasting for two days (dotted areas). After one day we found about 25 cGMP-ir cells (N=6/3) compared to about 45 cGMP-ir cells in vehicle-injected animals (N=8/4; $P<0.001$); after two days, cell numbers declined to about 20 cGMP-ir cells (N=8/6) compared to 40 cells (N=7/5) for controls ($P<0.001$). Three to five days after injection, no difference in cGMP-ir cells compared to control-injected animals was found (3 days: vehicle- (N=6/3) and ODQ-injected animals (N=7/4) around 15 cGMP-ir cells; 4 days: both around 8 cGMP-ir cells (both N= 6/3); 5 days: about 5 cGMP-ir cells (control: N=4/2, ODQ: N=6/3; Fig. 2).

sGC exclusively upregulates antennal nerve-dependent cGMP-immunoreactivity

Previously it was shown that electrical stimulation as well as cutting the antennal nerve were both equally sufficient to induce cGMP-immunoreactivity exclusively in a subset of LC cells (Schachtner et al. 1999). This result suggested that cutting an antennal nerve resulted in electrical activity of the damaged ORNs, which in an activity dependent manner release NO. This in turn activates soluble guanylyl cyclases, which eventually led to cGMP increases in LC cells (Schachtner et al. 1999). To examine whether the cGMP-increase which can be inhibited by ODQ-injection (as shown in Fig. 2) is solely due to antennal nerve activity, we performed the same experiment, but instead of dissecting out the whole brain only one antenna was cut, followed by *in situ* fixation after ten minutes (Fig. 3). The experiment consisted of animals injected with saline alone (controls) and animals injected with ODQ at stages P7 and P9. In both groups one antenna was severed one or two days after injection. As stimulation of one antenna resulted in similar cell numbers in both ALs of one animal, we used both ALs in our analysis. Saline injections at P7 and cutting of the antennal nerve one or two days later resulted in about 20 cGMP-ir cells in LC (Fig. 3A). These numbers nicely correspond to the differences of cGMP-ir cells between controls and ODQ-injected animals (see Fig. 2; for better comparison, dotted areas representing differences after one and two days respectively are included in Fig. 3A as dotted bars)). In contrast, cutting antennal nerves in animals which have been injected with ODQ resulted in nearly no cGMP-positive cells in LC one and two days after ODQ was injected (Fig. 3A). These results clearly suggest that ORNs are obviously the only source for NO and is consistent with previous reports using in-situ hybridization (Gibson and Nighorn 2000).

To determine whether the cGMP-immunoreactivity three days after ODQ-injection (Fig. 2) was due to other, non-ODQ sensitive

guanylyl cyclases or if this was rather due to a wearing off of ODQ, we also performed ODQ and saline injections at P9 (Fig 3B). Indeed, compared to saline injections, cGMP-immunoreactivity in ODQ-injected animals was again nearly completely abolished one or two days after the injection (1 day: control, N=12/6, ODQ, N=12/6, P<0.005; 2 days: control, N=19/11, ODQ, N=14/8, P<0.001).

To test whether the ability of neurons in the LC to upregulate cGMP concentrations in a NO-dependent manner depends on the ingrowth of the ORN axons during early pupal development, we removed one antenna from P0 animals. This developmental deantennation led to a total loss of ORN ingrowth, resulting in small ALs lacking proper glomerular organization (Sanes et al. 1977). Repeating the experiments performed above (see Fig. 3B) with these animals resulted in about 20 cGMP-ir cells in both ALs for the saline injections, and in nearly no cGMP-cells for the ODQ-injected animals (Fig. 4). This result suggests that the ability of LC neurons to upregulate cGMP in a NO dependent manner is independent of the ingrowth of the ORN axons from the antenna. To rule out some rudimentary innervations of ORN axons after developmental deantennation, we labeled the brains additionally with an antiserum against the transmembrane domain of *M. sexta* fasciclin II (TM-MFasII, Fig. 4A). TM-MFasII has been shown to be transiently expressed during pupal development in a subset of ORN axons including the axons from the labial pit organ (Higgins et al. 2002). The immunostaining nicely demonstrates that the only glomerulus on the developmentally deantennated AL positive for TM-MFasII is the labial pit organ glomerulus (LPOG), while all other glomeruli lack TM-MFasII staining. In contrast, the contralateral AL which is normally innervated by ORN axons showed the typical TM-MFasII positive glomeruli including the LPOG (Fig. 4A).

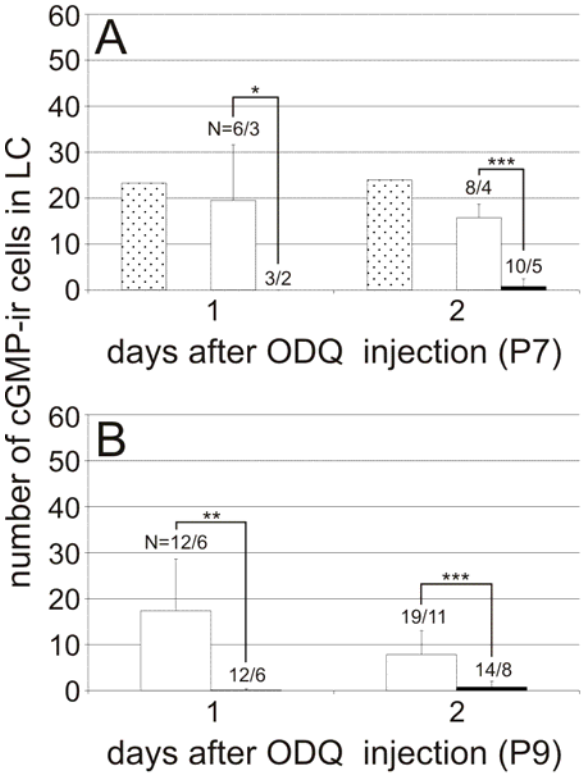

Figure 3 Effect of the soluble guanylyl cyclase inhibitor ODQ on cGMP-immunoreactivity in the lateral cell group after antennal stimulation. Animals were injected with ODQ (black bars) or vehicle alone (white bars, controls) **A)** shortly before the beginning of phase II (P7) or **B)** in the middle of phase II (P9). 1 and 2 days later one antenna was cut, followed by fixation with 4% formaldehyde 10 minutes later, thus warranting exclusive stimulation via the antennal nerve. **A)** The dotted bars represent the numbers of ODQ-sensitive cGMP-ir cells after standard dissection (see Fig.2, dotted areas). Note that numbers of cGMP-ir cells in control animals (white bars) equals the numbers of ODQ-sensitive cells after standard dissection. The combination of ODQ injection and antennal nerve stimulation 1 or 2 days later resulted in no or only a few cGMP positive cells in LC. **B)** Similar to ODQ injection at P7, the combination of ODQ injection at P9 and antennal nerve stimulation on subsequent days abolished number of cGMP-ir cells almost completely. Remaining cGMP-ir cells after 2 days are probably due to wearing off of ODQ and new sGC synthesis. N = ALs/animals, Bars = standard deviation, * = P<0.05, ** = P<0.005, *** = P<0.001.

Developmental time course and localization of ODQ-sensitive GC in the AL (MsGCα1)

Staining with an antiserum specifically recognizing the α1-subunit of *M. sexta* soluble guanylate cyclase (MsGCα1) revealed immunoreactive cells in all three cell groups during AL development. The intensity of MsGCα1 staining in cells of the AL varies to a massive degree; in case of strong staining, it is not restricted to somata but extends into primary neurites (Fig. 5E, F). Between P5 and P16, we sometimes found 3 to 32 MsGCα1-ir cells in the median cell group (MC; in 17 of 75 animals observed; Fig. 5A). Due to the infrequent occurrence no developmental pattern could be identified. The same holds true for the anterior cell group (AC); between P5 to P18, 14 of 75 animals exhibited up to two MsGCα1-ir cells (Fig. 5A). Schachtner et al. (1999) described one to two cells exhibiting cGMP immunoreactivity in the AC of P10 animals after treatment with a phosphodiesterase inhibitor. According to Homberg et al. (1989) the AC and MC are exclusively housing projection neurons (PNs). Wilson et al. (2007) confirmed MsGCα1-immunoreactivity in some, but not all PNs belonging to both MC and AC by intracellular filling of single neurons in adult moths. Also in adult *M. sexta*, Collmann et al. (2004) describe 90% of all PNs as MsGCα1-ir. Neither in these studies nor in our study MsGCα1-immunoreactivity was observed in tracts leaving the AL, so MsGCα1 activity in PNs seems to be restricted to the AL.

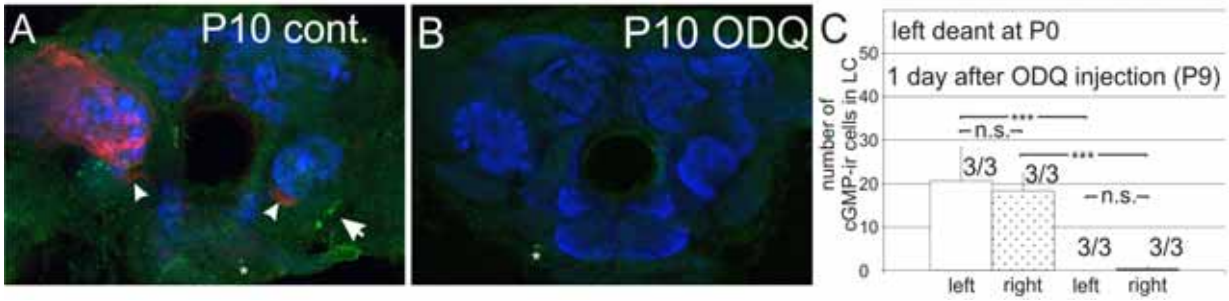

Figure 4 ODQ-effect on numbers of cGMP-ir cells after antennal stimulation in animals unilateral deantennated at P0. At stage P0, shortly after pupal formation, the left antenna was completely removed resulting in P10 animals with normal developed AL containing glomeruli on the right side, and an aglomerular left AL of reduced size (**A, B**). As visualized by anti-TM-MFasII staining (**A**, arrowheads), sensory innervation on the antennectomized side basically was reduced to the labial palp organ glomerulus, which receives sensory input coming from labial palps exclusively (Kent et al. 1999). Analogous to the protocol in Fig. 3, one day after ODQ injection the right antenna was cut, followed by fixation 10 minutes later, thus warranting exclusive stimulation via the right antennal nerve. As expected, on the stimulated ipsilateral right side approximately 20 cells responded with cGMP-upregulation (**A; C,** second column, dotted, N=3). Comparable to Fig. 3, this cGMP-signal was completely suppressible by ODQ injection (**B; C,** 1 weakly stained cell in one of three ALs, fourth column, N=3). Unexpectedly, almost the same numbers of cGMP-ir cells were found on the deantennated contralateral left side in controls (**A**, arrow; **C**, first column, white, N=3) which were also sensitive to ODQ (**C**, 0 cells, in third column; N=3). Note the ODQ-independent cGMP-immunoreactivity in the subesophageal ganglion (**A, B**, asterisk). Bars = standard deviation, *** = P<0.001, n.s. = not significant.

In contrast to the staining observed in AC and MC, in LC we regularly found cells immunopositive for the MsGCα1 antiserum. The individual range of cell numbers obtained from ALs at defined developmental stages was however quite variable (Fig. 5G). In LC, MsGCα1 immunoreactivity is for the first time found at P4 - in about three cells in half of the ALs examined (Fig. 5G; n=8/4). From P4, numbers of MsGCα1-ir cells increase up to stage P8. A mean of ten MsGCα1-ir cells is found at P5 (n=6/3). The number of MsGCα1-ir cells rises further from about 20 at P6 (n=4/2) and P7 (n=10/5) significantly to almost 30 MsGCα1-ir cells at P8 (n=12/6). Despite massive individual variations, the mean of MsGCα1-ir cells stays at this level until the end of the pupal period. In freshly eclosed adults, we observed a second rise to about 60 MsGCα1-ir cells, again with high variability (numbers reaching from 31 to 101 cells; n=6/3).

Developmental time course and localization of an ODQ-insensitive GC in the AL (MsGC-I)

The antiserum against the receptor guanylyl cyclase MsGC-I resulted in massive staining in basal and central parts of the glomeruli, the coarse neuropil of the AL, as well as in most cells of the LC, but not in the MC (Fig. 5A-F). In early stages of pupal development, namely P3 to P4/5, MsGC-I-immunoreactivity is restricted to the neuropilar parts of the AL. Staining in cell bodies did not occur before P6. Interestingly, the staining intensity in the neuropil of the forming glomeruli reflects the developmental wave directed from distal to proximal during the formation of glomeruli in phase II (Fig. 5C; Tolbert 1989, Oland and Tolbert 1996, Hildebrand et al. 1997, Dubuque et al. 2001). Over all, from the beginning of phase II the neuropilar staining pattern reflects the pattern described for adults by Nighorn et al. (2001).

Colocalization of ODQ-sensitive and -insensitive GC in the AL

In two representative stages, P8 and P18, we looked for colocalization of MsGCα1-immunoreactivity and MsGC-I-immunoreactivity in cells of the LC. Almost all strongly labeled cells of either antiserum excluded immunoreactivity against the other antiserum. However, approximately 1/3 of weakly stained MsGCα1-ir cells also exhibited weak MsGC-I-immunoreactivity (Fig. 5C). Only one to two cells showed strong immunoreactivity against both antisera.

Reduction of synapse protein quantity after ODQ application

The transient pattern of NO-sensitive cGMP upregulation during the onset of phase II strongly suggested an involvement of the NO/cGMP signaling pathway during formation of the olfactory glomeruli. To test this hypothesis, we injected ODQ in stage P7 animals as described above and analyzed the intensity of immunostaining of the ubiquitous synaptic vesicle protein synaptotagmin at the end of phase II. The synaptotagmin antiserum can be used to follow neuropil development, especially glomerulus development, during metamorphic brain development of *M. sexta* (Dubuque et al. 2001). We measured relative differences in anti-synaptotagmin immunoreactivity in two ways.

First, we analyzed optical densities of synaptotagmin immunoreactivity from vibratome sections, keeping all conditions and settings identical (see method section). We performed three series of experiments including three to five ODQ and two vehicle injected animals. Inspecting the sections and comparing the staining intensities between ODQ and vehicle treated animals clearly displayed fainter staining intensity in AL glomeruli of ODQ injected animals compared to vehicle injected ones (Fig. 6A-C). To quantify this effect, each section was digitized and compared in respect of number of pixels above a defined gray value threshold between treated and control animals (see method section). The resulting RIODs (ratio of integrated optical densities) clearly show lower levels of staining intensities of ALs of ODQ injected animals compared to the controls (Fig. 6D).

In a second approach we performed ELISAs of defined brain areas including ALs, optic lobes, and central brain, to compare the amount of expressed

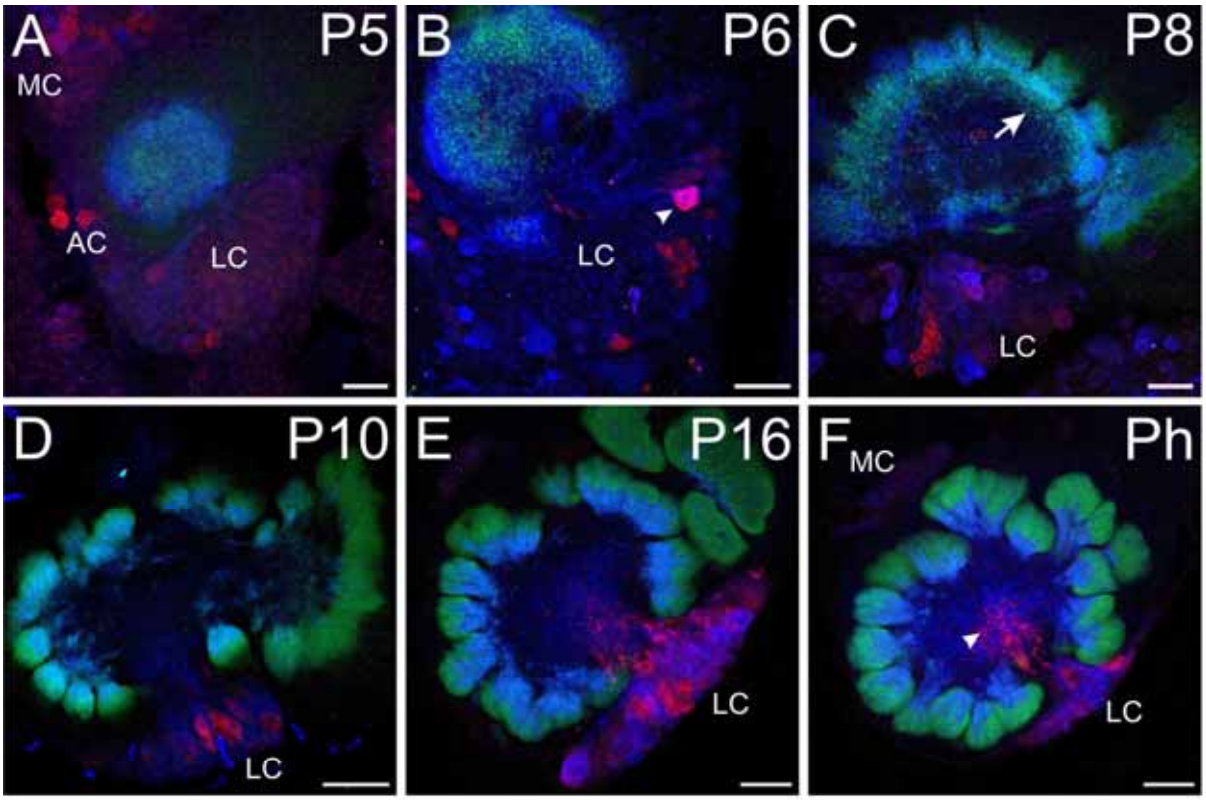

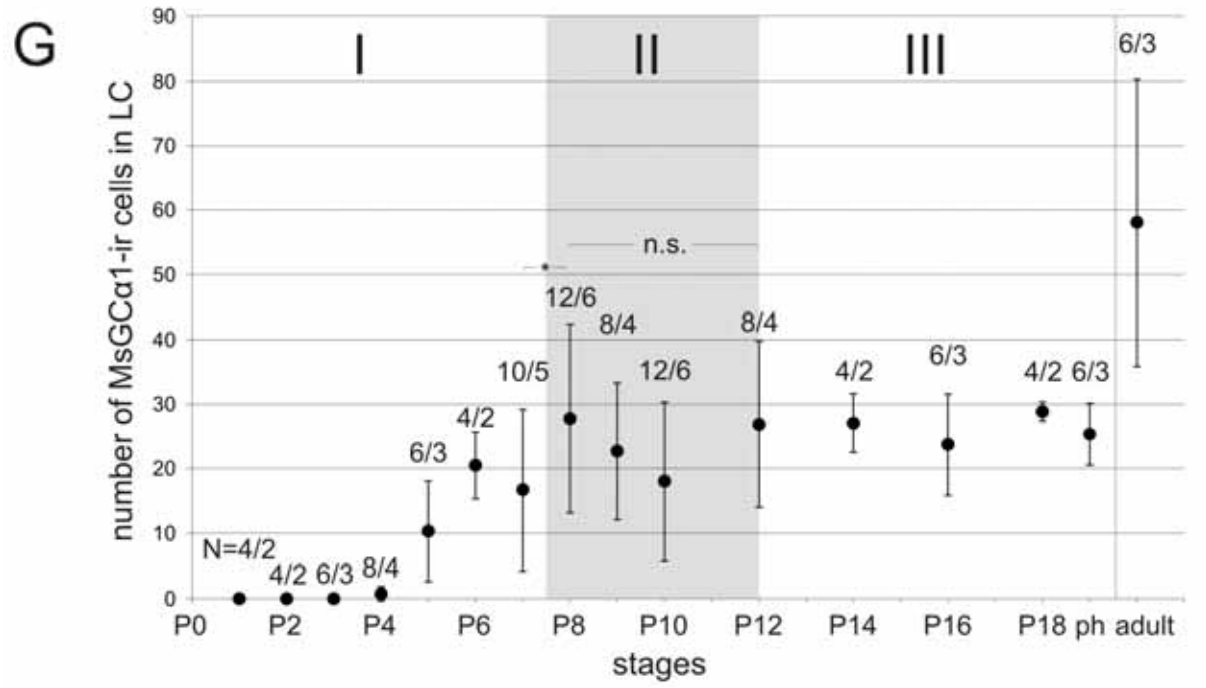

synaptotagmin protein between ODQ and vehicle injected animals. We chose this approach for two reasons: first to get a synaptotagmin measure different to the one obtained from the sections. Second we wanted to compare ALs with other brain areas to reveal whether the ODQ treatment is also influencing brain areas besides the AL. This seemed important to us, because systemic injection influences not only AL tissue but also other brain areas (optic lobes, central brain), which in an earlier study have been shown to also contain cGMP-ir neurons (Schachtner et al. 1998). The experiments were performed as described above for the measurements of the optical densities on sectioned material. Animals were injected with ODQ or vehicle alone shortly before onset of phase II (P7) and the brains were dissected out at the end of phase II (P12/13). To obtain the ELISA data, we performed three independent series of experiments with three ODQ and three vehicle injected animals. The results demonstrate that the only tissue which is clearly influenced by the ODQ treatment are the ALs with about 30 % lower amounts of synaptotagmin compared to the controls. Optic lobes and central brain also seem to have lower synaptotagmin concentrations of about 10 %, but are not significantly different to controls. In summary, the results obtained from optical density measurements from sections and from ELISAs clearly suggest a role for NO induced cGMP in the process of synapse formation during glomerulus formation (phase II).

Overall glomerulus morphology remains unchanged after ODQ application

To determine whether ODQ injection has an influence on glomerulus size, we performed similar experiments as described above, but performed 3D-reconstructions of ten selected individual glomeruli. Those glomeruli can, due to shape and position, easily be identified from animal to animal (Huetteroth and Schachtner 2005). For 3D reconstructions, we switched to synapsin immunostaining (see method section). Like synaptotagmin, the presynaptic vesicle-associated protein synapsin can equally be used to identify neuropil areas including olfactory glomeruli in the brain of insects (Rössler et al. 2002, Schachtner et al. 2005). Comparing the data between ODQ (n = 11/11) and vehicle treated animals (n = 11/11) revealed no difference in volume in none of the ten glomeruli. Visual inspection of the glomeruli also suggested that neither shape nor position in the AL seemed to be influenced. The additional result that ODQ has obviously no effect on glomerulus size, suggests an involvement directly on synapse formation, as defects in path finding or sprouting would very likely lead to smaller glomeruli.

DISCUSSION

The inducible rise of cGMP-concentrations in a defined set of local AL-neurons during glomerulus formation (phase II of metamorphic AL development) originates from different guanylyl cyclases. A subset of these local neurons increases cGMP-levels in response to NO. In a series of pharmacological experiments using the specific sGC-inhibitor ODQ, we demonstrated that the complete cGMP-increases evoked by antennal nerve activity are exclusively mediated by NO-dependent guanylyl cyclase. Using ODQ in long-term experiments, we provide evidence that these NO-dependent increases in cGMP affect central players in synapse formation during a critical phase in the development of the olfactory glomeruli.

The latter adds to previous studies which postulate such a role during formation of neural connectivity in the embryonic grasshopper (Truman

← **Figure 5** **MsGCα1-immunoreactivity and MsGC-I-immunoreactivity through development.** MsGCα1-immunoreactivity is found not before P4 in about three AL neurons, before MsGCα1-ir cell numbers rise around P5, exhibiting various degrees of staining intensity in cell somata (**A**). Irregularly, up to two somata in the anterior (AC) and up to 32 somata in the median cell group (MC) are stained with varying intensity. While MsGCα1-immunoreactivity in the LC is still confined to cell bodies at P5 (red), MsGC-I-immunoreactivity (blue) is already found in the coarse neuropil of the developing AL, as visualized with an antibody against the presynaptic vesicle protein synaptotagmin (green, A). The median cell group (MC) never stained with the anti-MsGC-I antiserum. The number of MsGCα1-ir cells continues to rise in P6 (**B**) and P8 (**C**), exhibiting increased staining intensity. Around P6, first somata in the lateral cell group (LC) are MsGC-I-ir (**B**), and some even show colocalization with MsGCα1-immunoreactivity (arrowhead). At the beginning of phase II, the developing glomeruli concentrate MsGC-I-immunoreactivity at their bases, with distal glomeruli having stronger staining than their proximal counterparts (arrow, **C**). Undergoing strong individual fluctuation, mean MsGCα1-ir cell number stays around 35 at P10 (**D**), and shows its typical staining pattern also at P16 (**E**) until pharate stage (Ph, **F**). At P10, all glomeruli exhibit robust MsGC-I-immunoreactivity in their basal part (**D**), which continues throughout the remaining pupal development (P16, **E**) until pharate stage (**F**). Staining of LC somata remains diffuse, but present. Note also the diffuse staining of MsGC-I-immunoreactivity and MsGCα1-immunoreactivity in the coarse neuropil (arrowhead in **F**). (**G**) Acquisition of MsGCα1-immunoreactivity in cells of the LC occurs in two steps. During the second half of phase I, around P4/5, the first somata are found to exhibit MsGCα1-immunoreactivity. This number rises until reaching almost 30 immunoreactive cells at about P8, just at the beginning of phase II, and thus corresponding to the rise of the 20-Hydroxyecdysone titer in the hemolymph. The MsGCα1-ir cell number remains roughly the same up to the pharate stage (ph). After adult eclosion, a second rise to about 60 immunoreactive cells occurs, again with high individual fluctuations. Bars = standard deviation, * = $P<0.05$, n.s. = not significant.

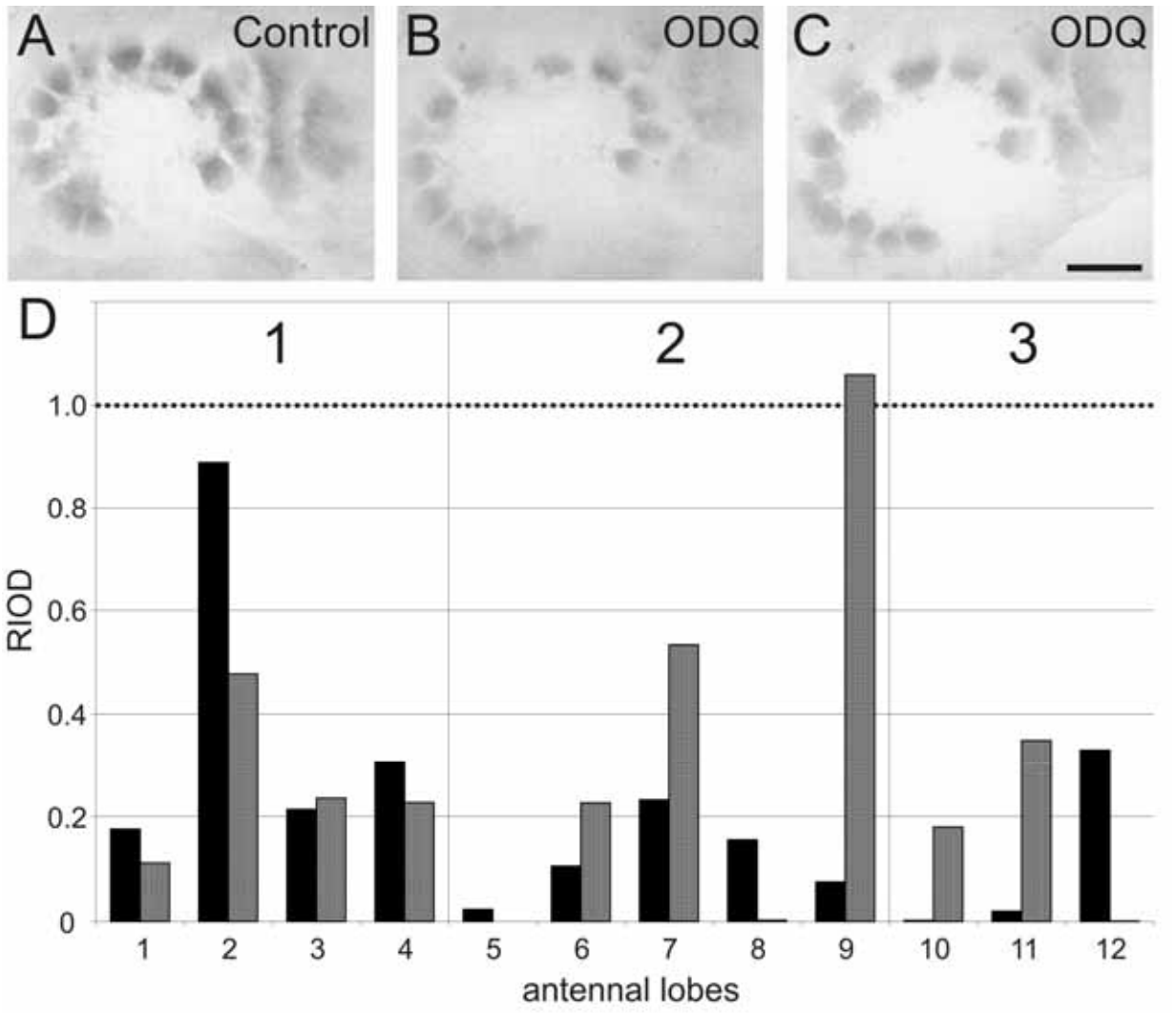

Figure 6 RIOD measurements in antennal lobe sections. Anti-synaptotagmin staining in comparable antennal lobe vibratome sections between equally processed control animals (A) and ODQ-injected animals (B, C) show a reduction of staining signal in ODQ-treated animals. If this staining signal is quantified in comparable glomerular regions of the antennal lobe (RIOD, ratio of integrated optical density; see method section for details), a massive signal reduction in ODQ-treated animals becomes obvious (D). Normalized to control animal values (RIOD = 1.0), both left (black) and right (gray) antennal lobes of 12 different animals exhibit almost always reduced RIOD, carried out in three different experiments (Sections 1-3). Scale: 50 µm.

et al. 1996, Ball and Truman, 1998) and during retinotopic pattern formation in the CNS of vertebrates and insects (e.g. Ferret: Leamey 2001; *Drosophila*: Gibbs and Truman 1998, Gibbs et al. 2001). During development and regeneration of the olfactory bulb of the rat NOS is transiently expressed in ORNs and the authors postulate an activity dependent involvement of NO in synapse formation (Roskams et al. 1994).

Transient cGMP-ir cells induced by antennal nerve activity are exclusively produced by sGC

The inducible cGMP production in local interneurons (LNs) of the AL follows a characteristic transient time pattern, which reaches a maximum of cGMP-ir cells at the onset phase II to drop down to zero cells at around stage P16 (Fig. 1). A subset of about 20 cGMP-ir cells which is selectively inducible via antennal nerve activity can completely be blocked with the sGC inhibitor ODQ (compare figs. 2 and 3, summarized in fig. 9). In contrast, the cGMP upregulation in the rest of the cells could not be blocked via ODQ, suggesting other, NO-independent guanylyl cyclases being involved. These results are in accordance with an earlier study, showing that *in vivo* application of NO-donors on the brain for 10 minutes as well as stimulation of the antennal nerve either by cutting or electrical stimulation are sufficient to upregulate cGMP in a similar number of cells in the lateral cell group of the *Manduca* AL (Schachtner et al.1999). The current study together with the studies by Schachtner et al. (1998, 1999) clearly reveal a transient NO- and activity-driven cGMP regulation provided by the ORNs in the antennal nerve during the phase of glomerulus formation. These results are also supported by a study from Gibson and

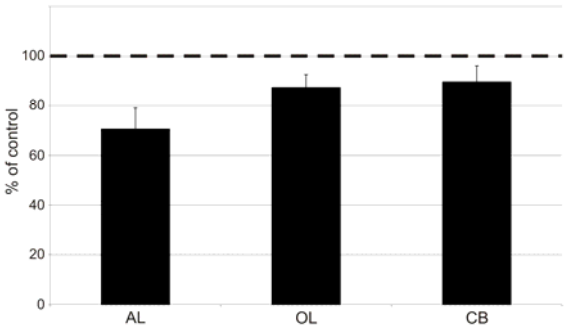

Figure 7 ELISA measurements with anti-Synaptotagmin in three different brain tissues. After ODQ application at P7/8 and dissection P12/13, dissected brains were divided into three different parts: antennal lobes (AL), optic lobes (OL), and central brain (CB). After homogenization, ELISA measurements of ODQ-treated animals were normalized to corresponding control tissues (100%). AL tissue clearly shows a reduction of signal intensity to about 70%, whereas OL and CB tissue exhibit less reduction reaching about 90%.

Nighorn (2000), who demonstrated expression of the NO producing enzyme NO-synthase exclusively in ORNs stemming from the antenna and from the labial pit organ. The developmental time course of numbers of cells immunoreactive against the α1-subunit of *M. sexta* sGC in the LC corresponds well with the time course of ODQ-sensitive cGMP-ir cells (compare figs. 2, 3, and 5). This provides additional evidence of the NO-stimulated MsGCα1/MsGCβ1 heterodimer being the only source of antennal nerve-dependent inducible cGMP for this critical phase during AL development.

Long-lasting blocking effect of ODQ *in vivo*

ODQ selectively inhibits sGC activity and has been widely used to study the function of the NO/cGMP signaling pathway in vertebrates as well as in invertebrates (e.g. Garthwaite et al. 1995, Friebe and Koesling 2003, Koesling et al. 2004, Bicker 2007). The blocking effect of ODQ-injections lasted up to two days; animals dissected later on (at P9) showed no differences in cGMP-ir cell numbers compared to controls (Fig. 2). If we injected ODQ at P9, we were again able to completely suppress cGMP-immunoreactivity (Fig. 3B). Thus, lacking ODQ-sensitivity was obviously not the reason for their reappearance after three days (Fig. 2). In *M. sexta*, and, to the best of our knowledge also in other insects, such a long lasting effect of ODQ has never been described earlier. This renders ODQ as a potent inhibitor of sGC also in longer lasting *in vivo* experiments. *In vitro* studies revealed that ODQ apparently leads to an irreversible inhibition of sGC (Friebe and Koesling 2003). Thus, we attribute the loss of the ODQ-effect three days after injection to *de novo* synthesis of sGC combined with complete catabolization of ODQ-blocked old sGC. However, it is not impossible although very unlikely, that long-lasting secondary effects

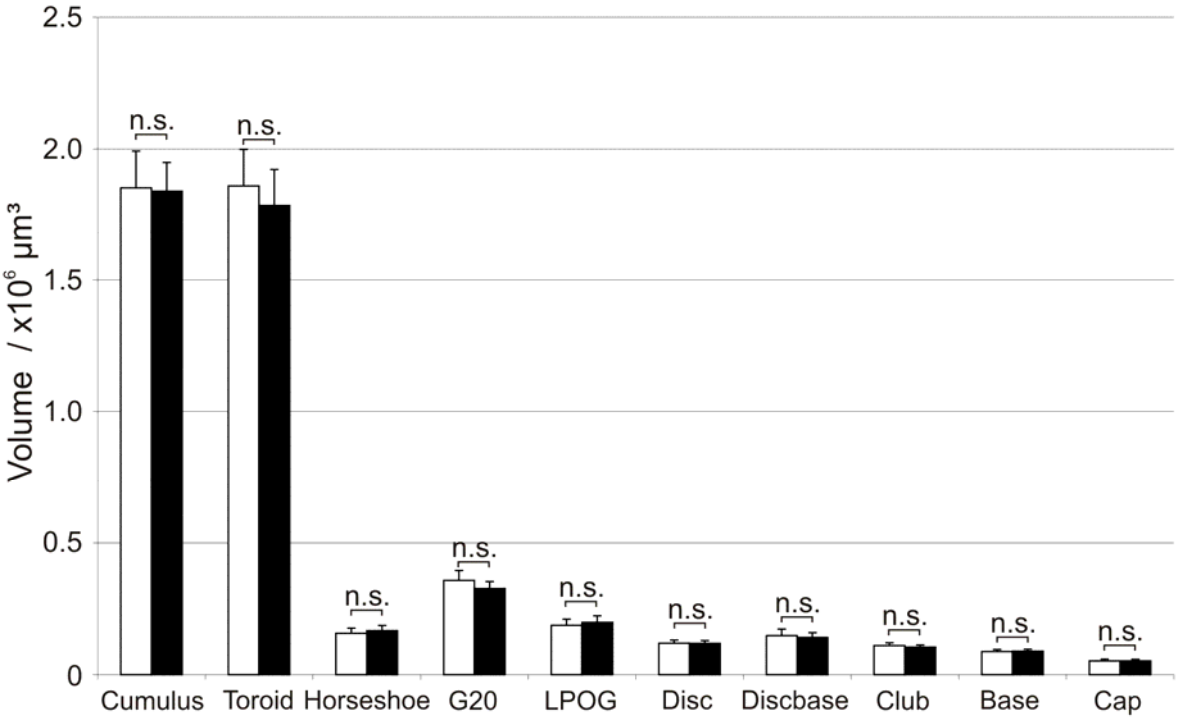

Figure 8 Volume measurements in 3D reconstructed antennal lobe glomeruli. ODQ was injected at P7 and animals were dissected at the end of phase II (P12). To see whether ODQ treatment has an effect on neuropilar volume, we compared volume and shape of ten identifiable glomeruli between equally processed animals (n=11/11), based on 3D-reconstructions of anti-synapsin staining. Those ten glomeruli are located in opposite corners of the antennal lobe, and were described before as being easily identifiable already at the end of phase II (Huetteroth and Schachtner 2005). In none of the selected glomeruli a significant difference of volume was found. Bars = SEM, n.s. = not significant.

downstream to inhibited cGMP led to this observed reduction in cGMP-immunoreactivity for two days.

Communication between left and right AL

Although we only cut the right antenna, we always counted approximately the same amount of cGMP-ir cells which were also sensitive to ODQ in the contralateral AL. Unlike in *Drosophila* (Vosshall et al. 2000), ORNs of *Manduca* only extend their axons to the ipsilateral AL (Schachtner et al. 2005). This implies that the ODQ-sensitive stimulation of cGMP neurons in the contralateral AL must have been mediated by interneurons, connecting both ALs. Since NOS in the AL is exclusively located in sensory neurons (Gibson and Nighorn 2000), this result demands an extrinsic stimulatory pathway onto sensory neurons, triggered by the contralateral stimulation. Although some few bilateral projection neurons exist (Kanzaki et al. 1989), far better candidate cells are centrifugal neurons (CNs) of the AL, which are thought to be involved in feedback mechanisms and bilateral integration (Homberg et al. 1988). Transmitter candidates of CNs are biogenic amines and neuropeptides. Known to date are a serotonergic neuron (Kent et al. 1987), a histaminergic neuron, about six dopaminergic (Homberg 1990), and three octopaminergic neurons (Dacks et al. 2005). For the peptidergic CNs account a RFamid-CN (Schachtner et al. 2004b), an Allatostatin-CN (Utz and Schachtner 2005), a Tachykinin-CN (in Heliothis virescens, Berg et al. 2007; in *M. sexta*, unpublished observation), and an Allatotropin-CN (Utz et al. 2008). Owing to their morphology, the above mentioned neurons are the only known neurons which could elicit activity in contralateral sensory neurons either directly or indirectly. Earlier experiments already showed 5HT- and histamine-dependent cGMP-upregulation in the developing *Manduca* AL (Schachtner et al. 1999). We interpret this data towards synchronization and an enhancement of NO-dependent sGC activation and subsequent cGMP synthesis between both ALs, mediated by either aminergic or peptidergic CNs.

Interestingly, the same number of cGMP-ir cells was found in animals which were antennectomized on one side at P0 and stimulated contralaterally at stage P10 (Fig. 4). Without the NOS containing ORNs, the major source for NO in the ALs is missing on the deafferented side. The only source of NO synthase in the developmentally antennectomized AL is provided by axons in the labial pit organ glomerulus (LPOG). The LPOG not only receives sensory innervation exclusively by the labial palps, but also extends its size in antennectomized animals (Kent et al. 1999). Intriguingly, the centrifugal activation of NO synthase in this hypertrophic contralateral LPOG obviously led to a sufficient amount of NO to induce the complete set of ODQ-sensitive cGMP-ir cells in the LC (Fig. 4). This result implies that either all LNs producing NO-dependent cGMP also innervate the LPOG, or the range of NO diffusing from the LPOG directly reaches to sGC-containing somata in the LC. Previous studies on the physiological range of NO allow for both possibilities (Philippides et al. 2005; Ott et al. 2007).

Other, NO-independent cGMP sources

Both, NO-sensitive and NO-insensitive cGMP upregulation seem to be dependent on activity. This is suggested by the fact that *in situ* fixation of brains resulted in none or only a few cGMP positive cells in the LC of the AL (Schachtner et al. 1999). Additionally to the NO-sensitive guanylyl cyclase other, NO-insensitive guanylyl cyclases (GC) have been described in the adult *Manduca* AL. These are the atypical receptor-like GC MsGC-I (Simpson et al. 1999, Nighorn et al. 2001) and the receptor GC MsGC-II (Morton and Nighorn 2003). Both GC are candidates to mediate NO-independent cGMP regulation during phase II of AL development. While MsGC-II is described as having only low basal synthesis levels, the opposite is true for MsGC-I. In the current study we performed immunostaining using a specific antiserum recognizing MSGC-I in the developing AL. The immunostainings showed the presence of MsGC-I from stage P4 including massive staining in glomeruli and in many cells in the LC (Fig. 5). The massive presence of MsGC-I suggests an

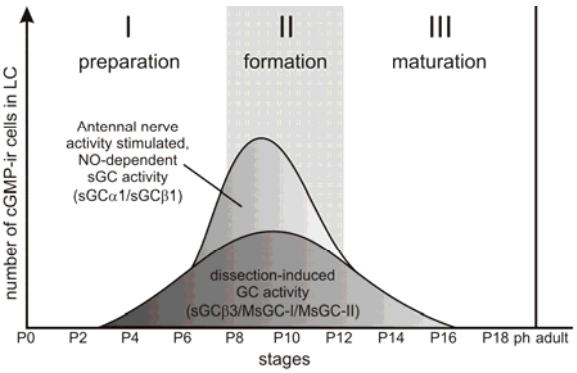

Figure 9 Schematic diagram showing the developmental time course of cGMP-ir cells in the lateral cell group of the antennal lobe (AL). A specific subset of cells exhibits antennal nerve activity-dependent cGMP-immunoreactivity, evoked by soluble guanylyl cyclase, a nitric oxide sensitive heterodimer (MsGCα1/MsGCβ1). This specific response is restricted to a narrow time window shortly before and during phase II of AL development, when glomeruli are formed and the main wave of synaptogenesis in the AL occurs. While the principle occurrence of inducible cGMP-immunoreactivity already starts around P2/3 and stops around P16, this underlying transient pattern is mainly due to other guanylyl cyclases also present in the developing AL.

involvement of this GC in the NO-independent upregulation of cGMP during phase II. Besides MsGC-I, also other NO-independent GC like MsGC-II might be involved in cGMP regulation during AL development and will be part of future studies.

Involvement of the NO/ cGMP signaling pathway in the formation of the olfactory glomeruli

The phase of glomerulus formation (II) is characterized by massive synaptogenesis (Dubuque et al. 2001, Tolbert et al. 2004) and the time course of glomerulus formation can be examined by using antisera against synaptic vesicle proteins like synaptotagmin or synapsin (Dubuque et al. 2001, Utz et al. 2008). To date, the exact mechanisms behind this process are still obscure. Intensity measurements of synaptotagmin immunostaining in sectioned material and in ELISAs revealed a downregulation of this synapse protein in ALs after ODQ treatment (Figs. 6, 7). This suggests lower synaptic strength in AL glomeruli and thus a role of the NO/cGMP signaling pathway in synapse formation during phase II.

Comparing the volumes of selected glomeruli revealed no significant differences between ODQ and vehicle injected animals (Fig. 8). Thus, inhibition of sGC is obviously not perturbing overall network architecture within glomeruli. We examined only 10 glomeruli of a total of about 63 glomeruli per AL, but as the selected glomeruli include the sex specific glomeruli, the LPOG and further six ordinary glomeruli at different locations in the glomerular shell, we conclude that they fairly represent also the rest of the glomeruli.

What factors influence glomerular formation and where can the NO/sGC/cGMP pathway be placed therein? The increasing hemolymph titer of the developmental hormone 20-hydroxyecdysone (20E) parallels the onset of phase II and injecting 20E into freshly eclosed pupa resulted in a concerted advancement of glomerular formation of three to four days (Schachtner et al. 2004b). Early injection of 20E also enhances the ability of LNs to react to NO with cGMP increases (Schachtner et al. 1999). 20E might thus directly or indirectly be responsible for the ability of LNs to respond to NO with cGMP upregulation. As the developmental time course of the numbers of MsGCα1-ir cells follows a similar time course as the 20E hemolymph titer (Warren and Gilbert 1986), 20E might very well be responsible for the expression of this subunit of the sGC.

Another event important in synaptogenesis might be spontaneous electrical activity of the ORNs starting at the onset of phase II (Oland et al. 1996). Electrical stimulation of ORNs during phase II leads to calcium increases in ORNs (Heil et al. 2007). Increased calcium concentrations evoked by spontaneous activity could in turn activate the calcium dependent NO synthase during phase II.The produced NO leads to transient cGMP production in about 20 LNs in the AL which then, by so far unknown mechanisms, enhance synaptic strength. Thus, spontaneous activity seems to be involved in synapse formation via NO/cGMP, without employing classical synaptic transmission pathways.

How can 20 NO-sensitive, presumably multiglomerular LNs of a total of approximately 350 LNs, 900 PNs, and around 255.000 ORNs in the AL (reviewed in Schachtner et al. 2005) account for 30% of the expression of a synaptic vesicle protein (Fig 7)? Those 20 NO-sensitive neurons must serve a promoting function by providing or modulating other signals which influence synapse formation on the AL level. Cyclic GMP increases have been shown to enhance the release of peptides in vertebrate and invertebrate neurosecretory cells (e.g. Moretto et al. 1993, Aguila 1994, Anderson et al. 2004). There is good evidence that NO/cGMP is one of the signaling pathways mediating the release of growth hormone from the pituitary (Anderson et al. 2004, Rodriguez-Pacheco et al. 2008). In *M. sexta*, cGMP increases are thought to be responsible for the release of peptides from endocrine Inka cells and from afferent Cell 27 in the context of eclosion behavior (Gammie and Truman 1997, Kingan et al. 1997). Several neuropeptides are also increasingly expressed in LNs during phase II (Schachtner et al. 2004b, Utz and Schachtner 2005, Utz et al. 2007, 2008). The possible connection between the NO/cGMP signaling pathway and other molecules involved in synapse formation has not yet been thoroughly investigated. We are currently examining whether cGMP increases lead to release of neuropeptides from LNs, and whether those neuropeptides play a role in glomerular formation during phase II.

The authors thank Drs. Erich Buchner (University of Würzburg, Germany), Philip F. Copenhaver (OHSU, USA) and Kaushiki P. Menon (CALTECH, USA) for kindly providing the various antisera. The authors are also grateful to Dr. Uwe Homberg and Dr. Frank Seeber for many fruitful discussions and Sabine Jesberg, Martina Kern, Karin Müller, and Cornelia Ellendt for expert technical assistance.

REFERENCES

Abercrombie M. 1946. Estimation of nuclear population from microtome sections. Anat Rec 94:239-247.

Ball EE and Truman JW. 1998. Developing grasshopper neurons show variable levels of guanylyl cyclase activity on arrival at their targets. J Comp Neurol 394:1-13.

Bell RA and Joachim FA. 1978. Techniques for rearing laboratory colonies of the tobacco hornworm, *Manduca sexta* and pink ballworms. Ann Entomol Soc Am 69:365-373.

Berg BG, Schachtner J, Utz S, and Homberg U. 2007. Distribution of neuropeptides in the primary olfactory

center of the heliothine moth *Heliothis virescens*. Cell Tissue Res 327:385-398.

Bicker G. 2001. Sources and targets of nitric oxide signalling in insect nervous systems. Cell Tissue Res 303:137-146.

Bicker G. 2007. Pharmacological approaches to nitric oxide signalling during neural development of locusts and other model insects. Arch Insect Biochem Physiol 64:43-58.

Boehning D and Snyder SH. 2003. Novel neural modulators. Annu Rev Neurosci 26:105-131.

Collmann C, Carlsson MA, Hansson BS, and Nighorn A. 2004. Odorant-evoked nitric oxide signals in the antennal lobe of *Manduca sexta*. J Neurosci 24:6070-6077.

Dacks AM, Christensen TA, Agricola HJ, Wollweber L, and Hildebrand JG. 2005. Octopamine-immunoreactive neurons in the brain and subesophageal ganglion of the hawkmoth *Manduca sexta*. J Comp Neurol 488:255-268.

Davies S. 2000. Nitric oxide signalling in insects. Insect Biochem Mol Biol 30:1123-1138.

de Vente J, Steinbusch HW, and Schipper J. 1987. A new approach to immunocytochemistry of 3',5'-cyclic guanosine monophosphate: preparation, specificity, and initial application of a new antiserum against formaldehyde-fixed 3',5'-cyclic guanosine monophosphate. Neuroscience 22:361-373.

de Vente J, Hopkins DA, Markerink-van Ittersum M, and Steinbusch HW. 1996. Effects of the 3',5'-phosphodiesterase inhibitors isobutylmethyl-xanthine and zaprinast on NO-mediated cGMP accumulation in the hippocampus slice preparation: an immunocytochemical study. J Chem Neuroanat 10:241-248.

Dubuque SH, Schachtner J, Nighorn AJ, Menon KP, Zinn K, and Tolbert LP. 2001. Immunolocalization of synaptotagmin for the study of synapses in the developing antennal lobe of *Manduca sexta*. J Comp Neurol 441:277-287.

Eisthen HL. 2002. Why are olfactory systems of different animals so similar? Brain Behav Evol 59:273-293.

Ephrussi B and Beadle GW. 1936. A Technique of Transplantation for *Drosophila*. Am Nat 70:218.

Ewer J, de Vente J, and Truman JW. 1994. Neuropeptide induction of cyclic GMP increases in the insect CNS: resolution at the level of single identifiable neurons. J Neurosci 14:7704-7712.

Fiala A, Müller U, and Menzel R. 1999. Reversible downregulation of protein kinase A during olfactory learning using antisense technique impairs long-term memory formation in the honeybee, *Apis mellifera*. J Neurosci 19:10125-10134.

Friebe A and Koesling D. 2003. Regulation of nitric oxide-sensitive guanylyl cyclase. Circ Res 93:96-105.

Gammie SC and Truman JW. 1997. An endogenous elevation of cGMP increases the excitability of identified insect neurosecretory cells. J Comp Physiol [A] 180:329-337.

Garthwaite J. 2008. Concepts of neural nitric oxide-mediated transmission. Eur J Neurosci 27:2783-2802.

Garthwaite J, Southam E, Boulton CL, Nielsen EB, Schmidt K, and Mayer B. 1995. Potent and selective inhibition of nitric oxide-sensitive guanylyl cyclase by 1H-[1,2,4]oxadiazolo[4,3-a]quinoxalin-1-one. Mol Pharmacol 48:184-188.

Gibbs SM and Truman JW. 1998. Nitric oxide and cyclic GMP regulate retinal patterning in the optic lobe of *Drosophila*. Neuron 20:83-93.

Gibbs SM, Becker A, Hardy RW, and Truman JW. 2001. Soluble guanylate cyclase is required during development for visual system function in *Drosophila*. J Neurosci 21:7705-7714.

Gibbs SM. 2003. Regulation of neuronal proliferation and differentiation by nitric oxide. Mol Neurobiol 27:107-120.

Gibson NJ and Nighorn A. 2000. Expression of nitric oxide synthase and soluble guanylyl cyclase in the developing olfactory system of *Manduca sexta*. J Comp Neurol 422:191-205.

Heil JE, Oland LA, and Lohr C. 2007. Acetylcholine-mediated axon-glia signaling in the developing insect olfactory system. Eur J Neurosci 26:1227-1241.

Higgins MR, Gibson NJ, Eckholdt PA, Nighorn A, Copenhaver PF, Nardi J, and Tolbert LP. 2002. Different isoforms of fasciclin II are expressed by a subset of developing olfactory receptor neurons and by olfactory-nerve glial cells during formation of glomeruli in the moth *Manduca sexta*. Dev Biol 244:134-154.

Hildebrand JG and Shepherd GM. 1997. Mechanisms of olfactory discrimination: converging evidence for common principles across phyla. Annu Rev Neurosci 20:595-631.

Hildebrand JG, Rössler W, and Tolbert LP. 1997. Postembryonic development of the olfactory system in the moth *Manduca sexta*: primary-afferent control of glomerular development. Semin Cell Dev Biol 8:163-170.

Homberg U, Montague RA, and Hildebrand JG. 1988. Anatomy of antenno-cerebral pathways in the brain of the sphinx moth *Manduca sexta*. Cell Tissue Res 254:255-281.

Homberg U, Christensen TA, and Hildebrand JG. 1989. Structure and function of the deutocerebrum in insects. Annu Rev Entomol 34:477-501.

Homberg U. 1990. Immunocytochemical demonstration of transmitter candidates in the central olfactory pathways in the sphinx moth *Manduca sexta*. In Olfaction and Taste X. K. Døving, editor. Oslo: University Press. p 151-158.

Huetteroth W and Schachtner J. 2005. Standard three-dimensional glomeruli of the *Manduca sexta* antennal lobe: a tool to study both developmental and adult neuronal plasticity. Cell Tissue Res 319:513-524.

Jindra M, Huang JY, Malone F, Asahina M, and Riddiford LM. 1997. Identification and mRNA developmental profiles of two ultraspiracle isoforms in the epidermis and wings of *Manduca sexta*. Insect Mol Biol 6:41-53.

Kanzaki R, Arbas EA, Strausfeld NJ, and Hildebrand JG. 1989. Physiology and morphology of projection neurons in the antennal lobe of the male moth *Manduca sexta*. J Comp Physiol [A] 165:427-453.

Kent KS, Hoskins SG, and Hildebrand JG. 1987. A novel serotonin-immunoreactive neuron in the antennal lobe of the sphinx moth *Manduca sexta* persists throughout postembryonic life. J Neurobiol 18:451-465.

Kent KS, Oland LA, and Hildebrand JG. 1999. Development of the labial pit organ glomerulus in the antennal lobe of the moth *Manduca sexta*: the role of afferent projections in the formation of identifiable olfactory glomeruli. J Neurobiol 40:28-44.

Kingan TG, Gray W, Žitňan D, and Adams ME. 1997. Regulation of ecdysis-triggering hormone release by eclosion hormone. J Exp Biol 200:3245-3256.

Koesling D, Russwurm M, Mergia E, Müllershausen F, and Friebe A. 2004. Nitric oxide-sensitive guanylyl

cyclase: structure and regulation. Neurochem Int 45:813-819.

Krumenacker JS and Murad F. 2006. NO-cGMP signaling in development and stem cells. Mol Genet Metab 87:311-314.

Leamey CA, Ho-Pao CL, and Sur M. 2001. Disruption of retinogeniculate pattern formation by inhibition of soluble guanylyl cyclase. J Neurosci 21:3871-3880.

Matsumoto SG and Hildebrand JG. 1981. Olfactory Mechanisms in the Moth *Manduca sexta*: Response Characteristics and Morphology of Central Neurons in the Antennal Lobes. Proc R Soc B 213:249-277.

Mombaerts P. 2006. Axonal wiring in the mouse olfactory system. Annu Rev Cell Dev Biol 22:713-737.

Moretto M, Lopez FJ, and Negro-Vilar A. 1993. Nitric oxide regulates luteinizing hormone-releasing hormone secretion. Endocrinology 133:2399-2402.

Morton DB and Nighorn A. 2003. MsGC-II, a receptor guanylyl cyclase isolated from the CNS of *Manduca sexta* that is inhibited by calcium. J Neurochem 84:363-372.

Nighorn A, Simpson PJ, and Morton DB. 2001. The novel guanylyl cyclase MsGC-I is strongly expressed in higher-order neuropils in the brain of *Manduca sexta*. J Exp Biol 204:305-314.

Oland LA, Pott WM, Bukhman G, Sun XJ, and Tolbert LP. 1996. Activity blockade does not prevent the construction of olfactory glomeruli in the moth *Manduca sexta*. Int J Dev Neurosci 14:983-996.

Oland LA and Tolbert LP. 1996. Multiple factors shape development of olfactory glomeruli: insights from an insect model system. J Neurobiol 30:92-109.

Oland LA and Tolbert LP. 2003. Key interactions between neurons and glial cells during neural development in insects. Annu Rev Entomol 48:89-110.

Ott SR, Philippides A, Elphick MR, and O'Shea M. 2007. Enhanced fidelity of diffusive nitric oxide signalling by the spatial segregation of source and target neurones in the memory centre of an insect brain. Eur J Neurosci 25:181-190.

Philippides A, Ott SR, Husbands P, Lovick TA, and O'Shea M. 2005. Modeling Cooperative Volume Signaling in a Plexus of Nitric Oxide Synthase-Expressing Neurons. J Neurosci 25:6520–6532.

Rodriguez-Pacheco F, Luque RM, Tena-Sempere M, Malagon MM, and Castano JP. 2008. Ghrelin induces growth hormone secretion via a nitric oxide/cGMP signalling pathway. J Neuroendocrinol 20:406-412.

Roskams AJ, Bredt DS, Dawson TM, and Ronnett GV. 1994. Nitric oxide mediates the formation of synaptic connections in developing and regenerating olfactory receptor neurons. Neuron 13:289-299.

Rössler W, Kuduz J, Schürmann FW, and Schild D. 2002. Aggregation of f-actin in olfactory glomeruli: a common feature of glomeruli across phyla. Chem Senses 27:803-810.

Sanes JR, Prescott DJ, and Hildebrand JG. 1977. Cholinergic neurochemical development of normal and deafferented antennal lobes during metamorphosis of the moth, *Manduca sexta*. Brain Res 119:389-402.

Schachtner J, Klaassen L, and Truman JW. 1998. Metamorphic control of cyclic guanosine monophosphate expression in the nervous system of the tobacco hornworm, *Manduca sexta*. J Comp Neurol 396:238-252.

Schachtner J, Homberg U, and Truman JW. 1999. Regulation of cyclic GMP elevation in the developing antennal lobe of the Sphinx moth, *Manduca sexta*. J Neurobiol 41:359-375.

Schachtner J, Huetteroth W, Nighorn A, and Honegger HW. 2004a. Copper/zinc superoxide dismutase-like immunoreactivity in the metamorphosing brain of the sphinx moth *Manduca sexta*. J Comp Neurol 469:141-152.

Schachtner J, Trosowski B, D'Hanis W, Stubner S, and Homberg U. 2004b. Development and steroid regulation of RFamide immunoreactivity in antennal-lobe neurons of the sphinx moth *Manduca sexta*. J Exp Biol 207:2389-2400.

Schachtner J, Schmidt M, and Homberg U. 2005. Organization and evolutionary trends of primary olfactory brain centers in Tetraconata (Crustacea + Hexapoda). Arthropod Structure and Development 34:257-299.

Schwartz LM and Truman JW. 1983. Hormonal control of rates of metamorphic development in the tobacco hornworm *Manduca sexta*. Dev Biol 99:103-114.

Simpson PJ, Nighorn A, and Morton DB. 1999. Identification of a novel guanylyl cyclase that is related to receptor guanylyl cyclases, but lacks extracellular and transmembrane domains. J Biol Chem 274:4440-4446.

Strausfeld NJ and Hildebrand JG. 1999. Olfactory systems: common design, uncommon origins? Curr Opin Neurobiol 9:634-639.

Tolbert LP, Matsumoto SG, and Hildebrand JG. 1983. Development of synapses in the antennal lobes of the moth *Manduca sexta* during metamorphosis. J Neurosci 3:1158-1175.

Tolbert LP. 1989. Afferent axons from the antenna influence the number and placement of intrinsic synapses in the antennal lobes of *Manduca sexta*. Synapse 3:83-95.

Tolbert LP, Oland LA, Tucker ES, Gibson NJ, Higgins MR, and Lipscomb BW. 2004. Bidirectional influences between neurons and glial cells in the developing olfactory system. Prog Neurobiol 73:73-105.

Truman JW, de Vente J, and Ball EE. 1996. Nitric oxide-sensitive guanylate cyclase activity is associated with the maturational phase of neuronal development in insects. Development 122:3949-3958.

Utz S and Schachtner J. 2005. Development of A-type allatostatin immunoreactivity in antennal lobe neurons of the sphinx moth *Manduca sexta*. Cell Tissue Res 320:149-162.

Vosshall LB, Wong AM, and Axel R. 2000. An olfactory sensory map in the fly brain. Cell 102:147-159.

Watson AH and Burrows M. 1981. Input and output synapses on identified motor neurones of a locust revealed by the intracellular injection of horseradish peroxidase. Cell Tissue Res 215:325-332.

Weevers RD. 1966. A lepidopteran saline: effects of inorganic cation concentrations on sensory, reflex and motor responses in a herbivorous insect. J Exp Biol 44:163-175.

Wilson CH, Christensen TA, and Nighorn AJ. 2007. Inhibition of nitric oxide and soluble guanylyl cyclase signaling affects olfactory neuron activity in the moth, *Manduca sexta*. J Comp Physiol A Neuroethol Sens Neural Behav Physiol 193:715-728.

Wright JW and Copenhaver PF. 2000. Different isoforms of fasciclin II play distinct roles in the guidance of neuronal migration during insect embryogenesis. Dev Biol 225:59-78.

Zayas RM and Trimmer BA. 2007. Characterization of NO/cGMP-mediated responses in identified motoneurons. Cell Mol Neurobiol 27:191-209.

CHAPTER III:

Mas-Allatotropin in the Developing Antennal Lobe of theSphinx Moth *Manduca sexta*: Distribution, Time Course Developmental Regulation, and Colocalization with Other Neuropeptides

Mas-Allatotropin in the Developing Antennal Lobe of the Sphinx Moth *Manduca sexta*: Distribution, Time Course, Developmental Regulation, and Colocalization with Other Neuropeptides

Sandra Utz, Wolf Huetteroth, Matthias Vömel, Joachim Schachtner*

Fachbereich Biologie, Tierphysiologie, Philipps-Universität Marburg, Karl-von-Frisch-Straße, D-35032 Marburg, Germany

Received 17 April 2007; revised 23 August 2007; accepted 30 August 2007

ABSTRACT: **The paired antennal lobes (ALs) of the sphinx moth *Manduca sexta* serve as a well-established model for studying development of the primary integration centers for odor information in the brain. To further reveal the role of neuropeptides during AL development, we have analyzed cellular distribution, developmental time course, and regulation of the neuropeptide *M. sexta* allatotropin (Mas-AT). On the basis of morphology and appearance during AL formation, seven major types of Mas-AT-immunoreactive (ir) cells could be distinguished. Mas-AT-ir cells are identified as local, projection, and centrifugal neurons, which are either persisting larval or newly added adult-specific neurons. Complementary immunostaining with antisera against two other neuropeptide families (A-type allatostatins, RFamides) revealed colocalization within three of the Mas-AT-ir cell types. On the basis of this neurochemistry, the most prominent type of Mas-AT-ir neurons, the local AT neurons (LATn), could be divided in three subpopulations. The appearance of the Mas-AT-ir cell types occurring during metamorphosis parallels the rising titer of the developmental hormone 20-hydroxyecdysone (20E). Artificially shifting the 20E titer to an earlier developmental time point resulted in the precocious occurrence of Mas-AT immunostaining. This result supports the hypothesis that the pupal rise of 20E is causative for Mas-AT expression during AL development. Comparing localization and developmental time course of Mas-AT and other neuropeptides with the time course of AL formation suggests various functions for these neuropeptides during development, including an involvement in the formation of the olfactory glomeruli.** © 2007 Wiley Periodicals, Inc. Develop Neurobiol 68: 123–142, 2008

Keywords: **insect; olfactory system; metamorphosis; neuropeptide; hormonal regulation**

INTRODUCTION

The antennal lobes (ALs) of the sphinx moth *Manduca sexta* serve as a well-established model for studying the neuronal development of the primary integration centers for odor information in the brain (Tolbert et al., 2004). ALs of insects compare to olfactory bulbs of vertebrates by sharing their principal morphological organization into so-called olfactory glomeruli, but also by a number of basic physiological properties with respect to information processing (Hildebrand and Shepherd, 1997; Strausfeld and

This article contains supplementary material available via the Internet at http://www.mrw.interscience.wiley.com/suppmat/1932-8451/suppmat.

**Present address:* Department of Biology, Animal Physiology, Philipps-University, Marburg 35032, Germany.

Correspondence to: J. Schachtner (schachtner@staff.uni-marburg.de).

Contract grant sponsor: DFG grant; contract grant number: Scha 678/3-3.

Published online 18 October 2007 in Wiley InterScience (www.interscience.wiley.com).
DOI 10.1002/dneu.20579

Hildebrand, 1999; Eisthen, 2002). Another characteristic of ALs and olfactory bulbs is the expression of a variety of neuropeptides (Smith et al., 1993; Caillol et al., 2003; Moody and Merali, 2004; Gutierrez-Mecinas et al., 2005; Schachtner et al., 2005). To further reveal the role of neuropeptides during ontogeny of the ALs, we focus in this study on the temporal expression pattern of the neuropeptide Mas-allatotropin (Mas-AT).

In *M. sexta* the ALs arise during metamorphosis, a hormonally-controlled postembryonic period lasting about 3 weeks. During this time, the whole brain undergoes reorganization and small larval antennal centers (LACs) develop into the adult ALs. AL development in *M. sexta* can be roughly divided into three phases (Oland and Tolbert, 1996; Dubuque et al., 2001). The preparation phase (phase I) lasts about 7–8 days beginning at pupal formation. It includes the birth of all AL neurons, the arrival of the axons of the olfactory receptor neurons (ORNs) in the ALs, and the formation of the protoglomeruli, the sites where the glomeruli form during phase II. The glomeruli formation phase (phase II) lasts about 5 days and is characterized by massive synaptogenesis between the involved neurons. It is assumed, that during phase II a basic network of synaptic contacts within and between the glomeruli is established, which ensures the principal correlation of in and output components of the AL (Dubuque et al., 2001). In contrast to phase II, in phase III, which lasts about 8 days up to adult eclosion, only little synaptogenesis occurs. During this last phase, the glomeruli grow in size between 40 and 130% (Huetteroth and Schachtner, 2005), probably because of the increasing neurite diameters, and the synaptic wiring in the glomeruli is thought to undergo further refinement and maturation (Tolbert et al., 1983; Tolbert, 1989; Dubuque et al., 2001). None of the neurons of the ALs undergo programmed cell death during phases I to III (Schachtner et al., 2004a), and, as all neurons of the ALs are born early in AL development (Hildebrand et al., 1997), the neuronal composition of the ALs does not change throughout formation of the ALs.

Immunocytochemical studies in a diversity of insects have indicated that several neuropeptides, including members of FMRFamide-related peptides (FaRPs), allatotropin, and A-type allatostatins (AST-A) are present in subpopulations of local AL neurons, which are responsible for information processing within and between glomeruli (for review see Schachtner et al., 2005). Mass spectrometric analysis of neuropeptides in the ALs of *M. sexta*, *Heliothis virescens*, the honeybee, and *Tribolium castaneum* even suggest about 40–50 different neuropeptides in the ALs of each of these species (Berg et al., 2007; Utz et al., 2007; and unpublished). Neuropeptides might operate as cotransmitters of GABA (γ-aminobutyric acid), the principle transmitter of local AL interneurons (Homberg and Müller, 1999). Concerning AL neurochemistry, the ALs of *M. sexta* are among the best studied (for review see Schachtner et al., 2005; Utz et al., 2007). Mapping of RFamides and AST-As throughout development of the sphinx moth ALs revealed unique developmental acquisition patterns in defined sets of neurons (Schachtner et al., 2004b; Utz and Schachtner, 2005). The occurrence of these neuropeptides is developmentally regulated by the steroid hormone 20-hydroxyecdysone (20E). Furthermore, for each neuropeptide family, the temporal pattern of their occurrence correlates with defined developmental phases, suggesting defined roles during AL development, including formation of olfactory glomeruli.

Mas-allatotropin, an amidated tridecapeptide (GFKNVEMMTARGF-NH_2) was isolated from heads of pharate adults of *M. sexta* (Kataoka et al., 1989). Since then, allatotropins (-TARGFamides) have been shown to be a highly conserved insect neuropeptide family (for reviews see Elekonich and Horodyski, 2003; Homberg et al., 2004; Nässel and Homberg, 2006). In *M. sexta*, the fall armyworm *Spodoptera frugiperda*, and the Eri silkworm *Samia cynthia ricini*, the allatotropin gene is expressed as at least three mRNAs that differ by alternative splicing. (*M. sexta*: Horodyski et al., 2001; Lee et al., 2002; *S. frugiperda*: Abdel-Latief et al., 2003, 2004; *S. cynthia ricini:* Sheng et al., 2007). The three different mRNAs in *M. sexta* encode Mas-AT itself and three allatotropin-like peptides (Mas-ATLs), which show bioactivities like Mas-AT, regarding stimulation of juvenile hormone (JH) biosynthesis in adults and inhibition of active ion transport on the larval midgut epithelium (Horodyski et al., 2001). Northern blot analysis revealed in the pupal brain expression of only one splice variant, which exclusively contains Mas-AT. In the pharate adult and adult brain additional low levels of a second splice variant, containing Mas-AT and Mas-ATL III, are expressed (Lee et al., 2002). A recent mass spectrometric study revealed only the ion signal of Mas-AT throughout AL development and in the adult AL, but no signal corresponding to the predicted mass of Mas-ATL III (Utz et al., 2007). This suggests that the splice form containing Mas-AT and Mas-ATL III is either not expressed in developing and adult ALs or the concentration of Mas-ATL III was too low for being detected. However, except for a single study which suggested the involvement of an allatotropin in photic entrainment of the circadian clock of the cockroach

Leucophaea maderae (Petri et al., 2002), nothing is known about possible functions of this neuropeptide family within brain circuits.

A prerequisite to understand the role of a certain neuromediator during nervous system development is the knowledge of its cellular and temporal localization. To further reveal the role of neuropeptides, we analyzed cell-type specific occurrence and hormonal regulation of allatotropin immunoreactivity during ontogeny of the ALs of *M. sexta*. Most of the Mas-AT-ir neurons are LNs which obtain their immunoreactivity with the beginning of the phase of glomeruli formation. This parallel and the developmental regulation via 20E, makes Mas-AT a candidate molecule for being actively involved during this defined phase of AL development.

With this study, we demonstrate for a third neuropeptide family distribution, time course, and regulation throughout AL development. Among the studied neuropeptides, the Mas-AT antiserum labels so far the largest amount of neurons in the ALs of *M. sexta*, including about one third of the LNs. In so far it was particularly interesting to study the developmental pattern of Mas-AT and to compare it with the earlier studies on RFamides and AST-As. This comparison revealed a third developmental pattern, namely the occurrence for Mas-AT immunoreactivity which contrasts the developmental pattern of the two other antisera.

MATERIALS AND METHODS

Animals

Manduca sexta (Lepidoptera: Sphingidae) were raised on an artificial diet under long-day photoperiod (L:D = 17:7) at 26°C in walk-in environmental chambers (Bell and Joachim, 1978). Under these conditions, the time required from hatching to pupal ecdysis is about 18 days, and the time from pupal to adult ecdysis is about 20 days. The start of the wandering stage (W0) occurs 3–4 days into the fifth larval instar (L5) and is characterized by the appearance of a red pigment along the heart. The following days are referred to as W1–W4. At about noon of W2, the animals go into a quiescent prepupal stage. Pupal ecdysis occurs on day W4, and the newly formed pupa is designated as day P0. Subsequent days of adult development are counted as P1–P20 and, after adult eclosion, as A0–A4. Larvae and pupae in this study have been staged according to the criteria described in Schwartz and Truman (1983) and Jindra et al. (1997). The criteria involve changes in structures that are either superficial or readily visible through the pupal cuticle under a dissecting microscope. To induce diapause, animals were reared under short-day photoperiod (L:D = 12:12; Bell and Joachim, 1978).

Immunocytochemistry

For immunostaining polyclonal rabbit antisera against *M. sexta* allatotropin (Mas-AT), *Diploptera* allatostatin 7 (Dip-AST7), RFamide, and γ-amino-butyric acid (GABA), and polyclonal antisera raised in guinea pigs against GABA and the transmembrane form of *Manduca sexta* Fasciclin II (TM-MFas II), and monoclonal antibodies from mouse against two ubiquitous synaptic vesicle proteins from *Drosophila* namely synaptotagmin and Synapsin I (SYNORF1) were used. Antiserum against Mas-AT was used at a concentration of 1: 4000 (No. 13.3.91, kindly provided by Dr. J. Veenstra, University of Bordeaux, Talence, France; Veenstra and Hagedorn, 1993). The antiserum recognizes Mas-AT (Kataoka et al., 1989) and *Locusta* myotropin (Veenstra and Hagedorn, 1993), both ending with TARGFamide. Specificity of the anti-Mas-AT antiserum has been shown by preadsorption of the antiserum with 100 μM synthetic Mas-AT (Bachem, Bubendorf, Switzerland) for 1 h at room temperature, which abolished all immunostaining in *M. sexta* brain sections (data not shown). Preadsorption of the antiserum with 100 μM synthetic FLRFamide, FMRFamide, or Dip-AST7 (all Sigma-Aldrich, St. Louis, MO) for 1 h at room temperature had no effect on immunostaining (data not shown). Antiserum against Dip-AST7, which is generally thought to recognize AST-A, was used at a concentration of 1:10,000 (kindly provided by Dr. H. Agricola, University of Jena, Germany; Utz and Schachtner, 2005). As shown previously by competitive ELISA the serum cross-reacts with other members of the AST-A peptide family, all characterized by their C-terminal Y/FXFGLamide sequence (Vitzthum et al., 1996). In a noncompetitive ELISA analysis, no cross-reactivity of the antiserum was found with corazonin, crustacean cardioactive peptide, FMRFamide, leucomyosuppressin, locustatachykinin II, perisulfakinin, or proctolin (Vitzthum et al., 1996). Preadsorption of the Dip-AST7 antiserum with 100 μM synthetic Dip-AST7 (Sigma-Aldrich) for 1 h at room temperature abolished all immunostaining in *M. sexta* brain sections, whereas preadsorption of the antiserum with 100 μM synthetic FLRFamide, FMRFamide (both Sigma-Aldrich), or *M. sexta* allatotropin (Bachem) for 1 h at room temperature had no effect on immunostaining (Utz and Schachtner, 2005). Anti-RFamide antiserum (#671, used at dilutions of 1:4000 to 1:10,000; Schachtner et al., 2004b) was kindly provided by Dr. E. Marder (Brandeis University, USA). The RFamide antiserum recognizes FMRFamide and FLRFamide peptides (Marder et al., 1987; Kingan et al., 1990), including the three FaRPs identified in *M. sexta* (Kingan et al., 1990, 1996; Miao et al., 1998).

To test whether the three used peptide antisera recognize proteins containing the short amino acid sequences, we performed Western blots. Peptide antisera were used at the same concentrations as for immunocytochemistry and preadsorptions were performed accordingly. We found for all three antisera several bands and preadsorption of the antisera resulted in the same pattern as found with the antiserum only (supplementary material Fig. S1). The results suggest that the bands recognized in the blots are due to

unspecific binding of the peptide antisera. However, as the same preadsorption protocol revealed no staining in brain sections, we conclude that the unspecific bands in the blots resulted from the sample preparation performed during the Western blot procedure.

The polyclonal anti-GABA antiserum (NT-108, Protos Biotech, New York, NY) raised in guinea pig was used at a concentration of 1:1000, the polyclonal anti-GABA antiserum raised in rabbits (kindly provided by Dr. T.G. Kingan, U.S. Dept. of Agriculture, Beltsville, MD) was used at a concentration of 1:2000. Both antisera were raised against conjugates of GABA covalently coupled to hemocyanin. The specificity of the rabbit GABA antiserum for *M. sexta* tissue has been shown in detail earlier (Hoskins et al., 1986). To demonstrate the specificity of the GABA antiserum raised in guinea pig, we performed double labeling experiments on 40 μm vibrating microtome sections with both anti-GABA antisera. Both antisera label the identical cells (Fig. S2).

The anti-TM-MFas II was used at a concentration of 1:2000 (kindly provided by Dr. P.F. Copenhaver, OHSU, USA). The specificity of the anti-TM-MFas II antiserum for *Manduca* nervous tissue was shown by Western blot analysis (Wright and Copenhaver, 2000). Anti-synaptotagmin (1:4000, kindly provided by Dr. K. Menon, Caltech, USA) and anti-synapsin antibodies (1:100, kindly provided by Dr. E. Buchner, University of Würzburg, Germany) were used to selectively label neuropil structures including olfactory glomeruli (Dubuque et al., 2001; Berg et al., 2002). *M. sexta* synaptotagmin was previously cloned and the specificity of the monoclonal anti-synaptotagmin antibody in *Manduca* brain tissue was shown by Western blot analysis and by cross comparison with a polyclonal anti-synaptotagmin antiserum recognizing a different region of the protein (Dubuque et al., 2001). Western blot analysis with the monoclonal anti-Synapsin I antiserum revealed one double band at a molecular weight of about 70 kDa in pupal (P8) and adult (A0) *M. sexta* brain tissue which is similar to the situation in *Drosophila* larval brain tissue (supplementary material Fig. S3, procedures see below). In homogenates of *Tribolium castaneum* pupal brain tissue only one band around 66 kDa was detected (Fig. S3). The result suggests a high specificity of the antiserum for all tested brain homogenates. The MW of 70 and 74 kDa for two isoforms of Synapsin 1 of *Drosophila* was shown by Klagges et al. (1996) in Western blots of whole head homogenates. An additional band at 80 kDa as shown by Klagges et al. (1996) was not detected, suggesting that this isoform is not highly enough expressed in larval brain tissue of *Drosophila* to be detected in Western blot.

Goat anti-rabbit antibodies conjugated to Cy2 and Cy3, goat anti-guinea pig conjugated to Cy3, and goat anti-mouse antibodies conjugated to Cy5 were used as secondary antisera (each 1:300; JacksonImmuno Research, Westgrove, PA). After dissection in cold saline (Weevers, 1966), brains of *M. sexta* were fixed in 4% formaldehyde in phosphate-buffered saline for 2 h (5 h using the anti-GABA antiserum) at room temperature or overnight at 4°C. For the double labeling with the two GABA antisera brains 0.1% glutaraldehyde was added to the fixative. After fixation, brains were either embedded in gelatin/albumin, postfixed overnight in 4% buffered formaldehyde and cut at 40 μm with a vibrating blade microtome (Leica VT 1000S) in the frontal, sagittal or horizontal plane, or processed as whole-mount. Immunostaining procedure was performed exactly as described in Schachtner et al. (2004b) or, for the whole-mounts, as described in Huetteroth and Schachtner (2005). For triple-labeling, the anti-Mas-AT, anti-GABA, and anti-synapsin antibodies were applied simultaneously and, likewise, the corresponding secondary antisera. Double labeling with anti-Mas-AT and anti-Dip-AST7 or anti RFamide antisera was performed according to a method modified from Negoescu et al. (1994), for double immunolabeling with primary antisera from the same species as recently described in Berg et al. (2007).

Western Blot Analysis

To demonstrate the specificity of the three peptide antisera and of Synapsin I for *M. sexta* tissue, we homogenized the brains of various pupal and adult *M. sexta* stages in ice-cold 10 m*M* Tris-HCl (pH 7.4) containing protease inhibitors (2 m*M* phenylmethylsulfonlyl fluoride (PMSF), 30 μM aprotinin, 20 μM leupeptin, 150 μM pepstatin). For Synapsin I we additionally homogenized pupal *Tribolium castaneum* and larval (L3) *Drosophila melanogaster* brains. Total protein concentrations of the samples were determined after Bradford (1976). Then, 10 μg of each sample was boiled for 3 min in an equal volume of reducing sample buffer (500 m*M* Tris-HCl, pH 6.8, containing 4% sodium dodecyl sulfate (SDS), 5% 2-mercaptoethanol, 20% glycerol, and 0.2% bromophenol blue). Samples were run on a discontinuous SDS-12.5% polyacrylamide gel and blotted onto Optitran BA-S 83 nitrocellulose membranes (Carl Roth GmbH & Co. KG, Karlsruhe, Germany). The blots were blocked in 0.1*M* phosphate-buffered saline (PBS; pH 7.4) plus 0.1% Tween 20, and 5% Slim.Fast vanilla powder (Slim.Fast, Englewood, NJ) for 2 h at room temperature (RT) and then incubated with the various antisera respectively (dilutions: Mas-AT 1:4000, Dip-AST7 1:10,000, RFamide 1:4000, Synapsin I 1:500) in PBS plus 0.05% Tween 20 at 4°C overnight. After washing for 45 min in PBS plus 0.05% Tween 20, 1% Triton X-100, and 1% SDS (PBT), the blots were incubated with a 1:5000 dilution of HRP-conjugated anti-rabbit or anti-mouse antibody (JacksonImmuno Research) in PBS plus 0.05% Tween 20 for 2 h at RT. After washing again for 1 h in PBT, the blots were incubated with chemiluminescent substrate according to the SuperSignal directions (PIERCE, Rockford, IL) and exposed to Fuji Super RX film (FUJIFILM, Düsseldorf, Germany).

Hormone Manipulation Experiments

20-hydroxyecdysone (20E, Sigma-Aldrich) was dissolved in saline (Ephrussi and Beadle, 1936) to a final concentration of 1 μg/μL. Pupae in stage P1 were chilled on ice for 2 min and then injected once with 15 μg 20E per gram body

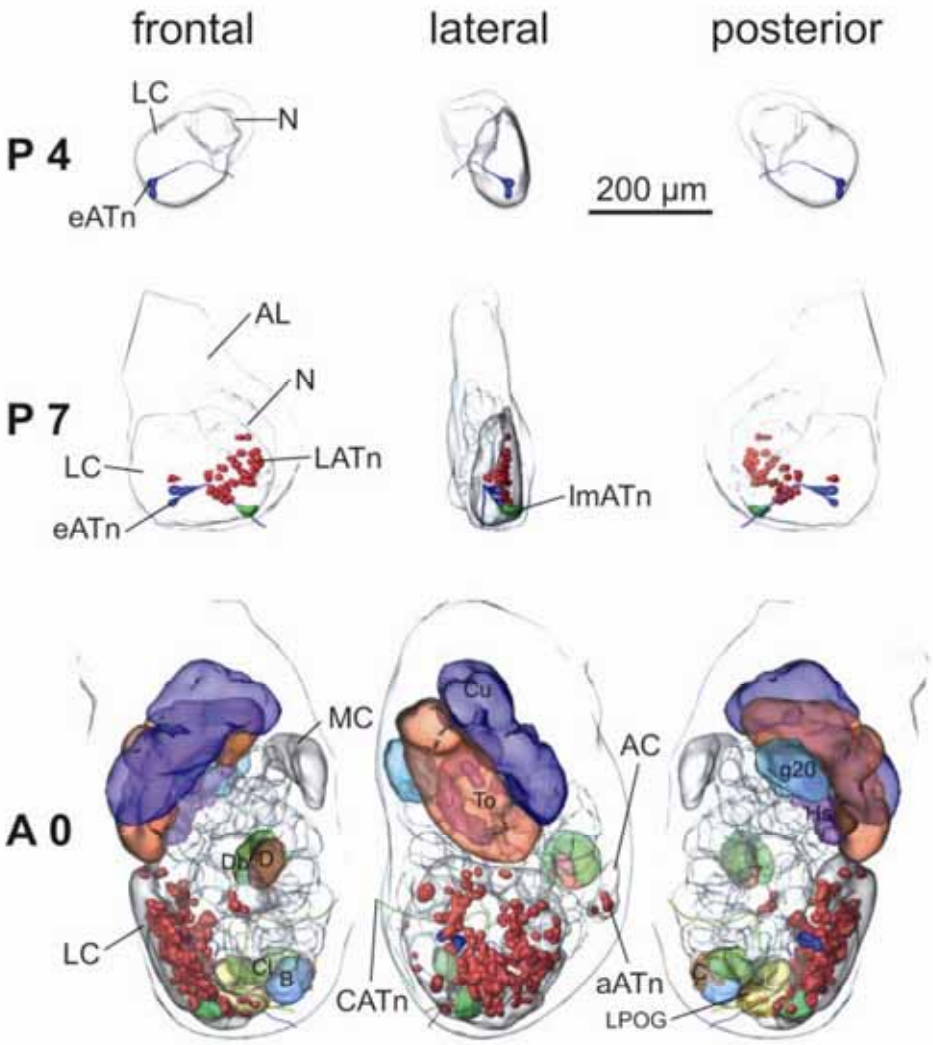

Figure 1 3D reconstructions of Mas-AT-ir cells during AL development (P4, P7) and in the adult AL. The outlines of the AL are shown in transparent light grey and the developing neuropil (N), glomeruli, and cell groups (LC, lateral cell group; MC, median cell group; AC, anterior cell group) are shown in dark grey. Recently standardized glomeruli are color coded according to Huetteroth and Schachtner (2005; B, base (blue); C, cap (light orange); Cl, club (light green); Cu, cumulus (dark blue); D, disc (red); Db, disc base (green); g20 (light blue); Hs, horseshoe (purple); LPOG, labial pit organ glomerulus (yellow); To, toroid (orange)). Note the continuous presence of the two early Mas-AT-ir neurons (eATn; blue somata) in all stages shown and their primary neurite leaving the AL [compare with Fig. 5(a)]. The single large median Mas-AT-ir neuron (lmATn, green soma) can easily be determined from P7/8 onwards. Most Mas-AT-ir cells, the local Mas-AT-ir neurons (LATn), reside in the LC, but Mas-AT-ir cells were also found in the AC (aATn) and outside any cell group (dlATn). The reconstruction of the "arc" of the centrifugal Mas-AT-ir neuron (CATn) in A0 is shown in light green. See also supplementary material (Fig. S4–animated 3D AL). Scale: 200 μm.

weight (Schachtner et al., 1999). Control animals were injected with 15 μL saline per gram body weight. All injections were performed with 100 μL Hamilton syringes dorsolaterally into the pupal thorax. Wounds were immediately sealed with melted wax, and animals were taken back to their walk-in environmental chambers. 3.5–11 days later, animals were dissected and processed according to the immunocytochemistry protocol described earlier.

Data Processing

Fluorescence was analyzed using a confocal laserscan microscope (Leica TCS SP2). Cell counts were performed at a magnification of 400×. As previously described (Utz and Schachtner, 2005) we used two strategies to obtain numbers of Mas-AT labeled cell bodies in the lateral cell group (LC). (1) For up to 35 cell bodies in total, we compared section by section to ensure that each cell was only counted once. (2) For a total of more than 35 cells, we counted every stained cell body including fragmented somata in each section and used the Abercrombie correction factor to obtain real cell numbers (Abercrombie, 1946). The mean diameter (d_m) of cell bodies (LATn) showing Mas-AT immunoreactivity in LCs from stage P7 up to the adult stage was 16.3 ± 2.7 μm. Comparing cell diameters between single stages revealed a slight increase in cell diameter between stages P7 to P12 of about 3.5 μm ($p < 0.001$ assessed by unpaired T-test) (stage P7: $d_m = 14.4 \pm 2.0$ μm ($n = 14$ of 4 ALs); stage P8: $d_m = 14.6 \pm 2.5$ μm ($n = 44$ of 11 ALs);

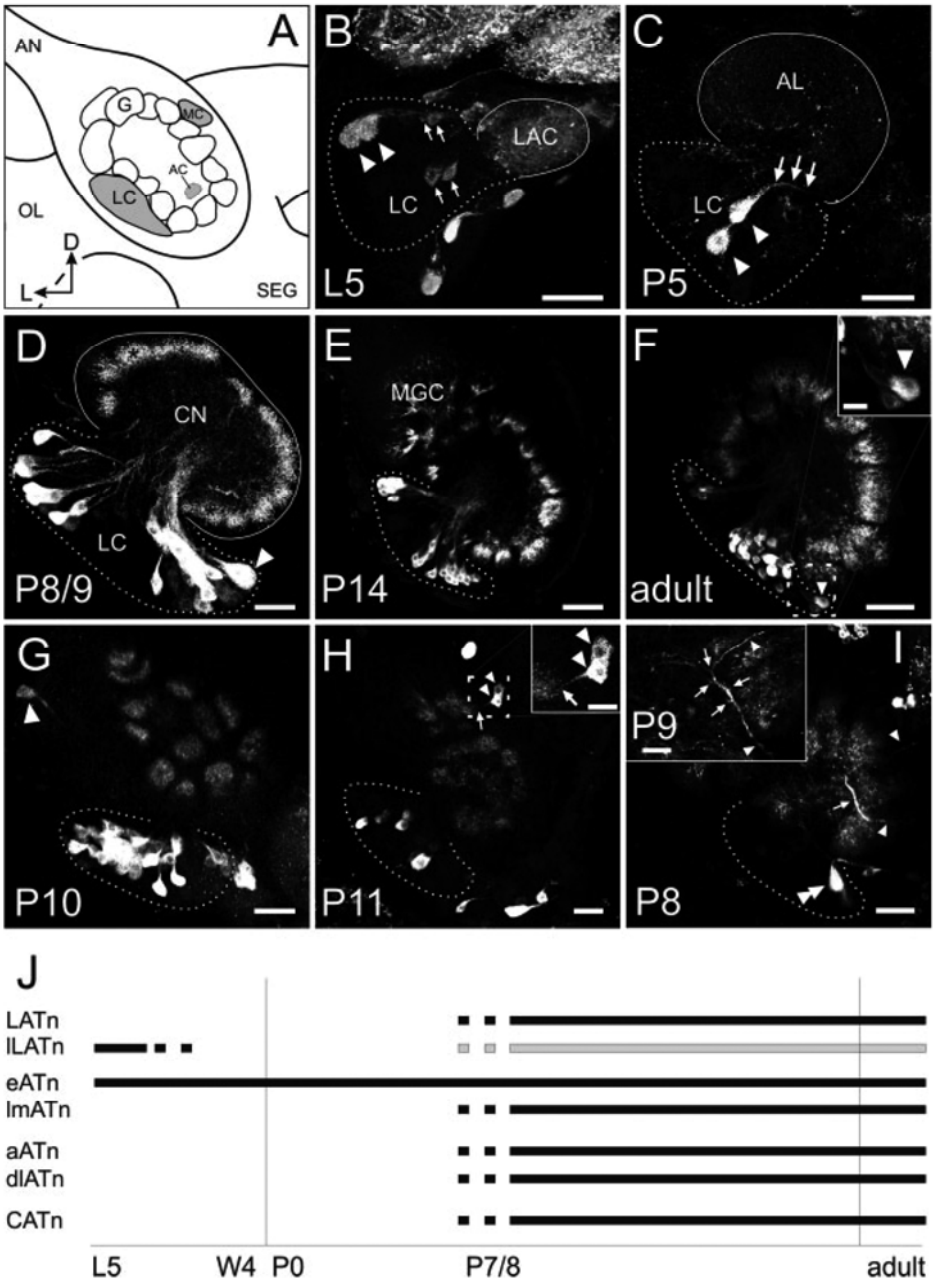

Figure 2

stage P9: $d_m = 15.7 \pm 2.3$ μm ($n = 113$ of 17 ALs); stage P10: $d_m = 16.3 \pm 2.7$ μm ($n = 89$ of 12 ALs); stage P11: $d_m = 16.8 \pm 2.7$ μm ($n = 58$ of 10 ALs); stage P12: $d_m = 18.1 \pm 3.0$ μm ($n = 72$ of 11 ALs)). Between stages P12 and adult we found a slight decrease in cell diameters of about 2.6 μm ($p < 0.001$ assessed by unpaired *T*-test) (stage P14–P16: $d_m = 17.8 \pm 2.9$ μm ($n = 66$ of 15 ALs); pharate: $d_m = 16.8 \pm 2.0$ μm ($n = 76$ of 17 ALs); adult: $d_m = 15.5 \pm 2.6$ μm ($n = 152$ of 21 ALs)). Since changes in diameter of the somata were only small, we decided to use one correction factor for whole developmental study. Thus, with a section thickness of 40 μm and a d_m of cell bodies of 16.3 μm, the Abercrombie correction factor used for cell counts in stage P7 up to adult was 0.71.

3D-Reconstruction

Digitization and 3D reconstructions of wholemount ALs labeled with anti Mas-AT and anti-synapsin antisera, visualized by corresponding secondary antisera coupled to Cy2 and Cy5, respectively, were performed with the Leica TCS SP2 and the 3D reconstruction software AMIRA 3.1–4.1.1 (Mercury Computer Systems, Chelmsford, MA) according to the protocol described in Huetteroth and Schachtner (2005). The AL outlines and cell group borders were labeled based on background staining of either data channel. The primary neurite of the early Mas-AT-ir neuron (eATn) in the P4 AL was reconstructed using the skeletonize plugin tool for AMIRA (Schmitt et al., 2004).

RESULTS

Mas-Allatotropin-ir Neurons During AL Development

On the basis of morphology and appearance during formation of the ALs, seven major types of Mas-AT-immunoreactive (ir) cell types could be distinguished (Figs. 1 and 2; Table 1). In the 5th instar larva (L5), the LAC contains numerous Mas-AT-ir fibers stemming from a cluster of about 10 smaller Mas-AT-ir larval LNs [lLATn, Fig. 2(B)]. The lLATn ceased their immunoreactivity between wandering stages W3 to W4. In contrast, two large neurons with strong Mas-AT immunoreactivity (early Mas-ATn or eATn) also present in the LAC of the 5th instar larva persisted during metamorphosis into the adult AL [Fig. 1, blue cells; Fig. 2(B,C)]. Typically, the eATn have cell bodies with diameters larger than 25 μm located in the ventral part of the lateral cell group. Without any projections in the glomeruli, the eATn send their

Figure 2 Confocal images of 40 μm sections showing frontal views of Mas-AT immunoreactivity during AL development. The dashed line encircles the lateral cell group (LC), the solid line encircles the neuropil of the LAC (B) or of the developing AL (C, D). (A) Schematic of the AL presenting the orientation (frontal) of the sections B–I with respect to the position of the three cell groups (grey); LC, median cell group (MC), anterior cell group (AC). Orientation bars: D, dorsal; L, lateral. (B) The two early Mas-AT-ir neurons (eATn, arrowheads) and about 10 smaller LNs (lLATn, small arrows) label in the larval (L5) LC. (C) In pupal stage P5, the two eATn (arrowheads) are the only neurons labeled in the LC–no staining in the neuropil could be detected. (D) P8/9: Local Mas-AT-ir neurons (LATn), which appear from stage P6/7 onwards and the large median Mas-AT-ir neuron (lmATn, arrowhead; compare with Fig. 1). Note the densely packed neurites, mainly stemming from the LATn, projecting into the central coarse neuropil (CN) and the dense Mas-AT immunoreactivity in the forming glomeruli (asterisks). (E) LATn innervating all glomeruli including the male specific macroglomerular complex (MGC) in a P14 AL. (F) Adult AL of a female *M. sexta*; the lmATn can be distinguished from the LATn by its typical median position, the leaf-like basal primary neurite, and the larger cell body (arrowhead, inset). (G) One Mas-AT-ir cell body in the anterior cell group (arrowhead) 10 days after pupal ecdysis. (H) In pupal stage P11, two dorsolateral Mas-AT-ir neurons (dlATn, arrowheads, inset) send their neurites (arrow) towards the AL neuropil. Typically, the neurites stained only a short distance from the cell body (arrow). (I) The "arc" neurite stemming from the centrifugal Mas-AT-ir neuron (CATn) gives rise to arborizations which intermingle with other Mas-AT-ir fibers in the AL neuropil (arrows). The arc-shaped neurite is formed by a large fiber entering/leaving the AL via the inner antenno-cerebral tract and entering/leaving the AL from/towards the tritocerebrum (arrowheads). Main figure shows a frontal view, inset a sagittal view. Note one of the eATn (double arrowhead) with its primary neurite leaving the AL. (J) Summary of the developmental time course for each of the Mas-AT-ir neuron types. The grey bar accounts for our hypothesis that the about 10 larval LNs (lLATn) might regain their Mas-AT identity during pupal development. The *x*-axis shows a simplified time scale starting during L5 larva and ending with early adult. W4, 4 days after beginning of wandering stage which is equivalent to a prepupa shortly before pupal formation. AN, antennal nerve; G, glomerulus; OL, optic lobe; SEG, subesophageal ganglion. Scale: 50 μm in B–D, G–I; 100 μm in E, F; 25 μm in insets in F, H, I.

Table 1 Mas-AT-ir Neuron Types

Mas-AT-ir Neuron Type	Number[a]		Origin	Identical To
Local neurons				
lLATn	~10		Larval	
LATn	P9/10	Adult		
Mas-AT	~20 to 30	~30	Adultsp.	
Mas-AT + AST-A	~30	~30	Adultsp.	Type Ia AST-A[b]
Mas-AT + RFamide	~20	~40	Adultsp.	Type I RFamide[c]
Projection neurons				
eATn	2		Larval	Type III RFamide[c]
lmATn	1		Larval	Type II RFamide[c]
aATn[d]	2–4		Adultsp.	
dlATn[d]	1–2		Adultsp.	
Centrifugal neurons				
CATn	1		Adultsp.	

Most of the Mas-AT-ir neurons are LNs (LATn), which can be subdivided into three groups with respect to their different neuropeptide chemistry. Adultsp., adultspecific.

[a] Number per AL.

[b] Utz and Schachtner, 2005.

[c] Schachtner et al., 2004b.

[d] Assignment as PN according to the location of the cell bodies.

primary neurite out of the AL towards the tritocerebrum. Owing to the numerous other Mas-AT-ir processes in the tritocerebrum, we could not further trace the neurites of the eATn.

In contrast to the lLATn and eATn, the other cell types did not obtain Mas-AT staining until after 6/7 days post-pupal eclosion (P6/7). The most prominent cell type, the local Mas-AT-ir neurons (LATn), consists exclusively of LNs located in the lateral cell group [LC; Figs. 1 and 2(D–H)]. The LATn with their smaller cell body diameter (<20 μm) could be clearly distinguished from the eATn with their large neurite leaving the AL [Figs. 1 and 6(J)]. Numbers of the LATn linearly increase between stages P6/7 and P13 from 0 to about 100 neurons [Figs. 2(J) and 3]. From P13 into adult stages, numbers of the LATn remained constant [Fig. 3]. A third cell type, the large median Mas-AT-ir neurons (lmATn), consists of a single cell with a large soma located in the median part of the LC and sends its neurite similar to the eATn into the tritocerebrum where it intermingled with other Mas-AT-ir fibers [Fig. 1, green cell; Fig. 2(D,F)].

Two other cell types (consisting of one to three cells) located outside the LC in anterior and dorsolateral positions in the AL and termed accordingly (aATn, dlATn), occurred not until after stage P7/8. Mas-AT staining in both cell types was always confined to the cell body and a neurite projecting towards the glomerular neuropil. Furthermore, aATn and dlATn were not observed in all, but a certain percentage of the preparations (of a total of 93 analyzed ALs: aATn, 45.2%; dlATn, 23.7%).

One Mas-AT-ir centrifugal neuron (CATn) could be identified from stage P7 onwards. The CATn consists of a large arc-shaped neurite in the basal median part of the AL, from where smaller fibers inter-

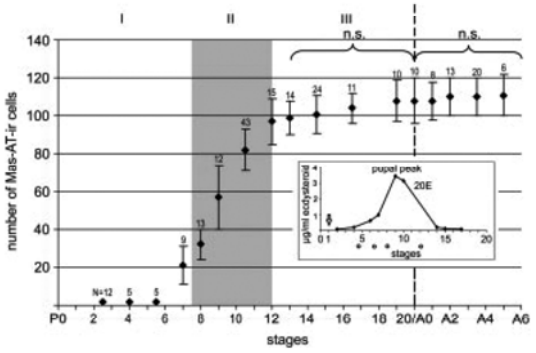

Figure 3 Developmental time course of numbers of Mas-AT-ir cell bodies in the lateral cell group (LC), mainly including the local Mas-AT-ir neurons (LATn). Acquisition of Mas-AT immunostaining in LATn occurred in a single step from 0 up to about 100 between stage P6/7 and P13. This prominent rise of number of the Mas-AT-ir neurons parallels the increasing titer of the hormone 20E in the hemolymph (inset) and the main wave of synaptogenesis (phase II, shaded area). Each data point indicates mean number ± standard deviation (*n* numbers of ALs, dotted line adult eclosion at P20/A0). Before stage P6 only the two eATn were labeled. Inset: Hemolymph concentrations of 20E during pupal-adult transition as reported by Warren and Gilbert (1986). The arrow indicates the time of 20E injection at stage P1. The small circles indicate times when injected animals were dissected and processed for immunocytochemistry (see Fig. 5).

mingled with the other Mas-AT-ir fibers in the coarse neuropil [inset in Fig. 2(I)]. The large neurite could be followed on one side into the inner antenno-cerebral tract (IACT, Homberg et al., 1988) and on the other side it was leaving the AL towards the tritocerebrum [Figs. 1 and 2(I)]. Owing to the fact that the immunostained fiber in the IACT usually faded out after a short distance and that the neurite in the tritocerebrum intermingled with numerous Mas-AT-ir fibers we could not trace the neurite back to its cell body.

Mas-AT-ir Projections in the Developing AL Neuropil

Sparse Mas-AT-ir projections appeared in the developing AL-neuropil 6–7 days after pupal eclosion (P6/7), which is the time when formation of the protoglomeruli begins. To examine whether Mas-AT-ir fibers enter the protoglomeruli, we labeled ingrowing axons of ORNs with an antiserum against the transmembrane domain of *M. sexta* fasciclin II (TM-MFas II). A recent study by Higgins et al. (2002) demonstrated the early expression of TM-MFas II in a subset of ORNs (including the axons) before glomerulus formation; this was taken as evidence for a role of TM-MFas II during the sorting and guidance of axons. Because of its early appearance in ORN axons, TM-MFas II can be used as a reliable marker for the formation of protoglomeruli, the templates for the later-forming glomeruli. In *M. sexta*, protoglomeruli are thought to be initially formed by axon endings of ORNs and uniglomerular PNs (uPNs; Malun et al., 1994; for a review, see Tolbert et al., 2004). Triple-immunolabeling with antisera against Mas-AT, TM-MFas II, and synapsin revealed between stage P6/7 to P7/8 no overlapping areas labeled with Mas-AT and TM-MFas II antisera (Fig. 4). Mas-AT-ir fibers stayed within the confinement of the central neuropil visualized by the synapsin antiserum [Fig. 4(A,A′)]. At the beginning of phase II (P7/8), Mas-AT-ir fibers start to project into the basal part of the newly forming glomeruli [Fig. 4(B,B′)] to eventually display finger-like protrusions from more basal to distal parts of each glomerulus in later developmental stages and in the adult, a pattern typical for LNs [Fig. 2(D–F); Schachtner et al., 2004b; Utz and Schachtner, 2005].

Hormone Manipulation

The rising number of LATn during AL development parallels the increasing titer of 20E in the hemolymph from P4 to P9 (inset in Fig. 3; Warren and Gilbert, 1986). To determine whether 20E is responsible for the increasing numbers of LATn, we injected 15 μg/g body mass of 20E into the hemolymph of stage P1 pupa (Schachtner et al., 1999, 2004b). Pupa were dissected 3.5–11 days after 20E injection and processed for immunocytochemistry (inset in Fig. 3). 3.5, 5.5, and 7 days after injection, the numbers of the LATn had increased to a level usually reached 2 days later during normal development. Eleven days after injection, the numbers of LATn in controls and 20E treated animals were the same as expected from normal development [Fig. 5(A,B,F)]. Across all preparations not only the soma numbers labeling with the Mas-AT antiserum increased after 20E injection but also the neurites of the cells showed strong staining [Fig. 5(B,C)].

As already shown in previous studies, formation of the olfactory glomeruli indicated by synaptotagmin immunostaining was advanced by 3–4 days compared to normal development [Fig. 5(A,B); Schachtner et al., 2004b; Utz and Schachtner, 2005]. A few of the animals which were dissected 3.5 days and all of the animals which were dissected 5.5 days after 20E injection showed an earlier occurrence of Mas-AT immunoreactivity in the lmATn and in the CATn, which normally do not appear before stage P7/8 [Fig. 5(D,E)]. Immunostainings of two pupae which had been in diapause for several weeks revealed only the two eATn, but no other Mas-AT-ir cells in the LC [Fig. 5(C)].

Colocalization of Mas-AT with GABA, RFamides, and A-Type Allatostatins

Most, if not all LNs in the LC are GABA-ir (Hoskins et al., 1986). Double immunostaining with antisera against GABA and Mas-AT demonstrated that in the LC, the eATn and the lmATn are not GABA-ir, while all of the LATn stain positively with the anti-GABA antiserum [Fig. 6(A–C)]. Inspecting the AL output tracts—in horizontal, sagittal, and frontal sections, as well as in wholemounts—revealed typically one Mas-AT-ir fiber in the IACT, belonging to the CATn, and, towards the SEG, the CATn fiber and two to three faintly labeled fibers very likely belonging to the eATn and the lmATn. Independently to the GABA double stainings, these results underline the identity of the LATn as LNs.

Schachtner et al. (2004b) described a large single RFamide-ir PN (type II) and two RFamide-ir somata (type III) in the LC which persisted from the larva into adulthood. Double labeling with anti-RFamide

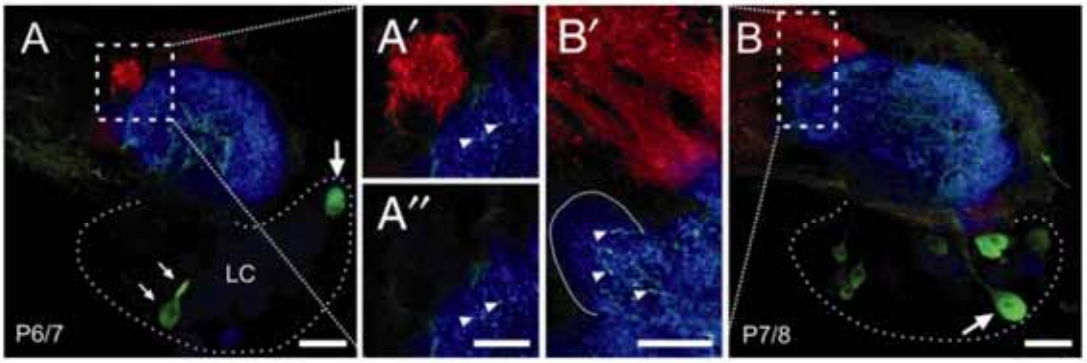

Figure 4 Confocal images showing triple-immunolabeling with antisera against Mas-AT (green), TM-MFas II (red), and synapsin (blue). All frontal views. (A) At stage P6/7, about one third of ingrowing axons of ORNs stains with the TM-MFas II antiserum and identifies protoglomerular templates. In this section, the two early Mas-AT-ir neurons (eATn, small arrows) and the large median Mas-AT-ir neuron (lmATn, large arrow) are labeled in the lateral cell group (LC, encircled). (A′, A″) Magnifications of A. Typically the Mas-AT-ir arborizations (arrowheads) are restricted to the synapsin-ir area. In A″ the red channel has been skipped to show that there is no immunostaining other then the TM-MFas II staining in the area of the shown protoglomerulus. (B, B′) At stage P7/8, Mas-AT-ir fibers (arrowheads in B′) start to enter the forming glomeruli at their basis (B′, encircled). In this section, a large median Mas-AT-ir neuron (lmATn, arrow) and several local Mas-AT-ir neurons (LATn) can be seen in the LC. (B′) magnification of B. Scales: 50 μm (A, B); 25 μm (A′, A″, B′).

and anti-Mas-AT antisera showed that the lmATn and the two eATn colocalize RFamide and Mas-AT staining and are thus identical with the type II and III RFamide neurons, respectively [Fig. 6(D–F,J,K)]. For the LATn, double immunostaining revealed that about 17 ($\sim$20% of the LATn; $n_{AL} = 6$) in P10 and about 37 ($\sim$35% of the LATn; $n_{AL} = 5$) in adults (A0/1) additionally to their Mas-AT staining exhibited RFamide immunoreactivity [Fig. 7(A)]. Corresponding to the RFamide neurons in the LC, about 65% in P10 and about 59% in A0/1 showed colocalization with Mas-AT immunostaining.

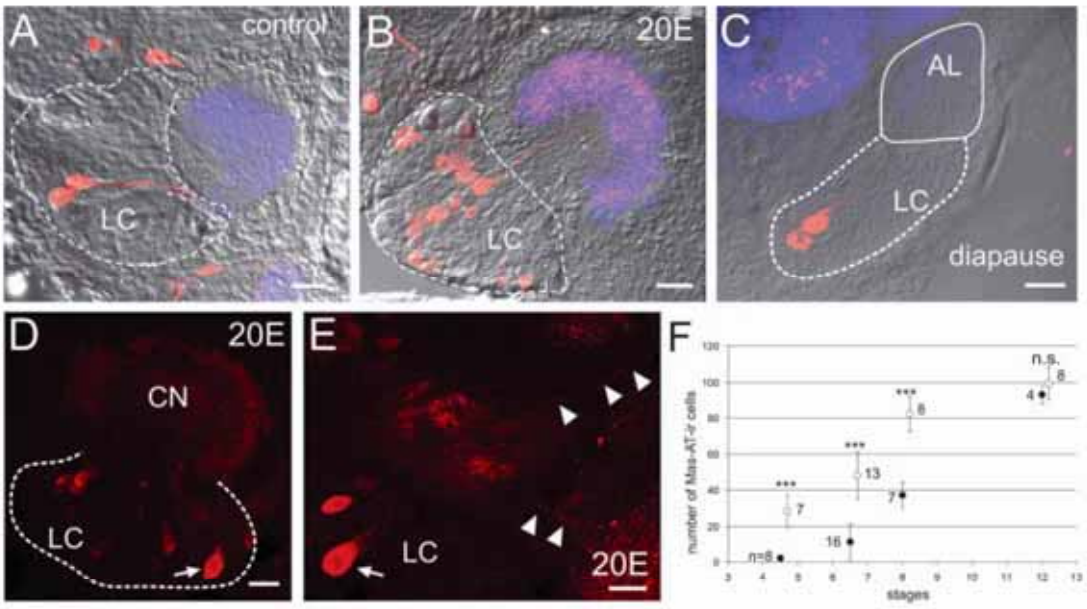

Figure 5

Double immunolabeling with antisera against Mas-AT and AST-A revealed colocalization in many LATn [Fig. 6(G–I)], but not in the other Mas-AT-ir cell types. The degree of colocalization for the LATn was examined in four developmental stages [Fig. 7(B)]. In stage P9/10 about 43% ($n_{AL} = 8$), in stage P13 about 38% ($n_{AL} = 10$), in pharate animals about 32% ($n_{AL} = 8$), and in adults (A0) about 30% ($n_{AL} = 6$) of the Mas-AT-ir neurons additionally labeled with the anti-AST-A antiserum. For about 30–40 AST-A-ir LC-neurons in the examined stages, the percentage of neurons which colocalized both immunoreactivities was about 70% in stage P9/10 ($n_{AL} = 8$), about 83% in stage P13 ($n_{AL} = 10$), about 89% in pharates ($n_{AL} = 8$), and about 81% in adults (A0; $n_{AL} = 6$). The AST-A-ir processes of a recently described centrifugal neuron are devoid of Mas-AT immunoreactivity [Fig. 6(G–I); Utz and Schachtner, 2005].

To test the possibility whether all three neuropeptide antisera (Mas-AT, AST-A, RFamide) colocalize in the same neurons, we double labeled P10 and adult animals with the anti-AST-A and the anti-RFamide antisera (Fig. 6L). The result showed no overlap between these two antibody stainings in the LC, suggesting that local AL neurons contain a combination of two of the three neuropeptides but not all three.

DISCUSSION

Specificity of the Mas-Allatotropin Antiserum

The polyclonal anti-Mas-AT antiserum used in this study recognizes peptides C-terminally ending with -TARGFamide (Veenstra and Hagedorn, 1993). In *M. sexta*, a single gene encodes for Mas-AT and for three allatotropin-like peptides (ATL I-III), which originate from three different mRNA splice-variants (Horodyski et al., 2001). Structurally, the three Mas-ATLs differ at their C-terminus by two to three amino acids from the conserved -TARGFamide of Mas-AT. Northern blot analysis suggested that in pupal and in adult brains predominantly the mRNA containing only Mas-AT and low amounts of the mRNA containing Mas-AT and Mas-ATL III are expressed (Lee et al., 2002). A recent mass spectrometric analysis revealed only Mas-AT, but none of the Mas-ATL

Figure 5 Hormone manipulation experiments and diapausing animals. Confocal images showing Mas-AT (red, A–E) and synapsin (blue, A–C) immunoreactivity. For better visualization of the outline of the AL, Nomarski contrast images of the sections are added in A–C (grey). All frontal views if not stated otherwise. (A, B) Mas-AT immunoreactivity (red) in ALs after injection of the vehicle alone (A) and after 20E injection (B) at stage P1 and dissection 3.5 days later at pupal stage P4/5. (A) After control injection, ALs was indistinguishable from ALs of untreated animals at stage P4/5. In the LC (dashed line), the two early AT-ir neurons (eATn) are labeled with their neurites leaving the AL. Typical for stage P4/5, the AL neuropil (blue, labeled with an antiserum against synaptotagmin) is undifferentiated and devoid of Mas-AT immunostaining. (B) By 3.5 days after 20E injection, the AL neuropil resembles the pattern normally observed about 2 days later (P6/7) with the Mas-AT immunoreactivity concentrated in an outer shell area (violet: colocalization of synaptotagmin and Mas-AT). In the LC (dashed line), LATn are labeled. (C) Mas-AT immunostaining in a diapausing animal revealed only the eATN in the lateral cell group. (D, E) Two examples of Mas-AT immunoreactivity after 20E injection at stage P1 and dissection 5.5 days later at pupal stage P6/7. (D) 5.5 days after 20E injection, the AL neuropil resembles the pattern normally observed about 2 days later (P8/9) with the Mas-AT-ir fibers projecting into the basis of the forming glomeruli [compare with Fig. 2(D)]. In the LC (dashed line), LATn and the lmATn (arrow) are labeled. (E) Oblique view, showing the fibers of the cATn entering/leaving the AL (arrowheads). In the LC, the lmATn (arrow) and LATn are labeled. (F) Numbers of Mas-AT-ir neurons in the lateral cell group after hemolymph injection of 20E at P1 and dissection 3.5 days (P4/5) to 11 days (P12) later (see inset in Fig. 3). 3.5–7 days after 20E injection, hormone-treated animals (open circles, means ± SD) showed a significant increase in the numbers of Mas-AT-ir neurons compared with controls (filled circles, means ± SD) injected with saline (***$p < 0.001$ for each data set as assessed by unpaired *t*-test). Compared with the normal developmental time course of Mas-AT-ir cell numbers (Fig. 3), controls gave the expected cell numbers, whereas 20E-injected animals showed a developmental advancement of about 2 days. Eleven days (P12) after 20E injection, cell numbers were not significantly different (n.s., $p > 0.05$) from control injected animals because, from stage P12 onwards, Mas-AT-ir cell numbers are more or less constant (compare with Fig. 3). Scale: 40 μm (A–E).

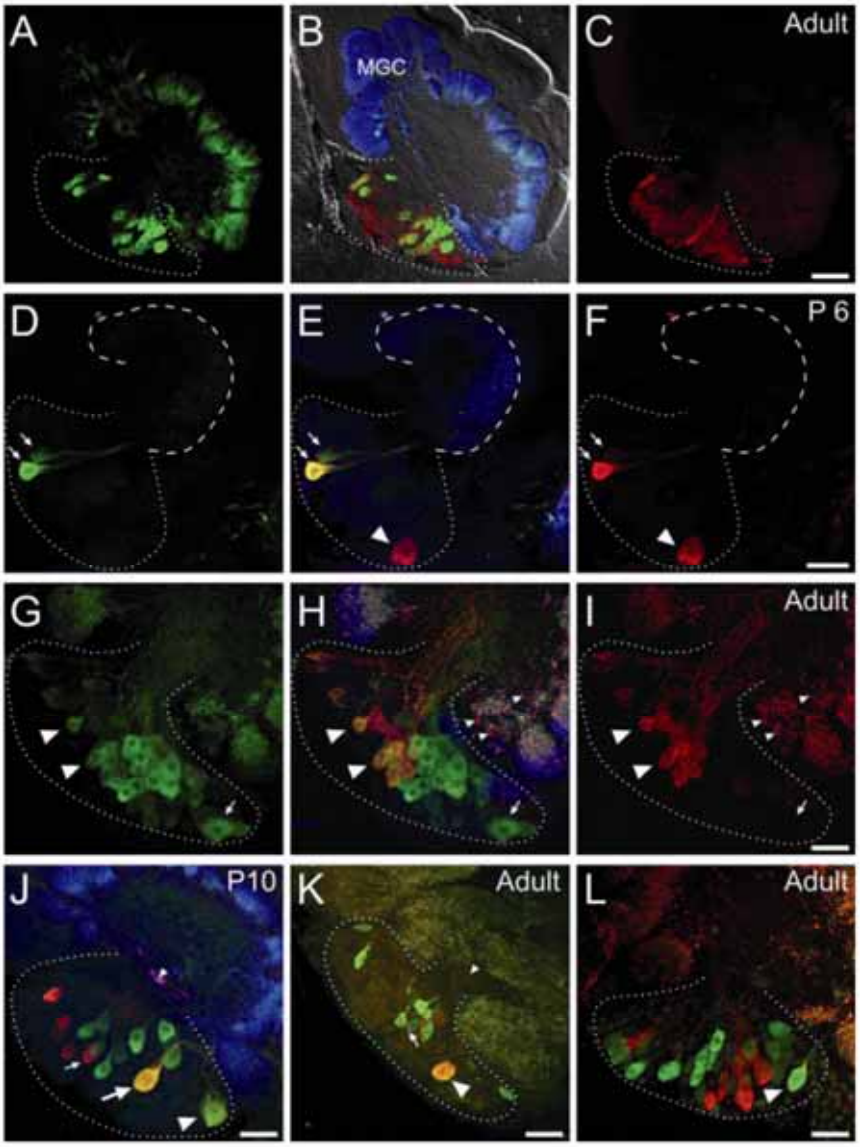

Figure 6 Confocal images of 40 μm sections showing triple immunostaining of Mas-AT-immunoreactivity (green, in (L) RFamide-ir cells are shown in green) and synapsin (blue) in the lateral cell group (LC) combined with antisera against GABA, RFamide or AST-A (red). In (B), an additional Nomarski contrast image is shown to better visualize the outline of the AL (grey). (A–C) Adult *Manduca* male AL. Comparing Mas-AT-ir cell bodies (A) and GABA-ir cell bodies (C) revealed that all cells containing Mas-AT staining also contain GABA immunoreactivity (B, overlay). (D–F) AL at pupal stage P6 showing the two early AT neurons (eATn; arrows) which are also labeled with antisera against RFamide. One large neuron, known as RFamide type II cell (Schachtner et al., 2004b), is at this stage devoid of Mas-AT immunoreactivity (arrowhead in E, F). Note the forming neuropil of the AL (dashed line) which faintly stains with the antibody against synaptotagmin (E). (G–I) LC of an adult labeled with antisera against Mas-AT (G) and AST-A (I). The overlay (H) shows a subpopulation of LATn labeling with both antisera (large arrowheads), while the lmATn only show Mas-AT immunoreactivity (arrow). Note that the AST-A-ir fibers and varicosities stemming from centrifugal type III AST-A-ir neurons (small arrowheads; Utz et al., 2005) are devoid of Mas-AT- immunoreactivity. The AST-A type III varicose meshwork is easily distinguishable from projections of the LNs, which typical for this neuron type project mainly into the basal area of each glomerulus. (J, K) In stage P10 (J) and adult (K) ALs, an antiserum against RFamide labels a subpopulation of the Mas-AT ir neurons including LATn (small arrows), eATn (large arrow), and lmATn (large arrowhead). The small arrowhead points the isthmus of the OATC which labels only with the RFamide antiserum. (L) Typically, as shown in an adult LC, RFamide staining (green) never colocalizes to cells containing AST-A immunoreactivity. Scale: 100 μm (A–C), 50 μm (D–K).

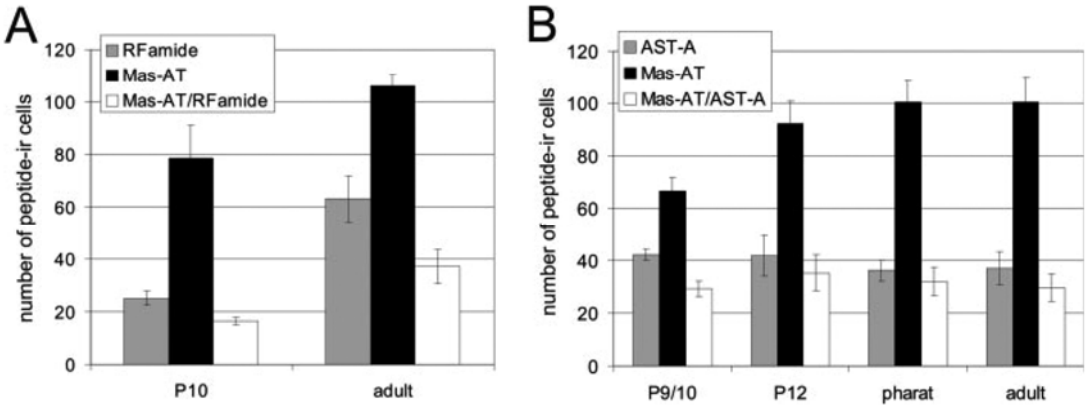

Figure 7 Colocalization of neuropeptides in local Mas-AT neurons (LATn). (A) Numbers of LATn labeling with antisera against RFamide (grey), Mas-AT (black) and both antisera (white) in stage P10 ($n = 6$ ALs) and in adult ALs ($n = 5$ ALs). (B) Numbers of LATn labeling with antisera against AST-A (grey), Mas-AT (black) and both antisera (white) in stage P10 ($n = 9$ ALs), P12 ($n = 10$), pharates ($n = 8$), and in adults ($n = 6$).

peptides in developing and adult ALs (Utz et al., 2007). This strongly suggests that the used antiserum recognizes selectively Mas-AT and no other neuropeptide.

Identity of Mas-AT-ir Neurons

Each AL of *M. sexta* contains three well-defined cell groups which house the somata of most of the LNs and PNs. All three cell groups can be easily recognized already early in AL development (Schachtner et al., 2004b). The largest of the cell groups, the lateral cell group, contains all LNs of the AL (about 360) and the largest group of PNs (about 600), while the other two cell groups contain only PNs; the median cell group about 200 and the anterior cell group about 20 PNs (Homberg et al., 1988). We describe Mas-AT immunoreactivity in seven different types of AL neurons, with four types located in the lateral cell group (lLATn, eATn, LATn, lmATn), one type located in the anterior cell group (aATn), one type located outside of any AL cell group (dlATn), and a centrifugal neuron (CATn). Owing to the projection pattern observed, the lLATn and the LATn belong to the LNs, while the eATn and the lmATn are PNs. For the neurons located outside the lateral cell group the situation is unclear. These cell types occur only in about 20–40% of the preparations, and their localization is varying. Immunostaining in the neurites of these cells typically faded out after a short distance from the soma and thus we cannot attribute them as LNs or PNs. However, as the aATn localize to the anterior cell group, they very likely are PNs because all neurons of this cell group are thought to be uniglomerular PNs (Homberg et al., 1988). Owing to the fact that all neurons outside the LC belong to the group of PNs, it seems very likely that also the dlATn belong to this group. The cell body of the large arc-shaped neurite of the CATn could not be traced by following the neurites in the IACT or the tritocerebrum. The "arc" formed by this neuron resembles a recently described centrifugal neuron immunoreactive to an antiserum against AST-A (Utz and Schachtner, 2005). We speculate that analogous to the AST-A-ir centrifugal neuron, the soma of the CATn could be located in the SEG.

For *M. sexta* we have a wealth of information on the developmental fates of identified neurons in the metamorphosing nervous system (for a review, see Truman, 1996a). Most neurons of the adult brain that differentiate during metamorphosis arise from neuroblasts that have been arrested during early larval stages and that start a second phase of proliferation in later larval stages. Among these cells are most of the neurons of the developing optic lobes and ALs, which are both newly formed during metamorphosis (adult specific neurons; Monsma and Booker, 1996a,b; Hildebrand et al., 1997; Champlin and Truman, 1998a, 2000). Other neurons of the CNS, which serve functions in the larva, are remodeled during metamorphosis to fit the requirements of the adult animal (larval neurons; Truman, 1996a; Weeks, 1999). A third fate of neurons during metamorphosis is programmed cell death, which has been described in many regions of the insect CNS (Weeks, 1999), but can be excluded for *M. sexta* AL development as shown by TUNEL-labeling experiments (Schachtner et al., 2004a).

Mas-AT immunoreactivity in the eATn persisted from the larva throughout pupal development and

thus these neurons can clearly be accounted for larval neurons. In contrast, in the pupa all other Mas-AT neuron types gain immunoreactivity not before stage P6/7. Judged from the acquisition of Mas-AT immunostaining these neuron types are adult specific neurons that are newly born during postembryonic development to serve functions in the adult (Truman, 1996a). In a few examples, however, it has been demonstrated that neurons can change their peptide identity (Loi and Tublitz, 1993; Tubliz and Loi, 1993; Witten and Truman, 1996). This raises the possibility, that some of the neurons could be larval neurons that change their peptide identity during metamorphosis. For a subpopulation of the LATn, the latter aspect is supported by the finding of a group of about ten Mas-AT-ir LNs (lLATn) which innervate the LAC. These larval Mas-AT-ir neurons lose their immunoreactivity during wandering stages W3 and W4. This strongly suggests that the about 100 LATn which become Mas-AT-ir from stage P6/7 to P13 consist of a mixed population of about 10 larval and about 90 adult specific LNs. A similar finding has been described for GABA-ir neurons (Homberg and Hildebrand, 1994). In the larva about 70, mostly LNs of the LAC display massive GABA-immunoreactivity. The immunostaining ceases during the wandering phase and around stage P8 over 400 mostly local AL neurons became GABA-ir. The authors could not find any typical signs of neuronal degradation in the AL of larval and wandering stages and thus suggested that the larval GABA-ir neurons regain their GABA-identity during metamorphosis. Very interestingly, the lmATn could be identified as a larval neuron by its colocalization with another neuropeptide antiserum (type II RFamide neuron (Schachtner et al., 2004b), for further discussion see later). The CATn were traced from stage P7/8. However, so far all centrifugal neurons which have been described during metamorphic development belong to the group of larval neurons (e.g. 5HT-ir and AST-A-ir centrifugal neurons; Kent et al., 1987; Utz and Schachtner, 2005). Thus it remains to be shown whether the CATn belongs to the larval or the adult specific group of neurons.

Time Course and Developmental Regulation of Mas-AT

The developmental occurrence, decrease, and increase of Mas-AT-ir neurons parallel fluctuations of the ecdysteroid titer in the hemolymph suggesting that the ecdysteroids could be causative for Mas-AT regulation. Transition from the 5th instar larva to pupa requires two surges of ecdysteroids, the commitment peak and the larger prepupal peak (Riddiford, 1985).

The disappearance of the lLATn during wandering stages coincides with the prepupal peak, which is known to initiate prepupal changes, including the reorganization of neuronal networks (Levine et al., 1986; Levine, 1989; Truman and Reiss, 1995) and alterations in neuroactive substances (Loi and Tublitz, 1993; Tublitz and Loi, 1993; Witten and Truman, 1996; Žitňan et al., 1999). The occurrence of Mas-AT-ir cell types and the subsequent increase of numbers of the LATn coincide with the change in circulating ecdysteroids from primarily α-ecdysone to 20E during pupal development (inset in Fig. 3; Warren and Gilbert, 1986). Since we are particularly interested in pupal development, we have experimentally shifted the onset of the pupal 20E peak by 20E injection into an earlier developmental stage. This manipulation resulted in the precocious appearance of the LATn, the lmATn and the CATn (Fig. 5) and thus clearly suggests a regulatory role of the pupal 20E rise for Mas-AT expression in at least three different neuronal types of the AL. Besides, the cell somata also the neurites showed robust staining with the Mas-AT antiserum after 20E injection [Fig. 5(B,C)]. This finding clearly suggests that the Mas-AT-ir neurons are involved in the increased neuropil formation after 20E manipulation. The two cell types located outside the LC have not been examined in this context, because of unreliable occurrence of at least Mas-AT immunoreactivity during normal development. We account this irregular appearance to neurons which exhibit individual variability of their soma localization.

The regulatory role of 20E is further supported by our findings in diapausing pupa, which lack the pupal ecdysteroid peak and which house only the two eATn but none of the other Mas-AT cells in the LC [Fig. 5(C)].

We have previously demonstrated a similar effect of 20E injections on the expression of AST-A and RFamides during AL development (Schachtner et al., 2004b; Utz and Schachtner, 2005). Furthermore, in both studies, synaptotagmin staining has revealed that not only the presence of the neuropeptides, but also the formation of glomeruli occurred earlier following 20E treatment than during normal development. Moreover, 20E injections early in metamorphosis lead to elevated concentrations of the second messenger molecule cyclic guanosine monophosphate in LC neurons; during normal development, this does not occur before stages P7/8 (Schachtner et al., 1998, 1999). Upregulation of transmitter and receptor expression could either be directly influenced by 20E

or indirectly via mechanisms induced by 20E in the course of inducing AL development. However, the current study together with our previous findings (Schachtner et al., 2004b; Utz and Schachtner, 2005) strongly supports a major role of 20E in the orchestration of metamorphic AL development with respect to glomeruli formation and transmitter and receptor acquisition.

Effects of the pupal 20E peak on the metamorphic development of the nervous system of *M. sexta* have been shown in several other studies: the regulation of the fusion of thoracic and abdominal ganglia (Amos et al., 1996), the control of cell proliferation during the genesis of the optic lobes and the retina and also of the programmed cell death of optic lobe neuroblasts (Champlin and Truman, 1998a,b, 2000). The 20E peak also regulates the pupal expression of tyramine β-hydroxylase, an essential enzyme for octopamine biosynthesis (Lehmann et al., 2000).

Colocalization of Mas-AT with GABA, RFamides, and A-Type Allatostatins

GABA is believed to be the principal transmitter of LNs in the ALs of insects (for a review see Schachtner et al., 2005). In *M. sexta* most of the GABA-ir neurons are LNs, while a small subpopulation belongs to the group of PNs (Hoskins et al., 1986; Homberg et al., 1989). Double labeling with Mas-AT and GABA antisera revealed that in the pupa and in the adult only one Mas-AT-ir type, the LATn, displays additional GABA immunoreactivity. This result supports our morphological finding that very likely all of the LATn belong to the group of LNs.

Double labeling with anti-Mas-AT and anti-RFamide antisera revealed that the two eATn, the lmATn, and a subpopulation of the LATn colocalize RFamide and Mas-AT immunoreactivity [Figs. 6(D–F,J,K) and 7(A)]. Comparing these results with a previous study on RFamides during *M. sexta* AL development revealed that the lmATn and the eATn are identical with the type II and type III RFamide neurons (Schachtner et al., 2004b). The single type II RFamide neuron is a persisting larval neuron, which according to our finding gains additional Mas-AT immunoreactivity at stage P7/8. This result not only identifies the lmATn as a larval neuron, but also is an example for a local peptidergic neuron which gains an additional neuropeptide identity during metamorphosis. The finding that the eATn colocalize RFamide identifies the type III RFamide neurons as PNs, which could not be determined in the earlier study from Schachtner et al. (2004b).

From double labeling experiments with antisera against GABA and RFamide, it has been concluded that about 10 RFamide-ir neurons in P10 (Schachtner et al., 2004b) and about 20 RFamide-ir neurons in adults (Homberg et al., 1990) in the lateral cell group might be PNs responsible for the staining in the outer antenno-cerebral tract (OACT) and the isthmus of the AL. Our double staining experiments revealed that the fibers in the root of the OACT stained selectively with the RFamide antiserum but not with the Mas-AT antiserum [Fig. 6(J,K)]. Furthermore, about 10 RFamide-ir neurons in P10 and about 25 RFamide-ir neurons in adults are devoid of Mas-AT immunoreactivity [Fig. 7(A)]. These results strongly suggest that Mas-AT and RFamide antisera colocalize exclusively in LNs, but not in PNs.

Double labeling experiments with antisera recognizing Mas-AT and members of the AST-A family of neuropeptides revealed that throughout development about 30 neurons (about 30% of the Mas-AT-ir neurons or about 75 % of the AST-A-ir neurons) show additional Mas-AT and AST-A immunoreactivity. This result suggests that during AL development about 30 local AL neurons have in addition to their principal transmitter at least two neuropeptides at their disposal. Double labeling experiments using antisera recognizing AST-A and RFamides revealed in stage P10 and in adult animals no colocalization.

Summarizing, our double labeling experiments clearly demonstrate for the LATn that there are at least three different populations of GABA-ir and Mas-AT-ir LNs: one group which additionally expresses RFamides, a second group which additionally expresses AST-As, and a third group which expresses Mas-AT but neither one of the two other neuropeptide families (Table 1).

A recent study on the distribution of various neuropeptides in the adult AL of the noctuid moth *Heliothis virescens* revealed about the same numbers of neuropeptide immunoreactive neurons in the lateral cell group for the same three antisera used in the various *M. sexta* studies (Mas-AT: ~87; AST-A: ~47; RFamide: ~64; Berg et al., 2007). Double immunostainings with antisera against Mas-AT and AST-A or RFamide antisera using the same method as in the current study, revealed a similar number of neurons which colocalize Mas-AT and AST-A (~32) but only about half of the number which colocalize Mas-AT and RFamide (~15) immunoreactivity. Sphingid and noctuid moth belong both to the group of Macrolepidoptera and have been evolutionary separated in the Paleocene about 65 Mio years ago (Grimaldi and Engel, 2005). The astonishing similarity observed in the anatomy of the neuropeptidergic systems between

these two species argues for a high conservation concerning the function of defined neuropeptides in the AL network within the Macrolepidoptera.

Possible Roles of Mas-AT and Other Neuropeptides During AL Development

Immunocytochemical studies in a diversity of insects have indicated that several neuropeptides are present primarily in subpopulations of local AL neurons (for a review see Schachtner et al., 2005). Direct profiling of ALs of several insects including *M. sexta*, *Heliothis virescens*, *Apis mellifera*, and the beetle *Tribolium castaneum* by MALDI-TOF mass spectrometry suggests about 40–50 different neuropeptides in the ALs of each of these species (Berg et al., 2007; Utz et al., 2007; and unpublished). Neuropeptides have often been considered as cotransmitters that are released in concert with a principal transmitter (Vilim et al., 2000; Nässel, 2002). In general, corelease is thought to enhance the repertoire of synaptic interactions within a neuronal network (for a review see Nusbaum et al., 2001). In the AL, neuropeptides might operate as cotransmitters of GABA (γ-aminobutyric acid), the principle transmitter of LNs (Homberg and Müller, 1999), but the function of cotransmission has so far not been studied in the AL or in general within the insect brain (Nässel and Homberg, 2006).

To date, neuropeptides are accepted as molecules responsible for shaping the activity pattern of neuronal circuits and thus as being of major importance for the functional condition and output pattern of the nervous system (Hökfelt, 1991; Marder and Bucher, 2001; Nusbaum et al., 2001; Nässel, 2002). In insects, a few studies on the role of neuropeptides revealed important functions in the brain, e.g. regulation of the insect molt (Truman, 1996b; Mesce and Fahrbach, 2002; Ewer, 2005), regulation of circadian control, and regulation of various aspects of feeding behavior (for a recent review see Nässel and Homberg, 2006).

Despite the large amount of neuropeptides present in the AL, so far only one study has addressed the question which function neuropeptides have in signal processing in the AL (Winther et al., 2006). In this study, knockdowns of the precursor gene coding for the tachykinine related peptides (TKRP), led to loss of sensitivity to three odors tested in a behavioral essay, thus suggesting an important role of the TKRPs in odor processing.

Knowledge on the functions of neuropeptides during ontogeny of the central nervous system is limited. Developmental studies attribute primarily tropic and trophic actions to certain peptides, including induction of neurogenesis and effects on neuronal migration (Strand et al., 1991; De Felipe et al., 1995; Voronezhskaya and Elekes, 1996; Croll, 2000; Hökfelt et al., 2000; Yacubova and Komuro, 2002). A few studies suggest important functions of peptides especially in the developing or regenerating olfactory system. Neuropeptide-Y and PACAP initiate proliferation of basal cells in the mouse olfactory epithelium (Hansel et al., 2001a,b), while prokineticin 2 serves as a trophic signal and induces neurogenesis in the mouse olfactory bulb (Ng et al., 2005).

The LATn start to increase their number at stage P6/7 which parallels the period when the protoglomeruli are formed. Analysis of Mas-AT-ir projections occuring at this period of AL development revealed that the protoglomeruli are devoid of Mas-AT immunostaining, suggesting that the LATn are not involved in the formation of the protoglomeruli. This fits the hypothesis that protoglomeruli are exclusively formed by ORNs and PNs, but not by LNs (Tolbert et al., 2004). With the beginning of the formation of the glomeruli (phase II) Mas-AT-ir processes enter the glomeruli, which is in accordance for a role of the LATn during formation of the synaptic network in the olfactory glomeruli. Such a role for peptidergic LNs during AL development has been postulated for interneurons displaying RFamide and AST-A immunoreactivity (Schachtner et al., 2004b; Utz and Schachtner, 2005). Comparing the developmental pattern of the three neuropeptide families, as judged by the number of immunopositive cells in LCs, suggests not only different mechanisms of developmental regulation but also distinct functions for selected developmental events (Fig. 8). Note that for the AST-

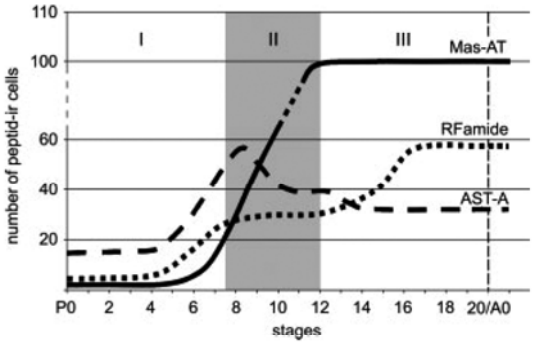

Figure 8 Summary of the developmental acquisition pattern of three antisera representing a single neuropeptide (Mas-AT) or neuropeptide families (RFamide, AST-A). Shown are numbers of cell bodies in the lateral cell group witch label at defined developmental stages with the neuropeptide antisera. RFamide and AST-A according to Schachtner et al., 2004; Utz and Schachtner, 2005.

A peptides transient increases occur, while with the other two neuropeptide antisera (Mas-AT and RFamide) only persisting increases are found. The increases around and during phase II (phase of glomeruli formation) are regulated via the increasing titer of the developmental hormone 20E, while all other fluctuations are regulated by so far unknown mechanisms (Schachtner et al., 2004b; Utz and Schachtner, 2005).

The presence of AST-A and RFamide immunoreactivity in cells of the LC and in centrifugal neurons during early AL development assigns these neurons and their neuropeptides as candidates being functionally involved during this period of AL formation. For the AST-A peptides, it has been speculated that they could provide a diffusible signal for the incoming ORN axons to find the AL and to guide the ORNs around the AL neuropil so that they can finally target their specific glomerular template sites (Utz and Schachtner, 2005).

From the beginning of phase II, processes of LNs, including those immunolabeled with the three neuropeptide antisera, enter the glomeruli to undergo massive synaptogenesis to eventually forming a glomerular network containing thousands of synapses between ORNs, PNs, and LNs. How could the neuropeptides be involved during the formation of the glomerular network during phase II and III? We hypothesize that neuropeptides could be involved (1) in generating and stabilizing neuronal activity in selected neurons establishing the glomerular network and (2) in the process of pathfinding and targeting of neurons towards their partners. The effects of the neuropeptides could be achieved by (1) a spatial and temporal release pattern which could result in a combination of transient gradients of the various peptides, and (2) by the availability and properties of the neuropeptide receptors in the developing AL. While nothing is known on the expression pattern of neuropeptide receptors during AL development, spontaneous electrical activity has been shown *in vivo* for the ORNs (starting at the beginning of phase II; Oland et al., 1996) and in cell culture for developing LNs and PNs (Mercer and Hildebrand, 2002). Furthermore, during phase II, application of the ORN transmitter ACh or of its agonist carbachol, and electrical stimulation of the antennal nerve elicits long lasting calcium transients as well as calcium oscillations in neurons of the LC (Lohr, 2003 and personal communication J. Schachtner). By means of calcium imaging and electrophysiological techniques we are currently examining how neuropeptides influence electrical activity in the developing AL.

The present study represents a detailed analysis of the cellular appearance and developmental expression of the neuropeptide Mas-AT in a defined brain area, the AL of *M. sexta*. A comparison of the time course of Mas-AT immunostaining and its neuronal localization with defined phases of AL development revealed parallels that are consistent with the hypothesis that Mas-AT is involved in certain aspects of AL development. Manipulation of the pupal 20E titer has further revealed that Mas-AT expression in different neuron types of the AL is under the developmental control of 20E. Double labeling experiments with antisera against GABA and two other neuropeptides revealed different populations of Mas-AT expressing neurons of the same morphological type, but with a different biochemical identity.

The authors thank Drs. Hans Agricola (University of Jena, Germany), Erich Buchner (University of Würzburg, Germany), Philip F. Copenhaver (OHSU, USA), Eve Marder (Brandeis University, USA), Kaushiki P. Menon (CALTECH, USA), and Jan Veenstra, (University of Bordeaux, Talence, France) for kindly providing the various antisera. The authors are also grateful to Dr. Uwe Homberg, Dr. Frank Seeber, and Ulrike Traeger for many fruitful discussions and Christa von Praun, Sabine Jesberg, Martina Kern, Karin Müller, and Cornelia Ellendt for expert technical assistance.

REFERENCES

Abdel-Latief M, Meyering-Vos M, Hoffmann KH. 2003. Molecular characterisation of cDNAs from the fall armyworm Spodoptera frugiperda encoding *Manduca sexta* allatotropin and allatostatin preprohormone peptides. Insect Biochem Mol Biol 33:467–476.

Abdel-Latief M, Meyering-Vos M, Hoffmann KH. 2004. Expression and localization of the *Spodoptera frugiperda* allatotropin (Spofr-AT) and allatostatin (Spofr-AS) genes. Arch Insect Biochem Physiol 55:188–199.

Abercrombie M. 1946. Estimation of nuclear populations from microtome sections. Anat Rec 94:239–247.

Amos TM, Gelman DB, Mesce KA. 1996. Steroid hormone fluctuations regulate ganglionic fusion during metamorphosis of the moth *Manduca sexta*. J Insect Physiol 42:579–591.

Bell RA, Joachim FA. 1978. Techniques for rearing laboratory colonies of the tobacco hornworm, *Manduca sexta*, and pink ballworms. Ann Ent Soc Am 69:365–373.

Berg BG, Galizia CG, Brandt R, Mustaparta H. 2002. Digital atlases of the antennal lobe in two species of tobacco budworm moths, the Oriental *Helicoverpa assulta* (male) and the American *Heliothis virescens* (male and female). J Comp Neurol 446:123–134.

Berg BG, Schachtner J, Utz S, Homberg U. 2007. Distribution of neuropeptides in the primary olfactory center of

the heliothine moth *Heliothis virescens*. Cell Tissue Res 327:385–398.

Bradford MM. 1976. A rapid and sensitive method for the quantitation of microgram quantities of protein utilizing the principle of protein-dye binding. Anal Biochem 72:248–254.

Caillol M, Aioun J, Baly C, Persuy MA, Salesse R. 2003. Localization of orexins and their receptors in the rat olfactory system: Possible modulation of olfactory perception by a neuropeptide synthetized centrally or locally. Brain Res 960:48–61.

Champlin DT, Truman JW. 1998a. Ecdysteroid control of cell proliferation during optic lobe neurogenesis in the moth *Manduca sexta*. Development 125:269–277.

Champlin DT, Truman JW. 1998b. Ecdysteroids govern two phases of eye development during metamorphosis of the moth, *Manduca sexta*. Development 125:2009–2018.

Champlin DT, Truman JW. 2000. Ecdysteroid coordinates optic lobe neurogenesis via a nitric oxide signaling pathway. Development 127:3543–2551.

Croll RP. 2000. Insights into early molluscan neuronal development through studies of transmitter phenotypes in embryonic pond snails. Microsc Res Tech 49:570–578.

De Felipe C, Pinnock RD, Hunt SP. 1995. Modulation of chemotropism in the developing spinal cord by substance P. Science 267:899–902.

Dubuque SH, Schachtner J, Nighorn AJ, Menon KP, Zinn K, Tolbert LP. 2001. Immunolocalization of synaptotagmin for the study of synapses in the developing antennal lobe of *Manduca sexta*. J Comp Neurol 441:277–287.

Eisthen HL. 2002. Why are olfactory systems of different animals so similar? Brain Behav Evol 59:273–293.

Elekonich MM, Horodyski FM. 2003. Insect allatotropins belong to a family of structurally-related myoactive peptides present in several invertebrate phyla. Peptides 24:1623–1632.

Ephrussi B, Beadle GW. 1936. A technique of transplantation for *Drosophila*. Nature 70:218–225.

Ewer J. 2005. Behavioral actions of neuropeptides in invertebrates: Insights from *Drosophila*. Horm Behav 48:418–429.

Grimaldi D, Engel M. 2005. Evolution of the Insects. Cambridge: Cambridge University Press.

Gutierrez-Mecinas M, Crespo C, Blasco-Ibanez JM, Gracia-Llanes FJ, Marques-Mari AI, Martinez-Guijarro FJ. 2005. Characterization of somatostatin- and cholecystokinin-immunoreactive periglomerular cells in the rat olfactory bulb. J Comp Neurol 489:467–479.

Hansel DE, Eipper BA, Ronnett GV. 2001a. Regulation of olfactory neurogenesis by amidated neuropeptides. J Neurosci Res 66:1–7.

Hansel DE, Eipper BA, Ronnett GV. 2001b. Neuropeptide Y functions as a neuroproliferative factor. Nature 410:940–944.

Higgins MR, Gibson NJ, Eckholdt PA, Nighorn A, Copenhaver PF, Nardi J, Tolbert LP. 2002. Different isoforms of fasciclin II are expressed by a subset of developing olfactory receptor neurons and by olfactory-nerve glial cells during formation of glomeruli in the moth *Manduca sexta*. Dev Biol 244:134–154.

Hildebrand JG, Rössler W, Tolbert LP. 1997. Postembryonic development of the olfactory system in the moth *Manduca sexta*: Primary-afferent control of glomerular development. Semin Cell Dev Biol 8:163–170.

Hildebrand JG, Shepherd GM. 1997. Mechanisms of olfactory discrimination: Converging evidence for common principles across phyla. Annu Rev Neurosci 20:595–631.

Hökfelt T. 1991. Neuropeptides in perspective: The last ten years. Neuron 7:867–879.

Hökfelt T, Broberger C, Xu ZQ, Sergeyev V, Ubink R, Diez M. 2000. Neuropeptides–An overview. Neuropharmacology 39:1337–1356.

Homberg U, Brandl C, Clynen E, Schoofs L, Veenstra JA. 2004. Mas-allatotropin/Lom-AG-myotropin-I immunostaining in the brain of the locust, *Schistocerca gregaria*. Cell Tissue Res 318:439–457.

Homberg U, Christensen TA, Hildebrand JG. 1989. Structure and function of the deutocerebrum in insects. Annu Rev Entomol 34:477–501.

Homberg U, Hildebrand JG. 1994. Postembryonic development of gamma-aminobutyric acid-like immunoreactivity in the brain of the sphinx moth *Manduca sexta*. J Comp Neurol 339:132–149.

Homberg U, Kingan TG, Hildebrand JG. 1990. Distribution of FMRFamide-like immunoreactivity in the brain and suboesophageal ganglion of the sphinx moth *Manduca sexta* and colocalization with SCP_B-, BPP-, and GABA-like immunoreactivity. Cell Tissue Res 259:401–419.

Homberg U, Montague RA, Hildebrand JG. 1988. Anatomy of antenno-cerebral pathways in the brain of the sphinx moth *Manduca sexta*. Cell Tissue Res 254:255–281.

Homberg U, Müller U. 1999. Neuroactive substances in the antennal lobe. In: Hansson BS, editor. Insect Olfaction. New York: Springer, pp 181–206.

Homberg U, Vitzthum H, Müller M, Binkle U. 1999. Immunocytochemistry of GABA in the central complex of the locust *Schistocerca gregaria*: Identification of immunoreactive neurons and colocalization with neuropeptides. J Comp Neurol 409:495–507.

Horodyski FM, Bhatt SR, Lee KY. 2001. Alternative splicing of transcripts expressed by the *Manduca sexta* allatotropin (Mas-AT) gene is regulated in a tissue-specific manner. Peptides 22:263–269.

Hoskins SG, Homberg U, Kingan TG, Christensen TA, Hildebrand JG. 1986. Immunocytochemistry of GABA in the antennal lobes of the sphinx moth *Manduca sexta*. Cell Tissue Res 244:243–252.

Huetteroth W, Schachtner J. 2005. Standard three-dimensional glomeruli of the *Manduca sexta* antennal lobe: A tool to study both developmental and adult neuronal plasticity. Cell Tissue Res 319:513–524.

Jindra M, Huang JY, Malone F, Asahina M, Riddiford LM. 1997. Identification and mRNA developmental profiles of two ultraspiracle isoforms in the epidermis and wings of *Manduca sexta*. Insect Mol Biol 6:41–53.

Kataoka H, Toschi A, Li JP, Carney L, Schooley DA, Kramer SJ. 1989. Identification of an allatotropin from adult *Manduca sexta*. Science 243:1481–1483.

Kent KS, Hoskins SG, Hildebrand JG. 1987. A novel serotonin-immunoreactive neuron in the antennal lobe of the sphinx moth *Manduca sexta* persists throughout postembryonic life. J Neurobiol 18:451–465.

Kingan TG, Shabanowitz J, Hunt DF, Witten JL. 1996. Characterisation of two myotropic neuropeptides in the FMRFamide family from segmental ganglia of the moth *Manduca sexta*: Candidate neurohormones and neuromodulators. J Exp Biol 199:1095–1104.

Kingan TG, Teplow DB, Phillips JM, Riehm JP, Rao KR, Hildebrand JG, Homberg U, et al. 1990. A new peptide in the FMRFamide family isolated from the CNS of the hawkmoth, *Manduca sexta*. Peptides 11:849–856.

Klagges BRE, Heimbeck G, Godenschwege TA, Hofbauer A, Pflugfelder GO, Reifegerste R, Reisch D, Schaupp M, Buchner S, Buchner E. 1996. Invertebrate Synapsins: A single gene codes for several isoforms in *Drosophila*. J Neurosci 16:3154–3165.

Lee KY, Chamberlin ME, Horodyski FM. 2002. Biological activity of *Manduca sexta* allatotropin-like peptides, predicted products of tissue-specific and developmentally regulated alternatively spliced mRNAs. Peptides 23: 1933–1941.

Lehman HK, Klukas KA, Gilchrist LS, Mesce KA. 2000. Steroid regulation of octopamine expression during metamorphic development of the moth *Manduca sexta*. J Comp Neurol 424:283–296.

Levine RB. 1989. Expansion of the central arborizations of persistent sensory neurons during insect metamorphosis: The role of the steroid hormone, 20-hydroxyecdysone. J Neurosci 9:1045–1054.

Levine RB, Truman JW, Linn D, Bate CM. 1986. Endocrine regulation of the form and function of axonal arbors during insect metamorphosis. J Neurosci 6:293–299.

Lohr C. 2003. Monitoring neuronal calcium signalling using a new method for ratiometric confocal calcium imaging. Cell Calcium 34:295–303.

Loi PK, Tublitz NJ. 1993. Hormonal control of transmitter plasticity in insect peptidergic neurons. I. Steroid regulation of the decline in cardioacceleratory peptide 2 (CAP2) expression. J Exp Biol 181:175–194.

Malun D, Oland LA, Tolbert LP. 1994. Uniglomerular projection neurons participate in early development of olfactory glomeruli in the moth *Manduca sexta*. J Comp Neurol 350:1–22.

Marder E, Bucher D. 2001. Central pattern generators and the control of rhythmic movements. Curr Biol 11:R986–R996.

Marder E, Calabrese RL, Nusbaum MP, Trimmer B. 1987. Distribution and partial characterization of RFamide-like peptides in the stomatogastric nervous system of the rock crab, *Cancer borealis*, and the spiny lobster *Panulirus interruptus*. J Comp Neurol 259:150–163.

Mercer AR, Hildebrand JG. 2002. Developmental changes in the electrophysiological properties and response characteristics of *Manduca* antennal-lobe neurons. J Neurophysiol 87:2650–2663.

Mesce KA, Fahrbach SE. 2002. Integration of endocrine signals that regulate insect ecdysis. Front Neuroendocrinol 23:179–199.

Miao Y, Waters EM, Witten JL. 1998. Developmental and regional-specific expression of FLRFamide peptides in the tobacco hornworm, *Manduca sexta*, suggests functions at ecdysis. J Neurobiol 37:469–485.

Monsma SA, Booker R. 1996a. Genesis of the adult retina and outer optic lobes of the moth, *Manduca sexta*. I. Patterns of proliferation and cell death. J Comp Neurol 367:10–20.

Monsma SA, Booker R. 1996b. Genesis of the adult retina and outer optic lobes of the moth *Manduca sexta*. II. Effects of deafferentiation and developmental hormone manipulation. J Comp Neurol 367:21–35.

Moody TW, Merali Z. 2004. Bombesin-like peptides and associated receptors within the brain: Distribution and behavioral implications. Peptides 25:511–520.

Nässel DR. 2002. Neuropeptides in the nervous system of *Drosophila* and other insects: Multiple roles as neuromodulators and neurohormones. Prog Neurobiol 68:1–84.

Nässel DR, Homberg U. 2006. Neuropeptides in interneurons of the insect brain. Cell Tissue Res 326:1–24.

Negoescu A, Labat-Moleur F, Lorimier P, Lamarcq L, Guillermet C, Chambaz E, Brambilla E. 1994. F(ab) secondary antibodies: A general method for double immunolabeling with primary antisera from the same species. Efficiency control by chemiluminescence. J Histochem Cytochem 42:433–437.

Ng KL, Li JD, Cheng MY, Leslie FM, Lee AG, Zhou QY. 2005. Dependence of olfactory bulb neurogenesis on prokineticin 2 signaling. Science 308:1923–1927.

Nusbaum MP, Blitz DM, Swensen AM, Wood D, Marder E. 2001. The roles of co-transmission in neural network modulation. Trends Neurosci 24:146–154.

Oland LA, Pott WM, Bukhman G, Sun XJ, Tolbert LP. 1996. Activity blockade does not prevent the construction of olfactory glomeruli in the moth *Manduca sexta*. Int J Dev Neurosci 14:983–996.

Oland LA, Tolbert LP. 1996. Multiple factors shape development of olfactory glomeruli: Insights from an insect model system. J Neurobiol 30:92–109.

Petri B, Homberg U, Loesel R, Stengl M. 2002. Evidence for a role of GABA and Mas-allatotropin in photic entrainment of the circadian clock of the cockroach *Leucophaea maderae*. J Exp Biol 205:1459–1469.

Riddiford LM. 1985. Hormone action at the cellular level. In: Kerkut GA, Gilbert LI, editors. Comprehensive Insect Physiology, Biochemistry, and Pharmacology. Oxford: Pergamon, pp 37–84.

Schachtner J, Homberg U, Truman JW. 1999. Regulation of cyclic GMP elevation in the developing antennal lobe of the sphinx moth, *Manduca sexta*. J Neurobiol 41:359–375.

Schachtner J, Huetteroth W, Nighorn A, Honegger HW. 2004a. Copper/zinc superoxide dismutase-like immunoreactivity in the metamorphosing brain of the sphinx moth *Manduca sexta*. J Comp Neurol 469:141–152.

Schachtner J, Klaassen L, Truman JW. 1998. Metamorphic control of cyclic guanosine monophosphate expression in the nervous system of the tobacco hornworm, *Manduca sexta*. J Comp Neurol 396:238–252.

Schachtner J, Schmidt M, Homberg U. 2005. Organization and evolutionary trends of primary olfactory brain centers in Tetraconata (Crustacea + Hexapoda). Artropod Struct Dev 34:257–299.

Schachtner J, Trosowski B, D'Hanis W, Stubner S, Homber U. 2004b. Development and steroid regulation of RFamide immunoreactivity in antennal lobe neurons of the sphinx moth *Manduca sexta*. J Exp Biol 207:2389–2400.

Schmitt S, Evers JF, Duch C, Scholz M, Obermayer K. 2004. New methods for the computer-assisted 3D reconstruction of neurons from confocal image stacks. Neuroimage 23:1283–1298.

Schwartz LM, Truman JW. 1983. Hormonal control of rates of metamorphic development in the tobacco hornworm *Manduca sexta*. Dev Biol 99:103–114.

Sheng Z, Ma L, Cao MX, Li S, Jiang RJ. 2007. Biochemical and molecular characterization of allatotropin and allatostatin from the Eri silkworm, *Samia cynthia ricini*. Insect Biochem Mol Biol 37:90–96.

Smith RL, Baker H, Greer CA. 1993. Immunohistochemical analyses of the human olfactory bulb. J Comp Neurol 333:519–530.

Strand FL, Rose KJ, Zuccarelli LA, Kume J, Alves SE, Antonawich FJ, Garrett LY. 1991. Neuropeptide hormones as neurotrophic factors. Physiol Rev 71:1017–1046.

Strausfeld NJ, Hildebrand JG. 1999. Olfactory systems: Common design, uncommon origins? Curr Opin Neurobiol 9:634–639.

Tolbert LP. 1989. Afferent axons from the antenna influence the number and placement of intrinsic synapses in the antennal lobes of *Manduca sexta*. Synapse 3:83–95.

Tolbert LP, Matsumoto SG, Hildebrand JG. 1983. Development of synapses in the antennal lobes of the moth *Manduca sexta* during metamorphosis. J Neurosci 3:1158–1175.

Tolbert LP, Oland LA, Tucker ES, Gibson NJ, Higgins MR, Lipscomb BW. 2004. Bidirectional influences between neurons and glial cells in the developing olfactory system. Prog Neurobiol 73:73–105.

Truman JW. 1996a. Metamorphosis of the insect nervous system. In: Gilbert LI, editor. Metamorphosis: Postembryonic Reprogramming of Gene Expression in Amphibian and Insect Cells. Orlando: Academic Press, pp 283–320.

Truman JW. 1996b. Ecdysis control sheds another layer. Science 271:40–41.

Truman JW, Reiss SE. 1995. Neuromuscular metamorphosis in the moth *Manduca sexta*: Hormonal regulation of synapses loss and remodeling. J Neurosci 15:4815–4826.

Tublitz NJ, Loi PK. 1993. Hormonal control of transmitter plasticity in insect peptidergic neurons. II. Steroid control of the up-regulation of bursicon expression. J Exp Biol 181:195–212.

Utz S, Schachtner J. 2005. Development of A-type allatostatin immunoreactivity in antennal lobe neurons of the sphinx moth *Manduca sexta*. Cell Tissue Res 320:149–162.

Utz S, Huetteroth W, Wegener C, Kahnt J, Predel R, Schachtner J. 2007. Direct peptide profiling of lateral cell groups of the antennal lobes of *Manduca sexta* reveals specific composition changes in neuropeptide expression during development. Dev Neurobiol 67:764–777.

Veenstra JA, Hagedorn HH. 1993. Sensitive enzyme immunoassay for *Manduca* allatotropin and the existence of an allatrotropin-immunoreactive peptide in *Periplaneta americana*. Arch Insect Biochem Physiol 23:99–109.

Vilim FS, Cropper EC, Price DA, Kupfermann I, Weiss KR. 2000. Peptide cotransmitter release from motorneuron B16 in *Aplysia californica*: Costorage, corelease, and functional implications. J Neurosci 20:2036–2042.

Vitzthum H, Homberg U, Agricola H. 1996. Distribution of dip-allatostatin I-like immunoreactivity in the brain of the locust *Schistocerca gregaria* with detailed analysis of immunostaining in the central complex. J Comp Neurol 369:419–437.

Voronezhskaya EE, Elekes K. 1996. Transient and sustained expression of FMRFamide-like immunoreactivity in the developing nervous system of *Lymnaea stagnalis* (Mollusca, Pulmonata). Cell Mol Neurobiol 16:661–676.

Warren JT, Gilbert LI. 1986. Ecdysone metabolism and distribution during the pupal-adult development of *Manduca sexta*. Insect Biochem 16:65–82.

Weeks JC. 1999. Steroid hormones, dendritic remodeling and neuronal death: Insights from insect metamorphosis. Brain Behav Evol 54:51–60.

Weevers RD. 1966. A lepidopteran saline: The effects of inorganic cation concentrations on sensory, reflex and motor responses in a herbivorous insect. J Exp Biol 44:163–176.

Winther AM, Acebes A, Ferrus A. 2006. Tachykinin-related peptides modulate odor perception and locomotor activity in *Drosophila*. Mol Cell Neurosci 31:399–406.

Witten JL, Truman JW. 1996. Developmental plasticity of neuropeptide expression in motoneurons of the moth, *Manduca sexta*: Steroid hormone regulation. J Neurobiol 29:99–114.

Wright JW, Copenhaver PF. 2000. Different isoforms of fasciclin II play distinct roles in the guidance of neuronal migration during insect embryogenesis. Dev Biol 225: 59–78.

Yacubova E, Komuro H. 2002. Stage-specific control of neuronal migration by somatostatin. Nature 415:77–81.

Žitňan D, Ross LS, Zitnanova I, Hermesman JL, Gill SS, Adams ME. 1999. Steroid induction of a peptide hormone gene leads to orchestration of a defined behavioral sequence. Neuron 23:523–535.

CHAPTER IV:

Direct peptide profiling of lateral cell groups of the antennal lobes of *Manduca sexta* reveals specific composition and changes in neuropeptide expression during development

Direct Peptide Profiling of Lateral Cell Groups of the Antennal Lobes of *Manduca sexta* Reveals Specific Composition and Changes in Neuropeptide Expression during Development

Sandra Utz,[1] Wolf Huetteroth,[1] Christian Wegener,[1,2] Jörg Kahnt,[3] Reinhard Predel,[4] Joachim Schachtner[1]

[1] Fachbereich Biologie, Tierphysiologie, Philipps Universität, Karl-von-Frisch-Straße, D-35032 Marburg, Germany

[2] Emmy Noether Neuropeptidgruppe, FB Biologie, Tierphysiologie, Philipps-Universität, Karl-von-Frisch-Straße, D-35032 Marburg, Germany

[3] Max Planck Institut für terrestrische Mikrobiologie, Karl-von-Frisch-Straße, D-35043 Marburg, Germany

[4] Institut für Allgemeine Zoologie und Tierphysiologie, Friedrich-Schiller-Universität, Ebertstraße 1, Jena D-07743, Germany

Received 24 September 2006; revised 13 December 2006; accepted 14 December 2006

ABSTRACT: **The paired antennal lobes are the first integration centers for odor information in the insect brain. In the sphinx moth *Manduca sexta*, like in other holometabolous insects, they are formed during metamorphosis. To further understand mechanisms involved in the formation of this particularly well investigated brain area, we performed a direct peptide profiling of a well defined cell group (the lateral cell group) of the antennal lobe throughout development by MALDI-TOF mass spectrometry. Although the majority of the about 100 obtained ion signals represent still unknown substances, this first peptidomic characterization of this cell group indicated the occurrence of 12 structurally known neuropeptides. Among these peptides are helicostatin 1, cydiastatins 2, 3, and 4, *M. sexta*-allatotropin (Mas-AT), *M. sexta*-FLRFamide (Mas-FLRFamide) I, II, and III, nonblocked Mas-FLRFamide I, and *M. sexta*-myoinhibitory peptides (Mas-MIPs) III, V, and VI. The identity of two of the allatostatins (cydiastatins 3 and 4) and Mas-AT were confirmed by tandem mass spectrometry (MALDI-TOF/TOF). During development of the antennal lobe, number and frequency of ion signals including those representing known peptides generally increased at the onset of glomeruli formation at pupal Stage P7/8, with cydiastatin 2, helicostatin 1, and Mas-MIP V being the exceptions. Cydiastatin 2 showed transient occurrence mainly during the period of glomerulus formation, helicostatin 1 was restricted to late pupae and adults, while Mas-MIP V occurred exclusively in adult antennal lobes. The power of the applied direct mass spectrometric profiling lies in the possibility of chemically identifying neuropeptides of a given cell population in a fast and reliable manner, at any developmental stage in single specimens. The identification of neuropeptides in the antennal lobes now allows to specifically address the function of these signaling molecules during the formation of the antennal lobe network.** © 2007 Wiley Periodicals, Inc. Develop Neurobiol 67: 764–777, 2007

Keywords: **MALDI-TOF mass spectrometry; insect; metamorphosis; olfactory system**

This article contains supplementary material available via the Internet at http://www.interscience.wiley.com/jpages/1932-8451/suppmat.

Correspondence to: J. Schachtner. (schachtj@staff.uni-marburg.de)

Contract grant sponsor: DFG; contract grant number: Scha678/3-3.

Published online 21 February 2007 in Wiley InterScience (www.interscience.wiley.com).
DOI 10.1002/dneu.20381

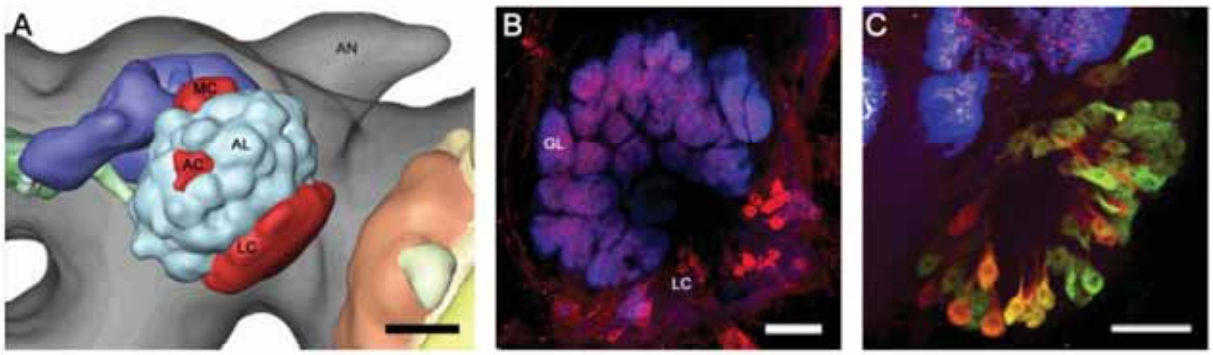

Figure 1 Antennal lobe (AL) morphology of *Manduca sexta*. (A) 3D reconstruction of a female left antennal lobe (AL, light blue) with respect to the localization of the three cell groups: anterior (AC), median (MC) and lateral (LC) cell group (all red). The AL is situated at the front of the brain (gray), anterior to the mushroom body (blue) and the central complex (green) and median to the neuropils of the optic lobe (orange/yellow). It receives its sensory input via the antennal nerve (AN, gray), which enters the brain laterodorsally. Scale: 200 μm. (B) Anti-myoinhibitory peptide antiserum (MIP-ir, red) labels a subpopulation of neurons in the lateral cell group (LC) at stage P17. According to their morphology, these cells are mainly local interneurons innervating the antennal neuropil, which is organized in about 60 olfactory glomeruli (GL). Glomeruli were visualized with an antiserum against the presynaptic vesicle protein synapsin (blue) (scale: 80 μm). (C) Immunostaining with antisera against the neuropeptides Mas-AT (green) and Dip-AST7 (red) also labels subpopulations of neurons of the lateral cell group, here at stage P12. Glomeruli were visualized with an antiserum against the presynaptic vesicle protein synaptotagmin (blue), scale: 80 μm.

INTRODUCTION

The antennal lobes (ALs) of the sphinx moth *Manduca sexta* serve as a well established model for the development of the olfactory system (Fig. 1; Hildebrand et al., 1997; Tolbert et al., 2004). ALs represent the primary integration centers for odor information in the insect brain and are compared to the olfactory bulb of vertebrates (Strausfeld and Hildebrand, 1999; Eisthen, 2002). AL and the olfactory bulb share not only their principal morphological organization into the so-called olfactory glomeruli, but also a number of basic physiological properties with respect to information processing (Hildebrand and Shepherd, 1997). Another characteristic of AL and the olfactory bulb is the expression of a variety of neuropeptides (Smith et al., 1993; Caillol et al., 2003; Moody and Merali, 2004; Gutierrez-Mecinas et al., 2005; Schachtner et al., 2005).

The ALs of *M. sexta* arise during ~3 weeks of hormonally-controlled pupal development (named pupal stages P0 to P20; Truman, 1996; Schachtner et al., 2004b). During this time, the whole brain undergoes reorganization and paired small larval antennal centers develop into the adult ALs (for reviews, see Oland and Tolbert, 1996; Tolbert et al., 2004). AL development in *M. sexta* can roughly be divided into three phases and, in contrast to other developing brain areas, no programmed cell death occurs (Dubuque et al., 2001; Schachtner et al., 2004a). During phase I which lasts from stage P0 to P7/8, the neuronal components of the ALs are provided – all neurons are born until stage P3, olfactory receptor neurons start to grow into the forming AL neuropil from P4 on, and the glomerular templates are formed between stages P6 and P7/8 (Hildebrand, 1985; Hildebrand et al., 1997; Oland et al., 1998). Phase II (P7/8 to P12/13) – the phase of glomeruli formation – is characterized by massive synaptogenesis between the involved neurons (Oland and Tolbert, 1996; Dubuque et al., 2001). It is assumed that at the end of phase II the principal network within and between glomeruli has formed (Dubuque et al., 2001). During phase III (P12/13 to adult eclosion) the main wave of synaptogenesis has ceased but the glomeruli grow in size, probably because of the increasing neurite diameters (Tolbert et al., 1983; Tolbert, 1989; Dubuque et al., 2001; Huetteroth and Schachtner, 2005). During this last phase, the synaptic connections in the glomeruli are thought to undergo further maturation and refinement (Tolbert et al., 1983; Dubuque et al., 2001).

Immunocytochemical studies in a diversity of insects have indicated that several neuropeptides,

including members of FMRFamide-related peptides (FaRPs), allatotropin, and allatostatins are present in subpopulations of local AL neurons, which are responsible for information processing within and between glomeruli (for review see Schachtner et al., 2005; Fig. 1). Neuropeptides might operate as cotransmitters of GABA (γ-aminobutyric acid), the principle transmitter of local AL interneurons (Homberg and Müller, 1999). Concerning AL neurochemistry, the ALs of *M. sexta* are among the best studied (for review see Schachtner et al., 2005). The cellular location and temporal occurrence of certain neuropeptides during ontogeny of the ALs of *M. sexta* have also been mapped by immunolabeling. Interestingly, each of the studied peptide families, including FaRPs, A-type allatostatins, and allatotropins revealed a unique developmental acquisition pattern in defined sets of AL neurons. The occurrence of these neuropeptides is developmentally regulated by the steroid hormone 20-hydroxyecdysone. For each neuropeptide family, the temporal pattern of their occurrence correlates with defined developmental phases, suggesting defined roles during AL development, including formation of olfactory glomeruli (Schachtner et al., 2004b; Utz and Schachtner, 2005; Utz et al., 2005).

In insects, peptides often occur in multiple isoforms within one neuropeptide family and members of the same family are usually encoded by the same gene (e.g., Vanden Broeck, 2001; Riehle et al., 2002; Predel et al., 2004; Hummon et al., 2006), but chemical identification of different isoforms by immunocytochemical methods is nearly impossible. The aim of the present study was first to determine the neuropeptidome of the AL, and second to reveal whether different isoforms are expressed during different times of development. For this purpose, direct peptide profiling of a defined neural cell cluster of individual moths by matrix-assisted laser desorption/ionization time of flight mass spectrometry (MALDI-TOF-MS) is an excellent tool to demonstrate the occurrence of such isoforms and their potential differential expression pattern during metamorphosis, which has not been reported so far. Recently, peptide fragmentation with tandem mass spectrometry parallel to the standardized MALDI-TOF-MS has emerged as an additional tool which provides enhanced capabilities for peptide sequencing directly from samples such as nervous tissues or even single cells of invertebrates, including those of insects (e.g., Yew et al., 2003; Billimoria et al., 2005; Neupert and Predel, 2005; Nachman et al., 2006; Wegener et al., 2006). This study is the first attempt to chemically describe development-dependent peptide expression in an identified neuronal cell cluster within a defined brain region, the AL.

MATERIALS AND METHODS

Insects

Manduca sexta (Lepidoptera: Sphingidae) were raised on artificial diet under long-day photoperiod (L:D = 17:7) at 26°C in walk-in environmental chambers (Bell and Joachim, 1978). Under these conditions, approximately 21 days were required from pupal to adult ecdysis. Newly formed pupae are designated as P0. Subsequent days of pupal development are counted as P1 to P20. Larvae and pupae were staged according to the criteria described by Jindra et al. (1997) and Schwartz and Truman (1983). The criteria involve changes in structures that are either superficial or readily visible through the pupal cuticle under a dissecting microscope.

MALDI-TOF Mass Spectrometry

To selectively obtain identified cell groups, we first detached ALs from isolated brains by pulling the antennal nerve and the attached AL in an anterior direction and then by cutting the ball-shaped AL off the protocerebrum with a pair of fine scissors. This technique ensured selective removal of the AL with no or negligible contamination by protocerebral tissue. The larger lateral and the smaller medial cell group can easily be distinguished on the surface of the isolated ALs. The cell groups were selectively peeled off from the underlying central neuropil by using ultra-fine scissors and microneedles, and were transferred onto a stainless steel sample plate for MALDI-TOF MS. All steps until tissue transfer onto sample plates were performed rapidly in cold saline (Weevers, 1966). After air-drying the tissue, the spots were covered with pure water for a few seconds, which was removed by cellulose paper. Approximately 50 nL matrix solution (recrystallized α-cyano-4-hydroxycinnamic acid dissolved in methanol/H_2O/TFA (trifluoroacetic acid); 60/39/1; v/v/v for stage P1 to P10 and ACN (acetonitril)/H_2O/TFA; 70/29/1; v/v/v or methanol/ethanol/H_2O/TFA; 30/30/39/1 for stage P11-adult) was pumped onto the dried preparations using a nanoliter injector (Neupert and Predel, 2005). Each preparation was allowed to dry again and was then covered with 0.1% TFA for a few seconds, which was removed by cellulose paper. Mass analyses were obtained using a Voyager DE MALDI-TOF biospectrometry workstation (PerSeptive Biosystems, Framingham, MA). Samples were analyzed in positive reflectron mode in the mass range of 830–3000 Da. Synthetic peptides were used for external calibration (angiotensin I, 1296.7 $[M+H]^+$; ACTH (clip 1-17), 1093.1 $[M+H]^+$). The ion signals of cydiastatin 3 (925.5 $[M+H]^+$) or cydiastatin 4 (909.5 $[M+H]^+$) and Mas-AT (1486.7 $[M+H]^+$) were later used for internal calibrations. For tandem MS experiments, analyses were performed on an Ultraflex TOF/TOF (Bruker Daltonics, Bremen, Germany) equipped with LIFT technology. Because of the limited nature of the samples, all acquisitions were taken in manual mode. To determine parent masses, the instrument was operated in reflectron mode prior to fragmentation. The fragmentation data obtained in these experiments were

handled using the flexAnalysis software package (Bruker Daltonics, Bremen, Germany).

Immunocytochemistry

For immunostaining in the AL of *M. sexta*, rabbit antisera against *M. sexta* allatotropin (Mas-AT), *Diploptera* allatostatin 7 (Dip-AST7), *Periplaneta americana* myoinhibitory peptide (Pea-MIP), and monoclonal antibodies from mouse against two ubiquitous synaptic vesicle proteins from *Drosophila* namely synaptotagmin and synapsin I (SYNORF1) were used. Antiserum against Mas-AT was used at a concentration of 1:4000 (No. 13.3.91, kindly provided by Dr. J. Veenstra, University of Bordeaux, Talence, France; Veenstra and Hagedorn, 1993). The antiserum recognizes Mas-AT (Kataoka et al., 1989) and *Locusta* myotropin (Veenstra and Hagedorn, 1993), both ending with TARGFamide. Specificity of the anti-Mas-AT antiserum has been shown by preadsorption of the antiserum with 100 μM synthetic Mas-AT (Bachem) for 1 h at room temperature, which abolished all immunostaining in *M. sexta* brain sections (data not shown). Preadsorption of the antiserum with 100 μM synthetic FLRFamide, FMRFamide, or Dip-AST 7 (all Sigma) for 1 h at room temperature had no effect on immunostaining (data not shown). Antiserum against Dip-AST7 was used at a concentration of 1:10,000 (kindly provided by Dr. H. Agricola, University of Jena, Germany; Utz and Schachtner, 2005). Competitive ELISA showed that the serum cross-reacts with other members of the A-type allatostatin family of peptides characterized by a Y/FXFGLamide C-terminus (Vitzthum et al., 1996). The antiserum against Pea-MIP (1:3000, kindly provided by Dr. M. Eckert, University of Jena, Germany) is thought to generally recognize myoinhibitory peptides. Preadsorption experiments and competitive ELISA showed that the anti Pea-MIP antiserum recognizes myoinhibitory peptides, but not Pea-adipokinetic hormones C-terminally ending with NWamide (Predel et al., 2001; Eckert and Wegener, unpublished). Anti-synaptotagmin (1:4000, kindly provided by Dr. K. Menon, Caltech) and anti-synapsin antibodies (1:100, kindly provided by Dr. E. Buchner, University of Würzburg, Germany) were used to selectively label neuropil structures including olfactory glomeruli (Dubuque et al., 2001; Berg et al., 2002).

Goat anti-rabbit antibodies conjugated to Cy2 and Cy3, and goat anti-mouse antibodies conjugated to Cy5 were used as secondary antisera (each 1:300; JacksonImmuno Research, Westgrove, PA). After dissection in cold saline (Weevers, 1966), the brains of *M. sexta* were fixed in 4% formaldehyde in phosphate-buffered saline overnight at 4°C. After fixation, the brain was either embedded in gelatin/albumin, postfixed overnight in 4% buffered formaldehyde and cut at 40 μm with a vibrating blade microtome (Leica VT 1000S) in the frontal plane, or processed as wholemount. Immunostaining procedure was performed exactly as described in Schachtner et al. (2004b) or, for the wholemounts, as described in Huetteroth and Schachtner (2005) and fluorescence analyzed using a confocal laser-scan microscope (Leica TCS SP2). Double labeling with anti-Mas-AT and anti-Dip-AST7 antisera was performed according to a method modified from Negoescu et al. (1994), for double immunolabeling with primary antisera from the same species as recently described in Berg et al. (2006).

RESULTS

Neurons of the *M. sexta* ALs are organized in three distinct cell groups [Fig. 1(A)]. This anatomical organization allowed the selective removal of the two larger cell groups for direct mass spectrometric profiling. The lateral cell group with about 980 somata contains a mixed population of local and projection neurons, while the median cell group contains only projection neurons (about 200 somata; Homberg et al., 1988). Immunostainings with antisera recognizing C-terminal sequences characteristic of several neuropeptide families (including A-type allatostatins, Mas-allatotropin, RFamides, and myoinhibitory peptides) revealed somata localized in the lateral cell group but not in the other two cell groups [Fig. 1(B–C); Schachtner et al., 2004b; Utz and Schachtner, 2005; Utz et al., 2005].

Direct peptide profiling of lateral cell group preparations revealed a total of about 100 different ion signals during pupal development and in the adult (see Fig. 2), with a maximum of over 50 different masses in single spectra of lateral cell groups of animals of stage P8 or older. Signal intensity obtained was overall small in comparison with other studies in which direct profiling of arthropod tissue or single neurons was performed (e.g. Ma et al., 2000; Predel et al., 2004; Neupert and Predel, 2005). At the beginning of this study, we encountered massive problems to obtain ion signals of peptides by direct mass profiling and had to test various combinations of solvents with the α-cyano-4-hydroxycinnamic acid to obtain reproducible results. For the younger stages (P2/3 to P10), best results were obtained with methanol/H_2O/TFA (60:39:1), while from P11 up to the adult stage methanol/ethanol/H_2O/TFA (30:30:39:1) turned out to be optimal. Nevertheless, many of the ion signals occurred only in some of the mass spectra obtained from a given developmental stage. Therefore, several spectra were collected for each stage, and the occurrence of ion signals was given as percentage of the total number of measurements for each stage (see S1 in supplementary material). Twelve mass peaks corresponded to known *M. sexta* peptides (Table 1; Fig. 3). An overview of the relative frequency of occurrence

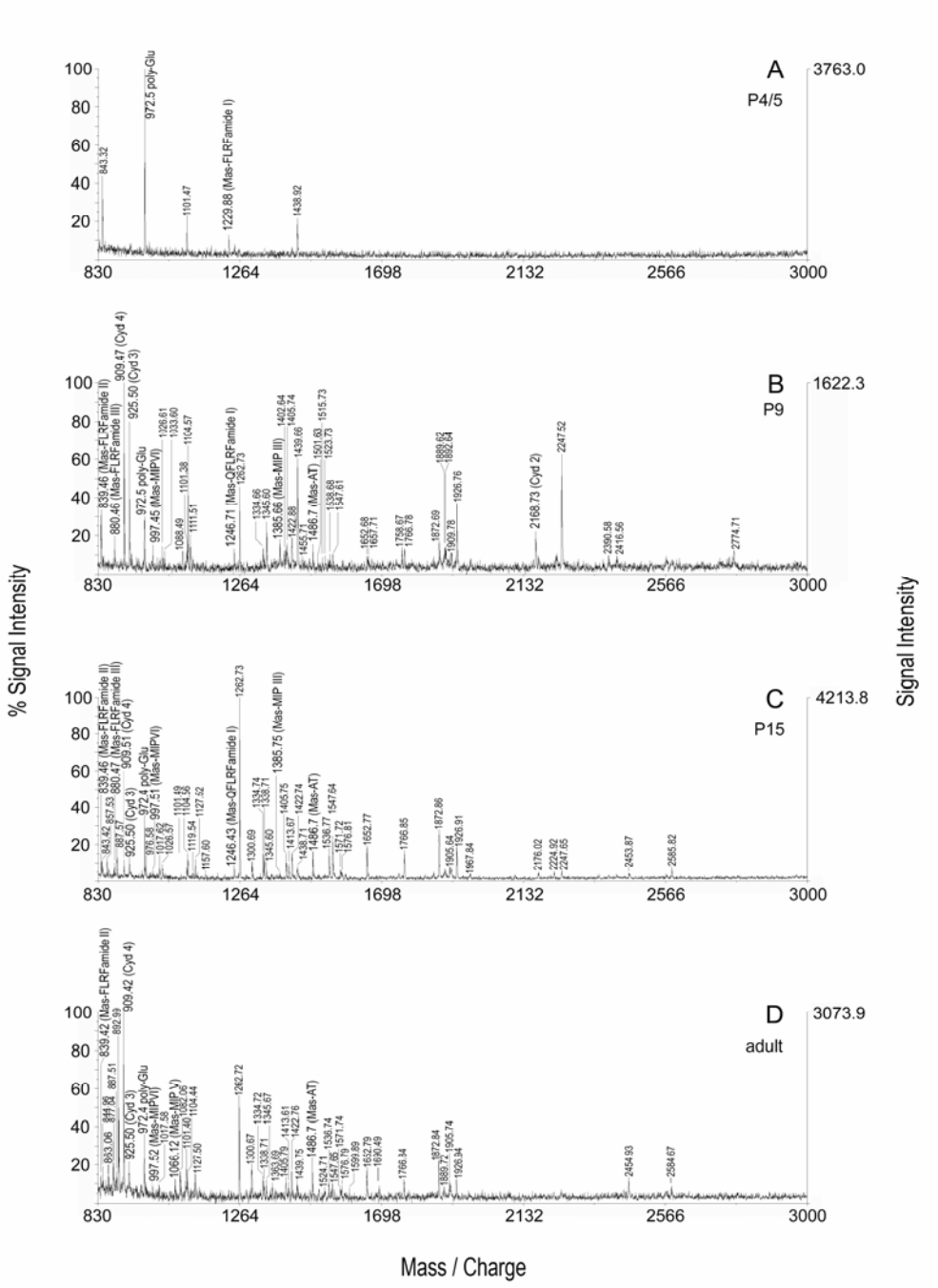

Figure 2 Representative MALDI-TOF mass spectra obtained after direct profiling of single lateral cell groups of the AL of *M. sexta* at different developmental stages. (A) In early pupal stages P2 to P5 spectra of the LC usually contain less than six ion signals ($n = 11$ of 15 evaluated spectra). Mass signal at *m*/*z* 1229.88 is identical with the mass of FLRFamide I. The mass peak at *m*/*z* 972.5, which regularly occurred in spectra of all stages, has been identified via tandem mass spectrometry as an unknown peptide probably ending with poly-glutamate (poly-Glu, see Fig. 6). (B–D) At pupal stage P8, the number of mass peaks measured strongly increased. As revealed by the analysis of 12 ion signals corresponding to known masses in the literature, the pattern of the mass peaks during the rest of development changed however (see text and Fig. 4). Left *y*-axis, relative signal intensity after autoscaling to maximum peak intensity in the selected mass range; right *y*-axis, peak intensity in absolute counts.

Table 1 Calculated and Measured Monoisotopic Masses $[M+H]^+$ of Identified Peptides in the Lateral Cell Group of Antennal Lobes of *M. sexta* and their Amino Acid Sequences

Peptide	Sequence	Calculated	Measured	Mean deviation	Reference
Helicostatin 1	SPHYDFGLa	934.4	934.5	±0.1	1, 3
Cydiastatin 2	AYSYVSEYKRLPVYNFGLa	2168.1	2168.6	±0.3	3, 4
Cydiastatin 3	**SRPYSFGLa**	925.5	925.5	±0.1	1, 3, 5
Cydiastatin 4	**ARPYSFGLa**	909.5	909.5	±0.1	1, 3, 5
Mas-allatotropin	GFKNVEMMTARGFa	1486.7	1486.7	±0.1	3, 8, 9
FLRFamide I	**pEDVVHSFLRFa**	1229.6	1230.1	±0.4	1, 2, 7, 8
FLRFamide I (Q^1)	QDVVHSFLRFa	1246.9	1246.7	±0.1	1, 2, 7
FLRFamide II	GNSFLRFa	839.5	839.4	±0.1	1, 6
FLRFamide III	DPSFLRFa	880.5	880.5	±0.0	1, 6
MIP III	APEKWAAFHGSWa	1385.7	1385.7	±0.1	2, 4
MIP V	GWQDMSSAWa	1066.4	1066.2	±0.1	2, 4
MIP VI	AWSALHGAWa	997.5	997.5	±0.1	1, 4

Peptides in bold have been verified in this study by tandem mass spectrometry. Sequences in bold have been verified by Audsley and Weaver (2003b).

(1) Audsley and Weaver, 2003a; (2) Audsley and Weaver, 2003b; (3) Audsley et al., 2005; (4) Blackburn et al., 2001; (5) Duve et al., 1997; (6) Kingan et al., 1997; (7) Kingan et al., 1990; (8) Predel et al., 2003; (9) Kataoka et al., 1989.

is shown in Figure 4. The sequences of cydiastatins 3 and 4, and Mas-AT were verified by fragmentation using MALDI-TOF/TOF MS (data not shown). In contrast to spectra obtained from lateral cell groups, direct profiling of median cell groups at two stages during development (P8, $n = 4$; P15, $n = 2$) and in adults ($n = 2$) typically revealed no (3 of 8 spectra) or only few ion signals (5 of 8 spectra) with typically overall very low signal intensity (Fig. 5). Some of the ion signals observed in the spectra of the median cell group were identical to ion signals found in the spectra of lateral cell groups, including FLRFamides I (in 1 of 8 spectra), II (in 2 of 8 spectra), III (2 of 8 spectra), Mas-AT (1 of 8 spectra), and some unknown masses, e.g., signals at *m/z* 927, 1101.5, 1338.8, and 1378.8. The majority of ion signals in the median cell group did not occur in the spectra of the lateral cell group, e.g., *m/z* 848.3, 1181.7, 1851.2, and 2892.2. MALDI-TOF/TOF fragmentation of the $[M+H]^+$ ion 972.4 ± 0.1, which was frequently observed in the lateral as well as in the median cell group, revealed fragments with mass differences of about 129 Da, which could indicate a poly-glutamate-containing peptide (Fig. 6).

A-Type Allatostatins

Four masses corresponding to Y/FXFGL-amide-type allatostatins (A-type-ASTs) were detected in preparations from lateral cell groups of ALs of different developmental stages. In mass spectra of stage P4/5 up to the adults, we obtained ion signals corresponding to cydiastatin 3 [925.5; SRPYSFGLa; Fig. 3(C)] and cydiastatin 4 [909.5; ARPYSFGLa; Fig. 3(C)]. Fragmentation by MALDI-TOF/TOF MS clearly identified these ions as cydiastatin 3 and 4, respectively (data not shown). In early stages from P4 to P6, detection of cydiastatin 3 and 4 was limited to a few spectra (4 of 14 evaluated spectra for cydiastatin 3 and 6 of 14 evaluated spectra for cydiastatin 4; Fig. 4). From stage P8 onwards, distinct signals of these two peptides could be detected in almost every evaluated mass spectrum for cydiastatin 3 (57 of 59) and cydiastatin 4 [58 of 59; Figs. 2(B–D) and 4]. The $[M+H]^+$ ion corresponding to *M. sexta* cydiastatin 2 [2168.1; AYSYVSEYKRLPVYNFGLa; Figs. 2(B) and 3(B)] occurred in about half of the spectra from preparations of lateral groups between stages P8 and P12 (14 of 29 evaluated spectra), in a single spectrum of a lateral cell group preparation at stage P5 (1 of 5 evaluated spectra) and P6 (1 of 4 evaluated spectra), and in two spectra of lateral cell groups of pharate animals (2 of 6 evaluated spectra; Fig. 4). In few spectra (7 of 30 evaluated spectra) obtained from lateral cell groups of P15 and older animals, we detected an ion signal corresponding to the calculated monoisotopic mass of helicostatin 1 [934.4; SPHYDFGLa; Figs. 3(A) and 4].

Mas-Allatotropin

A weak ion signal at 1486.6 [Fig. 3(D)] that matches with the monoisotopic mass ($[M+H]^+$) of Mas-AT (1486.7; GFKNVEMMTARGFa) was first detected in a single spectrum in developmental stage P6 (Fig. 4). From stage P8 and throughout the rest of development as well as in the adult stage, a distinct ion signal typical of Mas-AT was measured in most ($n = 44$) of

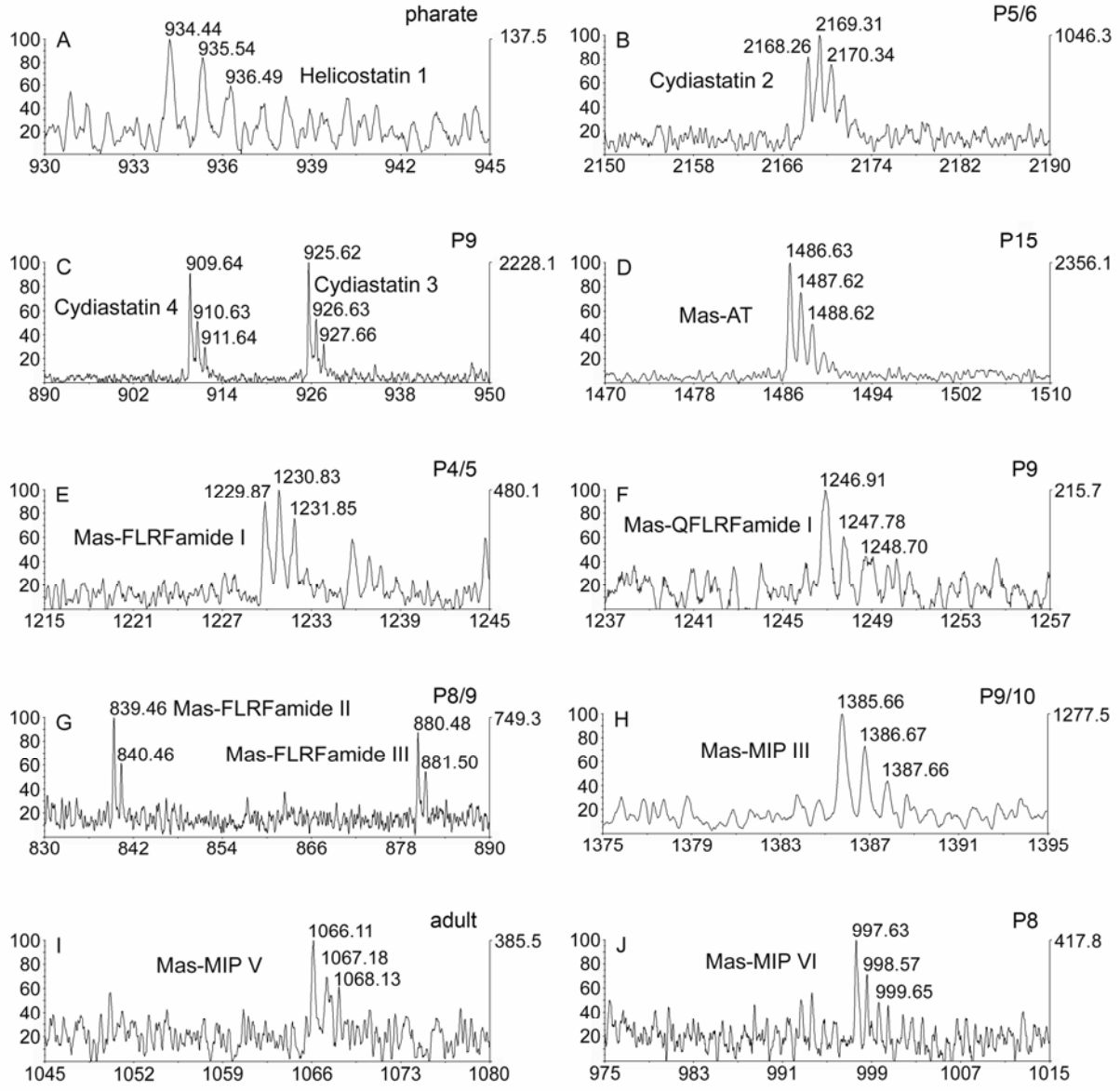

Figure 3 Close-ups showing typical examples for the 12 ion signals which matched masses of known neuropeptides after direct profiling of the lateral cell group at different stages. Left *y*-axis, relative signal intensity after autoscaling to maximum peak intensity in the selected mass range; right *y*-axis, peak intensity in absolute counts.

the 59 evaluated spectra [Figs. 2(B–D) and 4]. Fragmentation of the $[M+H]^+$ ion at 1486.7 by MALDI-TOF/TOF confirmed the identity of this substance with Mas-AT (data not shown).

Mas-FLRFamides

Ion signals corresponding to the calculated monoisotopic masses ($[M+H]^+$) of Mas-FLRFamide I (1229.6; pEDVVHSFLRFa; 11 of 78 evaluated spectra), Mas-FLRFamide II (839.5; GNSFLRFa; 23 of 78 evaluated spectra), and Mas-FLRFamide III (880.5; DPSFLRFa; 29 of 78 evaluated spectra) were found in mass spectra of lateral cell group preparations of different stages throughout pupal development and in adults (Fig. 4). Signal intensities have been low [Fig. 3(E,G)]. Additionally an ion signal corresponding to the $[M+H]^+$ of Mas-FLRFamide I with an unblocked N-terminus was present in 31 of the 78 evaluated spectra during whole study [1246.7; QDVVHSFLRFa; Figs. 2(B,C), 3(F), and 4]. The frequency of occurrence for Mas-FLRFamides II and III

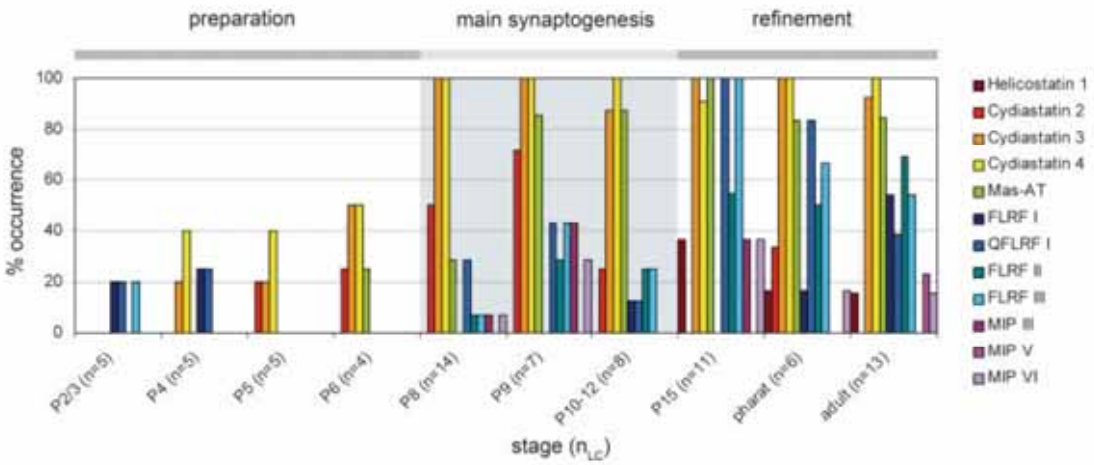

Figure 4 Relative frequency of occurrence of the 12 masses (color coded) matching identified peptides during development. At stage P8, which marks the beginning of formation of the olfactory glomeruli, the number and frequency of ion signals representing masses of the twelve identified peptides clearly increases in contrast to earlier stages. Analysis of the 12 ion signals revealed that the pattern of mass peaks during development was changing. Cydiastatin 2 (*m/z* 2168.73) primarily occurs between stage P8 and P12, while cydiastatins 3 and 4 occurred throughout development and in the adult. Helicostatin 1 occurred only in the spectra of adult animals. FLRFamides occurred throughout development and in the adult, with FLRFamide II not appearing before P8. Myoinhibitory peptide III (MIP III) exclusively occurred between stages P8 and P15, while MIP V occurred exclusively in the spectra of the lateral cell group of adult animals. For further explanation see text and compare with Figure 2; *n*, number of analyzed lateral cell groups.

was highest in the spectra of stage P15, pharates and adults ($\geq$50% of evaluated spectra). Nonblocked Mas-FLRFamide occurrence was highest in the spectra of stage P15 and pharates (100 and $\geq$80%, respectively). The ion signal corresponding to Mas-FLRFamide I occurred with highest frequency in adult spectra.

Mas-Myoinhibitory Peptides

Three masses corresponding to myoinhibitory peptides were detected in lateral cell groups between stage P8 and adult. A monoisotopic mass corresponding to the calculated monoisotopic mass ($[M+H]^+$) of Mas-MIP III [1385.7; APEKWAAFHGSWa; Figs. 2(B,C), 3(H), and 4] was measured at stage P8 (1 of 14 evaluated spectra), P9 (3 of 7 evaluated spectra), and P15 (4 of 11 evaluated spectra). In contrast, signals for Mas-MIP V (1066.4; GWQDMSSAWa) were observed in the adult stage exclusively [3 of 13 evaluated spectra; Figs. 2(D), 3(I), and 4]. The $[M+H]^+$ ion 997.6 [Fig. 3(J)] is in agreement with the $[M+H]^+$ signal of myoinhibitory peptide Mas-MIP VI (997.5; AWSALHGAWa) and occurred occasionally in single spectra of different stages starting at stage P8 up to the adult stage [10 of 59 evaluated spectra; Figs. 2(B–D), 3(J), and 4].

DISCUSSION

Direct peptide profiling of a selected cell group (lateral cell group) in a defined region of the brain (the AL) of the sphinx moth *M. sexta* by MALDI-TOF MS during metamorphosis and in the adult revealed a total of about 100 different mass peaks in the mass range of 830–3000 Da, suggesting the presence of a substantial number of different neuropeptides. Single spectra of lateral cell groups of animals of stage P8 or older contained a maximum of over 50 ion signals. In contrast, direct profiling of another identified cell group (median cell group) resulted in no or only few ion signals in the obtained spectra. Some of the ion signals observed in the median cell group could also be found in the lateral cell group, but typically the signal intensity was much lower in the spectra of the median cell group compared with the lateral cell group (compare Figs. 2 and 5). As we, in addition to the median cell group, dissected small pieces of glomerular tissue, one source for the ion signals occurring in the median cell group could be contamination stemming from peptidergic neurons of the lateral cell group projecting into the glomerular neuropil. Contamination is supported by the fact that we never detected any immunostaining with antisera against various neuropeptides (including antisera against A-

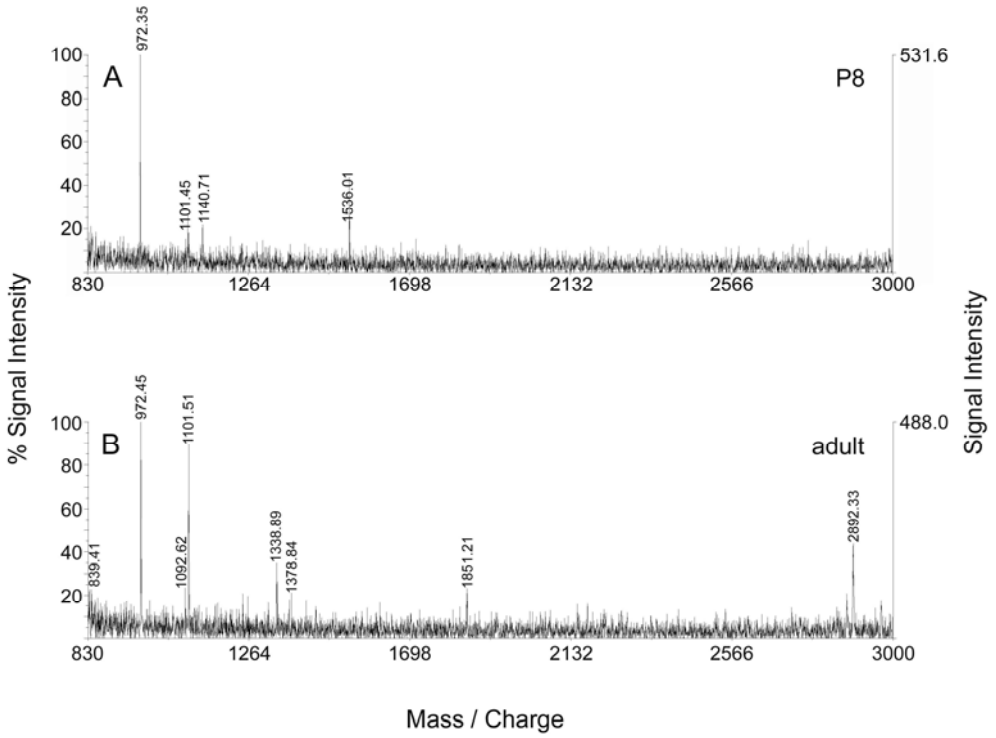

Figure 5 MALDI-TOF mass spectra obtained after direct profiling of single median cell groups of the AL of *M. sexta* at stage P8 (A) and of a freshly eclosed adult animal (B). Spectra obtained after direct profiling of the median cell group usually resulted in no or a few ion signals. Similar ion signals could also be measured in lateral cell groups, e.g., in (B) ion signals at *m/z* 839.4 (corresponds to Mas-FLRFamide II), 972.4, 1101.5, and 1338.8 (compare with Figs. 2 and 6). Left *y*-axis, relative signal intensity after autoscaling to maximum peak intensity in the selected mass range; right *y*-axis, peak intensity in absolute counts.

type allatostatins, Mas-AT, RFamides, and MIPs) in the median cell group of developing or adult *M. sexta* (Schachtner et al., 2004b; Utz and Schachtner, 2005; Utz et al., 2005; Utz et al., unpublished). However, the majority of the ion signals occurring in the spectra of the median cell group were not present in that of the lateral cell group and represent unknown masses. These ion signals might represent so far unknown peptides or other substances, similar as those observed for the ion signal at *m/z* 972.5.

The ion signals obtained from AL preparations were generally weak; a phenomenon which could indicate a low peptide quantity in these cells. Direct peptide profiling of nervous tissue or single cells in other insects revealed much higher signal intensities (e.g., Ma et al., 2000; Predel et al., 2005, 2006; Berg et al., 2006). The low signal intensity appears thus to be an intrinsic property of *M. sexta* tissue, as also mass spectra obtained by direct profiling of neurohemal organs of *M. sexta* show lower signal intensities than those obtained from homologous organs of other insects (Predel et al., 2003; Predel, unpublished observations). This might not be related to the total amount of peptide present, since even in CNS preparations of very small insects such as *Drosophila*, direct mass spectrometric profiling yields high inten-

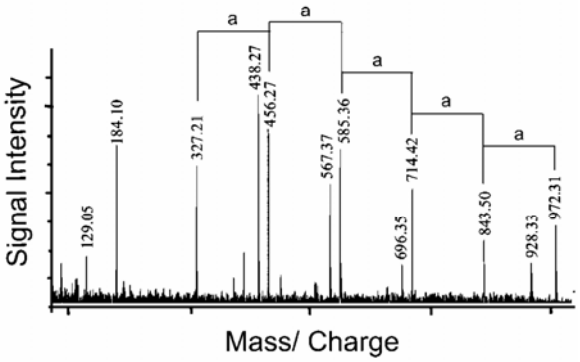

Figure 6 Fragmentation spectrum of the *m/z* 972.5 ion signal obtained by tandem mass spectrometry. The constant mass difference of 129 Da suggests the occurrence of a poly-glutamate. However, no immonium ions typical of Glu were observed. Thus, it remains unclear if the ion at *m/z* 972.5 represents a peptide. Note that the mass peak at 184.1 is not substance specific.

sity peptide signals (Predel et al., 2004). This suggests *M. sexta*-specific endogenous components in the nervous tissue that might prevent optimal cocrystallization of the peptides with the matrix solution or hinder efficient on-target peptide extraction.

Identity of Mass Peaks

Twelve of the about 100 mass peaks matched neuropeptide masses described in *M. sexta* or other moths (Table 1). Using tandem mass spectrometry we were able to confirm the identity of three of the more abundant peaks, namely Mas-allatotropin, cydiastatins 3 and 4. Of the remaining nine signals, which indicated the occurrence of known neuropeptides of *M. sexta*, Mas-FLRFamide I was verified by post-source decay using extracts of retrocerebral complex and larval nervous tissue by Audsley and Weaver (2003a,b). The other peptide signals have been shown to occur in mass spectrometric analyses of *M. sexta* retrocerebral complex, larval nervous tissue, perisympathetic organs and frontal ganglion, but are so far not verified by tandem mass spectrometry (Table 1, Audsley and Weaver, 2003a,b; Predel et al., 2003; Audsley et al., 2005). The four Mas-FLRFamides, three Mas-MIPs, and Mas-AT have been isolated from *M. sexta*, and their amino acid sequence was characterized (Kataoka et al., 1989; Kingan et al., 1990, 1996; Blackburn et al., 2001). Thus, it can be assumed that these peptides were indeed responsible for the ion signals in the respective mass spectra, particularly since immunocytochemical results indicated the presence of neuropeptides belonging to the above neuropeptide families. Amino acid sequences for helicostatin 1 and cydiastatin 2, however, have so far not been established for *M. sexta*, and it cannot be excluded that the ion signals at *m/z* 934.4 and 2168.3 belong to other substances with identical masses.

Developmental Pattern

To obtain best results for each developmental stage, we used different solvents for stages P2/3 to P10 and for P11 to adult. Importantly, changes of mass spectrometric profiles became clearly visible within the time window in which we used the same solvents, e.g., from P2/3 to P10/12. After changing the solvent in later stages, this pattern changed only slightly in pupae older than P12. A dramatic change in the composition of the mass peaks would have indicated that a change of solvent influences the mass spectra. As this is not the case, we conclude that solvent changes are not responsible for the mass peak changes observed; hence, what we see are indeed developmental changes.

A-Type Allatostatins. During AL development, ion signals of A-type allatostatins were not detected before stage P4 (Fig. 4). A recent immunocytochemical study revealed over 10 A-type allatostatin-immunoreactive (AST-A-ir) neurons in lateral cell groups of early pupal stages, with the number of immunoreactive neurons rising to over 50 until the onset of phase II (Utz and Schachtner, 2005). Before stage P4, these peptides are obviously present in such low amounts that we could not detect any ion signal. After stage P4, the frequency of occurrence of masses corresponding to cydiastatins 3 and 4 obtained by direct profiling increased until the beginning of phase II (P8). From stage P8 into adulthood, both masses were detected in nearly 100% of measurements (57/58 of 59 evaluated spectra for cydiastatin 3 and 4, respectively). The timing of their appearance may indicate that cydiastatins 3 and 4 play a role during all phases of development and in signal processing in the adult AL. In contrast, the ion signal corresponding to the mass of cydiastatin 2 was mainly concentrated on the transient time period between stage P8 and P10/12 which coincides with phase II—the phase of glomeruli formation. This result parallels the finding that during phase II a set of about 15 neurons of the lateral cell group transiently expresses peptides of the A-type allatostatin family (Utz and Schachtner, 2005). Deduced from this parallel, we hypothesize that these ~15 cells transiently express cydiastatin 2, which would make the neurons and this neuropeptide good candidates for being involved in the formation of olfactory glomeruli during phase II. It also remains a possibility, however, that the concentration of cydiastatin 2, which normally is below detection threshold, increases with the appearance of additional allatostatin-expressing neurons during phase II, and cydiastatin 2 becomes subsequently detectable.

The ion signal corresponding to helicostatin 1 appeared only in a small percentage of spectra starting in the last part of metamorphosis (P15) up to adulthood. This pattern suggests that helicostatin 1 is merely absent during glomeruli formation, but suggests a possible involvement in processes occurring during phase III and in the adult.

Mas-Allatotropin. Mas-AT was first isolated from heads of pharate adults of *M. sexta* (Kataoka et al., 1989) and could be identified in the mass spectra of frontal ganglia (Audsley et al., 2005), but not in the retrocerebral complex or larval brain extracts of the same species (Audsley and Weaver, 2003a,b).

The Mas-AT gene is expressed as at least three mRNA isoforms that differ by alternative splicing and which encode Mas-AT itself and three Mas-AT like peptides (Mas-ATLs; Horodyski et al., 2001). Northern blot analysis revealed that during pupal development only one splice variant, which exclusively contains Mas-AT, is expressed in the brain. In the adult brain additional low levels of a second splice variant, containing Mas-AT and Mas-ATL III, are expressed (Lee et al., 2002). The present study revealed throughout pupal development and in the adult only the ion signal of Mas-AT in the lateral cell group, but no signal corresponding to the predicted mass of Mas-ATL III. This suggests that the splice form containing Mas-AT and Mas-ATL III is either not expressed in the adult ALs or the concentration of Mas-ATL III was too low for being detected.

Mas-AT immunoreactive cell bodies localize to the lateral but not to the median cell group (Fig. 1). In the present study, the earliest ion signal corresponding to Mas-AT was detected at stage P6. From stage P8 onwards, the frequency in the appearance of the Mas-AT ion signal increased and reached a maximum of nearly 100% at stage P10/12. This corresponds to the finding that two Mas-AT immunoreactive somata are present in early pupae, with numbers increasing to about 100 from stage P6 to P12. The presence of Mas-AT shortly before and during formation of the glomeruli makes this peptide an additional candidate molecule involved in AL development during phases II and III (Utz et al., 2005; Utz et al., in preparation).

Mas-FLRFamides. Ion signals typical of Mas-FLRFamides have been observed throughout development. Signal intensities obtained for these ions, however, were relatively low as was their frequency of occurrence especially in the stages before P15. Owing to the small intensities, the FLRFamide ion signals could have easily been masked by larger peaks, which could explain the relative low frequency of their occurrence in the various measurements. Additionally, a general low amount of FLRFamides could also be responsible for the low frequency. The latter is suggested by an immunocytochemical study with an antiserum recognizing RFamides (Schachtner et al., 2004b) which revealed few immunoreactive neurons in the lateral cell group during early development. Numbers of immunoreactive cells increased then twice, in a first step up to about 30 neurons at the onset of phase II, and in a second step starting at about P12/13 to reach about 50 cells at stage P15. Thus, the higher reliability for the FLRFamide ion signals starting at P15 could be explained by the higher amount of the peptides, reflected by more cells expressing them.

In *M. sexta* it is assumed that Mas-FLRFamides I–III are encoded by three different genes (Lu et al., 2002). *In situ* hybridization revealed that FLRFamide I (F10 according to the authors' nomenclature) is newly expressed in at least 12 AL neurons during metamorphosis (Lu et al., 2002). With this study we confirm these *in situ* results, and additionally demonstrate the presence of three additional FLRFamides. The presence of more than one FLRFamide in the developing AL has already been postulated earlier (Schachtner et al., 2004b).

Myoinhibitory Peptides. In *M. sexta*, six myoinhibitory peptides (MIP I–VI) have been described, which are assumed to be encoded by a single gene (Blackburn et al., 1995, 2001). Similar to the FLRFamides, intensity and frequency of ion signals corresponding to MIP III, V, and VI were low in comparison to signals of, e.g., cydiastatins. The low frequency could be explained by larger mass peaks masking the low intensity MIP signals. Immunostaining with the Pea-MIP antiserum, which is thought to generally recognize myoinhibitory peptides, revealed about 60 somata in the lateral cell groups of adults (Huetteroth and Schachtner, unpublished). This number of Pea-MIP-ir neurons was already reached early during pupal development. Ion signals corresponding to MIP III and VI occurred not before P8, while MIP V signals occurred only in the adult. Comparison of these mass spectrometric data with the immunostainings suggests that, additionally, other so far unknown myoinhibitory or myinhibitory-related peptides are labeled with the Pea-MIP antiserum. Thus, ion signals of unknown peptides occurring in spectra of the lateral cell group during phase I could possibly account for these unknown myoinhibitory peptides.

Developmental Regulation. The developmental time window, during which the numbers of mass peaks within the lateral cell group dramatically increase, coincides with the onset of the formation of the olfactory glomeruli at stage P7/8 (Figs. 2 and 4). Formation of the glomeruli is under control of the rising titer of the developmental hormone 20-hydroxyecdysone, as is the number of cells in the lateral cell group immunoreactive to neuropeptide antisera including anti-RFamide, anti-allatostatin (A-type), and anti-Mas-AT (Schachtner et al., 2004b; Utz and Schachtner, 2005; Utz et al., 2005; Utz et al., in preparation). This strongly suggests that the rising hormone titer is causative for the expression of the neuropeptides. Further studies are on their way to reveal whether

neuropeptide expression is under direct or indirect control of 20-hydroxyecdysone.

In summary, mass spectrometric analysis of neuropeptides of the lateral cell group during AL development suggests a differential occurrence of neuropeptide isoforms encoded either altogether on one gene (A-type allatostatins, Mas-AT, MIPs), or on different genes (FLRFamides). To the best of our knowledge, this is the first mass spectrometric verification of a changing peptide complement in an identified cell group during ontogeny.

The differential expression pattern of individual neuropeptides during AL development suggested in this study clearly supports previous immunocytochemical studies which mapped neuropeptide immunoreactivity during AL ontogeny in the sphinx moth. Most importantly, this study chemically identified neuropeptides and characterized their temporal expression pattern, thus establishing them as candidate molecules involved in the regulation of AL development. We favor the idea that the described neuropeptides might be involved in both the formation of the AL network as well as adult signal processing. It may yet also be possible that the temporal expression pattern of neuropeptides simply is a consequence of AL development, with neuropeptides only serving a function in adult odor processing (Winther et al., 2006).

In any case, the chemical identification of single neuropeptides at defined phases of development allows now to specifically investigate the possible roles and developmental significance of these neuropeptides during the formation of the AL neuronal network.

The authors thank Drs. H. Agricola and M. Eckert (both University of Jena, Germany), E. Buchner (University of Würzburg, Germany), K. Menon (Caltech, USA), J. Veenstra (University of Bordeaux, Talence, France) for kindly providing the various antisera used in this study. We also thank Lotte Søgaard-Andersen (Max-Planck-Institute of Terrestrial Microbiology, Marburg) and Olaf Scheibner (Hans Knöll Institut, Jena) for the use of the MALDI-TOF and the Ultraflex TOF/TOF mass spectrometers.

REFERENCES

Audsley N, Matthews J, Weaver RJ. 2005. Neuropeptides associated with the frontal ganglion of larval Lepidoptera. Peptides 26:11–21.

Audsley N, Weaver RJ. 2003a. A comparison of the neuropeptides from the retrocerebral complex of adult male and female *Manduca sexta* using MALDI-TOF mass spectrometry. Regul Pept 116:127–137.

Audsley N, Weaver RJ. 2003b. Identification of neuropeptides from brains of larval *Manduca sexta* and *Lacanobia oleracea* using MALDI-TOF mass spectrometry and post-source decay. Peptides 24:1465–1474.

Bell RA, Joachim FA. 1978. Techniques for rearing laboratory colonies of the tobacco hornworm. *Manduca sexta*, and pink ballworms. Ann Entomol Soc Am 69: 365–373.

Berg BG, Galizia CG, Brandt R, Mustaparta H. 2002. Digital atlases of the antennal lobe in two species of tobacco budworm moths, the oriental *Helicoverpa assulta* (male) and the American *Heliothis virescens* (male and female). J Comp Neurol 446:123–134.

Berg BG, Schachtner J, Utz S, Homberg U. 2006. Distribution of neuropeptides in the primary olfactory center of the heliothine moth *Heliothis virescens*. Cell Tissue Res 327:385–398.

Billimoria CP, Li L, Marder E. 2005. Profiling of neuropeptides released at the stomatogastric ganglion of the crab *Cancer borealis* with mass spectrometry. J Neurochem 95:191–199.

Blackburn MB, Jaffe H, Kochansky J, Raina AK. 2001. Identification of four additional myoinhibitory peptides (MIPs) from the ventral nerve cord of *Manduca sexta*. Arch Insect Biochem Physiol 48:121–128.

Blackburn MB, Wagner RM, Shabanowitz J, Kochansky JP, Hunt DF, Raina AK. 1995. The isolation and identification of three diuretic kinins from the abdominal ventral nerve cord of adult *Helicoverpa zea*. J Insect Physiol 41:723–730.

Caillol M, Aioun J, Baly C, Persuy MA, Salesse R. 2003. Localization of orexins and their receptors in the rat olfactory system: Possible modulation of olfactory perception by a neuropeptide synthesized centrally or locally. Brain Res 960:48–61.

Dubuque SH, Schachtner J, Nighorn AJ, Menon KP, Zinn K, Tolbert LP. 2001. Immunolocalization of synaptotagmin for the study of synapses in the developing antennal lobe of *Manduca sexta*. J Comp Neurol 441: 277–287.

Duve H, Johnsen AH, Maestro JL, Scott AG, Winstanley D, Davey M. 1997. Lepidopteran peptides of the allatostatin superfamily. Peptides 18:1301–1309.

Eisthen HL. 2002. Why are olfactory systems of different animals so similar? Brain Behav Evol 59:273–293.

Gutierrez-Mecinas M, Crespo C, Blasco-Ibanez JM, Gracia-Llanes FJ, Marques-Mari A, Martinez-Guijarro. 2005. Characterization of somatostatin- and cholecystokinin-immunoreactive cells in the rat olfactory bulb. J Comp Neurol 489:467–479.

Hildebrand JG. 1985. Metamorphosis of the nervous system: Influence of the periphery on the postembryonic development of the antennal sensory pathway in the brain of *Manduca sexta*. In: Selverston A, editor. Model Neural Networks and Behavior. New York: Plenum, pp 129–148.

Hildebrand JG, Rössler W, Tolbert LP. 1997. Postembryonic development of the olfactory system in the moth *Manduca sexta*: Primary-afferent control of glomerular development. Cell Dev Biol 8:163–170.

Hildebrand JG, Shepherd GM. 1997. Mechanisms of olfactory discrimination: Converging evidence for common principles across phyla. Annu Rev Neurosci 20:595–631.

Homberg U, Montague RA, Hildebrand JG. 1988. Anatomy of antenno-cerebral pathways in the brain of the sphinx moth *Manduca sexta*. Cell Tissue Res 254:255–281.

Homberg U, Müller U. 1999. Neuroactive substances in the antennal lobe. In: Hanson BS, editor. Insect Olfaction. Berlin: Springer, pp 181–206.

Horodyski FM, Bhatt SR, Lee K-Y. 2001. Alternative splicing of transcripts expressed by the *Manduca sexta* allatotropin (Mas-AT) gene is regulated in a tissue-specific manner. Peptides 22:263–269.

Huetteroth W, Schachtner J. 2005. Standard three-dimensional glomeruli of the *Manduca sexta* antennal lobe: A tool to study both developmental and adult neuronal plasticity. Cell Tissue Res 319:513–524.

Hummon AB, Richmond TA, Verleyen P, Baggerman G, Huybrechts J, Ewing MA, Vierstraete E, Rodriguez-Zas SL, Schoofs L, Robinson GE, Sweedler JV. 2006. From the genome to the proteome: Uncovering peptides in the *Apis* brain. Science 314:647–649.

Jindra M, Huang JY, Malone F, Asahina M, Riddiford LM. 1997. Identification and mRNA developmental profiles of two ultraspiracle isoforms in the epidermis and wings of *Manduca sexta*. Insect Mol Biol 6:41–53.

Kataoka H, Toschi A, Li JP, Carney L, Schooley DA, Kramer SJ. 1989. Identification of an allatotropin from adult *Manduca sexta*. Science 243:1481–1483.

Kingan TG, Shabanowitz J, Hunt DF, Witten JL. 1996. Characterisation of two myotropic neuropeptides in the FMRFamide family from segmental ganglia of the moth *Manduca sexta*: Candidate neurohormones and neuromodulators. J Exp Biol 199:1095–1104.

Kingan TG, Teplow DB, Phillips JM, Riehm JP, Rao KR, Hildebrand JG. 1990. A new peptide in the FMRFamide family isolated from the CNS of the hawkmoth *Manduca sexta*. Peptides 11:849–856.

Lee K-Y, Chamberlin ME, Horodyski FM. 2002. Biological activity of *Manduca sexta* allatotropin-like peptides, predicted products of tissue-specific and developmentally regulated alternatively spliced mRNAs. Peptides 23:1933–1941.

Lu D, Lee KY, Horodyski FM, Witten LJ. 2002. Molecular characterization and cell-specific expression of a *Manduca sexta* FLRFamide gene. J Comp Neurol 446:377–396.

Ma PW, Garden RW, Niermann JT, O' Connor M, Sweedler JV, Roelofs WL. 2000. Characterizing the *Hez*-PBAN gene products in neuronal clusters with immunocytochemistry and MALDI MS. J Insect Physiol 46:221–230.

Moody TW, Merali Z. 2004. Bombesin-like peptides associates receptors within the brain: Distribution and behavioral implications. Peptides 25:511–520.

Nachman RJ, Russel WK, Coast GM, Russel DH, Miller JA, Predel R. 2006. Identification of PVK/CAP2b neuropeptides from single neurohemal organs of the stable fly and horn fly via MALDI-TOF/TOF tandem mass spectrometry. Peptides 27:521–526.

Negoescu A, Labat-Moleur F, Lorimier P, Lamarcq L, Guillermet C, Chambaz E, Brambilla E. 1994. F(ab) secondary antibodies: A general method for double immunolabeling with primary antisera from the same species. Efficiency control by chemoluminescence. J Histochem Cytochem 42:433–437.

Neupert S, Predel R. 2005. Mass spectrometric analysis of single identified neurons of an insect. Biochem Biophys Res Commun 327:640–645.

Oland LA, Pott WM, Higgins MR, Tolbert LP. 1998. Targeted ingrowth and glial relationships of olfactory receptor axons in the primary olfactory pathway of an insect. J Comp Neurol 398:119–138.

Oland LA, Tolbert LP. 1996. Multiple factors shape development of olfactory glomeruli: Insights from an insect model system. J Neurobiol 30:92–109.

Predel R, Eckert M, Pollák E, Molnár L, Scheibner O, Neupert S. 2006. Peptidomics of identified neurons demonstrates a highly differentiated expression pattern of FXPRLamides in the neuroendocrine system of an insect. J Comp Neurol 500:498–512.

Predel R, Herbert Z, Eckert M. 2003. Neuropeptides in perisympathetic organs of *Manduca sexta*: Specific composition and changes during development. Peptides 24:1457–1464.

Predel R, Neupert S, Roth S, Derst C, Nässel DR. 2005. Tachykinin-related peptide precursors in two cockroach species. FEBS J 272:3365–3375.

Predel R, Rapus J, Eckert M. 2001. Myoinhibitory peptides in the American cockroach. Peptides 22:199–208.

Predel R, Wegener C, Russell WK, Tichy SE, Russell DH, Nachman RJ. 2004. Peptidomics of CNS-associated neurohemal systems of adult *Drosophila melanogaster*: A mass spectrometric survey of peptides from individual flies. J Comp Neurol 474:379–392.

Riehle MA, Garczynski SF, Crim JW, Hill CA, Brown MR. 2002. Neuropeptides and peptide hormones in *Anopheles gambiae*. Science 298:172–175.

Schachtner J, Huetteroth W, Nighorn A, Honegger HW. 2004a. Copper/zinc superoxide dismutase-like immunoreactivity in the metamorphosing brain of the sphinx moth *Manduca sexta*. J Comp Neurol 469: 141–152.

Schachtner J, Schmidt M, Homberg U. 2005. Organization and evolutionary trends of primary olfactory brain centers in Tetraconata (Crustacea + Hexapoda). Arthropod Struct Dev 34:257–299.

Schachtner J, Trosowski B, D'Hanis W, Stubner S, Homberg U. 2004b. Development and steroid regulation of RFamide immunoreactivity in antennal lobe neurons of the sphinx moth *Manduca sexta*. J Exp Biol 207:2389–2400.

Schwartz LM, Truman JW. 1983. Hormonal control of rates of metamorphic development in the tobacco hornworm *Manduca sexta*. Dev Biol 99:103–114.

Smith RL, Baker H, Greer CA. 1993. Immunohistochemical analysis of the human olfactory bulb. J Comp Neurol 333:519–530.

Strausfeld NJ, Hildebrand JG. 1999. Olfactory systems: Common design, uncommon origins? Curr Opin Neurobiol 9:634–639.

Tolbert LP. 1989. Afferent axons from the antenna influence the number and placement of intrinsic synapses in the antennal lobes of *Manduca sexta*. Synapse 3:83–95.

Tolbert LP, Matsumoto SG, Hildebrand JG. 1983. Development of synapses in the antennal lobes of the moth *Manduca sexta* during metamorphosis. J Neurosci 3:1158–1175.

Tolbert LP, Oland LA, Tucker ES, Gibson NJ, Higgins MR, Lipscomb BW. 2004. Bidirectional influences between neurons and glial cells in the developing olfactory system. Prog Neurobiol 73:73–105.

Truman JW. 1996. Ecdysis control sheds another layer. Science 271:40–41.

Utz S, Huetteroth W, Schachtner J. 2005. Development and steroid regulation of Mas-allatotropin immunostaining in antennal lobe neurons of the sphinx moth *Manduca sexta*. In the 98th Meeting of the German Zooogical Society, Bayreuth, Germany. No. 1_Po_24

Utz S, Schachtner J. 2005. Development of A-type allatostatin immunoreactivity in antennal lobe neurons of the sphinx moth *Manduca sexta*. Cell Tissue Res 320:149–162.

Vanden Broeck J. 2001. Neuropeptides and their precursors in the fruitfly, *Drosophila melanogaster*. Peptides 22:241–254.

Veenstra JA, Hagedorn HH. 1993. Sensitive enzyme immunoassay for *Manduca* allatotropin and the existence of an allatotropin-immunoreactive peptide in *Periplaneta americana*. Arch Insect Biochem Physiol 23:99–109.

Vitzthum H, Homberg U, Agricola H. 1996. Distribution of Dip-Allatostatin I-like immunoreactivity in the brain of the locust *Schistocerca gregaria* with detailed analysis of immunostaining in the central complex. J Comp Neurol 369:419–437.

Weevers RD. 1966. A lepidopteran saline: The effects of inorganic cation concentrations on sensory reflex and motor responses in a herbiverous insect. J Exp Biol 44: 163–176.

Wegener C, Reinl T, Jänsch L, Predel R. 2006. Direct mass spectrometric peptide profiling and fragmentation of larval peptide hormone release sites in *Drosophila melanogaster* reveals tagma-specific peptide expression and differential processing. J Neurochem 96:1362–1374.

Winther ÅME, Acebes A, Ferrus A. 2006. Tachykinin-related peptides modulate odor perception and locomotor activity in *Drosophila*. Mol Cell Neurosci 31:399–406.

Yew JY, Dikler S, Stretton AO. 2003. De novo sequencing of novel neuropeptides directly from *Ascaris suum* tissue using MALDI-TOF/TOF. Rapid Commun Mass Spectrom 17:2693–2698.

CHAPTER V:

Standard three-dimensional glomeruli of the *Manduca sexta* antennal lobe: a tool to study both developmental and adult neuronal plasticity

Cell Tissue Res (2005) 319: 513–524
DOI 10.1007/s00441-004-1016-1

REGULAR ARTICLE

Wolf Huetteroth · Joachim Schachtner

Standard three-dimensional glomeruli of the *Manduca sexta* antennal lobe: a tool to study both developmental and adult neuronal plasticity

Received: 20 August 2004 / Accepted: 5 October 2004 / Published online: 26 January 2005

Abstract The metamorphosing antennal lobe (AL) of the sphinx moth *Manduca sexta* serves as an established model system for studying neuronal development. To improve our understanding of mechanisms involved in neuronal plasticity, we have analyzed the size, shape, and localization of ten identified glomeruli at three different time points during development and in the adult, viz., (1) 13 days after pupal eclosion (P13), which reflects a time when the basic glomerular map has formed, (2) immediately after adult eclosion (A0), which represents a time when the newly formed glomeruli are uninfluenced by external odors, and (3) 4 days after adult eclosion (A4), which reflects a time when the animals have been exposed to surrounding odors. Our data from normally developing ALs of male *M. sexta* from P13 to A0 revealed an increase in size of all examined glomeruli of between 40% and 130%, with the strongest increases occurring in two of the three sex-specific glomeruli (cumulus, toroid). From A0 to A4, the cumulus and toroid increased significantly when correlated to AL volume, whereas the other glomeruli reached the sizes gained after A0. This study was based on antibody staining against the ubiquitous synaptic vesicle protein synaptotagmin, confocal laser scan microscopy, and the three-dimensional (3D) analysis tool AMIRA. Tissue permeability and therefore reliability of the staining quality was enhanced by using formalin/methanol fixation. The standard 3D glomeruli introduced in this study can now be used as basic tools for further examination of neuronal plasticity at the level of the identified neuropil structures, viz., the glomeruli of the AL of *M. sexta*.

Keywords 3D reconstruction · AMIRA · Brain · Glomerular map · Olfactory system · *Manduca sexta* males, (Insecta)

W. Huetteroth · J. Schachtner (✉)
Fachbereich Biologie, Tierphysiologie, Philipps-Universität, 35043 Marburg, Germany
e-mail: schachtj@staff.uni-marburg.de

Introduction

The two antennal lobes of the adult sphinx moth *Manduca sexta* are the first relay stations for olfactory information processing in the brain. The neuropil of the antennal lobe (AL) is organized in globular structures, the so-called glomeruli (n=63±1), which are arranged in a sphere around a central coarse neuropil (Rospars and Hildebrand 2000). This glomerular assembly seems to be a conserved morphological principle among brain regions involved in the initial central processing of olfactory information, since it is, with variable numbers of glomeruli, common in insects and vertebrates (for reviews, see Hildebrand and Shepherd 1997; Strausfeld and Hildebrand 1999; Eisthen 2002).

The AL arises during approximately 3 weeks of hormonally controlled pupal development (regarded as pupal stages P0 to P20; Truman 1996; Schachtner et al. 2004b). During this time, the whole brain undergoes reorganization, and a small larval antennal center develops into the adult AL (Oland and Tolbert 1996). All neurons of the AL have been born by P3 (Hildebrand et al. 1997). Beginning with P4, the olfactory receptor neurons (ORNs) enter the AL and induce, in association with antennal glial cells, the formation of glomeruli during the subsequent stages (for a review, see Tolbert et al. 2004). After a short delay, mainly between P7/8 and P12, the interaction of ingrowing ORNs, glial cells, local (LNs) and projection (PNs) neurons leads to increased synaptogenesis in a distoproximally directed wave and to the stabilization of the glomeruli (Oland et al. 1990; Tolbert and Sirianni 1990; Dubuque et al. 2001). After P12, the glomeruli increase in size, probably because of the increasing neurite diameters, but the main wave of synaptogenesis seems to be complete (Tolbert et al. 1983; Tolbert 1989; for reviews, see Oland and Tolbert 1996; Tolbert et al. 2004). Nevertheless, the synaptic connections in the glomeruli are thought to undergo further maturation and refinement until eclosion (Tolbert et al. 1983; Dubuque et al. 2001).

Several authors have outlined the advantages of a 3D map not only of vertebrate brains (Ruffins et al. 2002; also reviewed in Van Essen et al. 2002), but also of insect brain

structures (Rohlfing et al. 2004; Zöckler et al. 2001; Chiang et al. 2001; Rein et al. 1999, 2002; Haddad et al. 2004), especially in the AL (*Drosophila melanogaster*: Laissue et al. 1999; *Apis mellifera*: Flanagan and Mercer 1989; Galizia et al. 1999; *Blaberus craniifer*: Chambille and Rospars 1981; *Mamestra brassicae*: Rospars 1983; *Helicoverpa assulta* and *Heliothis virescens*: Berg et al. 2002; *Spodoptera littoralis*: Sadek et al. 2002; *Agrotis ipsilon*: Greiner et al. 2004; *Cotesia glomerata* and *rubecula*: Smid et al. 2003). The identification and 3D representation of a set of "ordinary" glomeruli in an atlas allows for their repeatedly reliable identification irrespective of the original data (Galizia et al. 1999). Rospars and Hildebrand (1992, 2000) reconstructed ALs of adult *M. sexta* based on paraffin sections, but, although they provided the first map of *M. sexta* AL glomeruli, their work supplied only restricted information about glomerular volumes or shape. Because of the immense improvements in confocal laser scan microscopy (CLSM), computer power, and 3D reconstruction software during last few years, 3D maps have been constructed of various insect brains. However, a reconstruction of the AL of *M. sexta* by these methods has been absent until now, mainly because of its large size.

We have pursued two main aims in this study: (1) the quantification of the increase in glomerular size during the second half of pupal development and during the first few days after adult eclosion, and (2), for future studies, the establishment of an anatomical and volumetric standard of ten glomeruli of P13 pupae, freshly eclosed adults (A0), and 4-day old adults (A4). Within the scope of this study, we have found significant glomerular size increases in two of three sex-specific glomeruli in adult *M. sexta*. We have also found evidence for a higher variability in male-specific glomerular shape between individuals than has previously been reported (Rospars and Hildebrand 1992, 2000). Some of this study has been published before in abstract form (Huetteroth and Schachtner 2003).

Materials and methods

Animals

Moths (*Manduca sexta*; Lepidoptera: Sphingidae) were kept in walk-in environmental chambers at 26°C under a long-day photoperiod (L:D=17:7) and were fed on an artificial diet as described by Bell and Joachim (1978). Under this regime, pupal development from the day of pupal ecdysis (P0) until adult eclosion (A0) took approximately 20 days, each day corresponding to a pupal stage (P0-P20). Adult life was staged accordingly (A0–A4). Adult animals were supplied with water ad libitum; they were allowed to smell but not to reach the opposite sex. Pupae were staged according to criteria described in Jindra et al. (1997) and Schwartz and Truman (1983). Stages of other staging systems (Tolbert et al. 1983) used in cited studies were adapted accordingly. Only male moths were used.

Immunocytochemistry

As a primary antibody, we used a monoclonal anti-synaptotagmin antibody from mouse (1:2,000, kindly provided from Kaushiki Menon, Caltech, USA). Specificity controls for the anti-synaptotagmin antibody are described in Dubuque et al. (2001). As a secondary antibody, Cy3-coupled goat anti-mouse antibody (Jackson Immuno Research, Westgrove, Pa., USA) was used at a dilution of 1:300. After dissection in cold saline (Weevers 1966) or phosphate-buffered saline (PBS, 0.01 M), brains of various developmental stages of *M. sexta* were fixed in methanol containing 10% formalin for 50–100 min at room temperature and then rinsed in PBS for 1 h at room temperature. Because of the large brain size, two slabs containing the ALs were cut out of each brain (see also Figs. 2; 3a, A, A″). These slabs were preincubated overnight at 4°C in 5% normal goat serum (NGS; Jackson Immuno Research) in 0.1 M TRIS–HCl/0.3 M NaCl (SST) with 0.5% Triton X-100 (SST-TX 0.5, Sigma-Aldrich Chemie). The primary antibody was then diluted in SST-TX 0.5 with 1% NGS and incubated with the slabs for 5–6 days at 4°C. The brain slabs were rinsed 12 times over 6 h in SST-TX 0.1 at room temperature. Secondary antibody (in SST-TX 0.5/1% NGS) was applied for 2 days at 4°C, followed by rinsing in SST-TX 0.1 at room temperature for 4 h. Slabs were dehydrated in an ascending alcohol series (30%–100%, 5 min each), cleared in methyl salicylate (Merck, Gernsheim, Germany), and subsequently mounted in Permount (FisherScientific, Pittsburgh, Pa., USA). We used spacers to diminish squeezing of the preparations and two coverslips to allow scanning of the material from both sides.

CLSM image acquisition and processing

Fluorescently labeled slabs were scanned at 1024×1024 pixel resolution by using a 20× objective (HC PL APO 20×/0.70 Imm Corr CS; Leica, Bensheim, Germany) on a confocal laser scan microscope (Leica TCS SP2). No correction for *z*-axis refractive index mismatch was necessary, since the immersion oil, mounting medium, and tissue had refractive indices N_d^{20} of approximately 1.5 (Gahm and Witte 1986). Because of to the limited working distance of the objective (170 μm) and the size of the slabs (approximately 300 μm), we had to scan the material from two sides to obtain images of the whole preparation. This resulted in two image stacks. Further processing of images (reduction to 512×512 pixels and conversion to an 8-bit gray-scale) was performed by using Adobe Photoshop 6. Corresponding optical slices in the overlapping part of both image stacks were found by using the "Align Slices" tool of AMIRA 3.0 and 3.1 (Indeed-Visual Concepts, Berlin, Germany). Redundant slices of the stack were abolished. This led to image stacks of ALs and adjacent protocerebrum with a resolution of 1.4 μm×1.4 μm×1.01 μm/voxel and an overall size of about 720 μm×720 μm×272–325 μm.

Glomerular structures in the AL were labeled as described previously by using the AMIRA "brush" tool, "interpolate" tool, and "warp" tool (Galizia et al. 1999; Smid et al. 2003). To determine boundaries between two adjacent glomeruli more precisely, the "4viewer" mode was employed, which allows assessment of the glomerular extent in the XY plane, XZ plane, and YZ plane of each respective image stack (Fig. 1). The volumes of labeled glomeruli were read out with the tool "tissue statistics". The data were imported and further processed with Microsoft Excel XP.

Because of the variable orientation of the preparation, the CLSM sectioning of the AL could not always be achieved in orthogonal frontal planes corresponding to anatomical axes. This problem was solved by reslicing the CLSM stacks with the AMIRA "ObliqueSlice" tool until a corresponding plane consistent with previous data was detected.

Differences in absolute (measured glomerulus volumes) and relative (glomerulus volumes correlated to AL volume) glomerular volumes between P13 and A0 and between A0 and A4 were examined with the Mann–Whitney *U* test, since we observed no normal distribution of data within groups. We used the Friedman analysis of variance and Kendall coefficient of concordance test to determine whether there was constancy in glomerular size within the various stages. Significances were calculated with the Statistica"99 edition.

Results

Overall, we acquired image stacks of 37 ALs obtained from 26 male moths. Stages included P12 (3 ALs from 3 animals), P13 (6 ALs from 5 animals), A0 (16 ALs from 9 animals), A1 (4 ALs from 4 animals), and A4 (8 ALs from 5 animals). Most of this study including volumetric comparisons is based on P13, A0, and A4 ALs (see Table 1 for a comprehensive overview). The glomeruli of the macroglomerular complex (MGC), the labial pit organ glomerulus (LPOG), and six identifiable "ordinary" glomeruli were routinely analyzed. For reconstructing the whole set of AL glomeruli, 2 ALs of P12, 4 ALs of P13, 1 AL of A0, and 5 ALs of A4 animals were used (Table 1). The methanol-containing fixation allowed for antibody staining throughout the AL preparations; no labeling

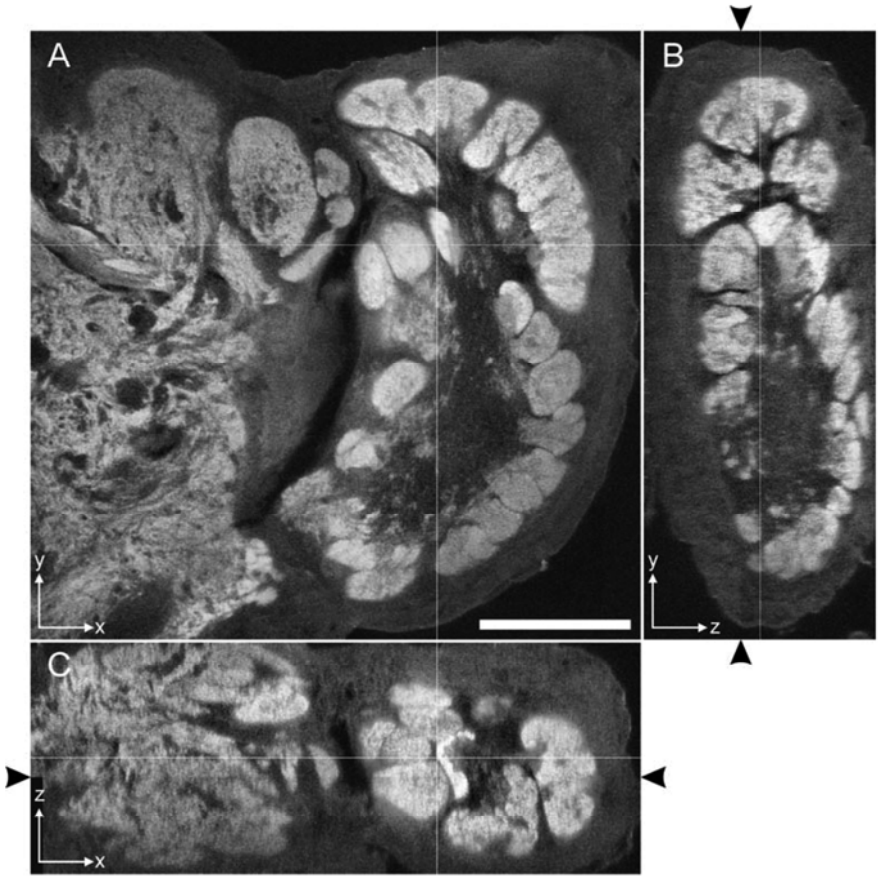

Fig. 1 Synaptotagmin immunostaining in three single planes of about 1 μm thickness of an AL whole-mount (male, A4). **A** One single optical slice from a stack of 282 approximately sagittal slices (XY). **B**, **C** The same image stack, viewed in YZ (frontal) and XZ (coronal) planes, respectively. *Lines* refer to corresponding intersection planes in **A**–**C**. This figure displays the quality of the optical slices taken with a lateral resolution of 1024×1024 pixels. Thus, the voxel resolution is 0.7 μm×0.7 μm×1.01 μm. Note the slight compression in the *z*-axis and the consistently good staining quality throughout the volume of the tissue slab. The alignment edge of the two image stacks can barely be seen (*arrowheads*). *Bar* 200 μm

Table 1 Comprehensive overview of antennal lobes (ALs) used in this study. From all listed ALs, the glomeruli of the MGC, the LPOG, and six "ordinary" glomeruli were routinely analyzed. Additionally, all glomeruli were labeled from 12 of the 37 ALs. The developmental stages (the figures in which the corresponding ALs are presented are indicated in *brackets*), weight of the animal, right (*r*) or left (*l*) AL side, number of optical slices per image stack, and additional labels (*All* all glomeruli labeled, *T* ring-shaped toroid, *Hs* horseshoe, *numbers* number of labels assigned to the corresponding glomerulus) are shown.

Stage	Weight (mg)	Side	Number of slices	Additional labels
P12[a]	3.78	r	139	
P12[a]	4.33	r	238	All; 2 Hs
P12[a]	4.80	r	310	All; T; 2 Hs
P13(Fig. 2)	3.73	r	289	All
P13	4.10	r	293	All; T; 2 Hs
P13	4.40	r	243	
P13(Fig. 3)	5.73	r	298	All; T; 2 Hs
P13	5.73	l	251	2 Hs
P13	5.87	r	254	All; T
A0(Fig. 2)	1.82	r	272	2 Hs
A0	1.84	r	277	2 Discbase
A0	1.84	l	276	2 Cumulus; 2 Hs; 2 Club
A0	2.00	r	289	2 Hs
A0	2.00	l	287	2 Hs
A0	2.02	r	268	2 Toroid
A0	2.02	l	299	2 Toroid; 3 Hs
A0	2.03	r	262	T; 2 Hs
A0	2.03	l	298	2 Hs
A0(Fig. 3)	2.07	r	299	All; 4 Hs
A0	2.07	l	280	2 Cumulus
A0	2.27	r	298	T; 2 Hs
A0	2.27	l	304	3 Hs
A0	2.62	r	279	2 Hs
A0	2.70	l	308	3 Hs
A0	2.70	r	326	
A1[a]	1.52	r	240	
A1[a]	1.63	r	283	2 Hs
A1[a]	1.78	r	275	2 Hs
A1[a]	1.80	r	288	T; 2 Hs
A4	1.20	r	270	All; T; 2 Hs
A4(Fig. 3)	1.34	r	294	All; 2 Hs
A4(Fig. 1)	1.37	r	282	All
A4	1.37	l	278	
A4	1.38	r	275	All; T; 3 Hs; 2 Discbase
A4	1.38	l	274	3 Hs
A4	1.49	r	292	All; 2 Hs
A4	1.49	l	279	2 Hs

[a]ALs not used for volumetric 3D analysis

gradient attributable to limited permeation was detected (Figs. 1, 2).

Organization of AL neuropil

In addition to the three sex-specific glomeruli of the MGC, we found 59–66 "ordinary" glomeruli of various shapes. Mainly bulb-like shapes were seen, but ellipsoid and sphere-like glomeruli were also observed. Typically, the glomeruli exhibited a more intensely stained apical cortex and a peduncle oriented toward the central coarse neuropil of the AL. With one exception, every single glomerulus contacted the AL core with its peduncle. Only one glomerulus, the "cap" glomerulus, was completely separated from the AL center by another glomerulus, viz., the "base" glomerulus (Figs. 2, 3, blue glomerulus), of which the "cap" might be a subcompartment (Figs. 2, 3, small light orange glomerulus).

The cumulus as the first and most distal glomerulus of the MGC almost always exhibited an elongated cylindrical shape that lay halfway embedded in the furrow of the toroid and oriented in an anteroventral manner (dark blue glomerulus in Figs. 2, 3). In two cases, two labels were assigned to the cumulus (Table 1). The two other sex-specific glomeruli, the toroid and the horseshoe (large orange glomerulus and purple glomeruli, respectively, in Figs. 2, 3), showed higher individual plasticity in shape: the toroid exhibited its name-giving toroidal shape (Homberg et al. 1995) in only 9 of 37 ALs examined; otherwise, it was "U"-shaped, with its opening oriented in an anteroventral fashion. In both ALs in one animal, we found two labels that were assigned to the toroid (Table 1). The horseshoe featured the highest range of shape and volume plastici-

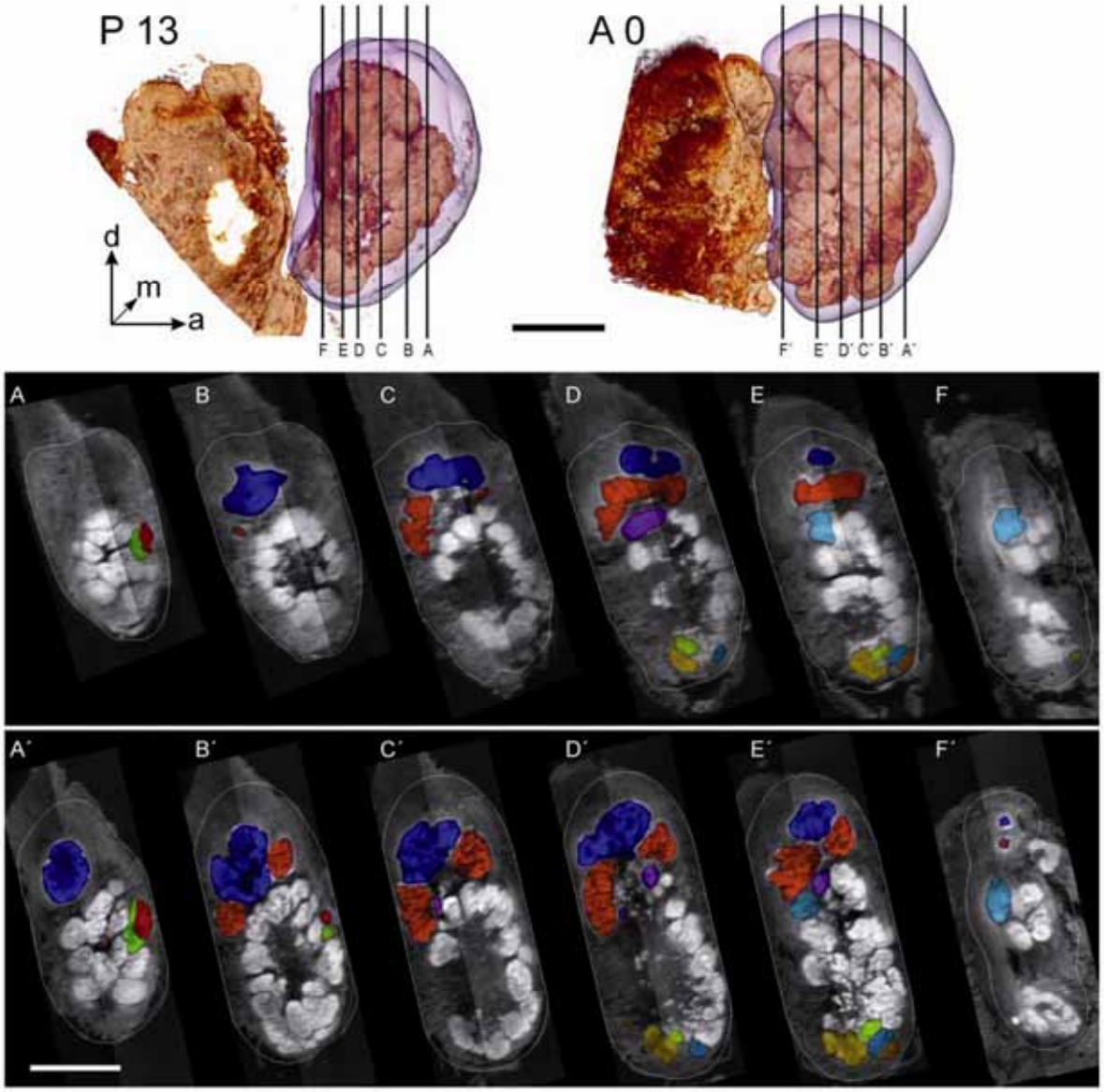

Fig. 2 Lateral view of 3D CLSM reconstructions of right male ALs of P13 and freshly enclosed *M. sexta* (A0). The reconstructed AL volume is visualized transparently. *Vertical lines* correspond to frontal sections in **A**–**F** (P13) or **A′-F′** (A0), respectively (*d* dorsal, *m* median, *a* anterior). **A**–**F** Frontal sections through P13 AL represented by *vertical lines* in P13 *above*. Labeled materials are either *outlined* (AL volume) or color-coded (*dark blue* cumulus, *orange* toroid, *purple* horseshoe, *light blue* G20, *dark red* disc, *green* discbase, *yellow* LPOG, *light green* club, *light orange* cap, *blue* base). **A′-F′** Corresponding sections through A0 AL represented by *vertical lines* in A0 *above*. Note the cumulus extending further anteriorly into section **A′**. Identical glomeruli can be found in similar positions during development, although slight individual variations of glomerular location and shape occur. The whole set of labeled frontal sections of both ALs are also available as animated slices online (http://online-media.uni-marburg.de/biologie/3d_brain/). *Bar* 200 μm

ty: in 20 of the 37 preparations, the horseshoe comprised two halves; in six cases, we even found that three to four parts had different sizes at the corresponding position of the horseshoe (Table 1). This high variation could explain why the horseshoe neuropil was initially assigned to three different glomeruli (Rospars and Hildebrand 1992, 2000). Normally, its form exhibits the shape and orientation of the toroid, but we found variations ranging from "U"-shapes to kidney shapes. All "ordinary" glomeruli exhibited shape plasticity to a lesser extent (Table 1).

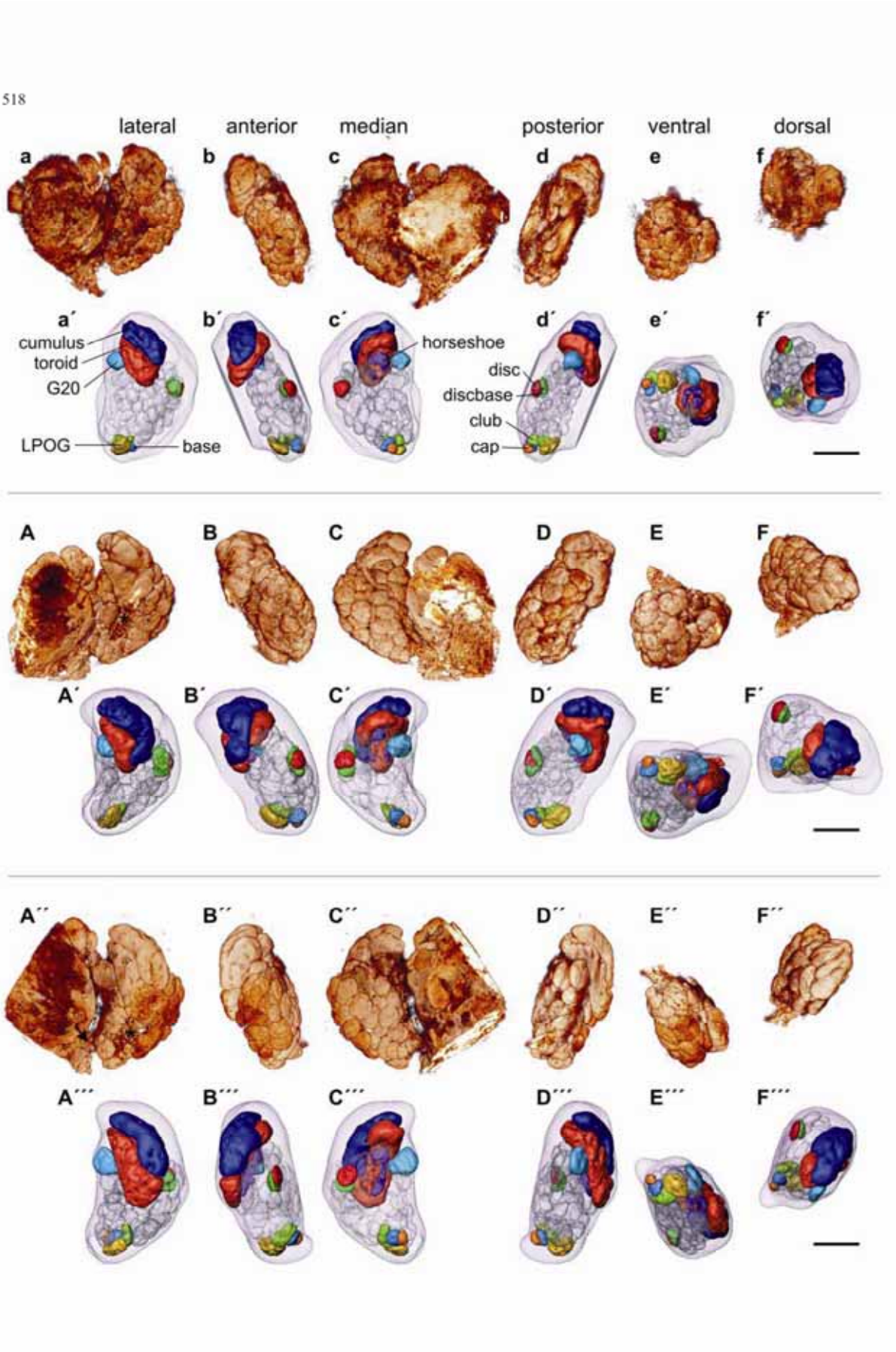
518
lateral
anterior
median
posterior
ventral
dorsal
a
b
c
d
e
f
a´
b´
c´
d´
e´
f´
cumulus
toroid
G20
LPOG
base
horseshoe
disc
discbase
club
cap
A
B
C
D
E
F
A´
B´
C´
D´
E´
F´
A´´
B´´
C´´
D´´
E´´
F´´
A´´´
B´´´
C´´´
D´´´
E´´´
F´´´

◀**Fig. 3** Surface-rendered views of synaptotagmin immunostaining in three representative ALs (**a**–**f** P13; **A**–**F** A0; **A″**–**F″** A4) with corresponding reconstructed glomerulus volumes (**a′**–**f′** P13; **A′**–**F′** A0; **A‴**–**F‴** A4). In the lateral and median view (*first and third columns*), additional protocerebral staining is shown, which was removed for clarification in other views. The ten labeled glomeruli are found in equivalent positions throughout stages and individuals. Note the variable number of horseshoe neuropils, i.e., three glomeruli in A0 (**C′**). Nonglomerular neuropil in the AL forms a neuropilar bridge between AL and protocerebrum (*arrow* in **A″**) or is found in the so-called coarse neuropil (*stars* in **A** and **A″**). Further clarification of glomerular 3D organization animations and interactive models of all these ALs are available online (http://online-media.uni-marburg.de/biologie/3d_brain/). *Bar* 200 μm

On its posteroventral side, the AL neuropil loses its highly ordered glomerular organization and strays into the protocerebrum (Fig. 3A″). Some scattered synaptotagmin immunostaining not correlated to the glomerular neuropil was found in the so-called coarse neuropil of the central AL (Fig. 3a, A, A″; Dubuque et al. 2001).

Reconstruction and identification of glomeruli

We reconstructed 13 whole ALs. In addition to the sex-specific glomeruli of the MGC, we chose seven glomeruli that were most easily and reliably identified, based on their shape, volume, and location, in all specimens throughout the examined developmental stages (Figs. 2, 3). Four of them could be referred to by the nomenclature of Rospars and Hildebrand (1992, 2000). These were the largest of the "ordinary" glomeruli: G20 (light blue glomerulus in Figs. 2E,E′,F,F′, 3), which lies posteromedial to the MGC (Rospars and Hildebrand 1992), the LPOG (yellow glomerulus in Figs. 2D,D′,E,E′, 3), which corresponds to G64 and has been extensively described by Kent et al. (1986, 1999) and Guerenstein et al. (2004), and two anteriorly located glomeruli that we have named disc and discbase, which might correspond to G27/28 and G22/29 (dark red and green glomeruli, respectively, in Figs. 2A,A′, B,B′, 3). The discbase always appeared to be "U"-shaped in frontal sections (not shown). This glomerulus almost completely surrounded the disc, leaving only a small gap for the basal peduncle of the overlying disc.

The other three glomeruli were an anteroposteriorly elongated glomerulus that was found in the ventral AL just above the LPOG and that we named club (G60/58; light green glomerulus in Figs. 2D,D′,E,E′, 3), and two ventromedian glomeruli that we called base (G61; blue glomerulus in Figs. 2D,D′,E,E′, 3) and cap (G62; light orange glomerulus in Figs. 2E,E′,F, 3), the latter exhibiting strong acetylcholine-esterase-like immunoreactivity (Homberg et al. 1995). Since the base and cap are closely associated, and since the cap lacks the typical proximal peduncle, they might have been considered as one glomerulus by Rospars and Hildebrand (1992, 2000).

In addition to the figures presented here, we have produced movies (.mpg files) of animated labeled slices and have reconstructed glomeruli for further clarification of the shape and organization in these ALs. We also provide interactive models (.vrml files) of reconstructed ALs (http://online-media.uni-marburg.de/biologie/3d_brain/).

Glomerulus volumes during pupal development

We chose P13 as a representative pupal stage, since at this stage, all glomeruli of the adult animal are present and become distinguishable units (Tolbert et al. 1983). Nevertheless, the volumetric ratio at which these newly formed P13 and adult glomeruli were comparable was unclear. The glomeruli increased in volume between 40% and 130% from stages P13 to A0 (Fig. 4a), and the relative size increases of glomeruli as a percentage of the overall AL volume ranged from almost 20% to 90% (Fig. 4b). Exceptions were the cap glomerulus, which exhibited no significant size differences at all, and the horseshoe, whose significant growth ($P<0.05$) was not mirrored in a relative size increase, adjusted to individual AL volumes (Fig. 4b).

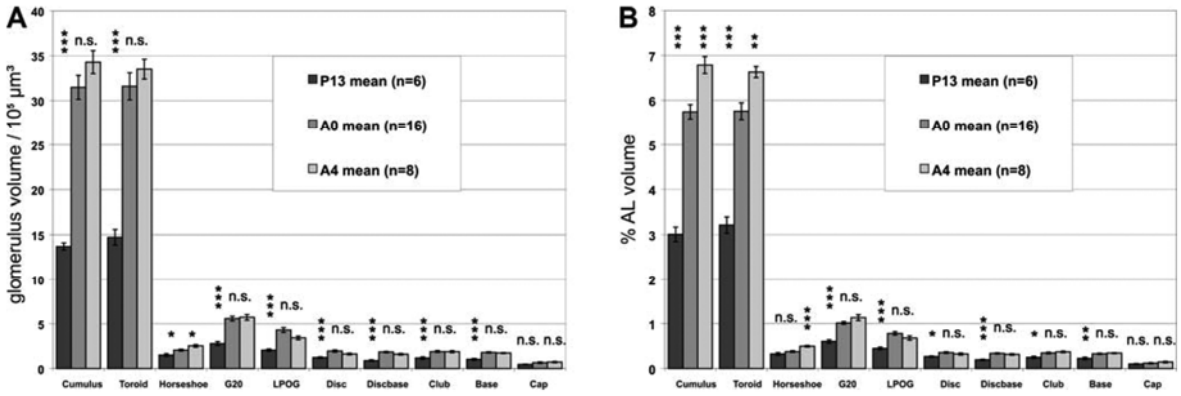

Fig. 4 Quantitative volume analysis of the three MGC glomeruli, the LPOG, and six "ordinary" glomeruli in P13 (*dark*, n=6 ALs) and adult animals (*gray* A0, n=16 ALs; *light gray* A4, n=8 ALs) of *M. sexta* (*bars* standard error, *stars* level of significance, ***$P<0.001$, **$P<0.01$, *$P<0.05$, *n.s.*not significant). **a** Mean values for absolute glomerular volumes. **b** Relative size of glomeruli as percentage of overall AL volume (glomerulus volume ×100/AL volume).

Table 2 Complementing Fig. 4 this table shows the exact mean values and standard errors of (*top*) the glomerular and AL volumes (μm^3) and (*bottom*) the percentage of the glomerular volume compared with AL volume (glomerulus volume×100/AL volume)

Stage	Cumulus	Toroid	Horseshoe	G20	LPOG	Disc	Discbase	Club	Base	Cap	Neurilemma
P13 mean (*n*=6)	1,369,997	1,472,315	149,581	278,000	204,442	121,715	88,609	116,996	102,275	45,241	46,225,583
P13 standard error	39,192	86,910	15,757	22,041	12,793	8,425	8,071	14,226	9,754	3,748	2,810,326
A0 mean (*n*=16)	3,148,000	3,159,776	204,837	556,702	429,475	194,286	183,534	188,934	178,832	65,306	54,782,744
A0 standard error	134,348	151,590	10,495	26,252	26,835	12,130	8,046	10,377	7,495	8,139	1,673,456
A4 mean (*n*=8)	3,429,388	3,351,816	252,591	570,906	340,824	162,077	158,752	187,322	172,660	71,703	50,644,375
A4 standard error	127,317	110,138	15,357	32,064	20,060	9,044	9,127	11,190	5,442	7,917	1,850,346

	Cumulus	Toroid	Horseshoe	G20	LPOG	Disc	Discbase	Club	Base	Cap
P13 mean (*n*=6)	3.01	3.21	0.32	0.60	0.45	0.27	0.19	0.25	0.23	0.10
P13 standard error	0.16	0.18	0.03	0.04	0.03	0.01	0.01	0.02	0.03	0.01
A0 mean (*n*=16)	5.74	5.76	0.38	1.01	0.78	0.36	0.34	0.35	0.33	0.12
A0 standard error	0.16	0.19	0.02	0.03	0.04	0.02	0.01	0.02	0.01	0.01
A4 mean (*n*=8)	6.79	6.63	0.50	1.13	0.68	0.32	0.31	0.37	0.34	0.14
A4 standard error	0.19	0.12	0.02	0.07	0.05	0.02	0.02	0.02	0.01	0.02

Interestingly, both the means of the cumulus and toroid almost doubled their volume (1.37×10^6 μm^3 and 1.47×10^6 μm^3 at P13 compared with 3.15×10^6 μm^3 and 3.16×10^6 μm^3, respectively, at A0) and thereby displayed the highest volume gains (Table 2). This was mirrored by the observation that approximately 27% of all glomerular volume in the P13 ALs compared with almost 30% in the A0 AL was allocated in the MGC. Thus, the relative percentage of pheromone-sensitive sensilla on the antennae (about one third) is reflected at the glomerulus volume level (Lee and Strausfeld 1990).

It is intriguing that the larger glomeruli exhibit higher growth rates than those of the smaller ones. This is not self-evident, since we have measured not surfaces but volumes and have compared relative size changes that are independent of the units involved (Fig. 4, Table 2). Within all P13 ALs, the size ranks of the corresponding glomeruli across individuals remain highly constant (coefficient of concordance=0.93737, $P<0.0001$), although there is no significant ranking between cumulus and toroid (coefficient of concordance=0.44444; $P<0.10248$).

Glomerulus volumes during early adult development

We found significant glomerulus size differences between adult moths differing by only 4 days in age. At A4, the means of the cumulus and toroid reached their highest values with 3.43×10^6 μm^3 and 3.35×10^6 μm^3, respectively, (Fig. 4a, Table 2); one third (33%) of all neuropil volume in the ALs was now allocated in the MGC. Although the absolute volume differences were not significant between A0 and A4 (Fig. 4a), they became so for the MGC glomeruli after AL volume correction (Fig. 4b). All other glomeruli examined exhibited no significant differences between adult stages A0 and A4, neither between absolute (Fig. 4a) nor between corrected volumes (Fig. 4b). Nevertheless, within both adult stages examined, the size ranks of corresponding glomeruli across individuals remained highly constant (coefficient of concordance: A0=0.87992, $P<0.0001$; A4=0.94242, $P<0.0001$). The cumulus and toroid, again, were still equally ranked (coefficient of concordance A0=0.06250, $P<0.31732$; A4=0.0000, $P<1.00000$).

Discussion

Reliability of whole-mount immunostaining for 3D brain reconstructions

Dubuque et al. (2001) have demonstrated the suitability of the anti-synaptotagmin antibody for labeling neuropilar structures and that these structures represent glomeruli during AL development and in the adult AL. The combination of methanol/formaldehyde fixation and synaptotagmin antibody staining has allowed us clearly to label glomerular neuropil in *M. sexta* brain whole-mounts with almost a complete lack of an intensity gradient attributable to poor tissue permeation (Figs. 1, 2; Ott and Elphick 2003). We emphasize the quality of our labeling, since realistic reconstructions rely on good tissue permeation of the labels used, especially in whole-mounts. The employed fixation has allowed an almost homogeneous refractive index throughout the tissue (Gahm and Witte 1986); different refractive indices otherwise have a high impact on axial mismatch (Bucher et al. 2000). Because of the large size of the AL and the working distance of the objective, we have had to scan from two sides. This has had no obvious consequences on image stack quality (Fig. 1). Dehydration of tissue leads to shrinkage artifacts, as outlined by Bucher et al. (2000). However, by retaining the same protocol throughout all preparations, the volume differences measured between the glomeruli of individual animals at various stages should unequivocally reflect real differences and not artifacts.

Usefulness of standard 3D glomeruli of the *M. sexta* AL

The usefulness of atlases and 3D databases in neuroscience is noncontentious (Ruffins et al. 2002; Van Essen 2002), and a plethora of 3D AL maps have arisen during the last few years (see Introduction). Computer-based 3D databases offer the opportunity to focus a variety of experimental approaches onto a standardized model system, even with respect to developmental events (Ruffins et al. 2002), whereas 3D atlases link these data to a common framework thereby compensating for individual differences (Van Essen 2002).

However, a comparable 3D map of the *M. sexta* AL has, to date, been missing. An existing map of the adult *M. sexta* AL, based on paraffin sections, provides an overview with regard to the absolute number, localization, and sex-specific dimorphisms of the glomeruli but does not provide 3D standard glomeruli (Rospars and Hildebrand 1992, 2000).

The *M. sexta* AL is a well-established model system for neurodevelopmental processes (for a review, see Tolbert et al. 2004). We have therefore provided not only a glomerular 3D standard for *Manduca* adults of various ages (A0, A4), but also for one stage (P13) during pupal development.

The formation of the glomeruli during pupal development can be divided into at least three phases. In a first phase including stages P5 to P7/8, the glomerular templates are formed by ORN axons and presumably by neurites of PNs (Malun et al. 1994; Oland and Tolbert 1996). In a second phase lasting from P7/8 to about P12, the principal glomeruli are formed. This phase is emphasized in the AL by a distoproximally directed wave of synaptogenesis (Malun et al.1994). A third phase from P13 to adult eclosion includes growth and refinement of the glomerular neuropil (Dubuque et al. 2001). Our P13 standard glomeruli provide a tool for studying mechanisms involved in basic glomerular formation during phase 2. A0 standard glomeruli allow the study of mechanisms involved in the growth and refinement during phase 3.

We have only provided 3D standards for ten of the approximately 60 glomeruli. Our existing data set obtained with the CLSM in principal allows the production of a 3D standard for any glomerulus of the *M. sexta* AL. With this in mind, we suggest that customizable 3D standards should be produced in cases in which labeling efforts are focused on specific glomeruli that are needed in the relevant study. For the across-individual identification of corresponding glomeruli, multiple atlases outclass single atlases (Rohlfing et al. 2004). Our 30 reduced 3D AL maps might serve as such atlases and might lead to less-time-consuming half-automated glomerulus identification. Some of these AL maps are available online in various forms, complementing the figures presented in this study; the others are available on request. In a phylogenetic context, the glomerular map presented in this work combined with existing atlases of other moths (*Agrotis*, Greiner et al. 2004; *Heliothis* and *Helicoverpa*, Berg et al. 2002; *Spodoptera*, Sadek et al. 2002) adds to a species-specific comparison of glomerular organization principles, as outlined by Greiner et al. (2004).

Comparison with existing data concerning the *M. sexta* AL

The first extrapolated estimates of overall glomerular volume during development of *M. sexta* ALs produced higher values (Tolbert 1989) than we have measured. This difference may be based on systematic differences in quantification techniques and on individual size differences between the animals used. However, what are the reasons for the glomerular volume increases? Mechanisms involved in volume increases are certainly different during development and in the adult but might share common principles depending on the stage of development.

Cell proliferation in the AL has finished at P3 (Hildebrand et al. 1997), and programmed neuronal cell death does not occur in the developing AL of *M. sexta* (Schachtner et al. 2004a). Moreover, glial cells, which significantly contribute to glomerulus formation during phase 2 of pupal AL development, presumably do not participate in glomerulus maturation and growth during later stages (Baumann et al. 1996; Oland et al. 1999; for a review, see Tolbert et al. 2004). This leaves anatomical changes in the neuronal components of the AL during phase 3 and in the adult as the basis for volume changes in the glomeruli.

These anatomical changes can principally result from three mechanisms: (1) changes in the branching pattern of neurites, (2) the swelling or shrinking of neurites, and (3) synapse formation or decomposition. (1) At the light-microscopical level, neurite elaboration in the AL of *M. sexta* appears to be finished by about P12 (Tolbert et al. 1983; Oland et al. 1990). We know of no information for *M. sexta* as to whether any of the neurons involved in glomerular composition change their branching pattern during phase 3 or in the adult. In honeybees, neuritic arbors in glomeruli undergo continuous maturation of their branching pattern during pupal and early adult AL development; this includes the pruning of dendritic arbors in a subset of LNs, but an effect of pruning on glomerulus volume has not been examined (Devaud and Masson 1999). (2) Tolbert (1989) has found, in an in-depth electron-microscopic study of the developing *M. sexta* AL, increasing diameters of glomerular processes during development, although the various cell types could not be resolved. Between P4 to P7, Tolbert described glomerular neuritic processes with diameters of 0.1–0.5 μm increasing, at P17, to a mean diameter of 0.2–1.0 μm, and finally reaching 2 μm in diameter at adult eclosion (Tolbert 1989). (3) The formation of new synaptic junctions seems to stall around stage P12 (Tolbert et al. 1983). These data are supported by a recent study from Dubuque et al. (2001) who have found the highest synaptotagmin immunostaining in P12 glomeruli. After P12, synaptotagmin density decreases, and the glomeruli grow in size (Dubuque et al. 2001). In vertebrates, similar results have been ob-

tained, supporting the view of a main phase of synaptogenesis followed by a second phase of maturation and refinement (Yuste and Bonhoeffer 2004). Thus, the net number of synapses might only contribute to volume changes to a small extent, but no studies are available that examine the correlation of the numbers of synapses with neuropilar size during development.

Correlates of adult neuronal plasticity

Data regarding neuronal plasticity in adult *M. sexta* is scarce. Daly et al. (2004) have recently shown that olfactory conditioning is combined with a restructuring of electrical odor response patterns in the AL. Work on adult neuronal plasticity in the honeybee has demonstrated that increases in adult glomerular volume are activity-dependent and correlated with better learning performance (Winnington et al. 1996; Sigg et al. 1997). Quantitative electron-microscopic studies have lead to the suggestion that volume increase and synapse number changes are independent processes that both contribute to structural plasticity in the AL, although synapse reorganization might only play a minor role on neuropilar volume (Brown et al. 2002). Age effects on bee mushroom body volumes must be distinguished from experience effects; the first 5 days of adult brain development seem to be functionally separated from later maturation effects (Farris et al. 2001); this is supported by synapse counts in certain glomeruli (Brown et al. 2004).

Devaud et al. (2003) also argue in this vein, as they have found a rapid increase in glomerulus size during late pupal development and ongoing heterogeneous glomerulus growth in young adults in *Drosophila*. This adult volume gain can be induced up to a critical age by specific odors and, unlike pupal growth, seems to involve a cAMP-dependent signalling pathway (Devaud et al. 2001). In *Agrotis ipsilon* pheromone-specific odor processing seems to be dependent upon juvenile hormone and age (Anton and Gadenne 1999; Gadenne and Anton 2000; Greiner et al. 2002). Two main possibilities may explain the induction of adult neuropilar growth: first, it might represent the final maturation processes, which are possibly hormonally controlled, or second, it might be a manifestation of early adult neural plasticity depending on sensory input (as discussed in Julian and Gronenberg 2002). A separation of these two possibilities may not be possible; indeed, they may build upon each other (Devaud et al. 2003).

We have observed the post-eclosional growth of sex-specific glomeruli. After eclosion, the animals are confronted with female pheromone for the first time. Thus, the neuronal activity of pheromone-specific olfactory receptor neurons might account for this early adult glomerular plasticity. For *M. sexta*, recent results further suggest the occurrence of a sensitive phase during early adult AL development. The reactive oxygen species scavenger Cu/Zn-superoxide dismutase (SOD) is present in a subset of AL neurons from A0 to A2/3 (Schachtner et al. 2004a). Schachtner et al. (2004a) discuss SOD as a cellular marker unmasking cells undergoing their last refinements to cope with the odor information provided from the olfactory receptor neurons. Furthermore, pheromone-specific MGC-ORNs maintain certain glycosylation patterns into adulthood (Gibson et al. 2004). At the behavioral level, adult female *M. sexta* exhibit changing responses to host plant volatiles, depending on age and mating status (Mechaber et al. 2002). The underlying principle might be comparable to that in males, since the female glomeruli specialized to host plant odors correspond to the MGC in males (Rospars and Hildebrand 2000).

Regarding the question as to which cell types contribute to adult volume plasticity, genetic work of Scott et al. (2003a,b) on the *Drosophila* visual system exclude second-order interneurons; if extrapolated to the olfactory system of *M. sexta*, this could mean that LNs and ORNs, but not PNs, are primarily responsible for glomerular volume differences. Of course, it has to be kept in mind that functional odor processing is not dependent on glomerular structure: if normal glomerular development is prevented, the animals are still competent to process odors (Oland and Tolbert 1988; Oland et al. 1988). Additionally, Willis et al. (1995) have demonstrated the odor-modulated flight of female moths lacking glomerular neuropil organization in the AL.

With respect to the questions that we initially raised, we have found (1) a tremendous increase in size in ten identified glomeruli during the last third of pupal development. These ten glomeruli are reliably identifiable in different individuals, and their volume gain has been quantified, thereby supplying (2) an anatomical and volumetric standard for future studies during development and in adults. Based on these glomerular standards, which are available online, we are now able to address issues of neuropilar development, such as the contribution of different cell types to size increase, or to investigate the influences of neuroactive compounds and electrical activity on neuropil growth in defined glomeruli.

Acknowledgements The authors thank Dr. Kaushiki Menon (Caltech, USA) for kindly providing the synaptotagmin antiserum and Dr. Robert Brandt (Zuse Institute, Berlin, Germany) for his excellent support with respect to the AMIRA software. This study was supported by a grant from the Deutsche Forschungsgemeinschaft (Grant Scha 678/3-3) to JS.

References

Anton S, Gadenne C (1999) Effect of juvenile hormone on the central nervous processing of sex pheromone in an insect. Proc Natl Acad Sci USA 96:5764–5767

Baumann PM, Oland LA, Tolbert LP (1996) Glial cells stabilize axonal protoglomeruli in the developing olfactory lobe of the moth *Manduca sexta*. J Comp Neurol 373:118–128

Bell RA, Joachim FA (1978) Techniques for rearing laboratory colonies of the tobacco hornworm, *Manduca sexta* and pink ballworms. Ann Entomol Soc Am 69:365–373

Berg BG, Galizia CG, Brandt R, Mustaparta H (2002) Digital atlases of the antennal lobe in two species of tobacco budworm moths, the Oriental *Helicoverpa assulta* (male) and the American *Heliothis virescens* (male and female). J Comp Neurol 446: 123–134

Brown SM, Napper RM, Thompson CM, Mercer AR (2002) Stereological analysis reveals striking differences in the structural plasticity of two readily identifiable glomeruli in the antennal lobes of the adult worker honeybee. J Neurosci 22:8514–8522

Brown SM, Napper RM, Mercer AR (2004) Foraging experience, glomerulus volume, and synapse number: a stereological study of the honey bee antennal lobe. J Neurobiol 60:40–50

Bucher D, Scholz M, Stetter M, Obermayer K, Pflüger HJ (2000) Correction methods for three-dimensional reconstructions from confocal images. I. Tissue shrinking and axial scaling. J Neurosci Methods 100:135–143

Chambille I, Rospars JP (1981) Le deutocérébron de la blatte *Blaberus craniifer* Burm. (Dictyoptera: Blaberidae). Etude qualitative et identification visuelle de glomérules. Int J Insect Morphol Embryol 10:141–165

Chiang AS, Liu YC, Chiu SL, Hu SH, Huang CY, Hsieh CH (2001) Three-dimensional mapping of brain neuropils in the cockroach, *Diploptera punctata*. J Comp Neurol 440:1–11

Daly KC, Christensen TA, Lei H, Smith BH, Hildebrand JG (2004) Learning modulates the ensemble representations for odors in primary olfactory networks. Proc Natl Acad Sci USA 101: 10476–10481

Devaud JM, Masson C (1999) Dendritic pattern development of the honeybee antennal lobe neurons: a laser scanning confocal microscopic study. J Neurobiol 39:461–474

Devaud JM, Acebes A, Ferrus A (2001) Odor exposure causes central adaptation and morphological changes in selected olfactory glomeruli in *Drosophila*. J Neurosci 21:6274–6282

Devaud JM, Acebes A, Ramaswami M, Ferrus A (2003) Structural and functional changes in the olfactory pathway of adult *Drosophila* take place at a critical age. J Neurobiol 56:13–23

Dubuque SH, Schachtner J, Nighorn AJ, Menon KP, Zinn K, Tolbert LP (2001) Immunolocalization of synaptotagmin for the study of synapses in the developing antennal lobe of *Manduca sexta*. J Comp Neurol 441:277–287

Eisthen HL (2002) Why are olfactory systems of different animals so similar? Brain Behav Evol 59:273–293

Farris SM, Robinson GE, Fahrbach SE (2001) Experience- and age-related outgrowth of intrinsic neurons in the mushroom bodies of the adult worker honeybee. J Neurosci 21:6395–6404

Flanagan D, Mercer AR (1989) An atlas and 3-D reconstruction of the antennal lobes in the worker honey bee, *Apis mellifera* L. (Hymenoptera: Apidae). Int J Insect Morphol Embryol 18:145–159

Gadenne C, Anton S (2000) Central processing of sex pheromone stimuli is differentially regulated by juvenile hormone in a male moth. J Insect Physiol 46:1195–1206

Gahm T, Witte S (1986) Measurement of the optical thickness of transparent tissue layers. J Microsc 141:101–110

Galizia CG, McIlwrath SL, Menzel R (1999) A digital three-dimensional atlas of the honeybee antennal lobe based on optical sections acquired by confocal microscopy. Cell Tissue Res 295:383–394

Gibson NJ, Hildebrand JG, Tolbert LP (2004) Glycosylation patterns are sexually dimorphic throughout development of the olfactory system in *Manduca sexta*. J Comp Neurol 476:1–18

Greiner B, Gadenne C, Anton S (2002) Central processing of plant volatiles in *Agrotis ipsilon* males is age-independent in contrast to sex pheromone processing. Chem Senses 27:45–48

Greiner B, Gadenne C, Anton S (2004) Three-dimensional antennal lobe atlas of the male moth, *Agrotis ipsilon*: a tool to study structure-function correlation. J Comp Neurol 475:202–210

Guerenstein PG, Christensen TA, Hildebrand JG (2004) Sensory processing of ambient CO_2 information in the brain of the moth *Manduca sexta*. J Comp Physiol [A] 190:707–725

Haddad D, Schaupp F, Brandt R, Manz G, Menzel R, Haase A (2004) NMR imaging of the honeybee brain. J Insect Sci 4:1–7

Hildebrand JG, Shepherd GM (1997) Mechanisms of olfactory discrimination: converging evidence for common principles across phyla. Annu Rev Neurosci 20:595–631

Hildebrand JG, Rössler W, Tolbert LP (1997) Postembryonic development of the olfactory system in the moth *Manduca sexta*: primary-afferent control of glomerular development. Cell Dev Biol 8:163–170

Homberg U, Hoskins SG, Hildebrand JG (1995) Distribution of acetylcholinesterase activity in the deutocerebrum of the sphinx moth *Manduca sexta*. Cell Tissue Res 279:249–259

Huetteroth W, Schachtner J (2003) 3D reconstructions of pupal and adult glomeruli in the antennal lobe of the sphinx moth *Manduca sexta*. Proc Fifth German Neurosci Soc Conf 689:735

Jindra M, Huang JY, Malone F, Asahina M, Riddiford LM (1997) Identification and mRNA developmental profiles of two ultraspiracle isoforms in the epidermis and wings of *Manduca sexta*. Insect Mol Biol 6:41–53

Julian GE, Gronenberg W (2002) Reduction of brain volume correlates with behavioral changes in queen ants. Brain Behav Evol 60:152–164

Kent KS, Harrow ID, Quartararo P, Hildebrand JG (1986) An accessory olfactory pathway in Lepidoptera: the labial pit organ and its central projections in *Manduca sexta* and certain other sphinx moths and silk moths. Cell Tissue Res 245:237–245

Kent KS, Oland LA, Hildebrand JG (1999) Development of the labial pit organ glomerulus in the antennal lobe of the moth *Manduca sexta*: the role of afferent projections in the formation of identifiable olfactory glomeruli. J Neurobiol 40:28–44

Laissue PP, Reiter C, Hiesinger PR, Halter S, Fischbach KF, Stocker RF (1999) Three-dimensional reconstruction of the antennal lobe in *Drosophila melanogaster*. J Comp Neurol 405:543–552

Lee JK, Strausfeld NJ (1990) Structure, distribution and number of surface sensilla and their receptor cells on the olfactory appendage of the male moth *Manduca sexta*. J Neurocytol 19:519–538

Malun D, Oland LA, Tolbert LP (1994) Uniglomerular projection neurons participate in early development of olfactory glomeruli in the moth *Manduca sexta*. J Comp Neurol 350:1–22

Mechaber WL, Capaldo CT, Hildebrand JG (2002) Behavioral responses of adult female tobacco hornworms, *Manduca sexta*, to hostplant volatiles change with age and mating status. J Insect Sci 2:1–8

Oland LA, Tolbert LP (1988) Effects of hydroxyurea parallel the effects of radiation in developing olfactory glomeruli in insects. J Comp Neurol 278:377–387

Oland LA, Tolbert LP (1996) Multiple factors shape development of olfactory glomeruli: insights from an insect model system. J Neurobiol 30:92–109

Oland LA, Tolbert LP, Mossman KL (1988) Radiation-induced reduction of the glial population during development disrupts the formation of olfactory glomeruli in an insect. J Neurosci 8:353–367

Oland LA, Orr G, Tolbert LP (1990) Construction of a proto-glomerular template by olfactory axons initiates the formation of olfactory glomeruli in the insect brain. J Neurosci 10:2096–2112

Oland LA, Marrero HG, Burger I (1999) Glial cells in the developing and adult olfactory lobe of the moth *Manduca sexta*. Cell Tissue Res 297:527–545

Ott SR, Elphick MR (2003) New techniques for whole-mount NADPH-diaphorase histochemistry demonstrated in insect ganglia. J Histochem Cytochem 51:523–532

Rein K, Zöckler M, Heisenberg M (1999) A quantitative three-dimensional model of the *Drosophila* optic lobes. Curr Biol 9:93–96

Rein K, Zöckler M, Mader MT, Grubel C, Heisenberg M (2002) The *Drosophila* standard brain. Curr Biol 12:227–231

Rohlfing T, Brandt R, Menzel R, Maurer CR Jr (2004) Evaluation of atlas selection strategies for atlas-based image segmentation with application to confocal microscopy images of bee brains. Neuroimage 21:1428–1442

Rospars JP (1983) Invariance and sex-specific variations of the glomerular organization in the antennal lobes of a moth, *Mamestra brassicae*, and a butterfly, *Pieris brassicae*. J Comp Neurol 220:80–96

Rospars JP, Hildebrand JG (1992) Anatomical identification of glomeruli in the antennal lobes of the male sphinx moth *Manduca sexta*. Cell Tissue Res 270:205–227

Rospars JP, Hildebrand JG (2000) Sexually dimorphic and isomorphic glomeruli in the antennal lobes of the sphinx moth *Manduca sexta*. Chem Senses 25:119–129

Ruffins SW, Jacobs RE, Fraser SE (2002) Towards a Tralfamadorian view of the embryo: multidimensional imaging of development. Curr Opin Neurobiol 12:580–586

Sadek MM, Hansson BS, Rospars JP, Anton S (2002) Glomerular representation of plant volatiles and sex pheromone components in the antennal lobe of the female *Spodoptera littoralis*. J Exp Biol 205:1363–1376

Schachtner J, Huetteroth W, Nighorn A, Honegger HW (2004a) Copper/zinc superoxide dismutase-like immunoreactivity in the metamorphosing brain of the sphinx moth *Manduca sexta*. J Comp Neurol 469:141–152

Schachtner J, Trosowski B, D'Hanis W, Stubner S, Homberg U (2004) Development and steroid regulation of RFamide immunoreactivity in antennal-lobe neurons of the sphinx moth *Manduca sexta*. J Exp Biol 207:2389–2400

Schwartz LM, Truman JW (1983) Hormonal control of rates of metamorphic development in the tobacco hornworm *Manduca sexta*. Dev Biol 99:103–114

Scott EK, Reuter JE, Luo L (2003a) Dendritic development of *Drosophila* high order visual system neurons is independent of sensory experience. BMC Neurosci 4:14

Scott EK, Reuter JE, Luo L (2003b) Small GTPase Cdc42 is required for multiple aspects of dendritic morphogenesis. J Neurosci 23:3118–3123

Sigg D, Thompson CM, Mercer AR (1997) Activity-dependent changes to the brain and behavior of the honey bee, *Apis mellifera* (L.). J Neurosci 17:7148–7156

Smid HM, Bleeker MA, Loon JJ van, Vet LE (2003) Three-dimensional organization of the glomeruli in the antennal lobe of the parasitoid wasps *Cotesia glomerata* and *C. rubecula*. Cell Tissue Res 312:237–248

Strausfeld NJ, Hildebrand JG (1999) Olfactory systems: common design, uncommon origins? Curr Opin Neurobiol 9:634–639

Tolbert LP (1989) Afferent axons from the antenna influence the number and placement of intrinsic synapses in the antennal lobes of *Manduca sexta*. Synapse 3:83–95

Tolbert LP, Sirianni PA (1990) Requirement for olfactory axons in the induction and stabilization of olfactory glomeruli in an insect. J Comp Neurol 298:69–82

Tolbert LP, Matsumoto SG, Hildebrand JG (1983) Development of synapses in the antennal lobes of the moth *Manduca sexta* during metamorphosis. J Neurosci 3:1158–1175

Tolbert LP, Oland LA, Tucker ES, Gibson NJ, Higgins MR, Lipscomb BW (2004) Bidirectional influences between neurons and glial cells in the developing olfactory system. Prog Neurobiol 73:73–105

Truman JW (1996) Metamorphosis of the insect nervous system. In: Gilbert LI (ed) Metamorphosis: postembryonic reprogramming of gene expression in amphibian and insect cells. Academic Press, Orlando, pp 283–320

Van Essen DC (2002) Windows on the brain: the emerging role of atlases and databases in neuroscience. Curr Opin Neurobiol 12:574–579

Weevers RD (1966) A lepidopteran saline: effects of inorganic cation concentrations on sensory, reflex and motor responses in a herbivorous insect. J Exp Biol 44:163–175

Willis MA, Butler MA, Tolbert LP (1995) Normal glomerular organization of the antennal lobes is not necessary for odor-modulated flight in female moths. J Comp Physiol [A] 176:205–216

Winnington AP, Napper RM, Mercer AR (1996) Structural plasticity of identified glomeruli in the antennal lobes of the adult worker honey bee. J Comp Neurol 365:479–490

Yuste R, Bonhoeffer T (2004) Genesis of dendritic spines: insights from ultrastructural and imaging studies. Nat Rev Neurosci 5:24–34

Zöckler M, Rein K, Brandt R, Stalling D, Hege H (2001) Creating virtual insect brains with AMIRA. ZIB Report 01–32:1–11

CHAPTER VI:

Anisometric brain dimorphism revisited: implementation of a volumetric 3D standard brain in *Manduca sexta*

Anisometric brain dimorphism revisited: implementation of a volumetric 3D standard brain in *Manduca sexta*

BASIL EL JUNDI*, WOLF HUETTEROTH*, ANGELA E. KURYLAS AND JOACHIM SCHACHTNER#
Department of Biology, Animal Physiology, Philipps-University
Karl-von-Frisch-Strasse 8, D-35043 Marburg, Germany

ABSTRACT

Lepidopterans like the giant sphinx moth *M. sexta* are known for their conspicuous sex dimorphism in the olfactory system, which is especially pronounced in the antennae and in the antennal lobe, the primary integration center of odor information. Even minute scents of female pheromone are detected by male moths, facilitated by a huge array of pheromone receptors on their antennae. The associated neuropilar areas in the antennal lobe, the glomeruli, are enlarged in males and organized in form of the so-called macroglomerular complex (MGC). In this study we searched for anatomical sex dimorphism more downstream in the olfactory pathway or in any other neuropil in the central brain. Based on freshly eclosed animals, we created volumetric female and male standard brains and compared 28 separate neuropilar regions.

Additionally, we labeled ten female glomeruli which were homologous to previously quantitatively described male glomeruli including the MGC. In summary, the neuropil volumes reveal an isometric sex dimorphism in *M. sexta* brains, which masks an anisometric dimorphism. This anisometric dimorphism is restricted to the sex-related glomeruli of the antennal lobes and neither mirrored in other normal glomeruli nor in higher brain centers like the calyces of the mushroom bodies. The standard brain is also used in interspecies comparisons, and may serve as future volumetric reference in pharmacological and behavioral experiments especially regarding development and adult plasticity. It is made available to the public on http://www.3d-insectbrain.com.

Indexing terms: brain; olfactory system; antennal lobe; insect; neuropil; amira

Unlike in vertebrates like humans, distinct brain subcompartments of the insect brain or supraoesophageal ganglion are more pronounced and can be recognized more easily already in the whole brain (Fig. 1). Analogue regions to vertebrate cortical areas are often well-separated neuropiles in insects, which exhibit – compared to vertebrate brain areas – highly invariant shape, size and localization (Van Essen and Dierker 2007). This leads to a big advantage regarding brain standardization in insects, including subsequent analysis of mutants or defined plasticity effects deviating from this standard. These defined morphological areas can principally be found in all insects, while their size and composition mainly depends on species (Strausfeld 1976, Chapman 1998), but also on sex, age, and environment interaction (Technau 2007, Molina and O'Donnell 2008).

Several of those neuropilar regions already have been ascribed to the processing of defined information, reaching from relaying primary sensory information to higher integration and learning. Most prominent examples of the sensory nervous system are found in the optic lobes (various aspects of visual information, reviewed in e.g. Douglass and Strausfeld 2003), and in the antennal lobes (olfactory information, reviewed e.g. in Schachtner et al., 2005), which both can already be discerned on the macroscopic level (Fig. 1).

* both authors contributed equally to the paper
# Correspondence to: Joachim Schachtner, Department of Biology, Animal Physiology, Philipps-University, Karl-von-Frisch-Str. 8, 35043 Marburg, Germany.
E-mail: schachtj@staff.uni-marburg.de

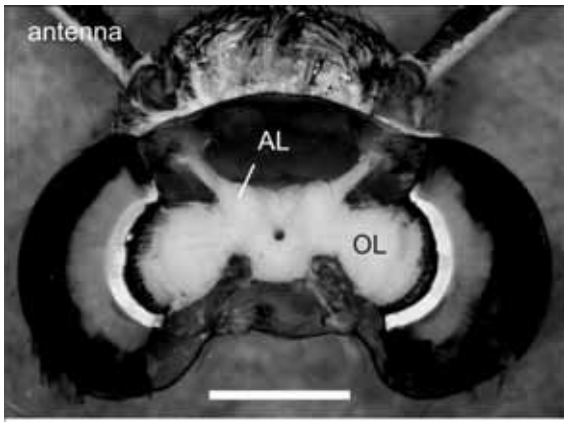

Fig. 1. Frontal view of the head of an adult *M. sexta* moth. Within the opened head capsule the brain is exposed in its natural position. Prominent brain areas are the optic lobe (OL), which receives its input from the eyes, and the antennal lobe (AL), which processes olfactory information coming from sensilla on the antenna. Scale bar: 2 mm.

Most of the optic lobe neuropiles can be attributed to special optic features, like color vision (lamina, medulla, and lobula; reviewed in Douglass and Strausfeld 2003), or motion- and orientation-dependent stimuli (lobula, lobula plate, Zeil 1983, Wicklein and Strausfeld 2000), or relaying Zeitgeber time to the circadian rhythm (accessory medulla, reviewed in Helfrich-Förster 2004). Also mainly linked to optic input is the anterior optic tubercle, which was shown to be involved in the polarization vision pathway in the locust (Homberg et al. 2003; Pfeiffer et al. 2005, Pfeiffer and Homberg 2007).

The deutocerebral antennal lobes house several globe-like neuropiles called glomeruli, which are arranged in a sphere around a coarse neuropil. Olfactory stimuli activate distinct subsets of glomeruli in a chemotopic manner, thus coding odors in time and space (Knüsel et al. 2007). Certain glomeruli are specialized to specific chemical compounds like pheromones, and may exhibit sex dimorphism (reviewed in Schachtner et al. 2005).

Deeper in the brain, neuropils subserve higher integration processes like the mushroom bodies or the central complex. Work from only a handful of species including *Drosophila*, but also larger insects like the honeybee or locust provided information on the function of mushroom bodies and central complex. For the mushroom bodies it is well accepted that they are primarily involved in odor learning (Wang et al. 2008), but also serve as multisensory integration units (cockroach: Strausfeld and Li 1999; hymenopterans: Gronenberg 2001, Gronenberg and Lopez-Riquelme 2004; moth: Sinakevitch et al. 2008). For the central complex, concepts on its function are diverse, reaching from the analysis of polarized light (Heinze and Homberg 2007) and visual memory formation (Liu et al. 2006) to coordination of movements (Strauss and Heisenberg 1993; Strauss 2002). The tritocerebrum as the third major neuromere of the insect brain seems to be involved in chemo- and mechanosensory stimulus integration, as shown by proboscis receptor backfills in moths (Jørgensen et al. 2006; Kvello et al. 2006). The tripartite subesophageal ganglion interconnects a- and efferent nerves of the appendages of its three neuromeres, namely of the mandibles, the maxillaries, and the labium. In adult moths, both the tritocerebrum and subesophageal ganglion are fused to the brain.

Increasing computer power over the last years combined with confocal 3D stacks and appropriate software led to a boost of 3D insect brain reconstruction and subsequent standardization. By now, we face standard insect brains of the fly *Drosophila* (Rein et al. 2002, Jenett et al. 2006), the honeybee (Brandt et al. 2005), and the desert locust (Kurylas et al. 2008). Two other major insect groups however, the coleoptera and the lepidoptera, are still missing, despite being first and second richest insect order regarding species number (Grimaldi and Engel 2005). In this study, we close this gap regarding lepidoptera and provide a standard brain for an insect, whose nervous system is being studied for decades - the giant sphinx moth *M. sexta* (e.g. Strausfeld and Hildebrand 1999, Tolbert et al. 2004).

The goals of this study were to 1) compare adult brain neuropil volumes regarding sex dimorphism, 2) supply adult standard brains of *M. sexta* as volume references for future pharmacological and behavioral studies, 3) check for allometric relations of neuropils in a lepidopteran species, 4) compare in detail homologous normal glomeruli in female and male antennal lobes regarding further sex-specific dimorphism apart from the described sex-dimorphic three glomeruli, and 5) place the *M. sexta* standard volume values into context to previously published insect brain volumes. Most of the 3D information is made available on an internet platform specially created for this purpose, http://www.3d-insectbrain.com.

MATERIALS AND METHODS

Animals

Moths (*Manduca sexta*; Lepidoptera: Sphingidae) were kept in walk-in environmental chambers at 26 °C under a long-day photoperiod (L: D=17:7) and were fed on an artificial diet (Bell and Joachim 1978). Under these conditions only freshly eclosed adults were weighed and prepared for reconstruction. For standard brain generation we used twelve female brains and six male brains. For the glomerulus volumes of the female antennal lobe we reconstructed nine antennal lobes of brains, which were in part also used for the standard brain.

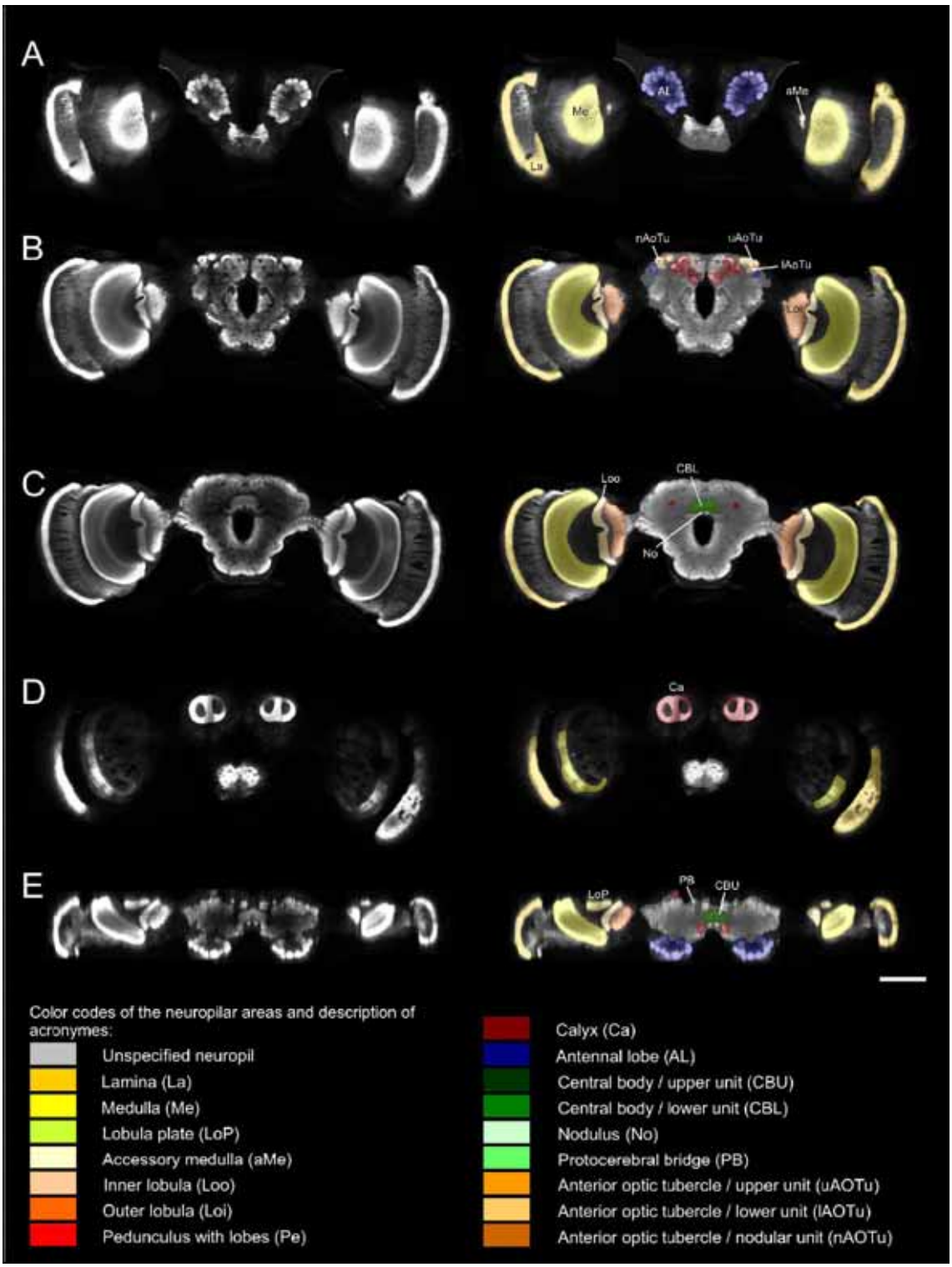

Fig. 2. Confocal images of an individual *M. sexta* brain stained with α-synapsin antibody. This brain was used as template for the VIB protocol. Right panel, confocal slices through the brain; left panel, all manually labelled neuropil areas as reconstructed in AMIRA. **A-D:** Anterior views. **E:** Dorsal view. **A:** Axial slice through the *M. sexta* brain at the level of the antennal lobes (AL) and the accessory medullae (aMe) at approximately 150 µm depth. The lamina (La) and medulla (Me) span over all slices. **B:** Axial slice at the level of the lobes of the mushroom bodies (Pe) and the three subunits of the anterior optic tubercle (upper, lower and nodular unit; uAOTu, lAOTu, nAOTu) at approximately 300 µm depth. Additionally, outer (Loo) and inner Lobula (Loi) appear. **C:** Image of the brain at the level of the central body subunits (upper and lower unit; CBU and CBL) and the noduli (No) at approximately 400 µm depth. Note the horizontally oriented pedunculi and continuing optic neuropils. **D:** At the posterior end of the brain at a depth approximately 600 µm the pedunculi of the mushroom bodies merged into the calyces (Ca) **E:** Horizontal slice through the brain at the level of the lower unit of the central body (CBL) at approximately 400 µm depth. Note the lobula plate (LoP) and the protocerebral bridge (PB) at their posterior position in the brain. The color code of the neuropilar areas is consistent with Brandt et al. (2005) and Kurylas et al. (2008). Scale bar: 500 µm.

Immunocytochemistry

For wholemount staining we adapted and refined the staining protocols described by Huetteroth and Schachtner (2005) and Kurylas et al. (2008). The whole brains were dissected under cold saline (Weevers 1966) and fixed subsequently at 4 °C overnight in a solution composed of one part formaldehyde, one part methanol and eight parts phosphate-buffered saline (PBS 0.01 M). These brains were then rinsed in 0.01 M PBS for 1 h at room temperature followed by preincubation overnight at 4 °C in 5% normal goat serum (NGS; Jackson ImmunoResearch, Westgrove, PA, USA) in 0.01 M PBS containing 0,3% Triton X-100 (PBST) and 0.02% sodium azide. The monoclonal primary antibody against the presynaptic vesicle protein synapsin I (SYNORF1, Klagges et al. 1996) from mouse was used to selectively label neuropilar areas in the brain (kindly provided by Dr. E. Buchner, Würzburg). Its specificity in *M. sexta* was shown in western blots in Utz et al. (2008). It was diluted 1:100 in PBST containing 1% NGS: in this solution the brains were incubated for 5-6 days at 4 °C.

Subsequently the brains were rinsed 6 times in 2 h with PBST before they were incubated with the secondary goat anti-mouse antibody conjugated to Cy5 (1:300, Jackson ImmunoResearch, Westgrove, PA, USA) in PBST and 1% NGS for 4 days at 4 °C. After this time the brains were rinsed again with PBST 6 times in 2 h. Thereafter the brains were dehydrated in an ascending alcohol series (50%-100%, 15 min each) and then cleared in methyl salicylate (Merck, Gernsheim, Germany) for about 40 min. At last the brains were mounted in Permount (Fisher Scientific, Pittsbourgh, PA.,

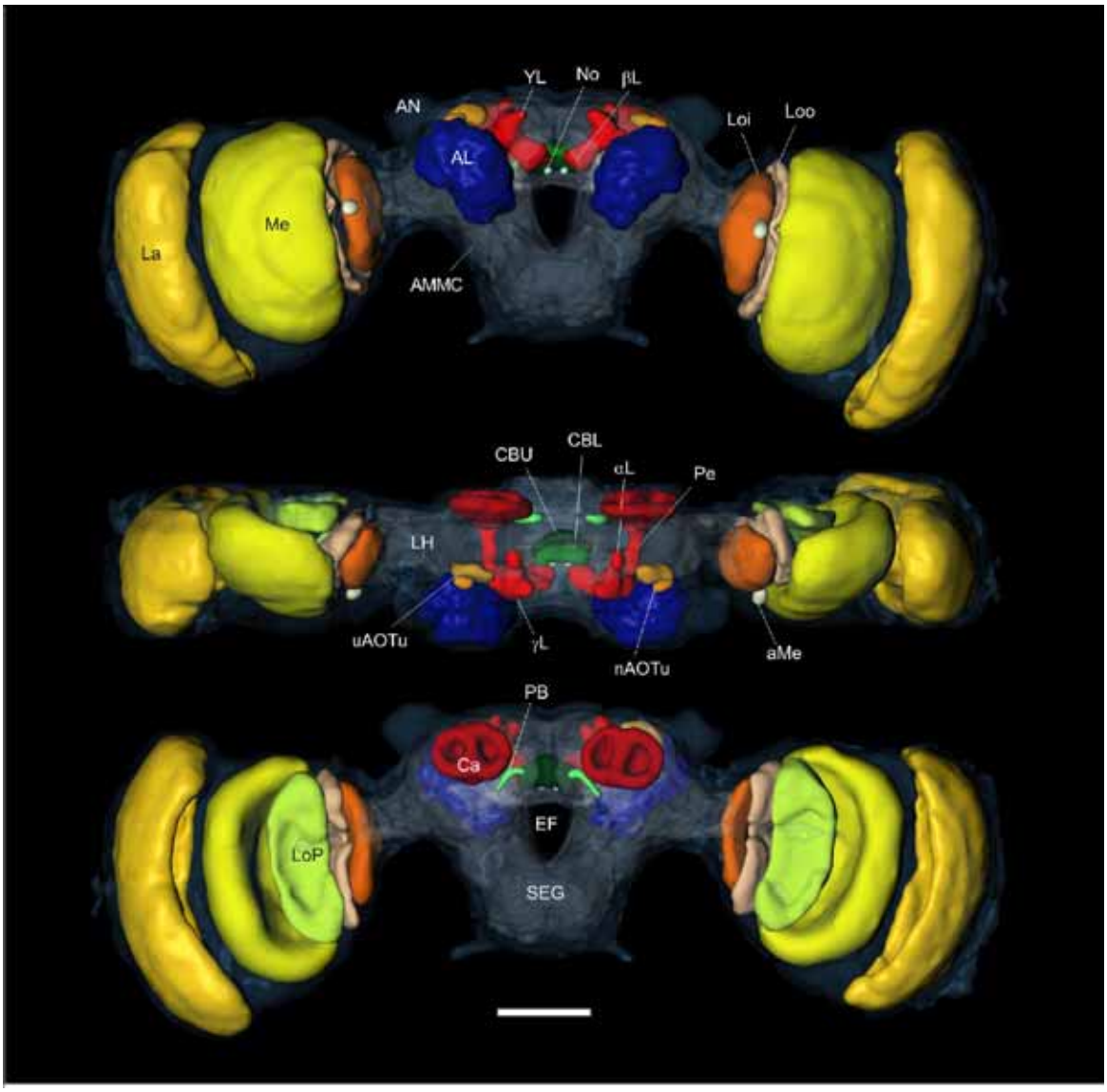

Fig. 3. The 3D female template brain of *M. sexta* in anterior (above), dorsal (middle), and posterior view (below). The different lobes of the mushroom bodies (α-; β-; γ-, and Y-lobes) are merged with the pedunculus neuropil, but can be discerned as distinct protrusions (see results). The lower unit of the anterior optic tubercle (lAOTu) is superposed by other neuropils and not visible here. In *M. sexta*, the subesophageal ganglion (SEG) is fused with the brain, thus forming the esophageal foramen (EF). See Fig. 2. for color code and abbreviations. Scale bar: 500 µm.

USA) between two coverslips using ten spacers (Zweckform, Oberlaindern, Germany) to prevent compression of brains.

CLSM image acquisition and processing

The wholemount preparations were scanned at 512 x 512 pixel resolution by using a 10x oil immersion objective (HC PL APO 10x / 0.40 Imm (0.36 mm); Leica, Bensheim, Germany) with a confocal laser scanning microscope (Leica TCS SP2). All brains were scanned with a voxel size of 2.9 x 2.9 x 2 µm. The thickness of the brain (approximately 700 µm) and the limited working distance of the objective (approximately 450 µm) made it necessary to scan the brain from both sides (anterior and posterior) to eventually acquire images of the whole brain. As a result of the brain width (approximately 4 – 5 mm) it was necessary to scan up to four batches of data from anterior and posterior. So we obtained a total of six to eight image stacks (three to four from anterior and the same from posterior) which together represented the complete brain.

Single antennal lobes were scanned at 512 x 512 pixel resolution by using the 10x oil immersion objective in one image stack. The antennal lobes were scanned with a voxel size of 1.46 x 1.46 x 1.5 µm and with a zoom factor of 2.

Processing of scanned stacks for reconstruction was performed basically as described in Kurylas et al. (2008): For the whole brains we found in the z direction corresponding optical slices in the overlapping part of both image stacks with the module "AlignSlices" in the program AMIRA 4.1 (Visage Imaging, Fürth, Germany). Redundant slices of the stacks were abolished and corresponding batches of data were merged with the module "AlignSlices". Thereby four batches of data were obtained. Before we merged these image stacks in xy direction, computation limits made it necessary to downsample the voxel size. With the module "Resample" we achieved image stacks with a voxel size of 6 x 6 x 6 µm, which allowed for merging the batch of data in xy direction. Again, we used the module "AlignSlices" for finding the corresponding optical slice and with the module "Merge" the four batches of data were merged into one batch of data which contained the whole brain.

Image segmentation, reconstruction, standardization and visualization

The brain areas and individual olfactory glomeruli were labeled with the segmentation editor in AMIRA on a PC running Windows XP Pro (Intel Core2 6600, 2 GB RAM, ATI Radeon X1800). For segmentation and reconstruction details we principally refer to Kurylas et al. (2008). In short, semi-automatically created voxel-based label fields of 14 paired and 2 unpaired neuropilar structures in twelve female and six male *M. sexta* brains provided the underlying matrix of all computation processes performed (i.e. polygonal surface models, morphometric analysis, shape averaging). Brain outlines were reconstructed separately and serve as orientational guidance only. The color codes for neuropilar areas and antennal lobe glomeruli are consistent with previous works (Brandt et al. 2005; Kurylas et al. 2008; Huetteroth and Schachtner 2005). AMIRA template label files of the brain, the female and the male antennal lobe can be downloaded online (Suppl. 6).

The application of the Virtual Insect Brain (VIB) protocol for registration and standardization was described in detail elsewhere (Jenett et al. 2006; Kurylas et al. 2008). For creation of standard brain neuropil labels, we chose an overlap threshold of 50% for large neuropils, and 30% for small neuropils.

Additional analysis of these data was achieved using Excel XP and SPSS 11.5 (SPSS, Chicago, IL; USA) for Windows. For visualization, respective label surfaces were exported from AMIRA and visualized with CINEMA 4D (Version 10.1; MAXON Computer GmbH, Friedrichsdorf, Germany).

RESULTS

Reconstructed Neuropils

We reconstructed all major discernible areas of the lepidopteran brain (14 paired and 2 unpaired neuropils). In the optic lobe, our female *M. sexta* brain standard is the first to include the lamina (La, Fig. 2). Median to the lamina is the medulla (Me) and posteromedian to this neuropil we reconstructed the lobula plate (LoP), a neuropil exclusively found in Ephemeroptera, Trichoptera, Coleoptera, Diptera and Lepidoptera (Strausfeld 2005). For the reconstruction we subdivided the lobula into two discernible subunits, the outer (Loo) and the inner lobula (Loi); anterior of the lobula we labeled the accessory medulla (aMe).

In the central brain we divided the mushroom bodies into two neuropiles, the pedunculus (Pe), which contained all lobes, and the calyx (Ca) according to earlier insect brain standards (*Drosophila*: Rein et al. 2002; honeybee: Brandt et al. 2005; locust: Kurylas et al. 2008). Although visible, we refrained from including subunits as described for the moth *Spodoptera littoralis* (Sjöholm et al. 2005); the resulting complexity of the pedunculi would have greatly interfered with standardization procedures, and would have also interfered with interspecies comparison. Nevertheless, all four lobes of the peduculus, the α-, β-, γ-, and Y-lobe (Pearson 1971) are discernible protrusions in our reconstruction. Between the mushroom bodies lies the central complex, which comprises the protocerebral bridge (PB), the upper and lower unit of the central body (CBU, CBL) and a small paired neuropil ventrally attached to the central body, the noduli (No). Synapsin-immunoreactivity (syn-ir) failed to label the connecting middle part of the two PB parts, which

consists of tracts only. We restricted the label for the PB to these two halves, because all labels here and in other insect standard brains are based on syn-ir exclusively. The anteriormost labeled neuropils were the deutocerebral antennal lobes (AL), right behind them in the protocerebrum we discerned three subunits of the anterior optic tubercle (AOTu), an upper (uAOTu), lower (lAOTu), and nodular unit (nAOTu).

All neuropilar areas which could not be associated to any of the neuropiles mentioned above or could not be separated clearly where assigned to "unspecified neuropil". Notably this material contains the antennal mechanosensory and motor center, the lateral accessory lobe, the superior, inferior, and lateral protocerebrum with the lateral horn, the subesophageal ganglion neuropil, and the tritocerebrum.

Representative outlines of all labels of these brain areas are shown in frontal slices (Fig. 2), an animation of all orthogonal sections of this brain can be found in the supplementary material (Suppl. 1). Additionally, all reconstructed neuropils are displayed threedimensionally to provide a 3D visualization of the whole brain (Fig. 3).

The standard brain

For the VIB protocol, one brain had to be chosen as positional reference. We calculated mean distances of all neuropilar centers to the calculated brain center and chose the individual brain with the least difference to the mean value as a template (Suppl. 2). This template brain is shown in Fig. 2 and 3.

For the standard brain we reconstructed the identifiable brain areas of twelve individual female brains of *M. sexta* mentioned above. To reduce bias between different individuals and to exclude adult-specific neuronal plasticity effects only freshly eclosed adults were used. The average weight of the twelve animals used was 2.99 g ± 0.56 g and lies within the mean weight of 3.03 ± 0.41 g (Fig. 4; N = 74).

With the VIB protocol we generated a three dimensional standard atlas consisting of 30 neuropils in both hemispheres of the brain. In the standardized gray image batch data the remaining neuropil was assigned to the material named "unspecified neuropil". The standard brain labels are shown in the left panel (Fig. 5) from anterior, dorsal and posterior. The displayed neurilemma (Fig. 5, left panel, transparent) is not standardized and used for orientation and approximate proportion reasons only. An animated view of the standard brain can be seen in the online supplement (Suppl. 3).

With the VIB protocol we generated the average volumes of twelve female brains. Table 1 gives mean volumes, standard deviation and standard error of absolute and relative volumes of all 30 areas plus the "unspecified neuropil". Volumes of corresponding neuropils on either hemisphere

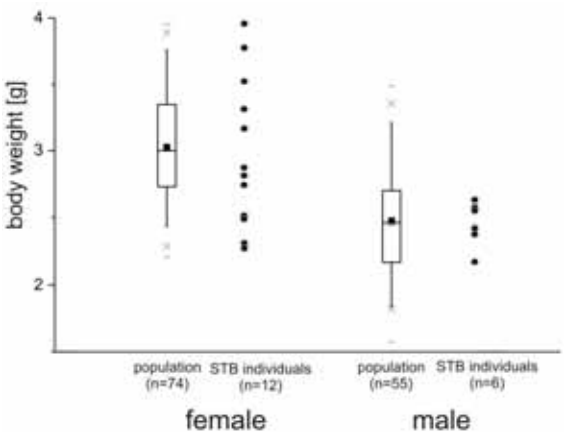

Fig. 4. Comparison of mean body weights of females (n=74) and males (n=55) on their first day after adult eclosion. Black squares = mean weight; black horizontal lines = median; boxes = interquartile range; whiskers = 5th and 95th percentile respectively; gray crosses = 1th and 99th percentile respectively; gray horizontal lines = maximal and minimal individual weights. Aside are individual weights of twelve females and six males (black dots) which were used for standard brain (STB) reconstruction.

exhibit no significant difference ($p > 0.19$, two-tailed t- test).

Brain size and body weight

In some insects, body weight was shown to correlate with brain size (Mares et al. 2005). In our study, we encountered notable differences in body weight (Fig. 4). Since the animals chosen for brain reconstruction span almost the whole weight range of adult *M. sexta*, it was straightforward to calculate neuropil size / body weight correlations. Although our heaviest female shows almost twice the weight than the smallest, we did not find significant allometric correlation between body weight and any neuropil volume in freshly eclosed animals. The only exception were the peduncles, which exhibited a positive correlation ($p<0.05$, Fig. 6). In males, no allometric correlation was found (data not shown).

Comparison of the female and male brains

Additionally to the female standard brain we created a male standard brain based on six freshly eclosed males, to allow for sex-specific comparison of brain neuropils (Fig. 7, Suppl. 4). The six male individuals have an average weight of 2.45 ± 0.17 g, which is also within 95 % of a population of 55 male animals with a mean weight of 2.47 ± 0.42 g. The weight of these six brains is significantly different from the female average weight of 3.03 ± 0.42 g ($p<0.05$, two-tailed t-test, Fig. 4). Accordingly, the brain areas of the male brain are smaller compared to the female brain. Congruent with allometric findings in ant brains (Wehner et al. 2007), we compared the average volumes of the female neuropils with corresponding average

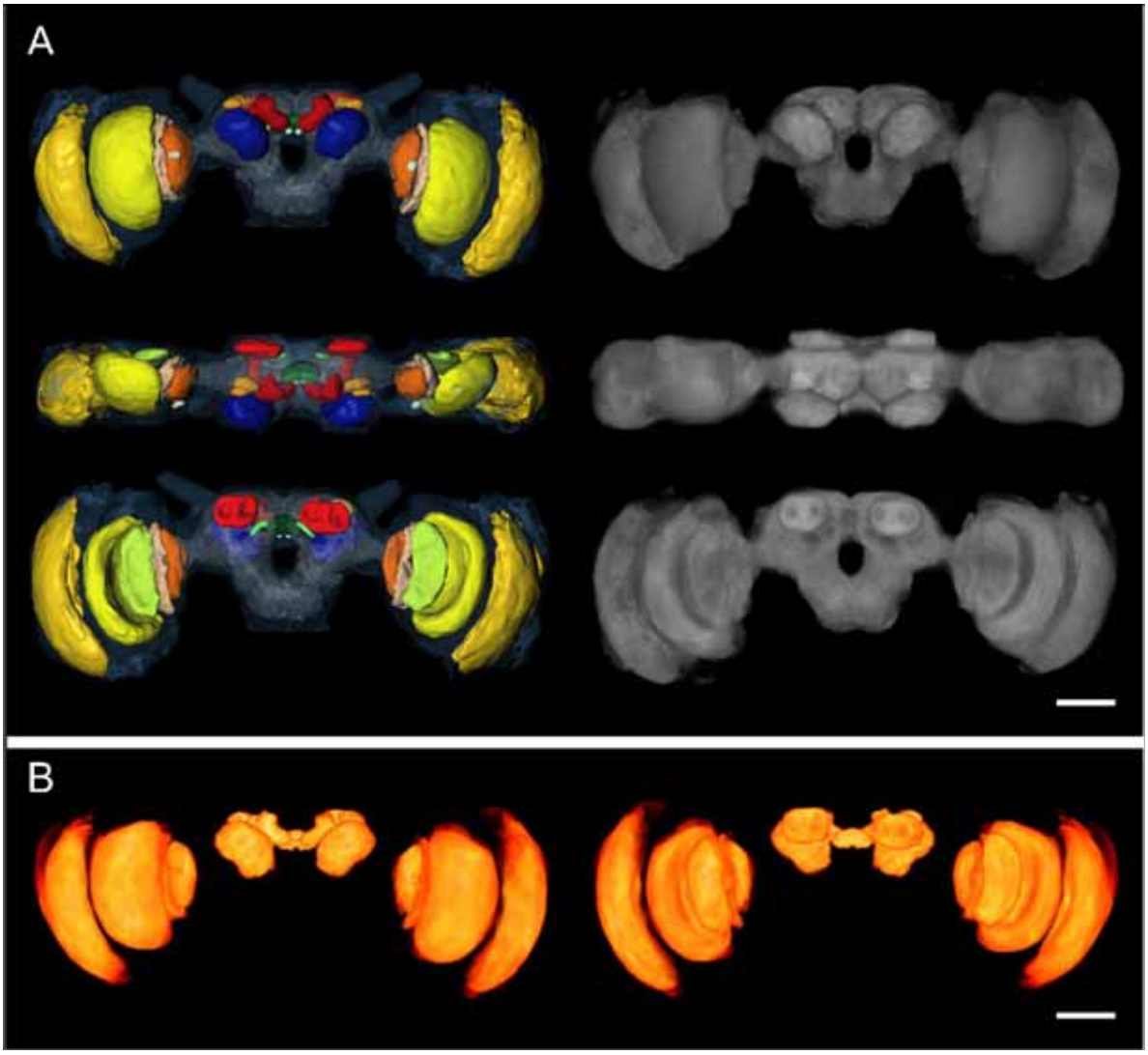

Fig. 5. The 3D female standard brain of *M. sexta* (n=12). **A:** Surface reconstructions of all 30 averaged labels in anterior (above), dorsal (middle), and posterior view (below). The right panel is a 3D visualization of the corresponding average intensity map by direct volume rendering. The transparent blue neurilemma surface in the left panel is not standardized and displayed for orientation only; the label of the unspecified neuropil (gray label) is based on the average image data on the right. The color code refers to Fig. 2. Even smaller neuropils retained their typical shape (e.g. protocerebral bridge, noduli) and give an optic measure of little brain variability as well as labeling quality. **B:** Direct volume rendered view of the resulting average label images from anterior (left) and posterior (right), exhibiting only minor deviations in the laminae. Scale bar: 500 µm.

volumes of the male brains, to study if neuropils are significantly different (Fig. 7).

For this comparison, we omitted the lamina for better comparability with existing insect brain standards and less preparation effort. Most neuropils of the female brain are bigger than their male counterparts (Fig. 9, left). Four neuropiles, namely the accessory medulla (aMe), the lower unit of the central body (CBL), the upper unit of the anterior optic tubercle (uAOTu), and the antennal lobe (AL) show no significant volume differences between female and male brains. After normalizing neuropilar volumes to overall neuropil volume (excluding lamina and unspecified neuropil), no significant differences in neuropil volumes between genders were left except for the aMe ($p<0.05$) and the AL ($p<0.001$) (Fig. 7, right). Because small neuropils like the aMe are especially prone to measuring errors and small labeling differences have big effects on overall volume (Julian and Gronenberg 2002; Kurylas et al. 2008), we do not overemphasize the difference in the aMe. Comparing overall brain neuropil volumes between females and males, males are 0.76 the size of the female, which mirrors the isometric sex dimorphism in all neuropils apart from the ALs.

Male – Female antennal lobe and glomerulus comparison

Since the antennal lobe (AL) remained as the only highly significant anisometric sex-dimorphic neuropil in the brain of *M. sexta*, we focused on this region in more detail and labeled the volumes of ten established glomeruli in eleven female ALs. These glomeruli included three well-described sex-specific glomeruli, the lateral (lLFG) and the

Table 1. Mean volume, relative volume (Rel. vol), standard deviation (SD), relative standard deviation (Rel. SD), standard error (SE), and relative standard error (Rel. SE) of all 31 segmented brain areas in the female standard brain of *M. sexta* (n=12).

Structure	Mean volume [µm³]	Rel. vol [%]	SD [µm³]	Rel. SD [%]	SE [µm³]	Rel. SE [%]
Unspecified neuropil	3.81×10^8	32.527	6.29×10^7	16.49	1.82×10^7	4.76
Lamina (r)	1.13×10^8	9.700	6.88×10^6	6.06	1.98×10^6	1.75
Lamina (l)	1.14×10^8	9.718	7.61×10^6	6.68	2.19×10^6	1.93
Medulla (r)	1.59×10^8	13.580	1.74×10^7	10.95	5.03×10^6	3.16
Medulla (l)	1.62×10^8	13.792	1.37×10^7	8.48	3.96×10^6	2.45
Outer Lobula (r)	1.81×10^7	1.548	1.54×10^6	8.52	4.46×10^5	2.46
Outer Lobula (l)	1.87×10^7	1.601	2.23×10^6	11.89	6.44×10^5	3.43
Inner Lobula (r)	1.75×10^7	1.496	3.26×10^6	18.61	9.43×10^5	5.37
Inner Lobula (l)	1.76×10^7	1.503	3.04×10^6	17.30	8.80×10^5	4.99
Lobula plate (r)	2.44×10^7	2.081	2.00×10^6	8.18	$5.76 \times 10^{\prime 5}$	2.36
Lobula plate (l)	2.45×10^7	2.093	2.96×10^6	12.05	8.53×10^5	3.48
Accessory medulla (r)	2.95×10^5	0.025	6.33×10^4	21.47	1.82×10^4	6.20
Accessory medulla (l)	2.94×10^5	0.025	5.90×10^4	20.11	1.70×10^4	5.81
Pedunculus (r)	8.54×10^6	0.728	9.88×10^5	11.57	2.85×10^5	3.34
Pedunculus (l)	8.28×10^6	0.706	$1.13. \times 10^6$	13.65	3.27×10^5	3.94
Calyx (r)	1.07×10^7	0.910	1.18×10^6	11.12	3.43×10^5	3.21
Calyx (l)	1.07×10^7	0.915	1.26×10^6	11.75	3.64×10^5	3.39
Central body upper unit	3.76×10^6	0.321	4.91×10^5	13.07	1.42×10^5	3.77
Central body lower unit	1.30×10^6	0.111	2.45×10^5	18.91	7.08×10^4	5.46
Protocerebral bridge (r)	4.09×10^5	0.035	6.05×10^4	14.81	1.75×10^4	4.27
Protocerebral bridge (l)	4.20×10^5	0.036	5.94×10^4	14.15	1.71×10^4	4.09
Nodulus (r)	1.13×10^5	0.010	1.57×10^4	13.90	4.54×10^3	4.01
Nodulus (l)	1.15×10^5	0.010	2.19×10^4	19.02	6.33×10^3	5.49
Antennal lobe (r)	3.62×10^7	3.090	3.20×10^6	8.82	9.23×10^5	2.55
Antennal lobe (l)	3.54×10^7	3.020	3.78×10^6	10.68	1.09×10^6	3.08
Anterior optic tubercle upper unit (r)	1.74×10^6	0.149	2.79×10^5	16.02	8.06×10^4	4.63
Anterior optic tubercle upper unit (l)	1.73×10^6	0.147	2.15×10^5	12.44	6.20×10^4	3.59
Anterior optic tubercle lower unit (r)	2.50×10^5	0.021	5.05×10^4	20.22	1.46×10^4	5.84
Anterior optic tubercle lower unit (l)	2.68×10^5	0.023	7.33×10^4	27.39	2.12×10^4	7.91
Anterior optic tubercle nodular unit (r)	4.74×10^5	0.040	7.46×10^4	15.73	2.15×10^4	4.54
Anterior optic tubercle nodular unit (l)	4.51×10^5	0.038	9.17×10^4	20.35	2.65×10^4	5.87

medial large female glomerulus (mLFG) as well as the small female glomerulus (SFG, Fig. 8C), which are homologous to the male-specific glomeruli cumulus, toroid, and horseshoe or toroid 2 (Rospars and Hildebrand 2000). Additionally, we labeled seven easily identifiable glomeruli which were described already in the male antennal lobe of *M. sexta* in an earlier study (Huetteroth and Schachtner 2005). Anterior in the antennal lobes we reconstructed the glomeruli disc and discbase, also known in the literature as mortar and pestle (Lipscomb and Tolbert 2006, Fig. 8B), and possibly homologous to flower and flowerbase in the silkmoth *Bombyx mori* (Terada et al. 2003). Most ventrally is the labial pit organ glomerulus (LPOG), the only glomerulus not innervated by the antennal nerve but by receptor neurons from the labial palps (Kent et al. 1986, Fig. 8C). This glomerulus received recent attention as being responsible for detecting CO2 (Guerenstein et al. 2004; Guerenstein and Hildebrand 2008). Further ventral glomeruli are the club, base, and cap (Fig. 8C). Right behind the sex-related glomeruli we labeled the largest of the "ordinary" glomeruli, G20 (Fig. 8D). The right panel in Fig. 8 shows frontal optical slices according to the planes named in Fig. 8A in an individual antennal lobe in the right hemisphere of the brain (Fig. 8B'-D'), on the left panel we show the labels of the identified glomeruli on the same image (Fig. 8B-D). For clarification, we included the AL outline, which surrounds all 63±1 glomeruli plus the

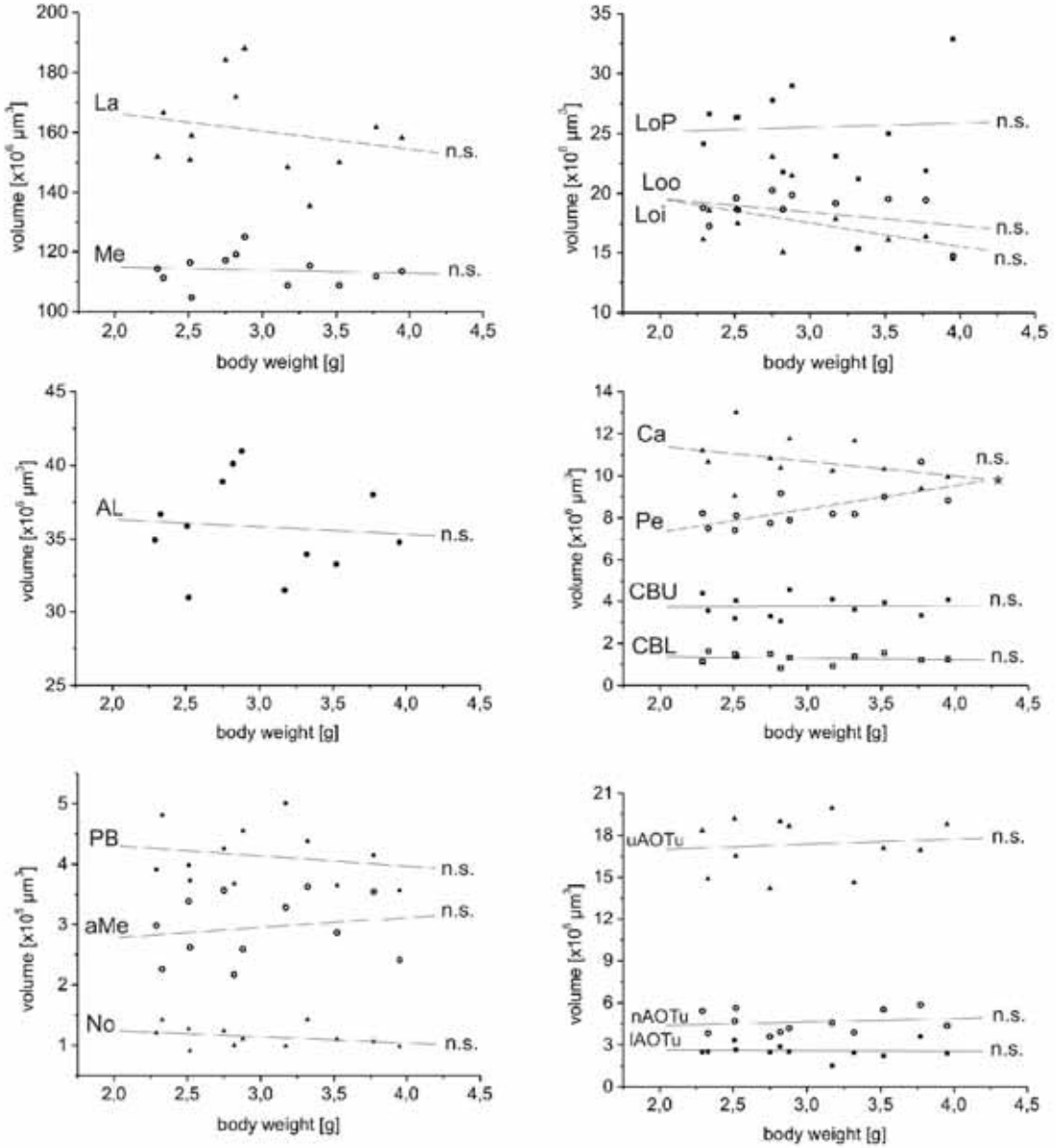

Fig. 6. Relation between body weight and neuropil volume. Regression lines indicate no significant correspondence between both parameters except for the pedunculi (Pe). La = laminae; Me = medullae; Loi, Loo = inner and outer lobulae; LoP = lobula plates; AL = antennal lobes; Ca = calyces; Pe = pedunculi; CBU, CBL = upper and lower unit of central body; PB = protocerebral bridges; aMe = accessory medullae; No = noduli; uAOTu, lAOTu, nAOTu = upper, lower and nodular units of anterior optic tubercles; n.s. = not significant, * = $p<0.05$.

lateral (LC), median (MC) and anterior cell group (AC) (Fig. 8A). Beside the identified ten glomeruli the remaining glomeruli are shown in gray transparent in the reconstruction (Fig. 8).

Suppl. 5 gives mean volumes, standard deviation and standard error of the absolute and relative volumes of the six already identified "ordinary" glomeruli, the LPOG, and the three sex-related glomeruli of the eleven antennal lobes. The weight of the eleven animals averages 2.92 ± 0.61 g, representative for the mean weight of all measured females. All female glomerular volumes (white bars) were compared to their corresponding male values (black bars) of freshly eclosed male brains (Fig. 9; Rospars and Hildebrand 2000; Huetteroth and Schachtner 2005). Not surprisingly, the volume of the male sex-related glomeruli cumulus and toroid are about 5.8-fold bigger than the homologous glomeruli mLFG and lLFG in the female antennal lobe. Taken together, the volumes of all three sex-related glomeruli of the male antennal lobe are 5.1-fold bigger than the volumes of the three female-specific glomeruli. The only non-significant exception is the third sex-specific glomerulus, the horsehoe/SFG (Fig. 9). All remaining six normal female glomeruli and the LPOG exceed their male counterparts significantly in absolute volume, similarly to the protocerebral brain neuropils. After taking this known size difference into account and correcting female glomerulus volumes by the factor 0.76 (gray bars, see section before), none of the normal glomeruli remains significantly larger in females. Even more pronounced than before, the three male sex-specific

glomeruli underline their bigger size, leaving them as the only real anisometric volume dimorphism found in *M. sexta* brain neuropils.

DISCUSSION

In this study, we provide evidence that the general isometric size dimorphism in moth brain anatomy masks an anisometric neuropil volume dimorphism. After compensating volumes for general isometric size dimorphism, we show that this anisometric brain difference between genders is indeed restricted to the three well-described sex-specific glomeruli in the antennal lobe, and neither reflected in higher brain centers nor in other identified homologous glomeruli of the AL.

To evaluate neuropilar volumes, we produced a volumetric standard brain based on twelve freshly eclosed female *M. sexta*, and compared it to a male standard brain of the same age. Additionally, we supply a realistic representation of a female *M. sexta* AL regarding volume, shape, and localization of ten previously identified glomeruli. Compared to existing insect standard brains, the *M. sexta* standard poses the largest brain so far with respect to absolute size.

Standard brain generation

To obtain a standard insect brain, two working protocols are established: the virtual insect brain (VIB) protocol, as used for the fruit fly *Drosophila* (Rein et al. 2002, Jenett et al. 2006), and the iterative shape averaging (ISA) method, as used for the honeybee (Brandt et al. 2005). As shown by Kurylas et al. (2008), "the" standardization protocol does not exist; rather the protocol has to be chosen according to its functional significance. In their work both VIB and ISA method were compared using the same individual locust brain reconstructions. While the VIB protocol was developed to ease comparison between different fly strains with mutant brain structures, the ISA method had the goal to register single reconstructed neurons from various individuals into one standard brain. The VIB script therefore keeps mean neuropilar volumes unchanged, while the ISA method tries to reduce anatomical differences on the cost of volume accuracy (Kuss et al. 2007, Kurylas et al. 2008). We used the virtual insect brain (VIB) protocol for standardization, since we wanted to use and compare mean volumes of neuropiles and did not aim for registration of reconstructed neurons (Rø et al. 2007, Kurylas et al. 2008). Given that both methods are established in

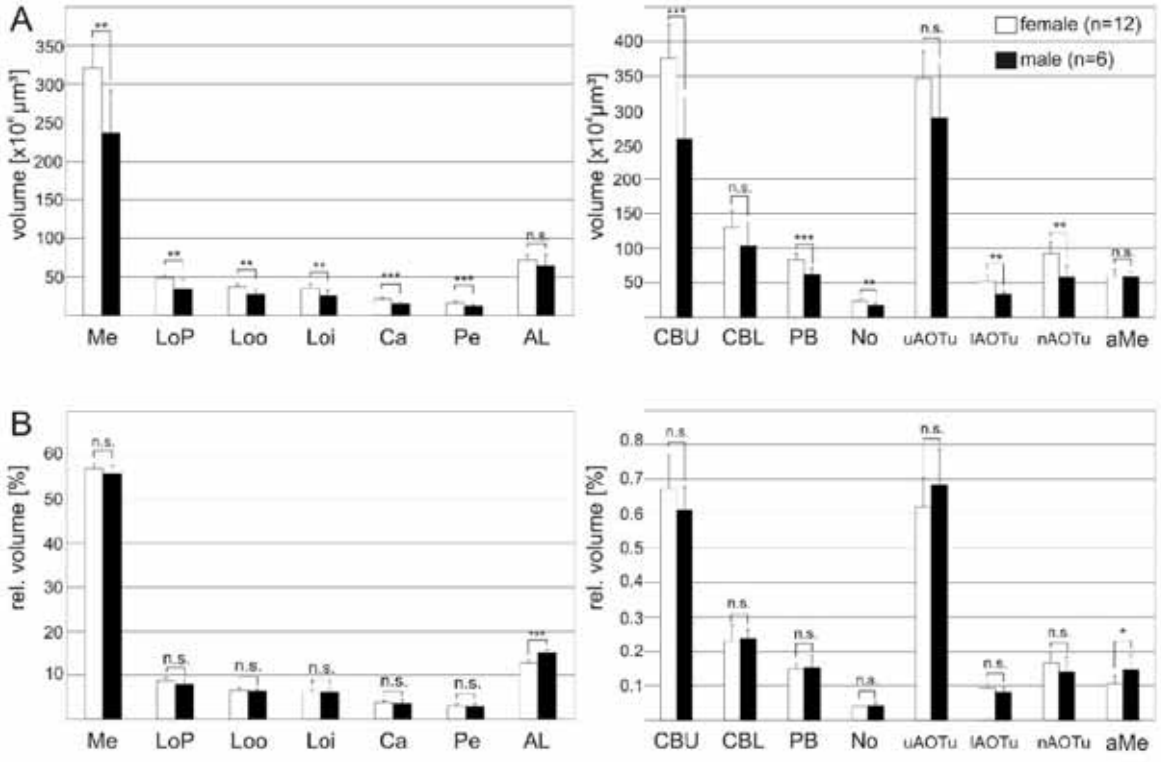

Fig. 7. Comparison of neuropil volumes between female (white) and male (black) brains. **A:** All female brain neuropil volumes are significantly larger than the corresponding male neuropil volumes apart from the antennal lobes (AL), the lower unit of the central body (CBL), the upper units of the anterior optic tubercles (uAOTu), and the accessory medullae (aMe). **B:** After normalizing all neuropil volumes to overall neuropil volume, almost all showed no significant differences apart from two neuropils. The accessory medullae (aMe) exhibited weakly significant differences, whereas the bigger antennal lobes of males became strongly significant. (Bars: standard deviation; *** = p< 0.001, ** = p< 0.01, * = p< 0.05, n.s. not significant).

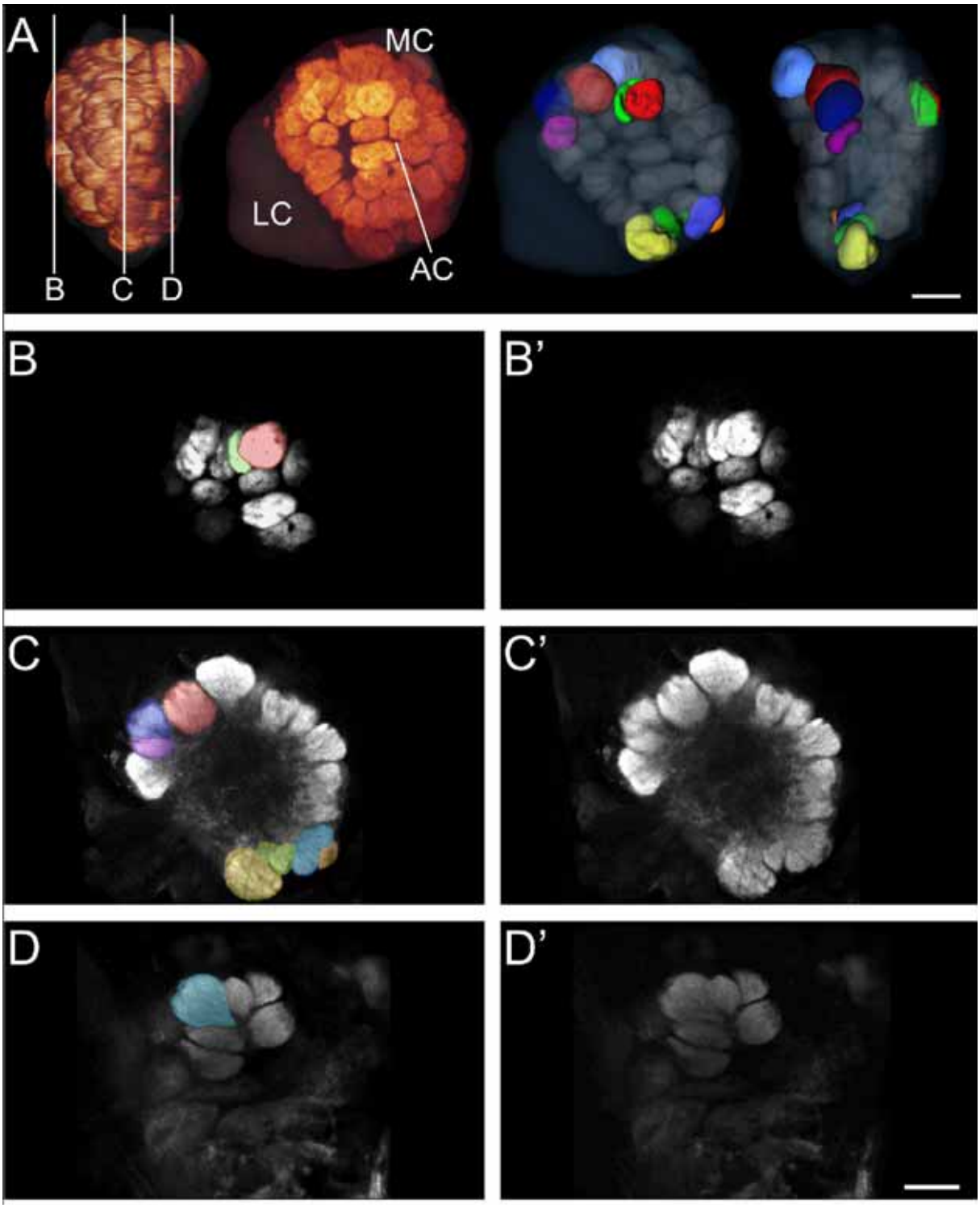

Fig. 8. Right antennal lobe of a female *M. sexta* brain. **A:** median and anterior view (left) of a right antennal lobe, shown by direct synapsin-immunoreactivity volume rendering; anterior and lateral view (right) of 3D-reconstructed glomeruli of the same antennal lobe. In the anterior view of the volume rendering the approximate location of the lateral (LC), median (MC), and anterior cell group (AC) is denoted. The vertical bars in the median view display section levels of B-D and B'-D' respectively. Ten identified glomeruli in the 3D reconstruction are colored according to ten homologous male glomeruli (see below; Huetteroth and Schachtner 2005). Other glomeruli are displayed in transparent gray; the neurilemma enclosing both AL neuropil and cell groups is shown in transparent blue. **B-D:** Axial slices through the antennal lobe at different levels. **B:** Two of the most anteriorly located glomeruli are disc (bright red) and discbase (green) **C:** Axial slice through the center of the antennal lobe containing the labial pit organ glomerulus (LPOG; yellow), club (green), base (blue) and cap (orange). Additionally, the sex-specific glomeruli of the female antennal lobe are visible, the small (SFG; purple), medial large (mLFG; dark red), and lateral large female glomerulus (lLFG; dark blue). **D:** Posterior part of the antennal lobe displaying G20 (bright blue), the largest of the "ordinary" glomeruli. **B'-D':** Confocal slices through the antennal lobe corresponding to B-D. Scale bars: 100 µm.

our lab, a standard brain calculated by the ISA method could be supplied on request.
It has to be noted that our wholemounts, like all immunocytochemical preparations, are subjected to considerable tissue shrinking (Bucher et al. 2000). Therefore absolute sizes are probably underestimated and make most sense in relative comparisons, i.e. comparisons might only be useful between brains after similar histological treatment. In a previous work, we already showed the usability of 3D reconstructions to quantify adult plasticity in the male antennal lobe (Huetteroth and Schachtner 2005). Since we carefully checked for animal age, this standard brain may be of additional use in future quantitative studies using pharmacological or behavioral approaches. Currently we are including the standard brain into a developmental framework, with volumetric data on neuropil growth during the pupal stages (Huetteroth et al., in preparation).

The *Manduca* standard brain

Detailed 3D information about lepidopteran mushroom body architecture was provided in three consecutive papers on *Spodoptera littoralis* (Sjöholm et al. 2005, Sjöholm et al. 2006, Sinakevitch et al. 2008). The authors demonstrated olfactory and optic input into the calyces, revised the pedunculus lobe organization, and revealed longitudinally organized subdivisions with different aminergic and peptidergic innervation patterns in the pedunculi and lobes. Rø et al. (2007) provided with *Heliothis virescens* the first complete 3D-reconstructed moth brain; in the mushroom bodies they adapted the proposed nomenclature of Sjöholm et al. (2005), and warped calyces of different animals together to ease comparability of reconstructed projection neuron arborizations. By using almost the same techniques of 3D reconstruction, we pursued in our work a completely different goal, namely to provide an average-volume standard as a future reference for comparative studies on brain neuropil.
Usually, larger animals of one species have larger brains; therefore head width as well as body weight corresponds to brain size (Mares et al. 2005, Wehner et al. 2007). For *M. sexta* we only measured body weight, but found no correlation between brain or single neuropil volume with body weight (Fig. 6). In different Nymphalid butterfly species Sivinsky (1989) also found no allometric relationship between brain and body size. Since our twelve female brains cover almost the whole span of weights encountered in a whole of 74 animals, our allometric comparisons of neuropil volumes might sufficiently represent the natural variance in animal size (Fig. 4). Still, individual body weight variances remained small in *M. sexta* (not quite x2). Mares et al. (2005) found a positive correlation of brain volume and body weight for bumblebees only, but not for honeybee workers. While honeybee workers exhibited a weight range similar to *M. sexta*, bumblebees are well-known for their

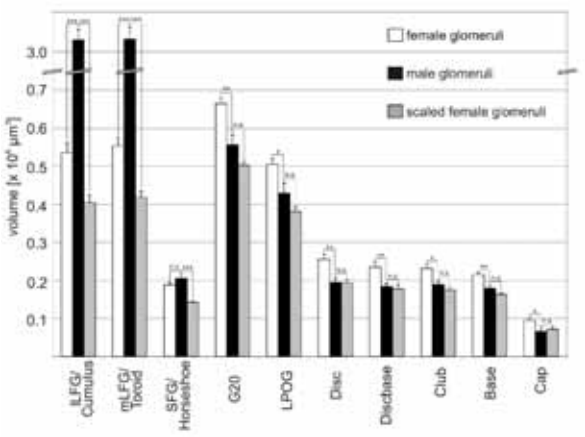

Fig. 9. Volume comparison between the ten identified glomeruli of the female (white; n=11) and the male antennal lobe (black; n=16, Huetteroth and Schachtner 2005) of *M. sexta*. All "ordinary" glomeruli and the LPOG are significantly larger in females ($p<0.05$). The three sex-specific glomeruli of the male antennal lobe (cumulus, toroid, and horsehoe) are together approximately 5.75-fold larger than the corresponding homologous glomeruli of the female antennal lobe (lateral and median large female glomerulus, lLFG and mLFG, and small female glomerulus, SFG). After normalizing female glomerulus volume by a factor of 0.76 (see results), all "normal" glomeruli and the LPOG exhibit equal volumes. Only the three sex-dimorphic glomeruli show highly significant larger volumes in males. (Bars: standard error; n.s. = not significant; *** = $p< 0.001$).

considerable variation in body size and weight (up to x10; Mares et al. 2005).

Intriguingly, no allometric relation could be found except for the pedunculus including the mushroom body lobes. We do not want to stress this exception, since increased N size might have eliminated this finding. Remarkably, it were also the pedunculi in honeybees which showed exceptional allometric behavior (Mares et al. 2005). It remains to be solved if this is of any significance; it should be noted however in this context, that ants seem to have an upper limit of mushroom body growth (Kühn-Bühlmann and Wehner 2006).
Notably, all variances and standard deviations of labeled neuropil volumes are comparable small, despite the fact that almost the complete weight range of animals was covered. Higher variances in smaller neuropils are an immanent problem of voxel-based labeling (Julian and Gronenberg 2002; Kurylas et al. 2008). As noted for other standardized insects, we also found no significant volume differences between left and right brain hemispheres.

Brain neuropil comparison between genders

Almost all neuropilar volumes in females are bigger than their male counterparts (Fig. 7). As noted previously, small neuropilar volumes are especially prone to labeling and measurement errors, leading

to higher standard deviations (Julian and Gronenberg 2002; Kurylas et al. 2008). This might account for the relatively high volume variability in smaller neuropils of both genders, as observed in the accessory Medulla (aMe), the lower unit of the central body (CBL), and the upper unit of the anterior optic tubercle (uAOTu). Apart from those small neuropils, we attribute the absolute size difference of brain neuropils between genders to general sex dimorphism, as it is found across animal phyla (Badyaev 2002).

However, if volumes are normalized to overall neuropilar volume, no significant differences in percentual neuropilar share were observed with two exceptions: as noted before, the bigger accessory medulla in males might be explained by its small size ($p<0.05$), but the difference in the relative antennal lobe neuropil volume between males and females became highly significant ($p<0.001$). Taken together, these results strongly imply no anisometric neuropilar sex dimorphism in the *M. sexta* brain apart from the antennal lobes, or better, the sex-specific glomeruli in the antennal lobes. This was not self-evident; a dimorphic correlate of the antennal lobe might have been present in one of the target regions of AL output neurons, the calyces. According to Homberg et al. (1988) males contain approximately 48 projection neurons more than females, and projection neuron number per glomerulus might be proportional to its size. Thus it would have been possible to detect a representation of the MGC in downstream neuropils on a volumetric level. Pearson (1971) states by citing Hanström (1928), that the size of the AL and the calyx in moths are correlated. The author explains this observation with the massive antennocerebral tracts which serve as main input to the calyces, thus strongly interlinking both neuropils. Although this sounds plausible, we did not find a significant correlation between AL and calyx in our preparations (data not shown). It has to be noted that we did not include the main target area of antennal lobe projection neurons, the inferior lateral protocerebrum or lateral horn. This neuropilar region exhibits no clear boundaries; therefore we refrained from including this region into the standard brain. It is known from the silkmoth *Bombyx mori*, that projection neurons originating in the MGC are targeting different areas in the inferior lateral protocerebrum (Kanzaki et al. 2003). It can be assumed that target areas innervated by projection neurons coming from ordinary glomeruli also have their distinct location, as it is the case in *Drosophila* (Jefferis et al. 2007). We interpret these results in this regard, that gender-specific olfactory information processing takes place mainly if not exclusively in the antennal lobes. Preprocessed olfactory information is transferred into higher brain centers, thereby targeting different regions depending on olfactory information. At least in the calyces however this preprocessed information is not handled differently between pheromonal and non-pheromonal odors, concerning absolute neuropil volume.

One might note that the optic neuropils are larger in females than in males even after normalizing, except for the aMe (Fig. 7). In a recent work, a sex dimorphic innervation of the lobula plate is described in hoverflies (Nordström et al. 2008), and a previous work describes male-specific neurons in fly lobulae (Strausfeld 1991). Generally, in Dipteran species sex dimorphic optic lobes seem to be rather the norm than the exception, although usually males exhibit more cells or more elaborate neuronal branching patterns than females (reviewed in Wehner 1981; Zeil 1983). Male-specific interneurons in the fly brain were shown to prevent programmed cell death by expressing fruitless, a factor being discussed as regulating sex dimorphism in the brain (Kimura et al. 2005). In intracellular recording studies on optic lobe neurons of both sexes of *M. sexta* no sex dimorphic arborizations were mentioned (Milde 1993; Wicklein and Strausfeld 2000).

Antennal lobe comparison between genders

Anatomical sex dimorphism in the antennal lobes has been found in several species (Schachtner et al. 2005). Usually in males enlarged glomeruli at the entrance site of the antennal nerve are described, as for cockroaches (Jawlowski 1948; Neder 1959), bees (Arnold et al. 1984), ants (Kleineidam et al. 2005; Nishikawa et al. 2008), flies (Kondoh et al. 2003), and of course moths (Bretschneider 1924) including *M. sexta* (Camazine and Hildebrand 1979, Matsumoto and Hildebrand 1981, Schneiderman et al. 1982). These glomeruli are cited as macroglomerulus or, if more than one, as macroglomerular complex (MGC). In *M. sexta*, and probably all other species as well, these glomeruli are involved in pheromone signal processing (Matsumoto and Hildebrand 1981).

Until now, the only 3D reconstruction of the female antennal lobe in *M. sexta* was based on two individuals and possessed only limited information about glomerulus shape or volume (Rospars and Hildeband 2000). Nevertheless, this work showed for the first time the correspondence of the three sex-specific glomeruli lLFG, mLFG and SFG to their male counterparts, the homologous glomeruli cumulus, toroid and horseshoe of the MGC. We revived some questions which arose in this work and compared corresponding male and female glomeruli on a quantitative basis. In two previous works male and female antennal lobes of the moths *Lobesia botrana* (Masante-Roca et al. 2002) and *Heliothis virescens* (Berg et al. 2002) were 3D-reconstructed and single glomeruli were identified; however, both works did not compare glomerular volumes quantitatively.

Our volumetric gender comparisons in the AL took advantage of a previously published work on glomerular volumes of 16 ALs of freshly eclosed male animals. We find in ten identified glomeruli

approximately the same dimorphism as for the remaining brain neuropils before; all glomeruli are significantly larger in females, apart from the three glomeruli homologous to the MGC. The MGC exceeds the combined size of homologous female glomeruli by far, paying tribute to its massive innervation by pheromone-sensitive ORNs (Lee and Strausfeld 1990). Interestingly, those significant differences in normal glomeruli all disappear if a correction factor derived from brain neuropils in males and females is applied (Fig. 9). The difference between dimorphic glomeruli becomes even more pronounced. So far, the six normal glomeruli and the LPOG should give a good estimate of all remaining glomeruli in the AL. We therefore conclude that the only anisometric volume dimorphism in *M. sexta* is limited to the primary integration center of pheromone odor information, or more specifically, to their main components bombycal or (E,Z)-10,12-hexadecadienal in the toroid and (E,Z)-11,13-pentadecadienal in the cumulus (Christensen and Hildebrand 1987).

Interspecies brain comparison

While volumetric sex dimorphism is still debated controversially in human brains (Good et al. 2001; Ekinci et al. 2008), it is repeatedly reported in eusocial insects like bees or ants, that primary sensory neuropils are enlarged in males (Molina and O'Donnell 2008). This is attributed to the differing behavioral task solely reduced to seek and find potential mating partners, either optically or olfactory. Neither male nor female *M. sexta* are known for elaborate behaviors apart from seeking either partners or proper plants for egg-laying. Since both genders of this non-social moth exhibit rather large primary sensory neuropils like antennal and optic lobes (table 2), their relative brain volumes somewhat resemble males in eusocial species.

Table 2. Comparison of relative neuropilar volumes between different insect species coming from four different insect orders, namely Diptera (*Drosophila melanogaster*, Rein et al. 2002), Hymenoptera (*Apis mellifera*, Brandt et al. 2005), Orthoptera (*Schistocerca gregaria*, Kurylas et al. 2008), and Lepidoptera (*M. sexta*, this work). We included the gender and the number of individuals, which were used for respective standardization. Only neuropils which have complements in all examined animals were compared (medulla, inner and outer lobula, lobula plate, antennal lobe, pedunculus, calyx, upper and lower unit of the central complex).

Order	Diptera	Hymenoptera	Orthoptera	Lepidoptera
Species	***D. melanogaster***	***A. mellifera***	***S. gregaria***	***M. sexta***
Gender	♀	☿	♂	♀
Number of individuals	28	20	10	12
Optic lobes	79,65 %	58,82 %	72,67 %	85,41 %
Antennal lobes	9,36 %	8,85 %	9,67 %	9,15 %
Central body	3,43 %	0,91 %	1,67 %	0,63 %
Mushroom bodies	7,56 %	32,65 %	15,98 %	4,80 %

Regarding the central complex, the sum of relative ellipsoid body volume and fan-shaped body volume in the fly exceed those of the upper and lower units of the central complex in locust, honeybee, and moth. The central complex is thought to play essential roles in locomotion control, which was mainly examined in flies (Strauss 2002). Another pivotal role of the central complex seems to be the integration of skylight information used for navigation, as examined mainly in locusts (Homberg 2004, Heinze and Homberg 2007), but also in hymenopterans like bees and ants (Wehner 1984, Müller and Wehner 2007). While a vision-based navigational role might be less important for the short-lived and night active moth *M. sexta*, it comes somewhat surprising that the navigational skills of the hymenopteran bees seem not to be reflected in their central complex volume. In this context, it would be interesting to have comparable standardized central complex volumes of ants and migratory lepidopterans, i.e. monarch butterflies (*Danaus plexippus*; Reppert 2006).

Much more pronounced than in the central complex are the differences in relative volume of the mushroom bodies. While the social honeybee by far exhibits the largest mushroom bodies, the smallest are found in *M. sexta* (table 2). Mushroom bodies, generally associated with higher integration processes and learning, vary considerably in relative size in different nymphalid butterflies, without correlating to optic or antennal lobe size. *Heliconius charitonius* for example stands out with having almost four times bigger mushroom bodies than other butterflies of that family (Sivinsky 1989). This is attributed to its relative long life combined with its occurrence in forested habitats with only scattered food recources, and a shared resting place with conspecifics. As discussed by the author, remembering a common resting place and good food sites might be a higher evolutionary constraint for learning ability than finding proper egg-laying sites, which does not necessarily involve memory tasks (Sivinsky 1989). For the ant *Cataglyphis*, Wehner et al. (2007) discussed social interaction rather than food gathering for being responsible of bigger mushroom bodies compared to other ant species. Newborn cells might contribute to bigger mushroom bodies, as adult neurogenesis does occur in moths (Dufour and Gadenne 2006). Despite the short lifespan of *M. sexta* and the smallest mushroom bodies in our comparison (table 2), we cannot exclude the possibility of behavior-dependent volume changes in adults. Classical conditioning was successfully tested (Daly and Smith 2000; Daly et al. 2001), learning of odors and colors in free-flying animals was shown (Riffell et al. 2008, Goyret et al. 2008), age- and mating-dependent behaviors towards odors (Mechaber et al. 2002), a persistent effect of odor learning onto olfactory network activity (Daly et al. 2004), and adult volume increases were at least found in antennal lobe glomeruli (Huetteroth and Schachtner 2005).

ACKNOWLEDGEMENTS

We are gratefully indebted to Dr. E. Buchner (Würzburg, Germany) for supplying us with anti-Synapsin antibody. We also like to thank Dr. U. Homberg for many fruitful discussions.

LITERATURE CITED

Arnold G, Masson C, and Budharugsa S. 1984. Demonstration of a sexual dimorphism in the olfactory pathways of the drones of *Apis-mellifica* L. (Hymenoptera, Apidae). Experientia 40:723-725.

Badyaev AV. 2002. Growing apart: an ontogenetic perspective on the evolution of sexual size dimorphism. Trends in Ecology & Evolution 17:369-378.

Bell RA and Joachim FA. 1978. Techniques for rearing laboratory colonies of the tobacco hornworm, *Manduca sexta* and pink ballworms. Ann Entomol Soc Am 69:365-373.

Berg BG, Galizia CG, Brandt R, and Mustaparta H. 2002. Digital atlases of the antennal lobe in two species of tobacco budworm moths, the Oriental *Helicoverpa assulta* (male) and the American *Heliothis virescens* (male and female). J Comp Neurol 446:123-134.

Brandt R, Rohlfing T, Rybak J, Krofczik S, Maye A, Westerhoff M, Hege HC, and Menzel R. 2005. Three-dimensional average-shape atlas of the honeybee brain and its applications. J Comp Neurol 492:1-19.

Bretschneider F. 1924. Über die Gehirne des Eichenspinners und des Seidenspinners (*Lasiocampa quercus* L. und *Bombyx mori* L.). Jena Z Naturw (Zool) 60:563-570.

Bucher D, Scholz M, Stetter M, Obermayer K, and Pflüger HJ. 2000. Correction methods for three-dimensional reconstructions from confocal images: I. Tissue shrinking and axial scaling. J Neurosci Methods 100:135-143.

Camazine SM and Hildebrand JG. 1979. Central projections of antennal sensory neurons in mature and developing *Manduca sexta*. Soc Neurosci Abstr 5:155.

Chapman RF. 1998. The Insects: Structure and Function. Cambridge: University Press.

Christensen TA and Hildebrand JG. 1987. Male-specific, sex pheromone-selective projection neurons in the antennal lobes of the moth *Manduca sexta*. J Comp Physiol [A] 160:553-69.

Daly KC and Smith BH. 2000. Associative olfactory learning in the moth *Manduca sexta*. J Exp Biol 203:2025-2038.

Daly KC, Durtschi ML, and Smith BH. 2001. Olfactory-based discrimination learning in the moth, *Manduca sexta*. J Insect Physiol 47:375-384.

Daly KC, Christensen TA, Lei H, Smith BH, and Hildebrand JG. 2004. Learning modulates the ensemble representations for odors in primary olfactory networks. Proc Natl Acad Sci U S A 101:10476-10481.

Douglass JK and Strausfeld NJ. 2003. Anatomical organization of retinotopic motion-sensitive pathways in the optic lobes of flies. Microsc Res Tech 62:132-150.

Dufour MC and Gadenne C. 2006. Adult neurogenesis in a moth brain. J Comp Neurol 495:635-643.

Ekinci N, Acer N, Akkaya A, Sankur S, Kabadayi T, and Sahin B. 2008. Volumetric evaluation of the relations among the cerebrum, cerebellum and brain stem in young subjects: a combination of stereology and magnetic resonance imaging. Surg Radiol Anat 30:489-494.

Good CD, Johnsrude I, Ashburner J, Henson RN, Friston KJ, and Frackowiak RS. 2001. Cerebral asymmetry and the effects of sex and handedness on brain structure: a voxel-based

morphometric analysis of 465 normal adult human brains. Neuroimage 14:685-700.

Goyret J, Pfaff M, Raguso RA, and Kelber A. 2008. Why do *Manduca sexta* feed from white flowers? Innate and learnt colour preferences in a hawkmoth. Naturwissenschaften 95:569-576.

Grimaldi DA and Engel MS. 2005. Evolution of the insects. Cambridge, UK: Cambridge University Press.

Gronenberg W. 2001. Subdivisions of hymenopteran mushroom body calyces by their afferent supply. J Comp Neurol 435:474-489.

Gronenberg W and Lopez-Riquelme GO. 2004. Multisensory convergence in the mushroom bodies of ants and bees. Acta Biol Hung 55:31-37.

Guerenstein PG, Christensen TA, and Hildebrand JG. 2004. Sensory processing of ambient CO2 information in the brain of the moth *Manduca sexta*. J Comp Physiol A Neuroethol Sens Neural Behav Physiol 190:707-725.

Guerenstein PG and Hildebrand JG. 2008. Roles and effects of environmental carbon dioxide in insect life. Annu Rev Entomol 53:161-178.

Hanström B. 1928. Vergleichende Anatomie des Nervensystems der Wirbellosen Tiere unter Berücksichtigung seiner Funktion. Berlin: Springer Verlag.

Heinze S and Homberg U. 2007. Maplike representation of celestial E-vector orientations in the brain of an insect. Science 315:995-997.

Helfrich-Förster C. 2004. The circadian clock in the brain: a structural and functional comparison between mammals and insects. J Comp Physiol [A] 190:601-613.

Homberg U, Montague RA, and Hildebrand JG. 1988. Anatomy of antenno-cerebral pathways in the brain of the sphinx moth *Manduca sexta*. Cell Tissue Res 254:255-281.

Homberg U, Hofer S, Pfeiffer K, and Gebhardt S. 2003. Organization and neural connections of the anterior optic tubercle in the brain of the locust, *Schistocerca gregaria*. J Comp Neurol 462:415-430.

Huetteroth W and Schachtner J. 2005. Standard three-dimensional glomeruli of the *Manduca sexta* antennal lobe: a tool to study both developmental and adult neuronal plasticity. Cell Tissue Res 319:513-524.

Jawlowski H. 1948. Studies on the insect brain. Ann UMCS C Lublin 3:1-30.

Jefferis GS, Potter CJ, Chan AM, Marin EC, Rohlfing T, Maurer CR, Jr., and Luo L. 2007. Comprehensive maps of *Drosophila* higher olfactory centers: spatially segregated fruit and pheromone representation. Cell 128:1187-1203.

Jenett A, Schindelin JE, and Heisenberg M. 2006. The Virtual Insect Brain protocol: creating and comparing standardized neuroanatomy. BMC Bioinformatics 7:544.

Jørgensen K, Kvello P, Almaas TJ, and Mustaparta H. 2006. Two closely located areas in the suboesophageal ganglion and the tritocerebrum receive projections of gustatory receptor neurons located on the antennae and the proboscis in the moth *Heliothis virescens*. J Comp Neurol 496:121-134.

Julian GE and Gronenberg W. 2002. Reduction of brain volume correlates with behavioral changes in queen ants. Brain Behav Evol 60:152-164.

Kanzaki R, Soo K, Seki Y, and Wada S. 2003. Projections to higher olfactory centers from subdivisions of the antennal lobe macroglomerular complex of the male silkmoth. Chem Senses 28:113-130.

Kent KS, Harrow ID, Quartararo P, and Hildebrand JG. 1986. An accessory olfactory pathway in Lepidoptera: the labial pit organ and its central projections in *Manduca sexta* and certain other sphinx moths and silk moths. Cell Tissue Res 245:237-245.

Kimura K, Ote M, Tazawa T, and Yamamoto D. 2005. Fruitless specifies sexually dimorphic neural circuitry in the *Drosophila* brain. Nature 438:229-233.

Klagges BR, Heimbeck G, Godenschwege TA, Hofbauer A, Pflugfelder GO, Reifegerste R, Reisch D, Schaupp M, Buchner S, and Buchner E. 1996. Invertebrate synapsins: a single gene codes for several isoforms in *Drosophila*. J Neurosci 16:3154-3165.

Kleineidam CJ, Obermayer M, Halbich W, and Rössler W. 2005. A macroglomerulus in the antennal lobe of leaf-cutting ant workers and its possible functional significance. Chem Senses 30:383-392.

Knüsel P, Carlsson MA, Hansson BS, Pearce TC, and Verschure PF. 2007. Time and space are complementary encoding dimensions in the moth antennal lobe. Network 18:35-62.

Kondoh Y, Kaneshiro KY, Kimura K, and Yamamoto D. 2003. Evolution of sexual dimorphism in the olfactory brain of Hawaiian *Drosophila*. Proc Biol Sci 270:1005-1013.

Kurylas AE, Rohlfing T, Krofczik S, Jenett A, and Homberg U. 2008. Standardized atlas of the brain of the desert locust, *Schistocerca gregaria*. Cell Tissue Res 333:125-145.

Kuß A, Hege HC, Krofczik S, and Borner J. 2007. Pipeline for the creation of surface-based averaged brain atlases. Proc of WSCG 1:17-24.

Kühn-Bühlmann S and Wehner R. 2006. Age-dependent and task-related volume changes in the mushroom bodies of visually guided desert ants, *Cataglyphis bicolor*. J Neurobiol 66:511-521.

Kvello P, Almaas TJ, and Mustaparta H. 2006. A confined taste area in a lepidopteran brain. Arthropod Struct Dev 35:35-45.

Lee JK and Strausfeld NJ. 1990. Structure, distribution and number of surface sensilla and their receptor cells on the olfactory appendage of the male moth *Manduca sexta*. J Neurocytol 19:519-538.

Lipscomb BW and Tolbert LP. 2006. Temporally staggered glomerulus development in the moth *Manduca sexta*. Chem Senses 31:237-247.

Liu G, Seiler H, Wen A, Zars T, Ito K, Wolf R, Heisenberg M, and Liu L. 2006. Distinct memory traces for two visual features in the *Drosophila* brain. Nature 439:551-556.

Mares S, Ash L, and Gronenberg W. 2005. Brain allometry in bumblebee and honey bee workers. Brain Behav Evol 66:50-61.

Masante-Roca I, Gadenne C, and Anton S. 2002. Plant odour processing in the antennal lobe of male and female grapevine moths, *Lobesia botrana* (Lepidoptera: Tortricidae). J Insect Physiol 48:1111-1121.

Matsumoto SG and Hildebrand JG. 1981. Olfactory Mechanisms in the Moth *Manduca sexta*: Response Characteristics and Morphology of Central Neurons in the Antennal Lobes. Proc R Soc B 213:249-277.

Mechaber WL, Capaldo CT, and Hildebrand JG. 2002. Behavioral responses of adult female tobacco hornworms, *Manduca sexta*, to hostplant volatiles change with age and mating status. J Insect Sci 2:5.

Milde JJ. 1993. Tangential medulla neurons in the moth *Manduca sexta.* Structure and reponses to optomotor stimuli. J Comp Physiol A 173:783-799.

Molina Y and O'Donnell S. 2008. Age, sex, and dominance-related mushroom body plasticity in the paperwasp *Mischocyttarus mastigophorus*. Dev Neurobiol 68:950-959.

Müller M and Wehner R. 2007. Wind and sky as compass cues in desert ant navigation. Naturwissenschaften 94:589-594.

Neder R. 1959. Allometrisches Wachstum von Hirnteilen bei drei verschieden großen Schabenarten. Zool Jb , Abt allg Zool u Physiol 77:411-467.

Nishikawa M, Nishino H, Misaka Y, Kubota M, Tsuji E, Satoji Y, Ozaki M, and Yokohari F. 2008. Sexual Dimorphism in the Antennal Lobe of the Ant *Camponotus japonicus*. Zoolog Sci 25:195-204.

Nordström K, Barnett PD, Moyer dM, I, Brinkworth RS, and O'Carroll DC. 2008. Sexual dimorphism in the hoverfly motion vision pathway. Curr Biol 18:661-667.

Pearson L. 1971. The Corpora Pedunculata of *Sphinx ligustri* L. and Other Lepidoptera: An Anatomical Study. Proc R Soc B 259:477-516.

Pfeiffer K, Kinoshita M, and Homberg U. 2005. Polarization-sensitive and light-sensitive neurons in two parallel pathways passing through the anterior optic tubercle in the locust brain. J Neurophysiol 94:3903-3915.

Pfeiffer K and Homberg U. 2007. Coding of azimuthal directions via time-compensated combination of celestial compass cues. Curr Biol 17:960-965.

Rein K, Zöckler M, Mader MT, Grübel C, and Heisenberg M. 2002. The *Drosophila* standard brain. Curr Biol 12:227-231.

Reppert SM 2006. A colorful model of the circadian clock. Cell 124:233-236.

Riffell JA, Alarcon R, Abrell L, Davidowitz G, Bronstein JL, and Hildebrand JG. 2008. Behavioral consequences of innate preferences and olfactory learning in hawkmoth-flower interactions. Proc Natl Acad Sci U S A 105:3404-3409.

Rospars JP and Hildebrand JG. 2000. Sexually dimorphic and isomorphic glomeruli in the antennal lobes of the sphinx moth *Manduca sexta*. Chem Senses 25:119-129.

Rø H, Müller D, and Mustaparta H. 2007. Anatomical organization of antennal lobe projection neurons in the moth *Heliothis virescens*. J Comp Neurol 500:658-675.

Schachtner J, Schmidt M, and Homberg U. 2005. Organization and evolutionary trends of primary olfactory brain centers in Tetraconata (Crustacea + Hexapoda). Arthropod Structure and Development 34:257-299.

Schneiderman AM, Matsumoto SG, and Hildebrand JG. 1982. Trans-sexually grafted antennae influence development of sexually dimorphic neurones in moth brain. Nature 298:844-846.

Sinakevitch I, Sjöholm M, Hansson BS, and Strausfeld NJ. 2008. Global and local modulatory supply to the mushroom bodies of the moth *Spodoptera littoralis*. Arthropod Struct Dev 37:260-272.

Sivinski J. 1989. Mushroom body development in nymphalid butterflies: A correlate of learning? Journal of Insect Behavior 2:277-283.

Sjöholm M, Sinakevitch I, Ignell R, Strausfeld NJ, and Hansson BS. 2005. Organization of Kenyon cells in subdivisions of the mushroom bodies of a lepidopteran insect. J Comp Neurol 491:290-304.

Sjöholm M, Sinakevitch I, Strausfeld NJ, Ignell R, and Hansson BS. 2006. Functional division of intrinsic neurons in the mushroom bodies of male *Spodoptera littoralis* revealed by antibodies against aspartate, taurine, FMRF-amide, Mas-allatotropin and DC0. Arthropod Struct Dev 35:153-168.

Strausfeld NJ. 1976. Atlas of an insect brain. Berlin, New York: Springer Verlag.

Strausfeld NJ. 1991. Structural organization of male-specific visual neurons in calliphorid optic lobes. J Comp Physiol [A] 169:379-393.

Strausfeld NJ. 2005. The evolution of crustacean and insect optic lobes and the origins of chiasmata. Arthropod Struct Dev 34:235-256.

Strausfeld NJ and Li Y. 1999. Organization of olfactory and multimodal afferent neurons supplying the calyx and pedunculus of the cockroach mushroom bodies. J Comp Neurol 409:603-625.

Strausfeld NJ and Hildebrand JG. 1999. Olfactory systems: common design, uncommon origins? Curr Opin Neurobiol 9:634-639.

Strauss R and Heisenberg M. 1993. A higher control center of locomotor behavior in the *Drosophila* brain. J Neurosci 13:1852-1861.

Strauss R. 2002. The central complex and the genetic dissection of locomotor behaviour. Curr Opin Neurobiol 12:633-638.

Technau GM. 2007. Fiber number in the mushroom bodies of adult *Drosophila melanogaster* depends on age, sex and experience. J Neurogenet 21:183-196.

Terada M, Kazawa T, Seki Y, and Kanzaki R. 2003. Three-dimensional reconstruction and identification of the antennal lobe glomerular structures in *Bombyx mori*. Zool Sci 20:1580.

Tolbert LP, Oland LA, Tucker ES, Gibson NJ, Higgins MR, and Lipscomb BW. 2004. Bidirectional influences between neurons and glial cells in the developing olfactory system. Prog Neurobiol 73:73-105.

Utz S, Huetteroth W, Vömel M, and Schachtner J. 2008. Mas-allatotropin in the developing antennal lobe of the sphinx moth *Manduca sexta*: distribution, time course, developmental regulation, and colocalization with other neuropeptides. Dev Neurobiol 68:123-142.

Van Essen DC and Dierker DL. 2007. Surface-based and probabilistic atlases of primate cerebral cortex. Neuron 56:209-225.

Wang Y, Mamiya A, Chiang AS, and Zhong Y. 2008. Imaging of an early memory trace in the *Drosophila* mushroom body. J Neurosci 28:4368-4376.

Weevers RD. 1966. A lepidopteran saline: effects of inorganic cation concentrations on sensory, reflex and motor responses in a herbivorous insect. J Exp Biol 44:163-175.

Wehner R. 1981. Spatial vision in arthropods. In Autrum H, editor. Handbook of Sensory Physiology. Berlin: Springer Verlag. p 471-592.

Wehner R. 1994. The polarization-vision project: championing organismic biology. Fortschr Zool 39:103–105.

Wehner R, Fukushi T, and Isler K. 2007. On being small: brain allometry in ants. Brain Behav Evol 69:220-228.

Wicklein M and Strausfeld NJ. 2000. Organization and significance of neurons that detect change of visual depth in the hawk moth *Manduca sexta*. J Comp Neurol 424:356-376.

Zeil J. 1983. Sexual dimorphism in the visual system of flies: the divided brain of male Bibionidae (Diptera). Cell Tissue Res 229:591-610.

CHAPTER VII:

A 4D representation of antennal lobe output based on an ensemble of identified projection neurons

A 4D Representation of Antennal Lobe Output Based on an Ensemble of Identified Projection Neurons

Erich M. Staudacher [a*], Wolf Huetteroth [b], Joachim Schachtner [b], Kevin C. Daly [a]

[a*] *Department of Biology, West Virginia University, Morgantown, WV, United States*
[b] *Department of Biology, Animal Physiology, Philipps-University, Marburg, Germany*

ARTICLE INFO

Keywords:
Moth
Manduca sexta L.
Olfaction
Intracellular recording and staining
Identified glomeruli
3D reconstruction
Ensemble analysis
Spike time resolution

ABSTRACT

A central problem facing studies of neural encoding in sensory systems is how to accurately quantify the extent of spatial and temporal responses. In this study, we take advantage of the relatively simple and stereotypic neural architecture found in invertebrates. We combine standard electrophysiological techniques, recently developed population analysis techniques, and novel anatomical methods to form an innovative 4-dimensional (4D) view of odor output representations in the antennal lobe of the moth *Manduca sexta*. This novel approach allows quantification of olfactory responses of identified neurons with spike time resolution. Additionally, arbitrary integration windows can be used for comparisons with other methods such as imaging. By assigning statistical significance to activity changes in neuronal firing, this method can visualize activity across the entire antennal lobe. This resulting 4D representation of antennal lobe output complements imaging and multi-unit experiments yet provides a more comprehensive and accurate glomerular activation pattern at spike time resolution.

1. Introduction

How much neural activity is necessary to encode sensory or motor information? This seemingly simple question has not been satisfactorily answered in any sensory or motor system. So far, we know that single neurons play major roles only in rare cases (Eaton and Bombardieri, 1978; Hedwig, 1996; Hedwig and Heinrich, 1997) and even then, not under all circumstances (Hedwig, 2000). In most cases, neural populations underlie sensory or motor encoding (Ruiz et al., 1995; Georgopoulos, 1996), but the necessary population size, in other words the amount of influence a single neuron exerts, is still under debate (Groh et al., 1997; Houweling and Brecht, 2008; Huber et al., 2008).

In the last decade, multi-unit recording and imaging techniques, which allow recording of ensemble activity, became widely available. Both approaches have greatly expanded our knowledge about and understanding of odor processing in the vertebrate olfactory bulb (OB) and the insect antennal lobe (AL). Imaging studies have allowed us to understand spatial aspects of odor processing. They show, that an odor consistently excites roughly same subset of glomeruli in a species specific manner (Galizia et al., 1999b; Rubin and Katz, 1999). These activation patterns differ for different odors (Friedrich and Korsching, 1997; Joerges et al., 1997; Uchida et al., 2000; Meister and Bonhoeffer, 2001; Ng et al., 2002; Wachowiak et al., 2002; Hansson et al., 2003). In most animals, both the glomerular pattern and their degrees of activation change with odor concentration (Rubin and Katz, 1999; Sachse and Galizia, 2003). The only exception seems to be the turtle, where the pattern of activated glomeruli is concentration invariant (Wachowiak et al., 2002). Usually, the percentage of glomeruli, which are activated in response to an odor stimulus, is not quantified in imaging studies, but it seems to be in the range of approximately 13-30% (Joerges et al., 1997; Uchida et al., 2000; Sachse and Galizia, 2002; Silbering and Galizia, 2007).

Recently, it has been shown for mammals and insects that olfactory receptor neurons (ORNs), which express the same receptor protein (Buck and Axel, 1991; Clyne et al., 1999; Gao and Chess, 1999; Vosshall et al., 1999), project into the same glomerulus in the primary olfactory neuropils (Mombaerts et al., 1996; Wang et al., 1998; Vosshall et al., 2000). For some insects, the glomeruli of the AL were identified early on (*Apis*: Flanagan and Mercer, 1989; *Drosophila*: Pinto et al., 1988; Stocker et al., 1990; Laissue et al., 1999; *Manduca*: Rospars and Hildebrand, 1992; Rospars

and Hildebrand, 2000). The finding that ORNs with the same receptor proteins project to the same glomeruli provides an anatomical basis for imaging studies. Furthermore, recently novel tools for anatomically correct reconstructions of brains and their neuropils have been developed. Together, they lead to the development of new reference atlases of the AL for a number of insects (*Apis*: Galizia et al., 1999a; *Drosophila*: Laissue et al., 1999; *Helicoverpa*: Berg et al., 2002; *Manduca*: Huetteroth and Schachtner, 2005).

Multi-unit recoding studies on the other hand have enhanced our understanding of the temporal aspects of odor processing. Current estimates from *Manduca sexta* ALs suggest that in response to brief stimulation (100 ms) with undiluted odors about 40% of recorded units in an ensemble are excited, about 30% are inhibited and 30% are not affected by an odor stimulus (Daly et al., 2004b). This suggests that odor-driven responses are more distributed than imaging studies imply. Ensemble responses evolve in an odor-dependent manner over time. That is, they are dynamic in that different units fire at different times and with different temporal patterns during an odor response (Laurent et al., 1996; Wehr and Laurent, 1999; Friedrich and Laurent, 2001; Stopfer et al., 2003; Daly et al., 2004b; Lei et al., 2004).

Both, imaging and multi-unit methods have, thus, added much more meaning to the conceptual term "across fiber" pattern (Pfaffmann, 1955). However, because of the inherent limitations of these methods, we still have no clear understanding of how little or how much activity is necessary to represent an odor at behaviorally defined detection thresholds and/or behaviorally relevant concentrations. Optical recording methods for example are restricted to a single 2 dimensional optical section and, thus, activity in the third dimension is not accounted for. Furthermore, the temporal resolution of optical recordings in these kinds of studies is usually about 3-5 Hz, which is too slow to resolve neural dynamics. Multiunit recordings, although revolutionizing our view of neural dynamics, do not permit a morphological identification of the recorded units and provide no, or at best limited (Lei et al., 2004) evidence about their spatial distribution. Moreover, because of physical constraints, the recorded units can only stem from a restricted area near the electrode site and, thus, typically only 10–25 units (up to 43; Daly et al., 2004b) of the approximately 1200 AL interneurons (Homberg et al., 1989) are recorded.

Therefore, we sought to complement these approaches by combining a number of established and more recent methods in a novel way. We take advantage of the very successful "identified neuron" approach in invertebrate neurobiology (e.g. Nolen and Hoy, 1984; Jacobs and Miller, 1985; Brodfuehrer and Friesen, 1986; Boehm and Schildberger, 1992; Borst and Egelhaaf, 1994; Poulet and Hedwig, 2006) by recording intracellularly from single AL projection neurons (PN) and staining each of them (e.g. Matsumoto and Hildebrand, 1981; Kanzaki et al., 1989; Anton and Hansson, 1994; Christensen et al., 1998; Kloppenburg et al., 1999; Reisenman et al., 2005). We combine this with recently advanced anatomical reconstruction methods (AMIRA; e.g. Lin et al., 2007; Rø et al., 2007) and created a 3D reference AL of *Manduca sexta* based on previously standardized 3D glomeruli (Huetteroth and Schachtner, 2005). The physiological data of all the sequentially recorded and identified PNs are combined to create a population of PNs (Georgopoulos et al., 1988), which we call a "virtual" ensemble (Skaggs and NcNaughton, 1998). Subsequently, this can be analyzed in a similar way as neural ensembles from multi-unit recordings (Stopfer et al., 2003; Daly et al., 2004b; Brown et al., 2005). The final combination of the anatomical and physiological results in a 4D representation of odor responses, which allows quantification of both the spatial and the temporal aspects of odor output representations across the AL. Previous accounts of this work have been published as abstracts (Staudacher et al., 2007a; Staudacher et al., 2007b).

2. Materials and Methods

2.1 Animals

Each of the *Manduca sexta* L. pupae received from the Arizona Research Laboratories Division of Neurobiology was placed in a separate paper bag. They were kept in an incubator (Percival Scientific, Inc.; I66VLC8) on a reversed light:dark cycle of 16:8 hours. Ambient temperature and relative humidity were kept constant at 25ºC and 75%, respectively. Every day, bags with newly eclosed moths were dated and only 3–10 day old males were used (median: 6; 1st quartile: 5; 3rd quartile: 7; N=78). To account for the nocturnal activity pattern of the moths, all experiments were performed within the first four hours of their subjective night.

2.2 Electrophysiology

The dissection followed an established protocol (Christensen and Hildebrand, 1987). In short, parts of the head capsule, all mouthparts and musculature inside the head and part of the tentorium were removed to expose the brain. Both antennal joints and antennae were left intact. The brain was superfused with *Manduca* saline throughout dissection and experiment (Heinbockel et al. 1998). A small area of the left antennal lobe was desheathed to enhance electrode penetration.

Borosilicate glass tubing (Sutter Instruments, Inc.; BF100-50-10; OD 1.0 mm, ID 0.5 mm) was pulled to form microelectrodes with a Brown-Flaming type puller (Sutter Instruments, Inc.; P-2000). Electrode tips were filled with 5% Neurobiotin in distilled water (Vector Laboratories, Inc.; SP-1120), while shoulders and part of the stems were filled with 2M potassium acetate. Connection to

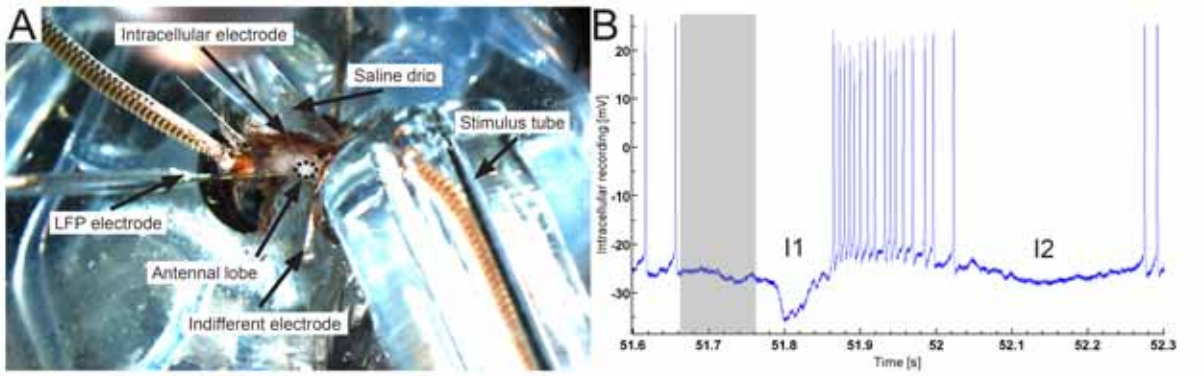

Fig. 1. (A) The photograph of the preparation shows brain with the AL, the glass tube with the left flagellum inserted and other details of the recording situation. (B) The original recording of an odor driven response of a PN shows the low spontaneous activity, a strong, high frequency response, and both I_1 and I_2 inhibition. Abbreviations: I1(2) inhibition No. 1 (2, respectively).

the amplifier was made with a silver/silver chloride (Ag/AgCl) wire, the tip of which was immersed in the potassium acetate solution. Electrode resistances were about 238 ± 48 MΩ (mean ± stdev, N=78). Another Ag/AgCl wire served as reference electrode (Fig. 1A). Neural signals were amplified in bridge mode with an Axoclamp 2B amplifier (Molecular Devices, Inc.; Fig. 1B). Intracellular recordings from neurites lasted up to 137 min with an average duration of 39 ± 29 min (mean ± stdev, N=78). Recording times longer than seven minutes were usually sufficient to passively stain the recorded neuron.

All data were recorded onto the hard disk of a personal computer with 10 kHz sampling rate (16 bit; Molecular Devices; Digidata 1440A) using Clampex (version 10.1; Molecular Devices) as software interface.

2.3 Odor stimulation

Compressed air was dried and cleaned by passing it through Drierite (W. A. Hammond Drierite, Ltd.) and activated charcoal (Sigma; C3014). The output of this filter array was then split into three lines, each of which passed through a separate three-way valve (The Lee Company; LFAA1200118H). They joined again via a 4-port stainless steel manifold, the fourth port of which was used as a common output into a glass tube. Two of the lines had custom-made odor cartridges with Luer fittings (inner diameter: 6 mm; length: 70 mm; volume: 1.5 ml) inserted between valve and glass tube. These lines were used for odor stimulation, while the third line provided a constant, blank air stream. The left flagellum was inserted into the glass tube, which had a diameter of 2 mm and was 65 mm long (Fig. 1A). Airflow through the three lines could be regulated (Cole Parmer; PMR1-01293) and was calibrated to 250 ml/min with a flow meter (Agilent Technologies; ADM100).

Odor cartridges were loaded with a strip of filter paper (Whatman International, Ltd.; No. 1), which was impregnated with 3 µl of odorant. When no stimulus was presented, the valve, which had no odor cartridge in-line was open to provide a constant airflow across the flagellum. For odor stimulation, this valve was closed, while one of the other two valves was opened simultaneously under software control (Clampex, version 10.1; Molecular Devices). Each odor presentation consisted of five 100 ms pulses per odor at neat concentration separated by 10 seconds of clean air. Neat concentration was chosen to compare the data to an earlier study (Daly et al., 2004b). To develop the method described here, we used undiluted 2-hexanone (Aldrich; 103004), 1-hexanol (Sigma; 471402), 2-octanone (Sigma; O4709), 1-octanol (Sigma; O4500), 2-decanone (Aldrich; 196207) and 1-decanol (Aldrich 150584). These odors have been used previously in behavioral studies with *M. sexta* and are known to elicit a conditioned feeding response and can be discriminated between (Daly and Smith, 2000; Daly et al., 2001a; Daly et al., 2001b).

2.4 Histology

After the experiments, the brains were fixed in 4% formaldehyde in 0.1 M Millonigs buffer (pH 7.4) for two hours at room temperature, washed with and then stored in Millonig's buffer (pH 7.4) for up to four weeks at 4ºC. Then, brains were embedded in 7.5% Agarose (Low EEO; Fisher Scientific; BP160-500) and sectioned with a vibratome (Leica; VT1000S). Free-floating sections (70 µm or 240 µm) were washed before they were incubated at 4ºC either for 20 hours with Avidin-Texas Red conjugate (Molecular Probes; A820; 70 µm) or for 40 hours with Streptavidin-CY3 conjugate (Jackson ImmunoResearch; 016-160-084; 240 µm). After washing and dehydration, the mounted sections were coverslipped with Permount (Fisher Scientific; SP15-500).

A compound microscope (Olympus; BX61) equipped with a confocal laserscanning unit (Olympus; FV1000) and controlled by the appropriate software (Olympus; FV10-ASW,

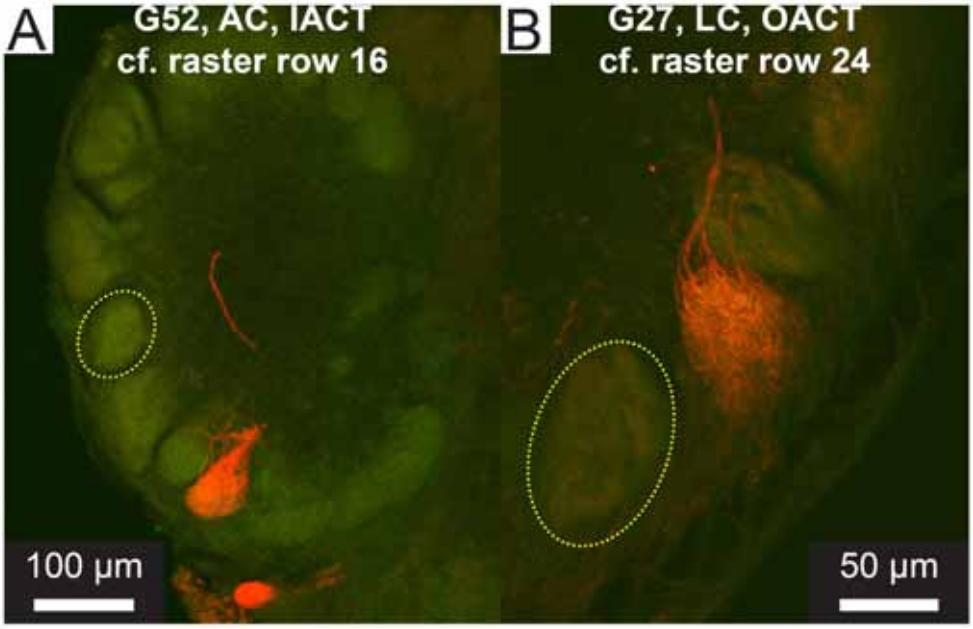

Fig. 2. (A, B) Two examples of recorded and filled projection neurons. Maximum projections show the dendritic trees of two PNs (red) and the outlines of AL glomeruli (green). Yellow dotted lines indicate the borders of two individual glomeruli. Abbreviations: AC/LC anterior/lateral soma cluster; lACT/OACT: inner/outer antennocerebral tract; G52, G27: identity of innervated glomerulus.

version 01.06b) was used to evaluate and scan the specimen. Sections were either scanned with a 10x or 20x objective (Olympus; UplanSApo 10x/0.40 or 20x/0.75, respectively) with XY pixel sizes of 1.242 or 0.621 µm/pixel and Z steps of 0.66 or 0.35 µm, respectively. Each section was simultaneously scanned at λ 488 nm and λ 543 nm to record the green autofluorescence of the brain tissue, especially the glomeruli of the antennal lobe, and the morphology of the cells in red. All data were exported as tagged image file (TIF) stacks for further analysis in AMIRA (version 4.1; Visage Imaging, Inc.). All anatomical descriptions are based on the head axis, not the embryonal neuroaxis.

2.5 Identification of glomeruli

A 3D antennal lobe reference atlas was created and subsequently used to determine, (1) in which glomerulus a PN arborized, (2) in which tract the axon was located, and (3) where the soma was located. For this, the TIF-stacks of all the sections of each brain were loaded into AMIRA and aligned in all dimensions. By using the "merge"-module of AMIRA, they were combined to one single 3D stack. Comparing this stack with the reference antennal lobe and the reconstructed ALs of Rospars and Hildebrand (1992) allowed identification of the glomeruli, in which individual PNs arborized. Antennocerebral tract identity and cell group of the recorded PN were also determined on the basis of this aligned 3D stack. The labels of identified glomeruli were false color coded according to anatomical or physiological data. Pictures of different views were taken with the snapshot tool of AMIRA.

2.6 Ensemble analysis

Physiological data were imported from Clampex (version 10.1; Molecular Devices) to Matlab (R2007a; The Mathworks, Inc.) for all analysis. As a first step, the time of occurrence of each action potential (AP) was extracted by thresholding the spike train. Ensemble raster plots are based on aligning the responses of all neurons to the same odor/concentration by stimulus onset. These aligned data sets were the basis for calculating peri-stimulus-time histograms for each trial of the seven stimuli. For every PN the 10 seconds of each trial were divided into 500 separate 20 ms bins and the number of APs per bin was counted. These AP count based data were saved for later analysis. These counts were also transformed into z-score based data sets in the following way. For every bin, the mean AP count across the trial was subtracted from the AP count of the current bin and then divided by the AP count standard deviation across the trial. The resulting z-score value expresses how many standard deviations the AP count of a given bin is above or below the mean AP count across the trial.

Euclidean distance (ED) analysis was then performed on ensemble response vectors (Stopfer et al., 2003; Daly et al., 2004b; Brown et al., 2005). EDs were calculated separately, but in the same way for AP count and z-score based data. Each data set contained one trial, had 500 columns (bins) and one row for each of the PNs. At each bin, the 19-25 different PN values (rows) define a single point in a multi-dimensional space of equal size. ED between two points of the same time bin, but different trials, is the length of a straight line between these points. ED was calculated for all time bins in pair-wise

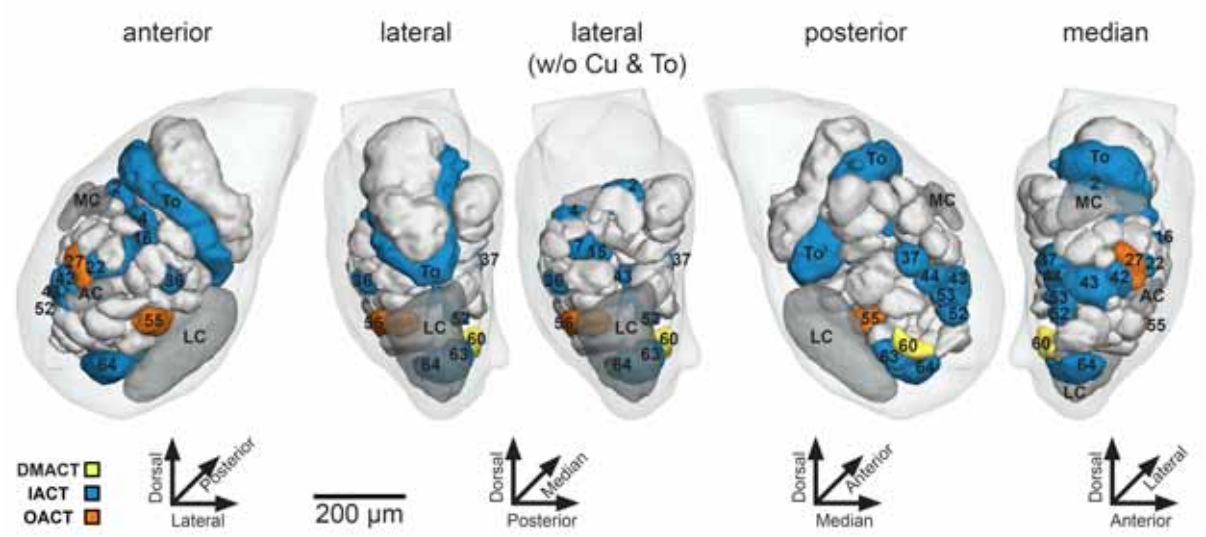

Fig. 3. Colored and numbered glomeruli in these four views of the 3D reference AL represent the locations of the dendritic trees of the uniglomerular PNs recorded and stained in this study. The three colors represent the output tracts through which the axons of these neurons leave the antennal lobe and project to the protocerebrum. Abbreviations: AC/LC/MC anterior/lateral/median soma cluster; DMACT/IACT/OACT: dorsomedian/inner/outer antennocerebral tract.

comparisons across all trials. Then, the appropriate mean ED values and standard errors were calculated and plotted.

Finally, to create a 4D activity map of antennal lobe responses to each odorant, the z-score data of each neuron were translated into a normalized color code. The colors representing the neuronal activity from identified glomeruli were then transferred to Amira and the respective glomeruli were then false color coded.

3. Results:

Of the 78 recorded neurons 29 PNs were stained successfully. Of these, the recordings of 25 neurons were complete enough to be included in this analysis. The steps towards a 4D representation of their activity across the AL were as follows: (1) each neuron was identified and the relevant morphological parameters extracted, (2) information on the glomerulus each cell arborized in was inserted into the AL map, (3) the physiological data were analyzed, and (4) the AL map was color coded based on the analysis of the physiological data.

3.1 Morphological parameter extraction

All sections containing AL structures and/or parts of the stained PN were scanned. In all cases, the recorded tissue auto-fluorescence showed the outlines of dense neuropils, e.g. glomeruli (Fig. 2A, B). The red fluorescence clearly showed the morphology and in all PNs allowed a complete reconstruction of their AL ramifications. Axon terminals in the mushroom body calyces were stained well in 14 cells, weakly in five neurons, but were not stained in six cells. Projection images of the relevant tif-stacks were usually sufficient to determine, in which cluster the soma of a PN was located and through which tract the axon projected to the protocerebrum. The somata of the 25 PNs were located in all three clusters (anterior cluster (AC): nine; lateral cluster (LC): five; medial cluster (MC): 11). Their axons ran in three tracts (dorso-medial antenno-cerebral tract (DMACT): one; inner antenno-cerebral tract (IACT): 22; inner antenno-cerebral tract (OACT): two).

However, the identification of the glomerulus, in which a given PN arborized, was only possible by using a species-specific 3D AL map (Fig. 3). For this, the tif-stacks of the relevant sections were combined. The auto-fluorescent channel of the stacks was essential to morph these data to the reference AL and to identify, in which glomerulus each PN ramified. The 25 PNs shown had dendrites in 19 of the 66 glomeruli. Two cells each arborized in glomeruli 15, 16, 36, 37, 52, and the toroid. Based on these single cell data, we created a 3D representation of these glomeruli (Fig. 3). Additionally, they were color-coded according to the tract in which the axon of a PN runs towards the protocerebrum. Fig. 3 shows that the glomeruli we recorded from are not located in one plane, but rather distributed across the entire AL. Furthermore, this representation can be viewed from all angles without loosing details. That any desired color-coding scheme can be applied easily and efficiently is important for linking physiological data to this anatomical map.

3.2 Analysis of physiological data

The raster plots in Figure 4 show that the spiking responses of single PNs and, consequently, the activity patterns of the ensemble constructed with 25 PNs change in an odor dependent manner. In all PNs that responded, an initial inhibition (I_1 inhibition) was observed (cf. Fig. 1B). This I_1

Fig. 4. Raster plots of odor dependent changes in the responses of single PNs and, consequently, of the virtual ensemble. Stimulus marker: grey vertical bar. Tables on the left side of the plots provide details on the glomerulus, in which the corresponding PN ramified in, soma cluster and output tract. Horizontal grey bars indicate specific stimuli that were not tested in a given PN. Abbreviations: AC/LC/MC anterior/lateral/median soma cluster; DMACT/IACT/OACT: dorsomedian/inner/outer antennocerebral tract.

inhibition varies in an odor dependent manner in terms of both onset latency and duration. In most cases, the stimulus-response latencies of PNs are between 160 and 220 ms of the command voltage initiating the odor valve opening, but they can be as short as 100 ms (cf. Fig. 4, 2-hexanone: cell 4: 7, AC, IACT). Spike frequency during the excitatory phase of the response was both odor and cell dependent (Fig.4). However, not all PNs responded with excitation or at all. Three of the 25 cells never responded to odor (cell 6: 15 (+25), AC; cell 19: 63, LC; cell 23: Toroid, LC; all IACT), two cells were always inhibited (cell 21: labial pit organ glomerulus (LPOG), LC, IACT; cell 25: 55 (+60), LC, OACT), and five were excited by every odor (cell 7: 16, AC; cell 12: 37, AC; cell 15: 44, MC; cell 18: 53, AC; cell 20: Discbase, MC; all IACT). Thus, about 50% of the 25 PNs were excited, 25% were inhibited and 25% remained inactive in response to an odor stimulus (11.43 ± 2.64, 5.86 ± 2.04, 6.29 ± 1.38, respectively). Excitatory responses were terminated by the so-called I_2

inhibition (Fig. 4; cf. also Fig. 1B), which is visible in the peri-stimulus raster plots as a distinct spike suppression following the excitatory response. The details of these I_2 epochs were also cell and odor dependent. Despite the fact that each cell was recorded in a different animal, all of these findings are consistent with results of multiunit experiments. Thus, constructing a virtual ensemble from single, identified neurons does not seem to introduce obvious artifacts.

Raw spike trains are, however, not suited for use in a 4D-representation of AL activity, because neuronal activity has to be comparable across PNs with very different baseline and response firing rates. Thus, the raw spike train data have to be transformed. This transformation should not change the dynamics of the neural activity patterns and should not lead to distortions of the results of subsequent analyses.

Therefore, we binned the AP train data of each cell (bin width: 20 ms) and afterwards transformed these binned data to z-score values. A comparison of the histograms of raw and z-score data showed that the dynamics of the neural responses are preserved by this transformation (data not shown). In fact, because negative z-scores are possible, inhibitory events can be detected more easily. To test whether population analysis following this transformation is distorted, we implemented a Euclidean distance (ED) analysis. This analysis also allowed us to establish how our serially recorded virtual ensemble compares to similar ensembles from multi-unit recordings (cf. Brown et al., 2005). A comparison of the AP-based (Figs 5A, B) and z-score ED (Figs 5C, D) plots shows that the peaks and troughs are preserved in a one-to-one fashion throughout. The Pearson's correlation coefficients between the AP-based and z-score-based ED curves are between 0.91 and 0.99 (all $p << 0.0001$), which suggests highly significant linear correlations. The slopes of the AP- and z-score based ED plots seem different because of the different ordinates. However, this scaling effect does not change the time course of the ED dynamics of the z-score transformed ED (cf. below). In other words, z-score based ED measures are not distorted as compared to AP based EDs. Furthermore, using standard deviations as the measurement unit makes it possible to discern significant from non-significant changes of neuronal activity, which is arbitrary if based on AP counts (Stopfer et al., 2003).

As in ensembles based on multi-unit recordings, responses to the same odor ('within odors') show low distance values. This indicates that odor-driven responses are highly consistent (Figs 5A, B). For the various comparisons between different odors (Fig. 5), the ED values increase by at least two times. There is always a brief decrease in distance between 100 and 140 ms followed by a rapid increase in ED, which starts about 120 - 140 ms after stimulus onset. The initial drop in ED reflects the initiation of I1 across the artificial population, whereas the increasing ED is consistent in response time with the odor-dependent sequence of

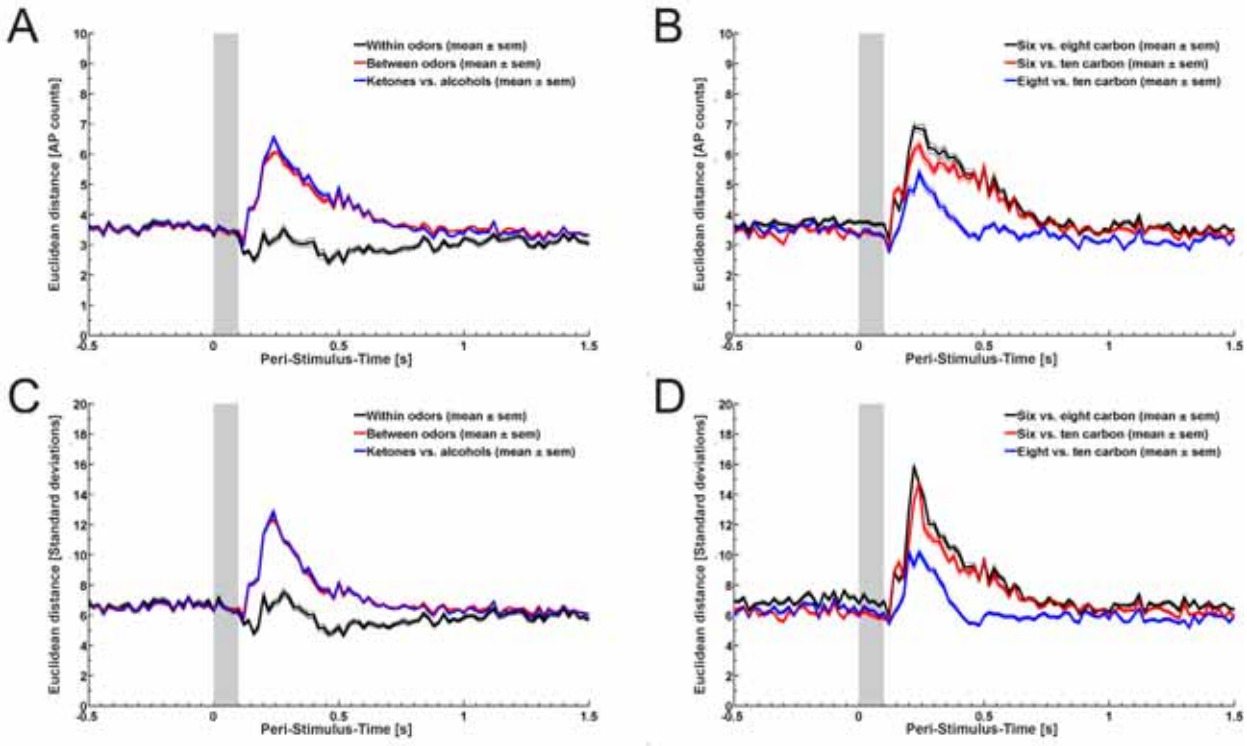

Fig. 5. Plots of ED based on binned (20 ms) AP data (A and B) and z-score transformed data (C and D) show that response dynamics is well preserved in z-score data and that this virtual ensemble could discriminate different odors very well. Stimulus marker: grey vertical bar.

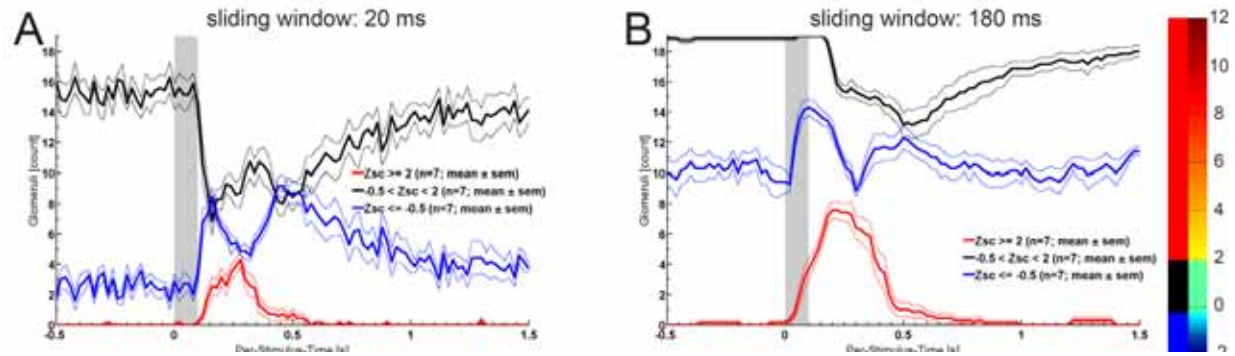

Fig. 6. z-score transformed data were used to quantify how many neurons increased, decreased or did not change their firing rate at any peri-stimulus time. For this, the normalized z-score colors-bar was broken into three appropriate regions. Data are plotted as means ± standard error of the mean (broken lines). In all cases n = 7, i.e. the blank and the six odors.

activations (cf. responses, and they decline over the subsequent 500 - 550 ms. These values are consistent with what has previously been reported for multi-unit data (Daly et al., 2004b).

3.3 Activity over time

The data have a sub-millisecond temporal resolution, which provides the opportunity to - post-hoc - compare glomerular activation patterns at different temporal resolutions. Thus, the analysis can emphasize the temporal or the spatial aspect of odor coding or any compromise between these extremes. A normalized color code makes it possible to display and to easily discern the number of positive and negative deviations from the mean firing rate (Figs. 6 and 7). In Figure 6, this color code has been further reduced to just discriminate between excitation (red: Zsc $\geq$ 2 std), inhibition (blue: Zsc $\leq$ -0.5 std) and non-significant variations in firing rate (black: -0.5 < Zsc < 2 std). Figure 6A, which emphasizes the temporal aspect, shows that up to four of the 19 glomeruli (21%) are excited per 20 ms time bin and this maximum activation is reached about 260 ms after stimulus onset (Fig. 6A red line). Because of their different response properties, not all glomeruli are simultaneously active. This means that the number of glomeruli, which are active during the whole odor response, is higher than at any one moment in response time. The blue curve shows, that 160 ms after stimulus onset about nine of the 19 glomeruli (47%) are inhibited, which can be explained by the occurrence of the I1 inhibition in a typical PN. Approximately the same number of PNs/bin is inhibited by about 450 ms, which is probably due to the I_2 inhibition. The black curve shows that in parallel with I_1, about seven PNs (37%) are not significantly excited or inhibited. At the peak of the response, nine of the 19 glomeruli (47%) are not activated at all. As expected, a longer integration window of 180 ms leads to different numbers (Fig. 6B). Here, eight of the 19 glomeruli (42%) are excited about 260 ms post stimulus onset (Fig. 6B red curve). The effects of I_1 and I_2 inhibition can still be observed (Fig. 6B blue curve). This shows that despite some smoothing by the sliding window the general dynamics of glomerular excitation/inhibition are preserved.

In the last step, we combined the 3D-AL representation of the recorded PNs (cf. Fig. 3) with the z-score transformed spike train data. This creates a 4D representation of neuronal activity. In contrast to the raster plots (Fig. 4), we can apply an objective criterion ($\geq$ 2 standard deviations) for significant activation of a glomerulus in the 4D-plots, because activity is represented by z-scores. In the normalized color code inhibition (Zsc $\leq$ -0.5 std) is marked by cool colors, excitation (Zsc $\geq$ 2 std) by warm colors, while green represents non-significant changes in firing rate (-0.5 < Zsc < 2 std). In Figure 7, maximum activity in a window of 100 ms to 400 ms after stimulus onset is shown for the 19 glomeruli recordings were obtained from. The use of such a long integration window provides a good basis for a comparison to imaging data. Glomeruli, of which two recordings are available, are represented by the activity of the PN with the more complete physiology and morphology. The long time window reveals how much of the AL is actively encoding for an odor. Figure 7 shows that glomeruli across the whole AL are, excited by, inhibited by or are not responding to odor stimulation. Currently, there is no obvious focal point of neural activity for any of the odors used. Active glomeruli are not located along single surfaces of the AL, but are found across the whole surface of the AL. Furthermore, the spatial patterns of glomerular activation are odor specific. This is obvious from a comparison of the activation patterns of some glomeruli, which are located in the posteriomedian plain. 2-hexanone elicits significant excitation in glomeruli 2, 27, 37, 43, 44, 52, 53 (plus four more out-of-view glomeruli), while glomeruli 42, 55, 60, 64 are inhibited. Stimulation with 1-hexanol leads to a different pattern. Now, glomeruli 27, 37, 43, 44 (plus four more glomeruli) are excited, while glomeruli 2, 42, 52, 53, 55, 60, and 64 are inhibited. In other words, there is an odor specific spatial code, which is distributed widely across the entire AL. Based on this

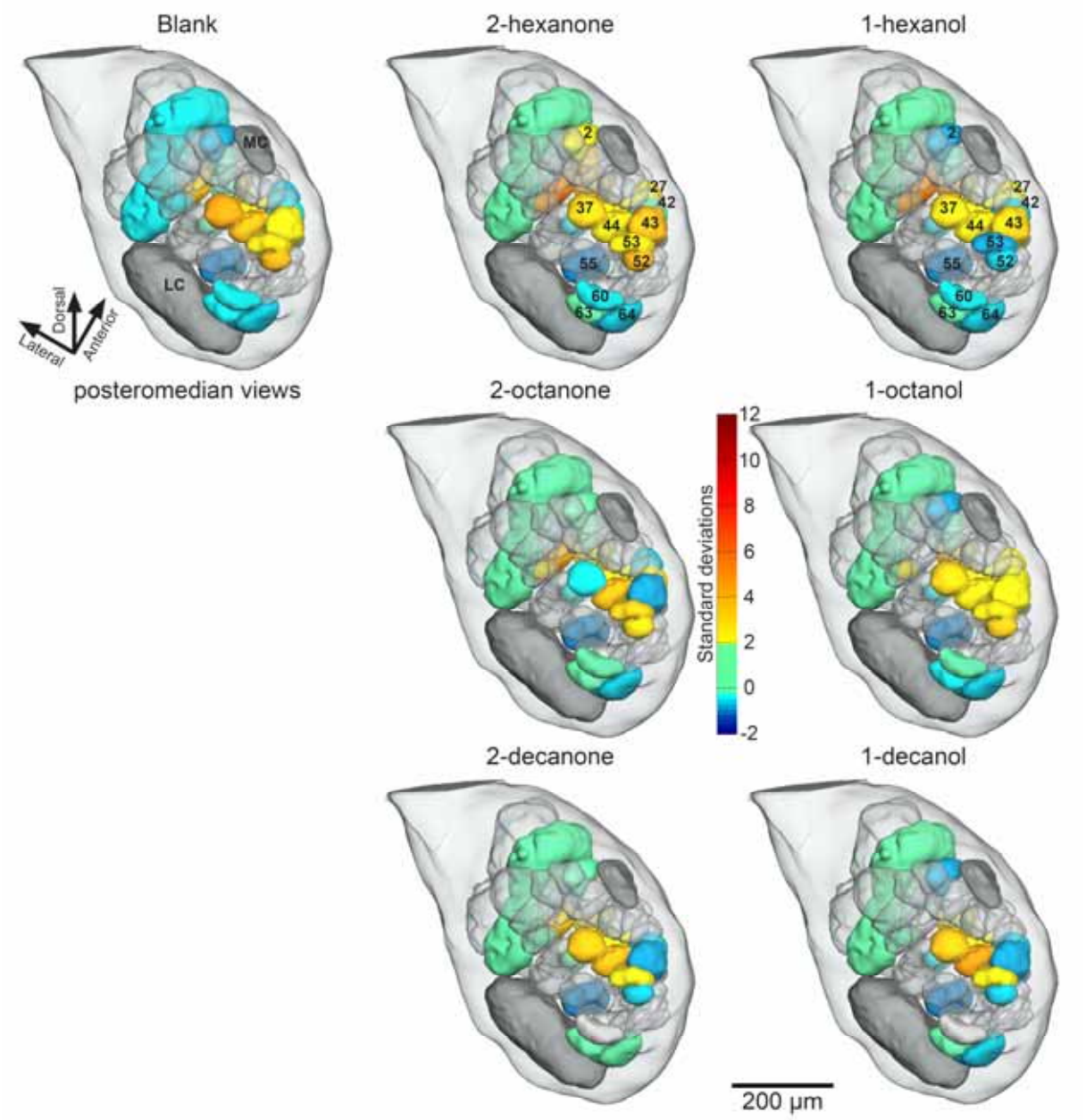

Fig. 7. Posteromedian views of the 3D reference AL show representations of stimulus driven PN activity for each condition, i.e. blank and six odors. Glomeruli are colored according to the normalized z-score colorbar. Their colors indicate the maximum z-score value for each glomerulus within the time window between 100 and 500 ms after stimulus onset. Abbreviations: LC/MC lateral/median soma cluster.

time window, which encompasses all the significant parts of the odor responses, about 47% of the 19 glomeruli are excited, 26 % inhibited and 27% do no change their activity in response to an odor. In other words, on average, about 73% of the AL actively contributes to the output code for any of the odors used.

4. Discussion

There is a gap between imaging based and multi-unit neural ensemble methods. On the one hand, imaging methods provide an indicator of the spatial distribution of neural population activity, but with limited temporal resolution. On the other hand, multi-unit methods reveal response dynamics across neural populations, but provide only very limited spatial information. The novel approach described here, is complementing imaging and multi-unit techniques. It takes advantage of the known species-specific pattern of glomeruli.

Sequentially recorded, stained and identified individual PNs are used to assign neural spiking activity to the specific glomeruli, they arborize in. Combining these serial recordings results in an output representation for each stimulus, which is visualized in the anatomical context of a newly created reference antennal lobe. Z-score transformed data preserve response dynamics and, thus, provide a good basis for further population analysis. Stimulus response dynamics of this virtual

ensemble is consistent with results from multi-unit data. The approach shown here adds spatial information for a more direct comparison with imaging methods. Therefore, this 4D representation of AL responses provides a meaningful tool to analyze odor output coding in primary olfactory neuropil.

4.1 Comparison to other techniques

Extracellular multi-site and multi-unit recording techniques have been used in a variety of vertebrate and invertebrate systems with great success (e.g. Wilson and McNaughton, 1993; Henze et al., 2000; Wessberg et al., 2000; Chapin, 2004; Daly et al., 2004a; Brown et al., 2005; Mazor and Laurent, 2005). Spike sorting allows classification of events based on a multitude of criteria and to form so-called units. However, the error rates of spike sorting depend on many physical, physiological, and other factors and can be rather high (Harris et al., 2000). Furthermore, except in locusts (Laurent and Davidowitz, 1994), most local interneurons in insect ALs produce sodium spikes (Christensen et al., 1993; Anton and Homberg, 1999; Wilson et al., 2004; Wilson and Laurent, 2005). Moreover, like LNs (Christensen et al., 1993), PNs can have short stimulus-response latencies (e.g. Fig. 4, raster #4: 7 AC IACT). These factors increase the difficulty of discriminating between PNs and LNs or subpopulations of these two major classes (Matsumoto and Hildebrand, 1981; Christensen et al., 1993; Anton and Homberg, 1999), because the cells actually recorded from are not stained in multi-unit experiments. However, only PN activity is read-out by and, thus, significant for higher brain centers. Thus, because multi-unit recordings represent both local processing (LN) and output (PN) activity in most insects except locusts, interpreting the significance and meaning of output by using extracellular methods is challenging. The new approach reported here, overcomes these limitations of extracellular recording, because each neuron is precisely classified and there is no issue of contamination or missing APs.

Neural activity can be optically recorded with voltage-sensitive dyes, Ca^{2+} sensitive dyes, by utilizing intrinsic signals or when synaptopHluorin is expressed by the targeted cells. These methods are used to study single cells (e.g. Single and Borst, 1998) and populations of neurons (e.g. Bonhoeffer and Grinvald, 1993; Shang et al., 2007). Ca^{2+}-imaging has been most prevalent in olfaction research (e.g. Friedrich and Korsching, 1997; Joerges et al., 1997; Wachowiak et al., 2002; Hansson et al., 2003; Spors et al., 2006; Silbering and Galizia, 2007). For this, the tissue is usually superfused with dye, which is taken up into cells over a preparation-specific staining period. It is, however, not known, which cells take the dye up and if this uptake occurs evenly across the preparation and the different cell types. Furthermore, when imaging large regions of neuropil, it is not possible to resolve individual unit activity patterns; this is true even when dye loading is restricted to a specific subpopulation (e.g. Sachse and Galizia, 2003). In all imaging systems, the light sensor, mostly a CCD camera, samples light from a relatively thin section within the tissue, i.e. the focal plane plus light from the depth of field and some scattered light. This works well in planar neuropils like parts of the olfactory bulb in vertebrates, but has limits in 3-dimensional structures like the insect AL. As Fig. 7 shows, a significant number of odor-activated glomeruli would be missed, if only a single plane of the AL were considered.

The fluorescent signals are usually very small, which means that light has to be sampled over relatively long periods of time. Therefore, with only few exceptions (Wachowiak et al., 2002; Spors et al., 2006; Wesson et al., 2008), the temporal resolution of Ca^{2+}-imaging experiments is usually not higher than 3-5 Hz when large neuropil areas are imaged. In other words, the temporal resolution of imaging techniques is two orders of magnitude slower than an action potential. As a corollary, odor driven glomerular activation patterns may seem similar based on the integration by the imaging technique. Furthermore, if the I_1 and I_2 phases are integrated with a brief excitatory response when using Ca^{2+} imaging, it may be possible to miss meaningful excitatory responses. In some circumstances, it may be possible that brief excitatory responses, which are flanked by I_1 and I_2 phases, may actually appear as suppression using these methods. Thus, because temporal dynamics of the neural response are not resolved well, differences in the sequence of glomerular activation may be invisible and, thus, missed in an interpretation of the results. In contrast to Ca^{2+}-imaging, the approach introduced here, works on a sub-millisecond temporal resolution, is not limited to a small volume around one focal plane, and is based on identifying each cell of a virtual ensemble.

The new approach shown here is complementary to imaging and multi-unit techniques and, like other methods, has a number of limitations. One is, that data from a serially recorded virtual ensemble cannot be used for studies on synchronous firing of populations of neurons, because there is no synchronous neural activity across animals. For the same reason, this method does not provide a means to quantify the relationship between population spiking and local field potentials. In addition, we make assumptions that should be clarified as well. For example, that stimulus delivery is precise and consistent between animals. To address this issue, we made certain that the velocity of airflow and distance from the odor cartridges to the antennae were identical across preparations. Nevertheless variability in delivery between preparations could introduce a small amount of variability in response latencies. But given that the delay from odor valve opening to the odor reaching the base of the antenna is on the order of 10 ms we estimate this

contribution to variability to be nominal. One indicator of stimulus consistency is that we observe little inter-trial variability in the responses of single PNs. Another assumption this approach makes is that the response latencies of cells, which arborize in the same glomerulus, but are recorded in different animals, are the same. The ultimate test of this assumption would require to record the same identified neuron in different animals, which is fairly difficult. However, when we consider the time course of odor-driven population responses from multiunit studies we find no difference, suggesting that between animal variability is minimal. Finally, from a practical standpoint, a serial reconstruction based on single cell recordings is not feasible in olfactory systems with a large number of glomeruli like in mammals.

4.2 Neural activity across the AL

The virtual ensemble shown here has a response dynamic that is essentially identical to what has been reported for multi-unit data. Odor responses evolve in time; that is, different PNs, which can be equated to identified glomeruli in this study, respond with different onset latencies and different PNs fire with different odor-dependent patterns (e.g. Daly et al., 2004b; Brown et al., 2005). ED analysis (Fig. 5) shows that odor representations evolve dramatically over time, producing unique output codes, which presumably contribute to unique odor representations and hence discrimination. About 100 ms after stimulus on31 set, ED briefly dips, then rapidly increases, reaching a peak within an additional about 140 ms, and then declines over about 500 ms. This time course is very similar to what has been reported for extracellular multi-unit data (Daly et al., 2004b; Brown et al., 2005). The large increase in z-score by four or more standard deviations is significant and indicates that this virtual ensemble could discriminate very well between classes of odorants (ketones vs. alcohols) and single odors of the same moiety that differ only in carbon chain length.

Our new approach allows the correlation of the temporal dynamics produced by action potentials with a 3D spatial perspective. We find that per response, about 47% of the glomeruli are excited, about 26% are inhibited, and about 27% do not change activity. These figures roughly match with previously reported distributions of excited, inhibited and unchanged units in multi-unit recordings (Daly et al., 2004b). Now, we can, however, relate these figures to the activity distribution across the AL. If one extrapolates this finding, it would mean that actually about 48 glomeruli of the 63 of an AL are actively involved in coding for a particular odor, 32 of them excited and 16 inhibited. This would contrast strongly with the results of imaging studies, which indicate that only about 13-30% of the glomeruli are actively involved in odor coding (Joerges et al., 1997; Uchida et al., 2000; Sachse and Galizia, 2002; Silbering and Galizia, 2007).

Why is the identity of the glomerulus important in regard with PNs? It was indicated by Buck and Axel (1991) and later shown (Mombaerts et al., 1996; Wang et al., 1998; Vosshall et al., 2000) that ORNs expressing the same receptor protein project to the same glomerulus. This seems to indicate that each glomerulus is not just an anatomically, but, based on ORN identity, a functionally distinct entity. Recently, it was shown that PNs have a broader odor tuning than the ORNs they are connected to (Wilson et al., 2004). This finding suggested the existence of excitatory connections between glomeruli by local excitatory interneurons, which were recently described (Olsen et al., 2007; Shang et al., 2007). Odor responses are, furthermore, shaped by interglomerular presynaptic inhibition (Olsen and Wilson, 2008). Because of these lateral interactions between different glomeruli of the AL, it follows that the more precise descriptor for any PN is the glomerulus it arborizes in and not the ORN it is connected with. The approach shown here accounts for this, because it takes advantage of the 3D reconstructed reference AL atlas and uses the identified PNs as a basis for identifying their respective glomeruli.

Along these lines, should odor responses of the approximately 14 PNs arborizing in the same glomerulus (66 glomeruli, 900 PNs; Anton and Homberg, 1999) not be identical? For six of the glomeruli two PNs were recorded in this study. Within these PN pairs, the responses to the blank and the six odors differ in most but not all cases. Differences in odor responses of PNs from the same glomerulus have been described in earlier studies too (Roche King et al., 2000; Sadek et al., 2002; Guerenstein et al., 2004; Masante-Roca et al., 2005). These results contrast with findings that PNs from the same glomerulus have very similar response properties (Reisenman et al., 2005) and also with the fact that the probability that they fire in synchrony is increased (Schoppa and Westbrook, 2001; Lei et al., 2002). To resolve the issue of how similar PNs are, which arborize in the same glomerulus, one would need to record the same identified neuron(s) in different animals.

In conclusion, the new approach shown herein will also contribute to clarifying this issue and, thus, contribute to a further understanding of odor encoding. As our database of cell reconstructions grows, it will allow exploration of whole AL responses to different odor as a function of various stimulus parameters, such as concentration and duration. This database will also provide unique opportunities to perform more focused population analyses of specific subpopulations of PNs based on morphological characteristics, such as differences between distinct cell clusters, and output tracks. This will allow us a deeper understanding of the functional role of multiple output cell types and

pathways, which are found in both vertebrates and invertebrates. Finally, future studies will match psychophysical experiments, which characterize detection and discrimination thresholds in this species, to the dynamic response patterns of a virtual ensemble of identified neurons. These data will be correlated with biologically relevant concentrations and sensory limits of the model system.

Acknowledgements
We thank Drs. Aric Agmon and Matt Wachowiak for discussions and comments on the manuscript. Oakland Peters helped translating the Clampex data format to Matlab format. Brittany L. Fredericks and Herbert L. Parsons helped with the histology and confocal imaging of some neurons. We are grateful to Drs. Thomas A. Christensen, Alan Nighorn and John G. Hildebrand of the Arizona Research Laboratories Division of Neurobiology for supplying animals. This work was supported by the following grants: NIH-NCRR RR015574 to KCD, NIH-NIDCD DC005652-04 to TAC, and DFG grant SCHA 678/3-3 to JS.

References

Anton S, Hansson BS. Central processing of sex-pheromone, host odor, and oviposition deterrent information by interneurons in the antennal lobe of female *Spodoptera littoralis* (Lepidoptera, Noctuidae). Journal of Comparative Neurology 1994; 350: 199-214.

Anton S, Homberg U. Antennal lobe structure. In Hansson BS, editor. Insect olfaction. Springer: Berlin ; New York, 1999; 97-124.

Berg BG, Galizia CG, Brandt R, Mustaparta H. Digital atlases of the antennal lobe in two species of tobacco budworm moths, the oriental *Helicoverpa assulta* (male) and the american *Heliothis virescens* (male and female). Journal of Comparative Neurology 2002; 446: 123-34.

Boehm H, Schildberger K. Brain neurons involved in the control of walking in the cricket *Gryllus bimaculatus*. J Exp Biol 1992; 166: 113-30.

Bonhoeffer T, Grinvald A. The layout of iso-orientation domains in area-18 of cat visual-cortex - optical imaging reveals a pinwheel-like organization. Journal of Neuroscience 1993; 13: 4157-80.

Borst A, Egelhaaf M. Dendritic processing of synaptic signals by sensory interneurons. Trends Neurosci 1994; 17: 257-63.

Brodfuehrer PD, Friesen WO. Initiation of swimming activity by trigger neurons in the leech subesophageal ganglion ii. Role of segmental swim-initiating interneurons. Journal of Comparative Physiology A Sensory Neural & Behavioral Physiology 1986; 159: 503-10.

Brown SL, Joseph J, Stopfer M. Encoding a temporally structured stimulus with a temporally structured neural representation. Nature Neuroscience 2005; 8: 1568-76.

Buck L, Axel R. A novel multigene family may encode odorant receptors – a molecular-basis for odor recognition. Cell 1991; 65: 175-87.

Chapin JK. Using multi-neuron population recordings for neural prosthetics.Nature Neuroscience 2004; 7: 452-5.

Christensen TA, Waldrop BR, Harrow ID, Hildebrand JG. Local interneurons and information-processing in the olfactory glomeruli of the moth *Manduca sexta*. Journal of Comparative Physiology A Sensory Neural and Behavioral Physiology 1993; 173: 385-99.

Christensen TA, Waldrop BR, Hildebrand JG. Multitasking in the olfactory system: Context-dependent responses to odors reveal dual GABA-regulated coding mechanisms in single olfactory projection neurons. Journal of Neuroscience 1998; 18: 5999-6008.

Clyne PJ, Warr CG, Freeman MR, Lessing D, Kim J, Carlson JR. A novel family of divergent seven-transmembrane proteins: Candidate odorant receptors in *Drosophila*. Neuron 1999; 22: 327-38.

Daly KC, Chandra S, Durtschi ML, Smith BH. The generalization of an olfactory-based conditioned response reveals unique but overlapping odour representations in the moth *Manduca sexta*. Journal of Experimental Biology 2001a; 204: 3085-95.

Daly KC, Christensen TA, Lei H, Smith BH, Hildebrand JG. Learning modulates the ensemble representations for odors in primary olfactory networks. PNAS 2004a; 101: 10476-81.

Daly KC, Durtschi ML, Smith BH. Olfactory-based discrimination learning in the moth, *Manduca sexta*. Journal of Insect Physiology 2001b; 47: 375-84.

Daly KC, Smith BH. Associative olfactory learning in the moth *Manduca sexta*. Journal of Experimental Biology 2000; 203: 2025-38.

Daly KC, Wright GA, Smith BH. Molecular features of odorants systematically influence slow temporal responses across clusters of coordinated antennal lobe units in the moth *Manduca sexta*. Journal of Neurophysiology 2004b; 92: 236-54.

Eaton RC, Bombardieri RA. Behavioral functions of the Mauthner neuron. In Faber DS, Korn H, editors. Neurobiology of the Mauthner cell. Raven Press: New York, 1978; 221-44.

Flanagan D, Mercer AR. An atlas and 3-D reconstruction of the antennal lobes in the worker honey bee, *Apis mellifera* (Hymenoptera, Apidae). International Journal of Insect Morphology & Embryology 1989; 18:145-59.

Friedrich RW, Korsching SI. Combinatorial and chemotopic odorant coding in the zebrafish olfactory bulb visualized by optical imaging. Neuron 1997; 18: 737-52.

Friedrich RW, Laurent G. Dynamic optimization of odor representations by slow temporal patterning of mitral cell activity. Science 2001; 291: 889-94.

Galizia CG, McIlwrath SL, Menzel R. A digital three-dimensional atlas of the honeybee antennal lobe based on optical sections acquired by confocal microscopy. Cell & Tissue Research 1999a; 295: 383-94.

Galizia CG, Sachse S, Rappert A, Menzel R. The glomerular code for odor representation is species specific in the honeybee *Apis mellifera*. Nature Neuroscience 1999b; 2: 473-8.

Gao Q, Chess A. Identification of candidate *Drosophila* olfactory receptors from genomic DNA sequence. Genomics 1999; 60: 31-9.

Georgopoulos AP. Arm movements in monkeys: Behavior and neurophysiology. J Comp Physiol A 1996; 179: 603-12.

Georgopoulos AP, Kettner RE, Schwartz AB. Primate motor cortex and free arm movements to visual targets in three-dimensional space. Ii. Coding of the direction of movement by a neuronal population. J Neurosci 1988; 8: 2928-37.

Groh JM, Born RT, Newsome WT. How is a sensory map read out? Effects of microstimulation in visual area mt on saccades and smooth pursuit eye movements. J Neurosci 1997; 17: 4312-30.

Guerenstein PG, Christensen TA, Hildebrand JG. Sensory processing of ambient CO2 information in the brain of the moth *Manduca sexta*. Journal of Comparative Physiology A Neuroethology Sensory Neural and Behavioral Physiology 2004; 190: 707-25.

Hansson BS, Carlsson MA, Kalinova B. Olfactory activation patterns in the antennal lobe of the sphinx moth, *Manduca sexta*. Journal of Comparative Physiology A Neuroethology Sensory Neural and Behavioral Physiology 2003; 189: 301-8.

Harris KD, Henze DA, Csicsvari J, Hirase H, Buzsaki G. Accuracy of tetrode spike separation as determined by simultaneous intracellular and extracellular measurements. J Neurophysiol 2000; 84: 401-14.

Hedwig B. A descending brain neuron elicits stridulation in the cricket *Gryllus bimaculatus* (de Geer). Naturwissenschaften 1996; 83: 428-9.

Hedwig B. Control of cricket stridulation by a command neuron: Efficiacy depends on behavioral state. J Neurophysiol 2000; 83: 712-22.

Hedwig B, Heinrich R. Identified descending brain neurons control different stridulatory motor patterns in an acridid grasshopper. J Comp Physiol A 1997; 180: 285-94.

Henze DA, Borhegyi Z, Csicsvari J, Mamiya A, Harris KD, Buzsaki G. Intracellular features predicted by extracellular recordings in the hippocampus in vivo. J Neurophysiol 2000; 84: 390-400.

Homberg U, Christensen TA, Hildebrand JG. Structure and function of the deutocerebrum in insects. In Mittler TE, editor. Ann Rev Entomol. Annual Reviews Inc: Palo Alto, California, USA, 1989; 34: 477-501.

Houweling AR, Brecht M. Behavioural report of single neuron stimulation in somatosensory cortex. Nature 2008; 451: 65-8.

Huber D, Petreanu L, Ghitani N, Ranade S, Hromadka T, Mainen Z, Svoboda K. Sparse optical microstimulation in barrel cortex drives learned behaviour in freely moving mice. Nature 2008; 451: 61-4.

Huetteroth W, Schachtner J. Standard three-dimensional glomeruli of the *Manduca sexta* antennal lobe: A tool to study both developmental and adult neuronal plasticity. Cell and Tissue Research 2005; 319: 513-24.

Jacobs GA, Miller JP. Functional properties of individual neuronal branches isolated in-situ by laser photoinactivation. Science 1985; 228: 344-6.

Joerges J, Kuettner A, Galizia GC, Menzel R. Representations of odours and odour mixtures visualized in the honeybee brain. Nature 1997; 387: 285-8.

Kanzaki R, Arbas EA, Strausfeld NJ, Hildebrand JG. Physiology and morphology of projection neurons in the antennal lobe of the male moth *Manduca sexta*. Journal of Comparative Physiology A Sensory Neural & Behavioral Physiology 1989; 165: 427-53.

Kloppenburg P, Ferns D, Mercer AR. Serotonin enhances central olfactory neuron responses to female sex pheromone in the male sphinx moth *Manduca sexta*. Journal of Neuroscience 1999; 19: 8172-81.

Laissue PP, Reiter C, Hiesinger PR, Halter S, Fischbach KF, Stocker RF. Three-dimensional reconstruction of the antennal lobe in *Drosophila melanogaster*. J Comp Neurol 1999; 405: 543-52.

Laurent G, Davidowitz H. Encoding of olfactory information with oscillating neural assemblies. Science 1994; 265: 1872-5.

Laurent G, Wehr M, Davidowitz H. Temporal representations of odors in an olfactory network. Journal of Neuroscience 1996; 16: 3837-47.

Lei H, Christensen TA, Hildebrand JG. Local inhibition modulates odor-evoked synchronization of glomerulus-specific output neurons. Nature Neuroscience 2002; 5: 557-65.

Lei H, Christensen TA, Hildebrand JG. Spatial and temporal organization of ensemble representations for different odor classes in the moth antennal lobe. Journal of Neuroscience 2004; 24: 11108-19.

Lin HH, Lai JSY, Chin AL, Chen YC, Chiang AS. A map of olfactory representation in the *Drosophila* mushroom body. Cell 2007; 128: 1205-17.

Masante-Roca I, Gadenne C, Anton S. Three-dimensional antennal lobe atlas of male and female moths, *Lobesia botrana* (Lepidoptera: Tortricidae) and glomerular representation of plant volatiles in females. J Exp Biol 2005; 208: 1147-59.

Matsumoto SG, Hildebrand JG. Olfactory mechanisms in the moth *Manduca sexta*: Response characteristics and morphology of central neurons in the antennal lobe. Proc R Soc Lond B 1981; 213: 249-77.

Mazor O, Laurent G. Transient dynamics versus fixed points in odor representations by locust antennal lobe projection neurons. Neuron 2005; 48: 661-73.

Meister M, Bonhoeffer T. Tuning and topography in an odor map on the rat olfactory bulb. Journal of Neuroscience 2001; 21: 1351-60.

Mombaerts P, Wang F, Dulac C, Chao SK, Nemes A, Mendelsohn M, Edmondson J, Axel R. Visualizing an olfactory sensory map. Cell 1996; 87: 675-86.

Ng M, Roorda RD, Lima SQ, Zemelman BV, Morcillo P, Miesenböck G. Transmission of olfactory information between three populations of neurons in the antennal lobe of the fly. Neuron 2002; 36: 463-74.

Nolen TG, Hoy RR. Initiation of behavior by single neurons: The role of behavioral context. Science 1984; 226: 992-4.

Olsen SR, Bhandawat V, Wilson RI. Excitatory interactions between olfactory processing channels in the *Drosophila* antennal lobe. Neuron 2007; 54: 89-103.

Olsen SR, Wilson RI. Lateral presynaptic inhibition mediates gain control in an olfactory circuit. Nature 2008; 452: 956-60.

Pfaffmann C. Gustatory nerve impulses in rat cat and rabbit. J Neurophysiol 1955; 18: 429-40.

Pinto L, Stocker RF, Rodrigues V. Anatomical and neurochemical classification of the antennal glomeruli in *Drosophila melanogaster* Meigen (diptera : Drosophilidae). Int J Insect Morphol Embryol 1988; 17: 335-44.

Poulet JFA, Hedwig B. The cellular basis of a corollary discharge. Science 2006; 311: 518-22.

Reisenman CE, Christensen TA, Hildebrand JG. Chemosensory selectivity of output neurons innervating an identified, sexually isomorphic olfactory glomerulus. Journal of Neuroscience 2005; 25: 8017-26.

Rø H, Müller D, Mustaparta H. Anatomical organization of antennal lobe projection neurons in the moth *Heliothis virescens*. J Comp Neurol 2007; 500: 658-75.

Roche King J, Christensen TA, Hildebrand JG. Response characteristics of an identified, sexually dimorphic olfactory glomerulus. Journal of Neuroscience 2000; 20: 2391-9.

Rospars JP, Hildebrand JG. Anatomical identification of glomeruli in the antennal lobes of the male sphinx moth *Manduca sexta*. Cell & Tissue Res 1992; 270: 205-27.

Rospars JP, Hildebrand JG. Sexually dimorphic and isomorphic glomeruli in the antennal lobes of the sphinx moth *Manduca sexta*. Chemical Senses 2000; 25: 119-29.

Rubin BD, Katz LC. Optical imaging of odorant representations in the mammalian olfactory bulb. Neuron 1999; 23: 499-511.

Ruiz S, Crespo P, Romo R. Representation of moving tactile stimuli in the somatic sensory cortex of awake monkeys. J Neurophysiol 1995; 73: 525-37.

Sachse S, Galizia CG. Role of inhibition for temporal and spatial odor representation in olfactory output neurons: A calcium imaging study. Journal of Neurophysiology 2002; 87: 1106-17.

Sachse S, Galizia CG. The coding of odour-intensity in the honeybee antennal lobe: Local computation optimizes odour representation. European Journal of Neuroscience 2003; 18: 2119-32.

Sadek MM, Hansson BS, Rospars JP, Anton S. Glomerular representation of plant volatiles and sex pheromone components in the antennal lobe of the female *Spodoptera littoralis*. Journal of Experimental Biology 2002; 205: 1363-76.

Schoppa NE, Westbrook GL. Glomerulus-specific synchronization of mitral cells in the olfactory bulb. Neuron 2001; 31: 639-51.

Shang Y, Claridge-Chang A, Sjulson L, Pypaert M, Miesenbock G. Excitatory local circuits and their implications for olfactory processing in the fly antennal lobe. Cell 2007; 128: 601-12.

Silbering AF, Galizia CG. Processing of odor mixtures in the *Drosophila* antennal lobe reveals both global inhibition and glomerulus-specific interactions. J Neurosci 2007; 27: 11966-77.

Single S, Borst A. Dendritic integration and its role in computing image velocity. Science 1998; 281: 1848-50.

Skaggs WE, NcNaughton BL. Neuronal ensemble dynamics in hippocampus and neocortex during sleep and waking. In Eichenbaum H, Davis JL, editors. Neuronal ensembles: Strategies for recording and decoding. Wiley-Liss: New York, 1998; x, 267 p.

Spors H, Wachowiak M, Cohen LB, Friedrich RW. Temporal dynamics and latency patterns of receptor neuron input to the olfactory bulb. J Neurosci 2006; 26: 1247-59.

Staudacher EM, Huetteroth W, Parsons HL, Schachtner J, Daly KC. Glomerular response mapping using virtual projection neuron populations: A step towards representing whole antennal lobe activity in realtime; 2007a; Sarasota, FL. AChemS. p 410.

Staudacher EM, Huetteroth W, Schachtner J, Daly K. Ensemble analysis of projection neurons from identified glomeruli in the moth *Manduca sexta*: Towards a 4D representation of odor processing in a virtual antennal lobe; 2007b; San Diego, CA. Society for Neuroscience. p 612.15/LL16.

Stocker RF, Lienhard MC, Borst A, Fischbach KF. Neuronal architecture of the antennal lobe in *Drosophila melanogaster*. Cell Tissue Res 1990; 262: 9-34.

Stopfer M, Jayaraman V, Laurent G. Intensity versus identity coding in an olfactory system. Neuron 2003; 39: 991-1004.

Uchida N, Takahashi YK, Tanifuji M, Mori K. Odor maps in the mammalian olfactory bulb: Domain organization and odorant structural features. Nature Neuroscience 2000; 3: 1035-43.

Vosshall LB, Amrein H, Morozov PS, Rzhetsky A, Axel R. A spatial map of olfactory receptor expression in the *Drosophila* antenna. Cell 1999; 96: 725-36.

Vosshall LB, Wong AM, Axel R. An olfactory sensory map in the fly brain. Cell 2000; 102: 147-59.

Wachowiak M, Cohen LB, Zochowski MR. Distributed and concentration-invariant spatial representations of odorants by receptor neuron input to the turtle olfactory bulb. Journal of Neurophysiology 2002; 87: 1035-45.

Wang F, Nemes A, Mendelsohn M, Axel R. Odorant receptors govern the formation of a precise topographic map. Cell 1998; 93: 47-60.

Wehr M, Laurent G. Relationship between afferent and central temporal patterns in the locust olfactory system. Journal of Neuroscience 1999; 19: 381-90.

Wessberg J, Stambaugh CR, Kralik JD, Beck PD, Laubach M, Chapin JK, Kim J, Biggs J, Srinivasan MA, Nicolelis MAL. Real-time prediction of hand trajectory by ensembles of cortical neurons in primates. Nature 2000; 408: 361-5.

Wesson DW, Carey RM, Verhagen JV, Wachowiak M. Rapid encoding and perception of novel odors in the rat. PLoS Biology 2008; 6: e82.

Wilson MA, McNaughton BL. Dynamics of the hippocampal ensemble code for space. Science 1993; 261: 1055-8.

Wilson RI, Laurent G. Role of gabaergic inhibition in shaping odor-evoked spatiotemporal patterns in the *Drosophila* antennal lobe. Journal of Neuroscience 2005; 25: 9069-79.

Wilson RI, Turner GC, Laurent G. Transformation of olfactory representations in the *Drosophila* antennal lobe. Science 2004; 303: 366-70.

DANKSAGUNG

Vielen Leuten gilt es zu danken:

Vorneweg Joachim Schachtner, meinem Betreuer und Doktorvater. Wir haben zusammen viel durchgemacht!

Uwe Homberg, der nicht nur bereitwillig die Zweitkorrektur übernahm, sondern auch sonst jederzeit gesprächsbereit war und viele wichtige Anregungen gab.

Monika Stengl und Christian Wegener, die die Chefriege abrundeten und immer mit Rat zur Seite standen.

Roland Brandl und Renate Renkawitz-Pohl, die freundlicherweise die Prüfungskommission vervollständigten.

Den Leuten der ersten Stunde bei denen ich viel lernte, z.B. die Wichtigkeit von 11:30 Uhr:
Björn Trosowski, Rudi Lösel, Jan Dolzer, Thomas Reischig, Michael Niehaus, Stephan Gebhardt, Sabine Hofer und Lucia Lennartz.

Der Boom-Crew, mit der es in jeder Hinsicht so richtig losging:
1000eram Pfeiffer (mieser kleiner...), Sandra Söhler, Sandra Utz (KONNichiwa Ützelsche, beschte Mit-Doktorandin!), Nils-Lasse Schneider, Martina Mappes, Jana Zimmermann, Julia ehem. Fischer, Wolfgang d'Hanis, Felix Scholz, Patrick Winterhagen, Angela Kurylas (dearest room mate!), Christian Flecke, Steffi Krannich, Matthias Vömel, Eva-Maria Rink, Karin Müller und Sabine Jesberg.

Ehemaligen und aktuellen AG-Mitgliedern, die vieles erleichtert haben, nicht nur den Arbeitsalltag. Insbesondere gilt mein Dank Achim Werckenthin, Nico Funk (der Super-Spreader), Julia Schuckel, Stanley Heinze, Ulrike Träger, Frauke Kepura, und Dominik Schumann.

Den guten Seelen im Labor: Jutta Seyfarth, Martina Kern, Conny Ellendt und Thorsten Bauschke.

„Meinen" Jungs, die sich nicht nur durch ihren Arbeitseinsatz jeweils einzelne Zeilen verdient haben. Es war ein langer Weg vom Love Lab zur Kompetenzzentrale!

Basil el Jundi,
David Dreyer,
Martin Kollmann,
Stefan Dippel.

Brigitte Götz, die die Kompetenzfiliale dank Augschburger Charisma überlebte. Keine ist härter…

Michiyo Kinoshita und Bente Berg, die internationales Flair nach Marburg brachten - Ryohei Kanzaki und Ryota Fukushima für ihre Gastfreundschaft und Hilfe in Tokyo - Reinhard Predel und Susanne Neupert u.a. dafür, mal richtiger Biologe sein zu dürfen - Petra Schachtner und den Wickelkindern – Claudio für vielerlei Support - der Felsenhof AG und den Kanupolo-Spielern für die Welt neben der Uni - meinen WGs, insbesondere Andi, Jonas, Sissi, sowie Kami für's Catering und Nina für die Formatierhilfe.

Schliesslich - nicht zuletzt und immer wieder - meinen Eltern.

CV

Wolf-Dietmar Moritz Hütteroth

Address

Steinweg 35a

35037 Marburg

Home:	+49(0)6421 / 608612
Office:	+49(0)6421 / 28-23380
Fax:	+49(0)6421 / 28-28941
Email:	huetteroth@staff.uni-marburg.de
Homepage:	http://www.uni-marburg.de/fb17/fachgebiete/tierphysio/neurobiologie

Personal

Born:	Erlangen, Germany June 16th 1976
Citizenship:	German
Marital status:	unmarried

Education

1982-1988	Elementary school, Erlangen-Dechsendorf, Germany
1988-1995	High school: Marie-Therese-Gymnasium Erlangen, Germany (intensive courses: Latin and Biology)
1995	General qualification for university entrance, Mark 2.6
1995-1996	Social service, Diakonie Erlangen
1996-1998	Undergraduate: Philipps-University Marburg, Germany
1998-1999	Visiting student: University of Edinburgh, Scotland, UK
1999-2002	Undergraduate: Philipps-University Marburg, Germany
2002-2008	PhD: Philipps-University Marburg, Germany
2007	JSPS Summer Program, University of Tokyo, Tokyo, Japan
2007-2008	PhD: Philipps-University Marburg, Germany

Degree

01.10.2002	Diploma in Biology, Mark 1.0 („Very good”) Title of thesis: „3D-Rekonstruktion der Glomeruli im Antennallobus des Tabakschwärmers *Manduca sexta* während der Metamorphose“ „3D-reconstruction of glomeruli in the antennal lobe of the sphinx moth *Manduca sexta* during metamorphosis“

Academic appointment

2002 – 2005	Research assistant Philipps-University Marburg

Scientific meetings

2004	Organizing committee, 15th Neurobiolocical PhD-students Workshop, Marburg, Germany

Awards

2006:	Travel grant of the German Neuroscience Society
2007:	JSPS summer program fellowship

Teaching

Tutor in undergraduate courses:

1999:	Zoology anatomy
1999-2001:	student assistant in lab, animal physiology („learning“)
2003-2006:	confocal microscopy course
2006:	multimedia in biology

Presentations

2001: “Cu,Zn-Superoxide dismutase-ir in the developing brain of *Manduca sexta*”, Justus-Liebig-University Gießen, Germany, Group of Dr. S. Trenczek

2003: “3D-Reconstructions of Pupal and Adult Glomeruli in the Antennal Lobe of the sphinx moth *Manduca sexta”*, Arthropod seminar, Kleinwalsertal, Germany

2004: “Pupal and Adult Glomeruli in the Antennal Lobe of the Moth *Manduca sexta*: a volumetric comparison based on 3D Reconstructions”, 97th DZG meeting, Rostock, Germany

2004: “The usability of standardized 3D glomeruli in the *Manduca sexta* antennal lobe during development”, Arthropod seminar, Eifel, Germany

2007: “Nitric oxide and cGMP signaling in the developing antennal lobe of the sphinx moth *Manduca sexta*”, 11th ISIN meeting, Tihany, Hungary

Publications

Reviewed Articles:

- Utz S, Huetteroth W, Vömel M, Schachtner J 2008
  Mas-allatotropin in the developing antennal lobe of the sphinx moth *Manduca sexta*: distribution, time course, developmental regulation and colocalization with other neuropeptides. Dev Neurobiol 68(1):123-142

- Utz S, Huetteroth W, Wegener C, Kahnt J, Predel R, Schachtner J 2007
  Direct peptide profiling of lateral cell groups of the antennal lobes of *Manduca sexta* reveals specific composition and changes in neuropeptide expression during development. Dev Neurobiol 67(6):764-777

- Huetteroth W, Schachtner J 2005
  Standard three-dimensional glomeruli of the *Manduca sexta* antennal lobe: a tool to study both developmental and adult neuronal plasticity. Cell Tissue Res 319(3):513-524

- Schachtner J, Huetteroth W, Nighorn A, Honegger HW 2004
  Copper/zinc superoxide dismutase-like immunoreactivity in the metamorphosing brain of the sphinx moth *Manduca sexta.* J Comp Neurol 469:141-152

Submitted:

- Staudacher EM, Huetteroth W, Schachtner J, Daly KC 2008
  Ensemble analysis of projection neurons from identified glomeruli in the moth *Manduca sexta*: towards a 4D representation of odor processing in a virtual antennal lobe. J Neurosci Methods

- el Jundi B*, Huetteroth W*, Kurylas AE, Schachtner J 2008
  Anisometric brain dimorphism revisited: implementation of a volumetric 3D standard brain in *Manduca sexta.* J Comp Neurol, * equal contribution

- Huetteroth W, Utz S, Winterhagen P, de Vente J, Müller U, Nighorn A, Schachtner J 2008
  Transient nitric oxide-dependent cGMP formation is involved in metamorphic development of the antennal lobes of *Manduca sexta.* Dev Neurobiol

In preparation:

- Neupert S, Huetteroth W, Schachtner J, Predel R 2008
  Peptidomics of pheromone biosynthesis activating neuropeptide (PBAN)-expressing neurons of an insect. PNAS

- Goetz B, Dippel S, Dreyer D, Huetteroth W, Schachtner J 2008
  The transition from the larval to the adult antennal lobe in the red flour beetle *Tribolium castaneum.* Dev Neurobiol

- Huetteroth W, Utz S, Schachtner J 2008
  Nitric oxide-induced cGMP influences synapse marker proteins in defined 3D neuropilar regions of the developing antennal lobe. Acta Biol Hung

Abstracts:

- Staudacher EM, Huetteroth W, Schachtner J, Daly KC 2007
  Ensemble analysis of projection neurons from identified glomeruli in the moth *Manduca sexta*: Towards a 4D representation of odor processing in a virtual antennal lobe. 37th SfN meeting, San Diego, California, USA, 612.15/LL16

- Schachtner J, Goetz B, Dippel S, Dreyer D, Huetteroth W 2007
  Metamorphic development of the antennal lobes of the red flour beetle *Tribolium castaneum*: 3D-reconstruction and neurochemistry. 37th SfN meeting, San Diego, California, USA, 135.2/F14

- Götz B, Dippel S, Dreyer D, Huetteroth W, Schachtner J 2007
  Ontogeny of the antennal lobes of the red flour beetle *Tribolium castaneum.* 100th DZG meeting Köln N14, p107

- Kollmann M, Huetteroth W, Schachtner J 2007
  Studies on a collembolan brain: 3D reconstruction and neurochemistry. 100th DZG meeting Köln N47, p124

- Huetteroth W, Utz S, Vömel M, Winterhagen P, Schachtner J 2007
  Nitric oxide and cGMP signaling in the developing antennal lobe of the sphinx moth *Manduca sexta*. 11th ISIN meeting, Tihany, Hungary

- Schachtner J, Utz S, Huetteroth W 2007
  Neuropeptides in the developing insect antennal lobe: localization, characterization, and putative functions. 11th ISIN meeting, Tihany, Hungary

- Staudacher EM, Huetteroth W, Parsons HL, Schachtner J, Daly KC 2007
  Glomerular response mapping using virtual projection neuron populations: A step towards representing whole antennal lobe activity in realtime. 29th AChemS meeting, Sarasota, Florida, USA

- Huetteroth W, Utz S, Schachtner J 2007
  Time course of NO dependent cGMP regulation and its influence on antennal lobe neuropil development in the sphinx moth *Manduca sexta.* 7th NWG meeting, Göttingen TS8-8B

- el Jundi B, Huetteroth W, Schachtner J 2007
  3D reconstruction of *Manduca sexta* adult brain and of brains during metamorphic development. 7th NWG meeting, Göttingen TS8-7B

- Dreyer D, Dippel S, Huetteroth W, Schachtner J 2007
  The *Tribolium* brain: 3D reconstruction and immunocytochemical mapping during metamorphosis and in the adult. 7th NWG meeting, Göttingen TS8-6B

- Dippel S, Goetz B, Dreyer D, Huetteroth W, Schachtner J 2007
  Pupal staging and metamorphic development of the antennal lobes of the red flour beetle *Tribolium castaneum*. 7th NWG meeting, Göttingen TS8-5B

- Schachtner J, Huetteroth W, Dreyer D, Dippel S, el Jundi B 2006
  3D-reconstructions of the *Tribolium* brain: a tool to study developmental and adult plasticity. 36th meeting of the Society for Neuroscience, Atlanta

- Dreyer D, Dippel S, el Jundi B, Huetteroth W, Schachtner J 2006
  3D reconstruction of the *Tribolium* brain: a tool to study developmental and adult plasticity. 99th DZG meeting Münster PM_NB_1.19, p44

- Dippel S, Dreyer D, Huetteroth W, Schachtner J 2006
  Staging of pupal development and brain metamorphosis of the red flour beetle *Tribolium castaneum*. 99th DZG meeting Münster PM_NB_1.20, p44

- Huetteroth W, Schachtner J 2005
  Standardized 3D glomeruli of the *Manduca sexta* antennal lobe as a tool to study the influence of nitric oxide-stimulated cGMP on neuropilar development. NWG Göttingen, Proc 6th German Neurosci Soc Conf, Thieme, Stuttgart 268B, p830

- Utz S, Huetteroth W, Schachtner J 2005
  Development and steroid regulation of Mas-allatotropin immunostaining in antennal lobe neurons of the sphinx moth *Manduca sexta.* 98th DZG meeting Bayreuth 1_Po_24, p87

- Huetteroth W, Utz S, Schachtner J 2005
  3D reconstructions of identified glomeruli of the *Manduca sexta* antennal lobe to study the influence of NO/cGMP on neuropil development. 98th DZG meeting Bayreuth 7_Po_06, p135

- Huetteroth W 2004
  The usability of standardized 3D glomeruli in the *Manduca sexta* antennal lobe during development. Arthropodenseminar Eifel

- Huetteroth W 2004
  Pupal and Adult Glomeruli in the Antennal Lobe of the Moth *Manduca sexta*: a volumetric comparison based on 3D Reconstructions. 97th DZG meeting Rostock V-S1.4, p97

- Huetteroth W 2003
  3D-Reconstructions of Pupal and Adult Glomeruli in the Antennal Lobe of the sphinx moth *Manduca sexta*. Arthropodenseminar Kleinwalsertal

- Huetteroth W-D, Schachtner J 2003
  3D reconstructions of pupal and adult glomeruli in the antennal lobe of the sphinx moth *Manduca sexta*. NWG Göttingen, Proc 5th German Neurosci Soc Conf, Thieme Verlag, Stuttgart, New York 689, p735

- Huetteroth W-D, Honegger H-W, Schachtner J 2001
  Transient Cu,Zn-superoxide dismutase (SOD)-like immunoreactivity in the metamorphosing brain of the sphinx moth *Manduca sexta*. NWG Göttingen, Proc 4th German Neurosci Soc Conf, Thieme Verlag, Stuttgart, New York 940

- Huetteroth W-D, Schachtner J, Honegger H-W, Homberg U 2000
  Developmental pattern of Cu, Zn-superoxide dismutase (SOD)-like immunoreactivity during metamorphosis of the brain of the sphinx moth *Manduca sexta*. 93th DZG meeting Bonn Zoology 103 Suppl. III, p9

- Hütteroth W, Honegger HW, Homberg U, Schachtner J 2000
  Cu, Zn-superoxide dismutase-like immunoreactivity in the brain of the sphinx moth *Manduca sexta* during metamorphosis. Soc Neurosci Abstr 26(1):1167

Marburg, August 13th 2008

_____
(Wolf Hütteroth)

ERKLÄRUNG

Ich versichere, dass ich meine Dissertation

Neuromediators in the developing olfactory system: 3D-reconstruction towards a functional understanding

(Neuromediatoren im sich entwickelnden olfaktorischen System: mittels 3D-Rekonstruktionen zu einem funktionellen Verständnis)

selbstständig, ohne unerlaubte Hilfe angefertigt und mich dabei keiner anderen als der von mir ausdrücklich bezeichneten Quellen und Hilfen bedient habe.

Die Dissertation wurde in der jetzigen oder einer ähnlichen Form noch bei keiner anderen Hochschule eingereicht und hat noch keinen sonstigen Prüfungszwecken gedient.

Marburg, den 13. August 2008

_____
(Wolf Hütteroth)